SEDIMENTATION AND NEOTECTONICS OF THE BURDUR REGION, SOUTHWEST TURKEY

Thesis submitted for the degree of

Doctor of Philosophy

at the University of Leicester

by

Simon Paul Price BSc (Nottingham)

Department of Geology

University of Leicester

September 1989

ProQuest LLC
789 East Eisenhower Parkway
P.O. Box 1346
Ann Arbor, MI 48106-1346

Sedimentation and Neotectonics of the Burdur Region, southwest Turkey.

Simon Paul Price.

The NE-SW trending Burdur-Acigöl-Baklan basin system of southwest Turkey represents the present-day configuration of a system initiated in late Miocene / early Pliocene times. During the Pliocene a half-graben, controlled by a NW-dipping planar fault system, developed in the area around Burdur. The Burdur Formation was deposited in this half-graben. Rapid subsidence is indicated by the lack of a well-developed footwall-sourced fan system. However, larger fans developed in the relay structures between en echelon fault segments. The centre of the basin was occupied by a deep saline lake. Orbitally-driven climatic change was the dominant control on sedimentation in this lake. The scarcity of wet-sediment deformation within the Burdur Formation suggests that levels of Pliocene seismicity were lower than twentieth century levels.

Towards the end of the Pliocene the fault system controlling the Burdur basin became inactive and renewed faulting took place in the hangingwall of the old system. This event gave rise to the present-day configuration of narrow basins in the study area and was due to instability of the end-Pliocene topography. Both margins of the present-day Burdur, Acigöl and Baklan basins are faulted. In each case the major throw is on the fault on the southeast margin. A β value of 1.18 calculated for the Burdur region assumes a planar fault geometry. As a curvature of up to 40° at depth cannot be ruled out this must be considered a minimum estimate.

Each of the Burdur, Acigöl and Baklan basins is extending in a NW-SE direction (compared to the N-S extension direction of the Aegean). It is proposed that the basins are within a N-S trending deforming zone between the rapidly-extending Aegean region (to the west) and the relatively stable Anatolian plateau (to the east). The model adopted explains the clockwise rotation of fault-bounded blocks in the Burdur region. The dextral motion across the deforming zone, predicted by the model, may be a result of the anticlockwise rotation of western Turkey.

ACKNOWLEDGMENTS.

Firstly, I would like to thank Barry Scott and John Hudson for instigating this project and for their supervision throughout.

In Turkey I would like to thank Celal Sengör and the Dean of the Faculty of Mines at Istanbul Technical University for their logistical support. Also, Celal Sengör and his family are thanked for making Pepsi Cola facilities available to me during my stay in Turkey. The Turkish Petroleum Corporation provided transport in the field and allowed me to study aerial photographs in their offices in Ankara. This was greatly appreciated. Altan Cin, Haldun Okurogullari and Emrah Can provided able assistance and fruitful discussions in the field. The driving skills of Hulki Tunç, Mustafa Karapinar and Erol Çakmak were also appreciated. Dr. Nuran Gökçen of Dokuz Eylül University studied the ostracode fauna collected from the Burdur Formation. Her contribution was greatly appreciated. Finally, Simon Lamb, of Victoria University (New Zealand) and Ali Bilgin and Erkan Karaman, both of Akdeniz University, are thanked for discussions in the field.

In the U.K. I would like to thank the following people: Graham Weedon (Cambridge University) for performing the spectral analysis of the Burdur Formation. Jim Marshall, Hilary Attenborough and Julie Sharman (all Liverpool University) for help with stable isotope analyses. David Rex (Leeds University) for providing K-Ar dating facilities. Richard Lisle (Swansea University) for providing me with a program to undertake palaeostress analyses. Jane Tongue (Leicester University) for migrating the seismic lines obtained from Ozan Sungurlu (Turkish Petroleum). James Jackson and Steve Roberts (both Cambridge University) and Rob Westaway (Durham University) for fruitful discussions.

Mark Allen, John Faithfull, John Hudson, Dave Martill, Barry Scott and Mark Williams are thanked for commenting on early drafts of parts of this thesis. I would also like to thank the technical, secretarial and academic members of the Geology Department at Leicester (too numerous to name here) for their help and advice over the last 3 years.

Finally, I would like acknowledge the N.E.R.C. (Grant No. GT4/86/GS/53) for financial support.

LIST OF CONTENTS.

CHAPTER ONE. Introduction.

1.1. INTRODUCTION..... 1.1
1.2. AIMS OF STUDY..... 1.1
1.3. OUTLINE OF THESIS..... 1.2
1.4. HISTORY OF RESEARCH..... 1.2
1.5. GEOLOGICAL BACKGROUND
1.5.1. Palaeotectonic history..... 1.3
(a) Regional..... 1.4
(b) Western Taurides..... 1.5
(i) Late Cretaceous to Palaeocene..... 1.5
(ii) Late Palaeocene to late Eocene..... 1.6
(iii) Early Oligocene to mid-Miocene..... 1.7
1.5.2. Causes of neotectonic extension..... 1.9
1.6. REFERENCES..... 1.11

CHAPTER TWO. Stratigraphy of the Burdur Formation.

2.1. INTRODUCTION..... 2.1
2.2. DEFINITION OF STRATIGRAPHIC UNITS..... 2.2
2.3. GEOMETRY OF THE BURDUR FORMATION..... 2.2
2.3.1. The whole formation..... 2.3
2.3.2. The individual members..... 2.4
(a) Çendik Member..... 2.4
(b) Akdere Member..... 2.4
(c) Günalan Member..... 2.4
2.4. DATING THE BURDUR FORMATION
2.4.1. Biostratigraphy..... 2.6
2.4.2. Chronostraigraphy..... 2.8
2.5. A REVISED LITHOSTRATIGRAPHY..... 2.9
2.5.1. Central basinal succession
(a) Çendik Member..... 2.9
(b) Akdere Member..... 2.11
(c) Günalan Member..... 2.12
2.5.2. Volcanic succession
(a) Lower Gölcük Member..... 2.13

(b) Upper Gölcük Member..... 2.14
2.6. CONCLUSIONS..... 2.15
2.7. REFERENCES..... 2.16

CHAPTER THREE. Sedimentology of the Burdur Formation.

3.1. INTRODUCTION..... 3.1
3.2. SEDIMENTARY FACIES..... 3.1
3.2.1. Facies Association A: Alluvial fan-fluvial deposits..... 3.1
3.2.2. Facies Association B: Fan-delta plain deposits..... 3.4
3.2.3. Facies Association C: Fan-delta front deposits..... 3.5
3.2.4. Facies Association D: Coastal plain deposits..... 3.6
3.2.5. Facies Association E: Interdeltaic shoreline deposits..... 3.7
3.2.6. Facies Association F: Nearshore lacustrine deposits..... 3.8
3.2.7. Facies Association G: Offshore lacustrine deposits..... 3.10
3.2.8. Facies Association H: Offshore turbidite deposits..... 3.11
3.2.9. Facies Association I: Air fall tuff/agglomerate deposits... 3.12
3.2.10. Facies Association J: Base surge deposits..... 3.15
3.2.11. Facies Association K: Lahar deposits..... 3.16
3.3. A SEDIMENTARY MODEL..... 3.17
3.3.1. Hangingwall-sourced fans..... 3.17
3.3.2. Footwall-sourced fans..... 3.19
3.3.3. Fan-lake interactions..... 3.20
3.3.4. Effect of fault migration..... 3.22
3.4. CONCLUSIONS..... 3.23
3.5. REFERENCES..... 3.25

CHAPTER FOUR. A spectral and geochemical study of cyclic sedimentation in Neogene Lake Burdur.

4.1. INTRODUCTION..... 4.1
4.2. SAMPLE ACQUISITION AND TREATMENT
4.2.1. Field sampling and sample preparation..... 4.2
4.2.2. Analytical techniques
(a) X-ray diffraction..... 4.2
(b) Trace elements..... 4.3
(c) Stable isotopes..... 4.3
4.3. DOLOMITE ORDERING AND STOICHIOMETRY..... 4.4

4.4. CYCLIC SEDIMENTATION
4.4.1. Periodicity of cycles
(a) Technique..... 4.5
(b) Results..... 4.6
4.4.2. Geochemical results and discussion
(a) Sediment texture..... 4.7
(b) Mineralogy..... 4.7
(c) Minor elements
(i) Strontium..... 4.9
(ii) Magnesium..... 4.10
(iii) Sodium..... 4.11
(d) Oxygen isotopes..... 4.13
(i) $\delta^{18}O$ of aragonite..... 4.14
(ii) Lake water temperature..... 4.15
(iii) Meteoric water composition..... 4.16
(e) Carbon isotopes..... 4.17
4.5. OSTRACODAL SEDIMENTS..... 4.19
4.6. DISCUSSION
4.6.1. Nature of cyclic sedimentation..... 4.21
4.6.2. Cause of cyclic sedimentation..... 4.23
4.7. CONCLUSIONS..... 4.25
4.8. REFERENCES..... 4.26

CHAPTER FIVE. The structure of the Burdur-Acigöl-Baklan basin system.

5.1. INTRODUCTION..... 5.1
5.2. BASEMENT FAULTS..... 5.1
5.2.1. Quaternary basement faults..... 5.2
(a) The Burdur basin..... 5.2
(b) The Acigöl basin..... 5.3
(c) The Baklan basin..... 5.3
5.2.2. Neogene basement faults..... 5.4
5.3. FAULTS WITHIN THE NEOGENE..... 5.5
5.3.1. Syn-depositional tectonic faults..... 5.5
5.3.2. Post-depositional tectonic faults..... 5.6
5.3.3. Landslips..... 5.6
5.3.4. Liquefaction-related faults..... 5.6
5.3.5. Compaction-related faults..... 5.7

5.4. PALAEOSTRESS ANALYSIS
5.4.1. The method..... 5.7
5.4.2. Data and results..... 5.8
5.5. STRUCTURE OF THE BURDUR BASIN
5.5.1. Seismic structure..... 5.9
5.5.2. Neogene–Quaternary boundary..... 5.11
5.6. EXTENSION..... 5.13
5.7. DISCUSSION..... 5.15
5.8. REFERENCES..... 5.17

CHAPTER SIX. The sub-surface geometry of basin-controlling faults from the Burdur region.

6.1. INTRODUCTION..... 6.1
6.2. QUATERNARY FAULT GEOMETRY..... 6.2
6.2.1. Surface fault dips..... 6.3
6.2.2. Surface slip vector dips..... 6.4
6.2.3. Seismological observations..... 6.4
6.3. NEOGENE FAULT GEOMETRY
6.3.1. Dip profiles..... 6.5
(a) Non-rotating listric faults..... 6.6
(b) Rotating planar faults..... 6.6
6.3.2. Burdur dip profiles..... 6.7
6.3.3. Discussion of dip profiles..... 6.8
6.4. GEOMETRICAL CONSIDERATIONS OF ROTATIONS ON A CURVED SURFACE.... 6.10
6.5. DISCUSSION
6.5.1. The controversy..... 6.12
6.5.2. Geometry of faults at Burdur..... 6.13
6.6. REFERENCES..... 6.15

CHAPTER SEVEN. Structural evolution of the Burdur-Acigöl-Baklan basin system: the nature of the eastern end of the graben sytem of western Turkey.

7.1. INTRODUCTION..... 7.1
7.2. SEISMOLOGY
7.2.1. Historical seismology..... 7.2
7.2.2. Pre-historical seismology..... 7.3

7.3. GEOGRAPHICAL DISTRIBUTION OF FAULT ACTIVITY..... 7.7
7.4. THE END-NEOGENE TECTONIC EVENT..... 7.9
7.5. DEFORMATION OF BLOCKS
7.5.1. Graben orientation..... 7.12
7.5.2. Regional σ_3 orientation..... 7.12
7.5.3. Block rotations..... 7.13
7.5.4. Deformational models..... 7.13
(a) Cross-graben model..... 7.14
(b) Rotational block model..... 7.14
(i) The width of the deforming zone, a..... 7.15
(ii) The angle θ..... 7.16
(iii) The rate of rotation, $d\theta/dt$..... 7.16
7.6. DISCUSSION..... 7.16
7.7. CONCLUSIONS..... 7.18
7.8. REFERENCES..... 7.20

CHAPTER EIGHT. Summary of conclusions.

.....8.1

APPENDIX I..... I.1

APPENDIX II..... II.2

CHAPTER ONE

INTRODUCTION AND GEOLOGICAL BACKGROUND

1.1. INTRODUCTION.

The Burdur, Acigöl and Baklan basins (see enclosure 2), situated at the western end of the Taurus Mountain range of western Turkey (Fig.1.1), form a basin system which was initiated in late Miocene to early Pliocene times and is still active. This introductory chapter describes the main aims of this study, which was conducted over 3 years between July 1986 and August 1989 and involved 3 field seasons, each of about 3 months duration. A brief outline of the layout of the thesis is given as well as a history of research of the study area. Finally, a summary of the geological history of the region prior to basin development and some ideas as to why basins have developed in this region are given. These latter discussions form the main part of this chapter.

1.2. AIMS OF STUDY.

The main objective of this study was to investigate the age, structure and evolution of the Burdur-Acigöl-Baklan basin system. This is an actively evolving system of extensional basins and, therefore, provides a useful modern analogue to many ancient basins. This study area was chosen for the following reasons:

(a) The basinal sediments of the Burdur region constitute the most well-exposed Neogene succession in western Turkey.

(b) The study area is situated at the boundary between the rapidly extending Aegean region and the relatively stable Anatolian plateau. Studies in this area will therefore yield potentially useful information concerning the nature of this boundary.

(c) The area has received little attention from geologists in the past.

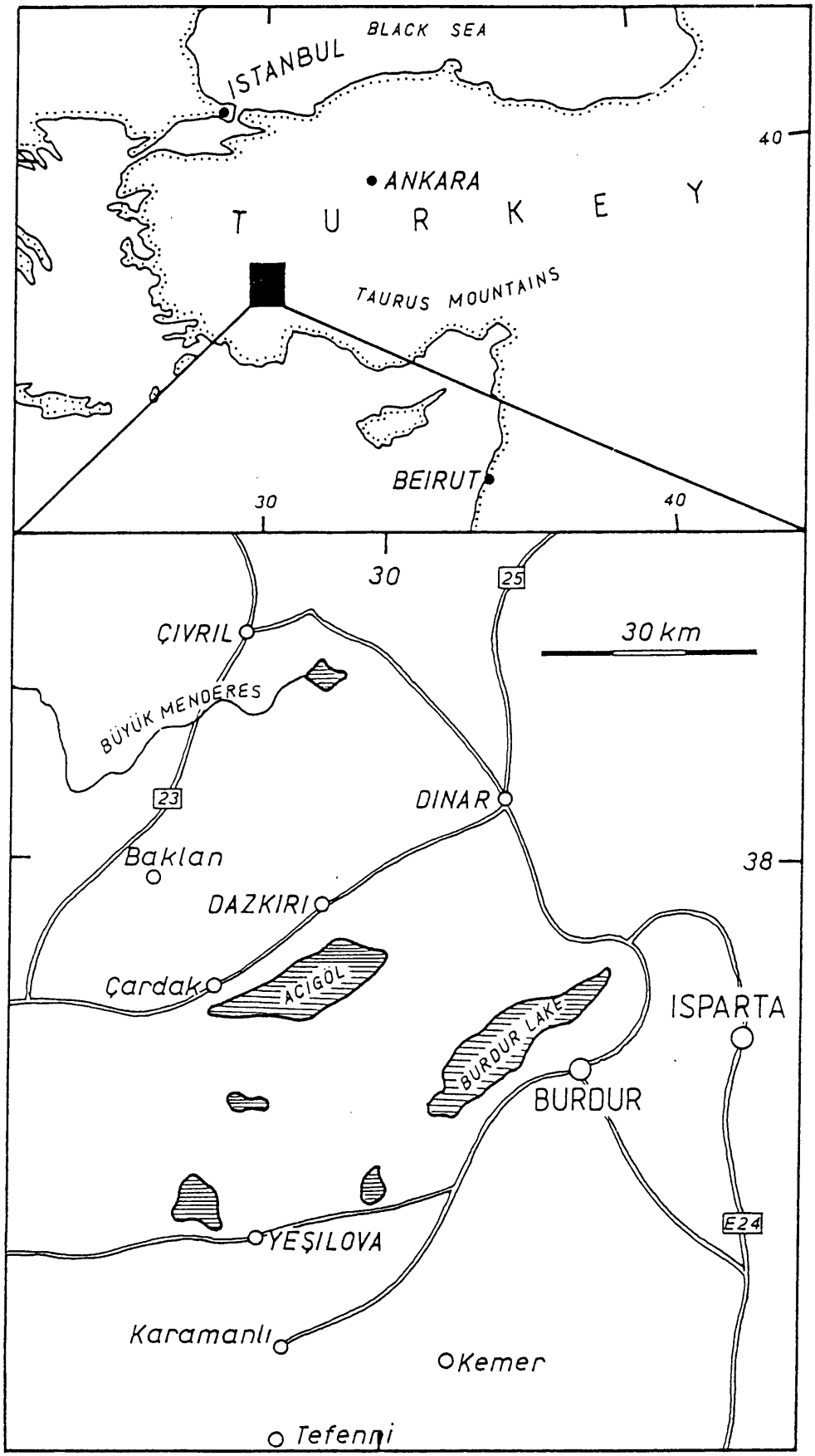

Fig.1.1. Locality map of the study area.

1.3. OUTLINE OF THESIS.

The thesis is divided into 8 chapters. Following this chapter, Chapter 2 deals with the stratigraphy of the well-exposed Neogene succession of the Burdur region (the Burdur Formation). A lithostratigraphy is proposed and new biostratigraphic and chronostratigraphic data are presented. In Chapter 3 the sedimentological evolution of the Burdur Formation is described, with particular emphasis on the interaction between tectonics and basin margin fan geometry. Chapter 4 is a detailed spectral and geochemical study of cyclicity within Neogene Lake Burdur. The nature and cause of this cyclicity is investigated. Chapters 5, 6 and 7 deal with the structure and evolution of the Burdur, Acigöl and Baklan basins. In Chapter 5 the structure of both Neogene and Quaternary basins in the study area is outlined. Chapter 6 is an investigation of the sub-surface geometry of faults controlling both the Neogene and Quaternary Burdur basin. In Chapter 7, a model for the evolution of the 3 basins in the study area is proposed and this is discussed with reference to the general tectonics of the Aegean region. Finally, Chapter 8 gives a summary of the conclusions drawn from this study.

1.4. HISTORY OF RESEARCH.

Because of its excellent exposure, most of the work published on the study area has been about the Neogene succession of the Burdur basin (the Burdur Formation). The first geological description of the study area was by Penck (1918) who believed the Neogene and Quaternary sediments of the Burdur basin to have been deposited in a depression formed by a pre-Neogene syncline. Lahn (1946) was the first to give a description of the Burdur Formation. Wedding (1966) and Wedding and Inque (1967) produced a geological map of the Burdur area and proposed the first formal lithostratigraphy of the Burdur Formation. The geological map published by Bering (1971a) covers the whole of the Burdur Formation outcrop, from Keçiborlu in the NE to Tefenni in the SW. His lithostratigraphy is similar to that of Wedding and Inque (1967) although includes the volcanic deposits of the Gölcük Lake area at the NE end of the Burdur Formation oucrop (Bering 1971a). Bering also studied the deposits of other continental basins in southern Anatolia and, by comparison, was able to propose tentative biostratigraphic ages (Bering 1971a,1971b). Karaman (1986a) again revised the lithostratigraphy of the

Burdur Formation based on more detailed mapping in the Burdur area.

The volcanic deposits of the Gölcük Lake area were first described by Ardel and de Planhol (1951), who believed volcanism to have been of lower Neogene age with caldera collapse occurring in the late Pliocene/early Quaternary. Subsequent K-Ar dating by Lefèvre et al. (1983) showed volcanism to have started at the beginning of the Pliocene. De Planhol (1956) believed that the downfaulting of the present-day Burdur basin was initiated during the closing stages of the last Glacial period. In his extensive studies of the Quaternary deposits (and geomorphology) of Anatolia, however, Erol (1975) concluded that this downfaulting event occurred over a period of time starting in the late Pliocene.

The structure of the basins in the study area has received little attention. Karaman (1986b) published some structural data from the Burdur area and attributed the major topographic break on the SE side of Lake Burdur to faulting. The 3 basins in the study area were shown on a cross-section by Koçyigit (1984) to be symmetrical grabens.

1.5. GEOLOGICAL BACKGROUND.

1.5.1. Palaeotectonic history.

The pre-rifting geological history of the Burdur-Acigöl-Baklan area is complex and a detailed study is beyond the scope of this thesis. However, it is important to be able to recognise the main lithological units of the palaeotectonic period (collectively termed "basement" throughout this study) and to have an understanding of how the region evolved prior to the onset of neotectonic extension. The reason for this is twofold. Firstly, the neotectonic study covered in this thesis is a small part of the long and complex history of the area and should only be considered in the light of earlier events. An understanding of the evolution of the crust in western Turkey is of importance when considering the possible mechanisms involved in the later extensional phase. Also, older structures are often thought to influence the pattern of younger structures (Sengör et al. 1985), which are of interest here, and therefore an understanding of their geometries is essential. The following is therefore a brief summary of the palaeotectonic history of the Alpine-Himalayan mountain belt and, more particularly, the western

Taurus Mountains of Turkey. The various palaeotectonic units of the study area are described and their evolution is summarized in a geological history. For a more detailed description of the palaeotectonic history of the western Taurides the reader is referred to Brunn et al. (1971) and for a summary of the palaeotectonic history of Turkey see Sengör and Yilmaz (1981).

(a) Regional.

Turkey is situated towards the western end of the Alpine-Himalayan mountain chain. The "roots" of this mountain chain are largely composed of Precambrian and Lower Palaeozoic rocks deformed during the Pan-African orogenic phase (900Ma to 450 Ma (Kröner 1984)), which was responsible for the initial assembly of Gondwanaland. Lower Palaeozoic Pan-African terrains form the basement in western Turkey (Sengör et al. 1984). The Alpine-Himalayan orogenic belt marks the destruction of the former oceanic embayment in the Pangean Supercontinent born in the Triassic and first recognised by Neumayr (1885) and later linked with the Alpine-Himalayan Belt by Suess (1893). This ocean was called Tethys, after the sister and wife of Okeanos, the Greek god of the ocean (Suess 1893). The notion of Tethys has been modified by more recent authors to take account of an ocean which existed before the classical Tethys of Suess (1893) (Sengör 1984). Thus Sengör (1984,1985) puts forward a model involving 2 separate collisions to account for the evolution of the Alpine-Himalayan mountain belt. In this model the former ocean, called Palaeo-Tethys (after Sengör 1979), closed in late Triassic to mid-Jurassic times, when the Eurasian continent collided with what was essentially a thin continental east-west trending sliver called the Cimmerian continent to form an east-west trending orogenic belt, called the Cimmerides (Sengör 1979, Bernoulli and Lemoine 1980). Behind the Cimmerian continent was a younger ocean, called Neo-Tethys (Sengör 1979, Argyriadis et al. 1980), which opened in the mid-Jurassic, possibly as a back-arc basin over a south-dipping Palaeo-Tethyan subduction zone (Windley 1982). This corresponds to the Permo-Triassic embayment of Pangaea (the "classical" Tethys of Suess (1893)). The closure of this ocean during the early Tertiary was brought about by the northward collision of continental fragments of Gondwanan origin with the southern margin of Eurasia, which now was composed largely of accreted Cimmerian blocks. This closure may have involved northward subduction (Smith and Woodcock 1976) and the ultimate collision gave rise to the second

orogenic belt, the Alpides (Sengör 1984), which largely overprints the earlier Cimmeride belt. The two together form the Alpine-Himalayan mountain belt and are collectively termed, the Tethysides (Sengör 1984).

(b) Western Taurides.

The Taurus Mountains of Turkey form an arcuate east-west trending belt, stretching across southern Turkey. The development of Turkey (and the western Taurides in particular) throughout the late Mesozoic and Tertiary is summarized below and in Fig.1.2.

(i) Late Cretaceous to Palaeocene.

During the middle to late Cretaceous a large carbonate platform, the Anatolide-Tauride Platform, existed in an area approximately equivalent to the present-day Anatolian Plate (Sengör and Yilmaz 1981). This platform had separated from Gondwanaland during the Triassic. Its exact position during the Mesozoic is uncertain, but the similarity of European and Turkish Mesozoic faunas suggests a strong link with Europe (Ager 1988). The Anatolide-Tauride Platform was separated into a southern Menderes Taurus block and a northern Kirsehir block (Görür et al. 1984) by the Inner Tauride Ocean, which had opened in the early Triassic (Özgül 1984). Oktay (1973) was the first to recognise the subdivision of the Anatolides into these two continental blocks, which had collided along a suture now underlying the Tuzgölü basin complex. This subdivision is highlighted by differences in the structural evolution between the Kirsehir Massif and the Menderes Massif (Seymen 1981, 1982). However, Sengör et al. (1988) believed that the Inner Tauride Ocean was only formed as a result of intracontinental rifting as the closure of the Karakaya Basin to the north of the Kirsehir block affected the Menderes Taurus block to the south of the Inner Tauride Ocean (Sengör et al. 1984).

The basement rocks of the study area are dominated by the "Mesozoic Comprehensive Series" (M.T.A. 1:500000 Map of Turkey). These consist mainly of massive, hard white sparry limestones, which often contain Rudist bivalves (Brunn et al. 1971) and represent Upper Cretaceous reefs deposited on an extensive carbonate platform (Brinkmann 1971; Brunn et al. 1971), the Anatolide-Tauride Platform.

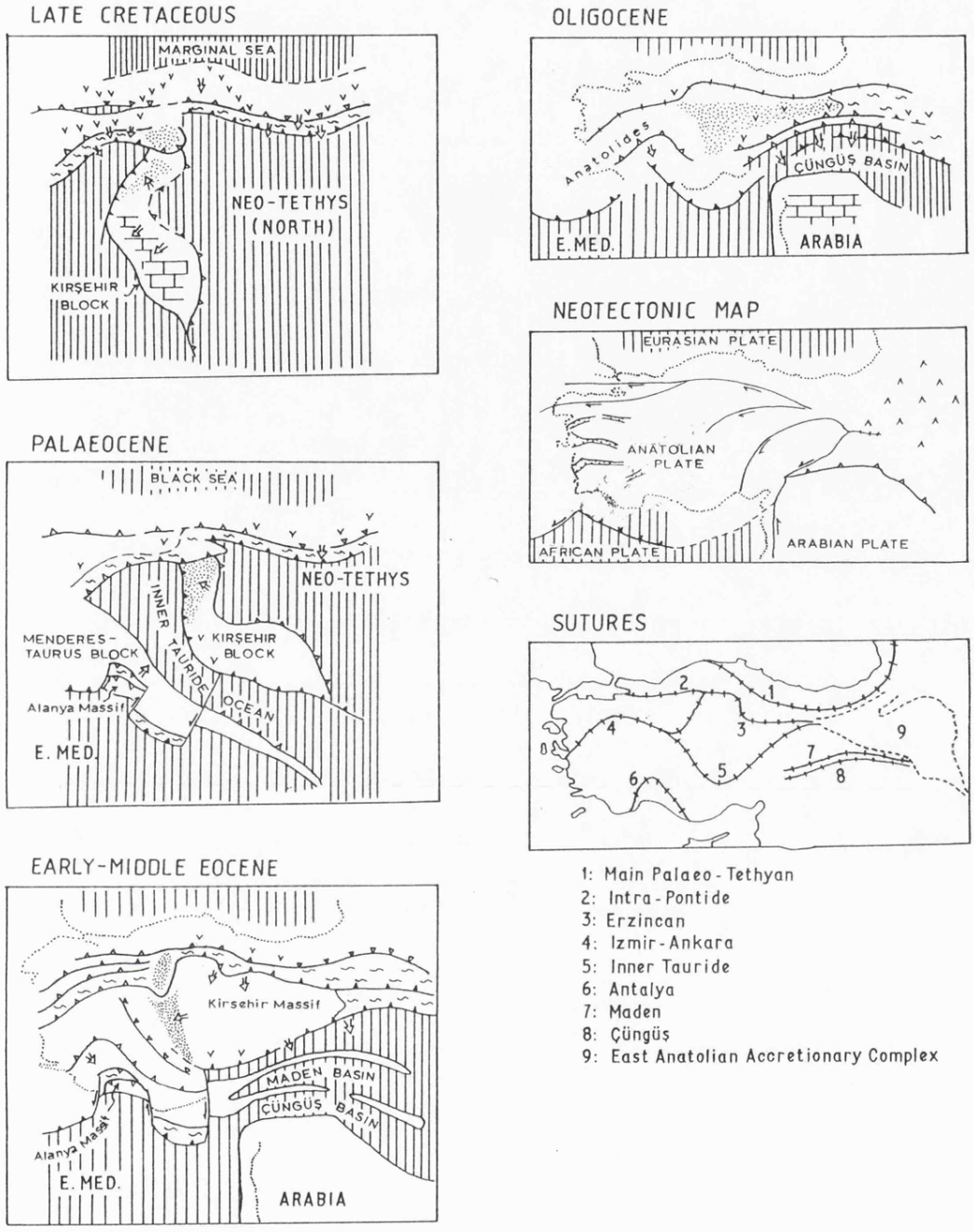

1: Main Palaeo-Tethyan
2: Intra-Pontide
3: Erzincan
4: Izmir-Ankara
5: Inner Tauride
6: Antalya
7: Maden
8: Çüngüş
9: East Anatolian Accretionary Complex

Fig.1.2. Maps depicting the palaeotectonic evolution of Turkey. Maps show oceans (ruled), continents (white), predominant lithologies (carbonate pattern = neritic carbonates, stippled = turbidites, wavy lines = ophiolitic mélanges). Open arrows show flysch dispersal directions. v = arc volcanics, ∧ = Tibet-type volcanics. Lines with hachures are passive continental margins, heavier lines with black triangles are subduction zones and lines with half-arrows are transform faults. Lines with open triangles are major thrust faults and lines with upside-down triangles are "rétrocharriages". Taken from Görür et al. (1984); partly after Sengör et al. (1981).

Towards the end of the Cretaceous extensive ophiolite obduction took place throughout the Anatolide-Tauride Platform (Ricou 1971; Ricou et al. 1975). These ophiolites comprise harzburgites, chromitite deposits and deep sea radiolarian cherts (Karamata 1980) and their geochemistry indicates that they originated in back-arc basins behind a series of arcs (Pearce 1980). Advancing ophiolite nappes caused the platform to subside and become a site for either pelagic or flysch deposition depending on distance from the nappes (Sengör and Yilmaz 1981). The late Cretaceous "wildflysch" (an olistostrome deposit containing assorted blocks to 1000 metres) terminates the Çamlik Formation on the eastern branch of the Isparta Angle and the Koyçegiz Formation on the western branch. This deposit, according to Brunn et al. (1971) gives the first indication of Alpine (i.e. Alpide) movements at the western end of the Taurus Mountains. Brinkmann (1971) considered changes in sea level throughout southern Anatolia during the Cenozoic. During the middle Cretaceous he envisaged radiolarite-ophiolite sediments depositing in individual basins within the "Taurus Geosyncline", followed by thick reef limestone sedimentation in the Late Cretaceous. At the end of the Cretaceous he describes a regressive event, which was probably due to shallow water sedimentation on thickened mélange wedges during the Palaeocene (Sengör and Yilmaz 1981). Rebound of the crust after ophiolite obduction also contributed to this regression.

(ii) Late Palaeocene to late Eocene.

During the Late Palaeocene the Anatolide-Tauride Platform collided with the Pontide mountain chain to the north (a Cimmeride feature) causing large-scale internal deformation (Sengör and Yilmaz 1981). This collision occurred along the Izmir-Ankara Suture. Following this, during the latest Palaeocene-Eocene, the Alanya Massif was emplaced into the future Isparta Angle along the Antalya Nappes (Delaune-Mayer et al. 1977), thus closing the small Pamplylian oceanic basin, which had existed in Southwest Turkey before this time (Sengör and Yilmaz 1981, Özgül 1985).

The provenance of the Antalya Nappes has been the subject of some considerable debate in the past. The allochthonous Antalya and Lycian Nappes lie to the east and west of the autochthonous Bey Daglari platform. Sediments on the eastern margin of the Bey Daglari platform appear to have been derived from the east and northeast (i.e. from the Antalya Nappes), whereas Miocene flysch on its western margin, in the

Susuz Dag area, were derived from the northwest (i.e. from the advancing Lycian Nappes). This led Hayward (1984) to believe that the two allochthons developed in seperate oceanic basins on either side of the Bey Daglari platform. Also, sedimentation continued uninterrupted on the central Bey Daglari until Upper Miocene times, supporting the "external" origin of the Antalya Nappes (Hayward and Robertson 1982, Hayward 1984). However, many authors, still support an "internal" origin for the Antalya Nappes (i.e. a derivation across the Bey Daglari platform from the northwest) (e.g. Ricou et al. 1974, 1975, 1979, 1984, Monod 1976 and Dumont et al. 1980). Whitechurch et al. (1984) showed that ophiolites from the Antalya and Lycian Nappes are structurally very similar and he postulated that they were formed at an east-west spreading axis in a single oceanic basin.

Following the closure of the Pamplylian Basin, a post-Lutetian phase of compression in the Isparta Angle brought the nappes in the eastern branch (the Taurus Occidental) to their present position upon autochthonous Eocene flysch deposits. Any movements in the western branch (the Lycian Nappes) at this time was masked by later movements (Brunn et al. 1971). However, flysch sediments of Eocene age are present within the Lycian Nappes, although the composition of conglomerates within this Nummulitic Flysch was believed by Brunn et al. (1971) to indicate a source within the Antalya Nappes. Also, this unit has a diachronous base and becomes thinner and younger on the inner (i.e. convex) part of the Isparta Angle (Brunn et al. 1971), away from the Antalya Nappes. Throughout the Late Eocene to Middle Miocene period flysch (derived from the north and northwest) was deposited throughout region of the western Taurides (Sengör and Yilmaz 1981).

(iii) Early Oligocene to mid-Miocene.

The Oligocene saw the beginning of widespread uplift and exposure of the Anatolides (Görür et al. 1984), with the advancing Bozkir Nappes to the north of the study area feeding much continental material beneath the massifs, giving rise to crustal thickening and anatectic melting resulting in silicic volcanism in western Turkey and granite plutonism in the Aegean Islands (Sengör and Yilmaz 1981). Associated with this uplift was widespread flysch deposition from the north and northwest, which began in the late Eocene and continued until early Miocene times (Sengör and Yilmaz 1981).

Throughout the study area large areas of flysch conglomerates, sandstones and marls are exposed. The largest areas of outcrop occur at the northern end of the Burdur Basin and on the northwest side of the Acigol Basin, where conglomerates form the Maymun Mountains (see enclosure 2). Also, to the west of Tefenni, there are exposures of marl, fine sandstones and limestones. These are shown either as Eocene flysch or, simply, Eocene–Oligocene on the M.T.A. 1:500000 geological maps covering the area (Denizli, Konya, Ankara and Izmir sheets). The conglomerate succession north of Burdur Lake is approximately 300 metres thick and transgresses over the Eocene flysch formations. There is a slight unconformity between the two. This deposit contains reworked corals of Stampian age and is therefore not older than uppermost Oligocene (Brunn et al. 1971). For a list of the fossils found within these deposits see Pamir (1974). Apart from their derived fossil contents the Oligocene conglomerates can be differentiated from the Eocene conglomerates on the basis of their clast content. The Eocene conglomerates contain more than 90% serpentinised ultrabasic clasts, whereas the Oligocene conglomerates contain more than 90% Mesozoic–Palaezoic clasts. Also the Oligocene conglomerates tend to be more indurated (Pamir 1974). Throughout the study area the Oligocene flysch fines upwards from conglomerates into sandstones and marls. This can be observed by driving eastwards from Çardak to Dazkiri on the road north of Acigol, passing through the eastward tilting Oligocene flysch of the Maymun Mountains. The deposits become progressively finer towards Dazkiri. The Oligocene flysch is locally overlain by parts of the Lycian Nappes.

The final emplacement of the Lycian Nappes over the autochthonous Mesozoic carbonate platform of the Bey Daglari occurred during the Miocene. The Lycian Nappes contain a telescoped sequence of Mesozoic–early Tertiary continental margin sediments (Delaune–Mayere et al. 1977). "Ophiolitic" units of peridotite and mélange are intercalated between the nappes and the western part of the thrust pile is capped by the "Peridotite Nappe", consisting of harzburgites cut by pyroxenite and dolerite dykes (Graciansky 1972). These nappes were transported from the northwest to the southeast, extensively overriding a succession of Burdigalian molasse deposited during the Miocene marine transgression of the Mediterranean (Brunn et al. 1971, Waldron 1984). These Burdigalian molasse deposits occupy a neo–autochthonous position with respect to the Lycian Nappes (Gutnic and Poisson 1970) (i.e. in the west they underlie the Lycian Nappes, whereas in the north, at Isparta Cay, they are

transgressive over the Antalya Nappe unit and its autochthonous basement (Brunn et al. 1971)). The exact time of this final phase of thrusting is post-Langhian or post-late Langhian (Poisson 1984). The Burdigalian marine molasse of southwest Turkey has undergone considerable deformation, hindering an accurate estimate of its thickness. Brunn et al. (1971) suggest a thickness variation of 200 to 2000 metres. In the study area, the molasse sucession is poorly exposed as the outcrop areas are usually forested. However, in forest road cuttings northeast of Kemer, exposures indicate a succession of distal turbidite deposits.

On a more regional scale, the early-middle Miocene saw the closure of the Çüngüs Basin in eastern Turkey, by the collision of the Arabian Plate (with its Atlantic-type passive margin) with the Eurasian Plate, along the Bitlis Suture zone. Continued convergence was taken up in the East Anatolian Accretionary Complex until considerable crustal thickening caused a piece of Turkey (approximately equivalent to the Anatolide-Tauride Platform) to wedge westwards, out of the collision zone, along the North and East Anatolian Faults. The westward motion of this newly formed Anatolian Plate heralded the beginning of the neotectonic period, which is the subject of this thesis.

1.5.2. Causes of Continental Extension

Many authors have noted a time difference during the evolution of an area of continental crust between the cessation of compression and the onset of extension. For example, western North America has had a complex history of compression and extension and when split into smaller areas, the above relationship becomes apparent (Wernicke et al. 1987). Sonder et al. (1987) proposed a model to account for this time difference. They showed that the temperature of the Moho required to allow the strain rates observed in actively extending continental crust (typically about $10^{-16}s^{-1}$) is about 750°C. Using the method of England and Thompson (1984), they worked out the amount of time it takes for thickened continental lithosphere to reach this temperature, as a function of the initial Moho temperature and the vertical compressional strain, f. Their results are shown in Fig.1.3. This shows that a piece of cold lithosphere will take tens of millions of years to extend, whereas hot lithosphere will extend almost immediately following compression.

Extension in western Turkey began in the Tortonian (Sengör et al. 1985),

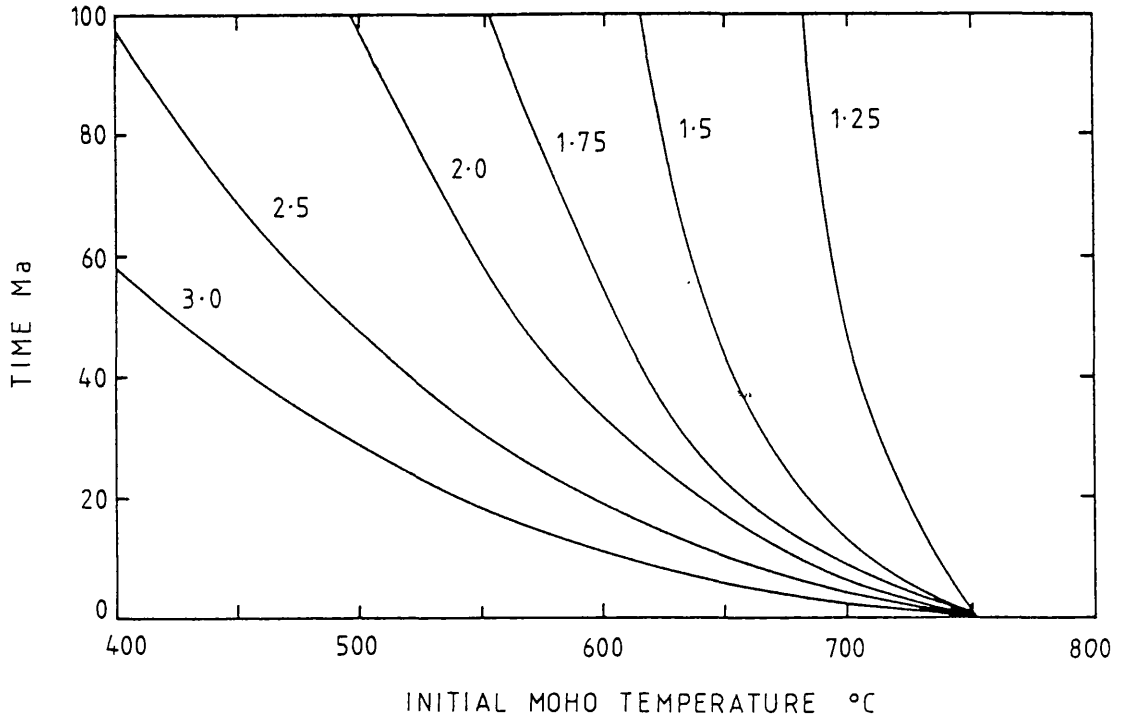

Fig.1.3. Time required for the Moho temperature to reach 750°C, as a function of initial Moho temperature and compressional strain f (f value shown beside each curve). From Sonder et al. (1987).

2-3Ma after the cessation of compression marked by post-late Langhian thrusting in the Lycian Nappes (Poisson 1984). The crust in western Turkey prior to extension probably had a thickness comparable to the present-day thickness of the relatively unstretched Anatolian plateau, believed to be between 40 and 50km (Makris 1976; Makris and Vees 1977; Mindevalli and Mitchell 1989). This compares favourably with a figure of 50km obtained by multiplying the present-day crustal thickness of western Turkey (approximately 35km according to Le Pichon and Angelier (1981)) by a factor of 1.5 to remove post-mid-Miocene extension (Sengör et al. 1985). The development of extension in western Turkey almost immediately after the cessation of compression, in crust initially overthickened by a factor of about 1.5, indicates an initial Moho temperature of 750°C or above (Fig.1.3). Wyllie (1984) showed that the Moho of the overriding plate in a subduction zone has a temperature of about 750°C. Throughout the Tertiary, Neotethyan oceanic crust was subducted beneath what is now western Turkey, so a Moho temperature of 750°C is likely.

The collapsing orogen model of Sonder et al. (1987) can be used to explain the short delay between the cessation of compression and the onset of extension in western Turkey. However, at present the rapidly extending Aegean region has a crustal thickness of only 22-32km (Makris 1976; Makris and Vees 1977). Rollback of the Hellenic subduction zone beneath the Aegean Sea accounts for this continued extension (Dewey 1988).

1.6. REFERENCES.

Ager, D.V. 1988. Mesozoic Turkey as part of Europe. In: Audley-Charles, M.G. and Hallam, A. (eds) Gondwana and Tethys. Special Publication of the Geological Society of London, No.37, p.241-245.

Ardel, A. and de Planhol, X. 1951. Isparta Gölcügü. Istanbul Üniversitesi Fen Fakultesi Mec. B., v.16.

Argyriadis, I., Graciansky, P.C. De., Marcoux, J. and Ricou, L.E. 1980. The opening of the Mesozoic Tethys between Eurasia and Arabia Africa. 26th International Geological Congress, Paris (Mem. B.R.G.M.), v.115, p.199-214.

Bering, D. 1971a. The developement of the Neogene and Quaternary intramontane basins within the Pisidic lake district in S. Anatolia. Newsletter on Stratigraphy, v.1, p.27-32.

Bering, D. 1971b. Lithostratigraphie, tektonische Entwicklung und Seengeschichte der neogenen und quatäran intramontanen Becken der Pisidischen Seenregion (Südanatolien) (Känozoikum und Braunkohlen der Türkei. 5.). Beihefte zum Geolischen Jahrbuch, v.101, 150pp.

Bernoulli, D. and Lemoine, M. 1980. Birth and early evolution of the Tethys: the overall situation. In: Geology of the Alpine Chains born of the Tethys. 26th International Geological Congress, Paris (Mem. B.R.G.M.), v.115, p.168-179.

Brunn, J.H., Dumont, J-F., De Graciansky, P.C., Gutnic, M., Juteau, T., Marcoux, J., Monod, O. and Poisson, A. 1971. Outline of the geology of the western Taurides. In: Campbell, A.S. (ed) Geology and History of Turkey. Petroleum Exploration Society of Libya, Tripoli, p.225-255.

Delaune-Mayere, M., Marcoux, J., Parrot, J-F. and Poisson, A. 1977. Modèle d'évolution Mèsozoique de la paleo-marge téthysienne au niveau des nappes radiolaritiques et ophiolitiques du Taurus Lycien, d'Antalya et du Baer-Bassit. In: Biju-Duval, B. and Montadert, L. (eds). Structural History of the Mediterranean Basins. Paris, p.79-94.

Dewey, J.F. 1988. Extensional collapse of orogens. Tectonics, v.7, p.1123-1139.

Dumont, J-F., Uysal, S., and Monod, O. 1980. La série de Zindan: un élément de liason entre plate-forme et bassin à l'oest d'Isparta (Taurides ocidentales, Turquie). Société Géologique de France Bulletin, v.22, p.225-232.

England, P.C. and Thompson, A.B. 1984. Pressure-temperature-time paths of regional metamorphism I. Heat transfer during the evolution of regions of thickened continental crust. Journal of Petrology, v.25, p.894-928..

Erol, O. 1975. Quaternary deposits of the Burdur Lake Basin. Congress of Earth Sciences 50th Anniversary of the Turkish Republic, Ankara, p.386-391.

Görür, N., Oktay, F.Y., Seymen, I. and Sengör, A.M.C. 1984. Palaeo-tectonic evolution of the Tuzgölü basin complex, Central Turkey: sedimentary record of a Neo-Tethyan closure. In: Dixon, J.E. and Robertson, A.H.F. (eds) The Geological Evolution of the Eastern Mediterranean. Special Publication of the Geological Society of London, No.17, p.467-482.

Graciansky, P.C. De. 1972. Recherches géologiques dans le Taurus Lycien Occidental. Unpublished Ph.D. thesis, Université de Paris-Sud, 571pp.

Gutnic, M. and Poisson, A. 1970. Un dispositif remarquable des chaines tauriques dans le sud de la courbure d'Isparta. Comptes Rendus Académie des Sciences Paris, v.270, p.672-675.

Hayward, A.B. 1984. Miocene clastic sedimentation related to the emplacement of the Lycian Nappes and the Antalya Complex, SW Turkey. In: Dixon, J.E. and Robertson, A.H.F. (eds) The Geological Evolution of the Eastern Mediterranean. Special Publication of the Geological Society of London, No.17, p.287-300.

Hayward, A.B. and Robertson, A.H.F. 1982. Direction of ophiolite emplacement inferred from Cretaceous and Tertiary sediments of an

adjacent autochthon, the Bey Daglari, southwest Turkey. Bulletin of the Geological Society of America, v.93, p.68-75.

Karaman, M.E. 1986a. Burdur Dolayinin Genel Stratigrafisi. Akdeniz Üniversitesi Isparta Mühendislik Fakültesi Dergisi, v.2, p.23-36.

Karaman, M.E. 1986b. Burdur ili ve çevresindeki yerlesim alanlarinin depremselligi. Mühendislik Jeolojisi Bülteni, No.8, p.23-30.

Karamata, S. 1980. Tethyan ophiolites: a short review and the main problems. In: Panayiotou, A. (ed) Ophiolites. Proceedings of the International Ophiolite Symposium, Cyprus 1979. Geological Survey of Cyprus, Nicosia, p.257-260.

Koçyigit, A. 1984. Güneybati Turkiye ve Yakin dolayinda levha içi yeni tektonik gelisim. Turkiye Jeoloji Kurumu Bülteni, v.27, p.1-16.

Kröner, A. 1984. Late Precambrian plate tectonics and orogeny: a need to redefine the term Pan-African. In: Klerkx, J. and Michot, J. (eds) African geology, Musée royal de l'Afrique centrale, Tervuren, p.23-28.

Lahn, E. 1946. Les depots pliocenes et quaternaires de la region de Konya-Burdur. Istanbul Üniversitesi Fen Fakultesi Mem. B., v.11, p.85-106.

Le Pichon, X. and Angelier, J. 1981. The Aegean Sea. Philosophical Transactions of the Royal Society of London, A300, p.357-372.

Lefèvre, C., Bellon, H. and Poisson, A. 1983. Présence de leucitites dans le volcanisme pliocène de la région d'Isparta (Taurides occidentales, Turquie). Comptes Rendus Académie des Sciences Paris, v.297(II-10), p.369-372.

Makrees, J. 1976. A dynamic model of the Hellenic arc deduced from geophysical data. Tectonophysics, v.36, p.339-346.

Makrees, J. and Vees, R. 1977. Crustal structure of the central Aegean Sea and the islands of Evvia and Crete, Greece, obtained from refraction seismic experiments. Journal of Geophysics, v.42,

p.329-341.

Mindevalli, O.Y. and Mitchell, B.J. 1989. Crustal structure and anisotropy in Turkey from seismic surface wave dispersion. Geophysical Journal International, v.98, p.93-106.

Monod, O. 1976. La "courbure d'Isparta": une mosaique de blocs autochtones surmontés de nappes composités à la jonction de l'arc hellénique et de l'arc taurique. Société Géologique de France Bulletin, v.18, p.521-532.

Neumayr, M. 1885. Die geographische Verbreitung der Juraformation. Denkschriften der kaiserlichen und königlichen Akademie der Wissenschaften zu Wien, mathematisch-naturwissenschaftliche Classe, v.15, p.57-114.

Oktay, F.Y. 1973. Sedimentary and tectonic history of the Ulukisla area, southern Turkey. Unpubl. Ph.D. thesis. University College, London, 414pp.

Özgül, N. 1984. Stratigraphy and tectonic evolution of the Central Taurides. In: Tekeli, O. and Göncüoglu, C. (eds) Geology of the Taurus Belt. Maden Tetkik ve Arama Enstitüsü, Ankara, p.77-90.

Özgül, N. 1985. Alanya tektonik penceresi ve bati kesiminin jeolojisi. Ketin Simpozyumu Kitabi, Türk. Jeol. Kur., Ankara, p.97-120.

Pamir, H.N. 1974. Explanatory text of the geological map of Turkey. Maden Tetkik ve Arama Enstitüsü, Ankara, 83pp.

Pearce, J.A. 1980. Geochemical evidence for the genesis and eruptive setting of lavas from Tethyan ophiolites. In: Panayiotou, A. (ed) Ophiolites. Proceedings of the International Ophiolite Symposium, Cyprus 1979. Geological Survey of Cyprus, Nicosia, p.261-271.

Penck, W. 1918. Die tektonische Grundzüge Westkleinasiens, Stuttgart.

Planhol, X de. 1956. Contribution àl'Etude Géomorphologique du Taurus occidental et de ses plaines bordières, Revue Géogr. Alpine, v.44, p.1-86.

Ricou, L.E. 1971. Le croissant ophiolitique périarabe, une ceinture de nappes mises en place au Crétacé superieur. Rev. Geogr. phys. Geol. Dynam., v.18, p.327-349.

Ricou, L.E., Argyriadis, I. and Lefèvre, R. 1974. Proposition d'une origine interne pour les nappes d'Antalya et le massif d'Alanya (Taurides occidentales, Turquie). Société Géologique de France Bulletin, v.16, p.107-111.

Ricou, L.E., Argyriadis, I. and Marcoux, J. 1975. L'Axe Calcaire du Taurus, un alignement de fenètres arabo-africaines sous des nappes radiolaritiques, ophiolitiques et metamorphiques. Société Géologique de France Bulletin, v.17, p.1024-1043.

Ricou, L.E., Marcoux, J. and Poisson, A. 1979. L'allochtonie des Bey Daglari orientaux. Reconstruction palinspastique des Taurides occidentales. Société Géologique de France Bulletin, v.21, p.125-133.

Ricou, L.E., Marcoux, J. and Whitechurch, H. 1984. The Mesozoic organization of the Taurides: one or several ocean basins? In: Dixon, J.E. and Robertson, A.H.F. (eds) The Geological Evolution of the Eastern Mediterranean. Special Publication of the Geological Society of London, No.17, p.349-360.

Sengör, A.M.C. 1979. Mid-Mesozoic closure of Permo-Triassic Tethys and its implications. Nature, v.279, p.590-593.

Sengör, A.M.C. 1984. The Cimmeride orogenic system and the tectonics of Eurasia. Special Paper of the Geological Society of America, No.195, 85pp.

Sengör, A.M.C. 1985. The story of Tethys: How many wives did Okeanos have? Episodes, v.8, p.3-12.

Sengör, A.M.C., Altiner, D., Cin, A., Ustaömer, T. and Hsü, K.J. 1988. Origin and assembly of the Tethyside orogenic collage at the expense of Gondwana Land. In: Audley-Charles, M.G. and Hallam, A. (eds) Gondwana and Tethys. Special Publication of the Geological Society of London, No.37, p.119-181.

Sengör, A.M.C., Görür, N. and Saroglu, F. 1985. Strike-slip deformation faulting and related basin formation in zones of tectonic escape: Turkey as a case study. In: Biddle, K.T. and Christie-Blick, N. (eds) Strike-slip Deformation, Basin Formation and Sedimentation. Special Publication of the Society of Economic Paleontologists and Mineralogists, No.37, p.227-264.

Sengör, A.M.C. and Yilmaz, Y. 1981. Tethyan evolution of Turkey: a plate tectonic approach. Tectonophysics, v.75, p.181-241.

Sengör, A.M.C., Yilmaz, Y. and Sungurlu, O. 1984. Tectonics of the Mediterranean Cimmerides: nature and evolution of the western termination of Palaeo-Tethys. In: Dixon, J.E. and Robertson, A.H.F. (eds) The Geological Evolution of the Eastern Mediterranean. Special Publication of the Geological Society of London, No.17, p.77-112.

Seymen, I. 1981. Stratigraphy and metamorphism of the Kirsehir massif around Kaman (Kirsehir, Turkey). Bulletin of the Geological Society of Turkey, v.24, p.101-108.

Seymen, I. 1982. Geology of the Kirsehir Massif in the neighbourhood of Kaman. Upublished thesis. Istanbul Teknik Üniversitesi, 164pp.

Smith, A.G. and Woodcock, N.H. 1976. Emplacement model for some "Tethyan" ophiolites. Geology, v.4, p.653-656.

Sonder, L.J., England, P.C., Wernicke, B.P. and Christiansen, R.L. 1987. A physical model for Cenozoic extension of western North America. In: Coward, M.P., Dewey, J.F. and Hancock, P.L. (eds) Continental Extensional Tectonics. Special Publication of the Geological Society of London, No.28, p.187-201.

Suess, E. 1893. Are great ocean depths permanent? Natural Science, v.2, p.180-187.

Waldron, J.W.F. 1984. Structural history of the Antalya Complex in the "Isparta Angle", Southwest Turkey. In: Dixon, J.E. and Robertson, A.H.F. (eds) The Geological Evolution of the Eastern Mediterranean. Special Publication of the Geological Society of London, No.17, p.273-286.

Wedding, H. 1966. Burdurun güneyindeki Kömür zuhurlari. Die Kohlenvorkommen südlich Burdur. M.T.A. Report (unpublished), Ankara.

Wedding, H. and Inque, E. 1967. Report on the lignite bearing Pliocene strata around Burdur city. M.T.A. Report 1-11 (unpublished), Ankara.

Wernicke, B.P., Chritiansen, R.L., England, P.C. and Sonder, L.J. 1987. Tectonomagmatic evolution of Cenozoic extension in the North American Cordillera. In: Coward, M.P., Dewey, J.F. and Hancock, P.L. (eds) Continental Extensional Tectonics. Special Publication of the Geological Society of London, No.28, p.203-221.

Whitechurch, H., Juteau, T. and Montigny, R. 1984. Role of the Eastern Mediterranean ophiolites (Turkey, Syria, Cyprus) in the history of the Neo-Tethys. In: Dixon, J.E. and Robertson, A.H.F. (eds) The Geological Evolution of the Eastern Mediterranean. Special Publication of the Geological Society of London, No.17, p.301-318.

Windley, B.F. 1982. The Evolving Continents. Wiley, 399pp.

Wyllie, P.J. 1984. Constraints imposed by experimental petrology on possible and impossible magma sources and products. Philosophical Transactions of the Royal Society of London, A310, p.439-456.

CHAPTER TWO

STRATIGRAPHY OF THE BURDUR FORMATION, SW TURKEY.

2.1. INTRODUCTION

This chapter describes more fully a revised stratigraphy of the Burdur Formation put forward by Price and Scott (1989). This revision takes into account studies on the geometry of the Burdur Formation and on its sedimentology. The revised lithostratigraphy is discussed in the light of these new findings.

The Burdur Formation is well-exposed and outcrops in a broad zone about 10km wide between the towns of Burdur and Tefenni (see enclosures 1 and 2). The succession was deposited in a northeast-southwest trending half-graben, which formed as a result of crustal extension during the Neogene. The basinal system in which the Burdur Formation was deposited is still actively evolving (Erinç et al. 1971, Karaman 1986a) and the excellent exposure of the formation is a result of uplift on the footwall of faults, which control the geometry of the present-day Burdur and Tefenni basins to the northwest (see Chapter 5).

The Burdur Formation has been described by various authors in the past. Wedding (1966) was the first to study the Neogene of the Burdur region in any detail, proposing the first lithostratigraphic sub-divisions. Wedding and Inque (1967) stated that its deposition occurred mainly after the Miocene and continued until the end of the Pliocene. A program of lignite prospecting by German geologists during the period 1966-67 produced much new lithostratigraphic (Becker-Platen 1971) and biostratigraphic (Benda 1971, Bering 1971a) data for the region. Bering (1971b) published the main biostratigraphical results of this study. He also produced a geological map of the region, which, although showing little structural detail, gives a clear indication of the spatial distribution of the main facies units. The more detailed map published by Karaman (1986b) is of a smaller area but indicates the structural complexity of the region. In his paper he proposed a general stratigraphy of the Burdur region from the Lutetian (Middle Eocene) through to the Holocene. The importance of the relationship of geomorphology to the neotectonic development of the Burdur region has been recognised by several authors, most notably in the

works of Erol (e.g. Erol 1975, 1978, 1981) and in a detailed geomorphological description of the Burdur region by Sungur (1978).

2.2. DEFINITION OF STRATIGRAPHIC UNITS.

The Burdur Formation is defined as the unit comprising the basinal and volcanic successions of the Burdur region, which postdate the youngest basement lithologies (early Miocene turbidites near Kemer) and predate the travertines at Yakaköy. It unconformably overlies (and is faulted against) the former and is unconformably overlain by the latter (Fig.2.1, Plate 2.1a).

Individual members within the Burdur Formation are structurally and sedimentologically identifiable lithological units. They are defined in terms of the sedimentary facies associations which they contain and the unconformable boundaries which locally separate them. Individual sedimentary facies associations are described in Chapter 3. Members are not defined on exclusive "suites" of facies associations; such a definition would require the Burdur Formation to be split into an unrealistically large number of members. However, each member is dominated by a single sedimentary facies association. 5 members in all are defined in this study; 3 forming a central basinal succession deposited within a subsiding tectonically-controlled basin and 2 forming a volcanic succession which overlaps the basin margin at the NE end of the basin. Fig.2.1 shows the schematic stratigraphic relationships between the members, which are defined and described fully in section 5.

2.3. GEOMETRY OF THE BURDUR FORMATION

In any stratigraphical consideration of a sedimentary body its 3-dimensional geometry must be taken into account. A series of traverses across the exposed formation working up through the stratigraphy is not sufficient to elucidate lateral facies variations which occur in the subsurface. A traverse from NW to SE across the Burdur Formation passes initially through a fluvially dominated unit (the Çendik Member) followed by a dominantly lacustrine unit (the Akdere Member) and finally through another fluvially dominated unit (the Günalan Member) (see enclosure 1). Noting the regional shallow southeast dip of the formation (a result of

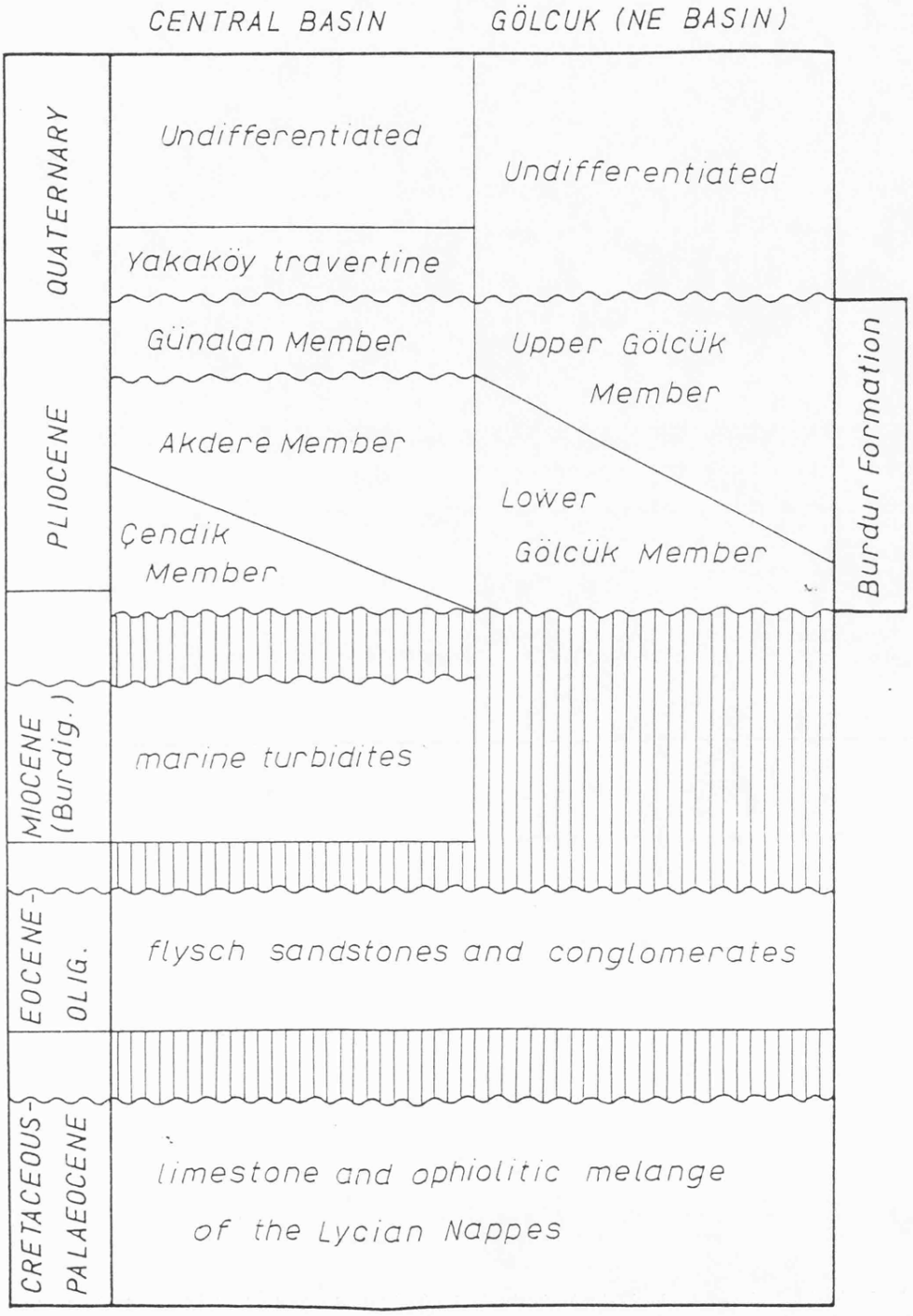

Fig.2.1. Stratigraphic units of the Burdur region.

progressive rotations on basement faults) the assumption could be made that the stratigraphy has a simple layer-cake geometry, in which a lacustrine layer is sandwiched between two fluvial layers. Summary stratigraphic logs of the Burdur Formation (Fig.2.2a) display just such a relationship. Although showing, quite correctly, the stratigraphic relationships between the various members as deduced in the field, such logs cannot be used to interpret the subsurface geometry of the formation. Other lines of evidence, which need to be taken into account are those which can be used to elucidate the shape of the body as a whole at depth (geophysical and structural field data) and those which can be used to delineate individual facies associations at depth. If available, borehole and high resolution seismic data is ideal for investigating the latter. If not sedimentological evidence such as facies characteristics and palaeocurrent data can be used. The following discussion outlines the subsurface geometry of the Burdur Formation and its individual members using such evidence.

2.3.1. The whole formation

There is considerable structural field evidence in the Burdur region to suggest that the Burdur Formation was deposited in a half-graben, which was active throughout most of the Pliocene. This is discussed in more detail in Chapter 5. The basement faults controlling this half-graben were located on the southeast side of the basin and dipped to the northwest. Towards the end of the Pliocene these faults became inactive and were buried by the basinal succession. They can still be observed in places where erosion has cut down into them, such as at Soganli (TG575625).

A seismic line from the southern end of the Burdur basin stretching from near Soganli (TG375682) in the northwest to near Karacaören (TG515557) in the southeast, crosses the entire uplifted Burdur Formation and the adjacent Quaternary basin. Several southeast dipping reflectors can clearly be seen within the uplifted Burdur Formation, which is seen to have a thickness of about 1100m against the syn-depositional basement fault (see Chapter 5; Plate 5.4 and Fig.5.7). Although no borehole data has been made available, gravity modelling of this line indicates the presence of a somewhat thinned prism of probable Pliocene sediment beneath the Quaternary basin (Chapter 5 and Fig.2.3).

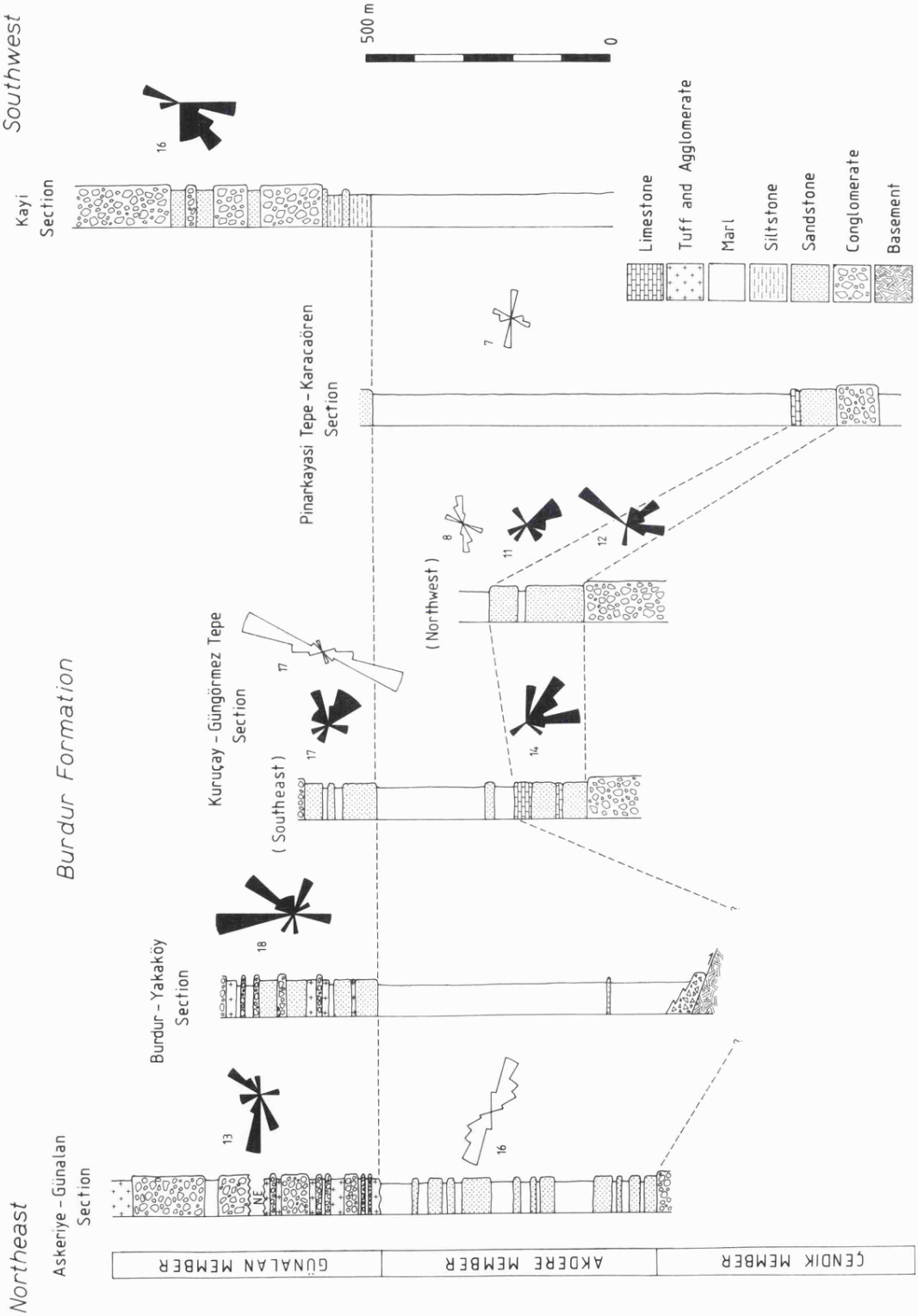

Fig.2.2a. Summary stratigraphic logs of the Burdur Formation. Each log was produced by traversing southeastwards across the Burdur Formation outcrop into progressively younger strata. Place names are indicated in enclosure 1.

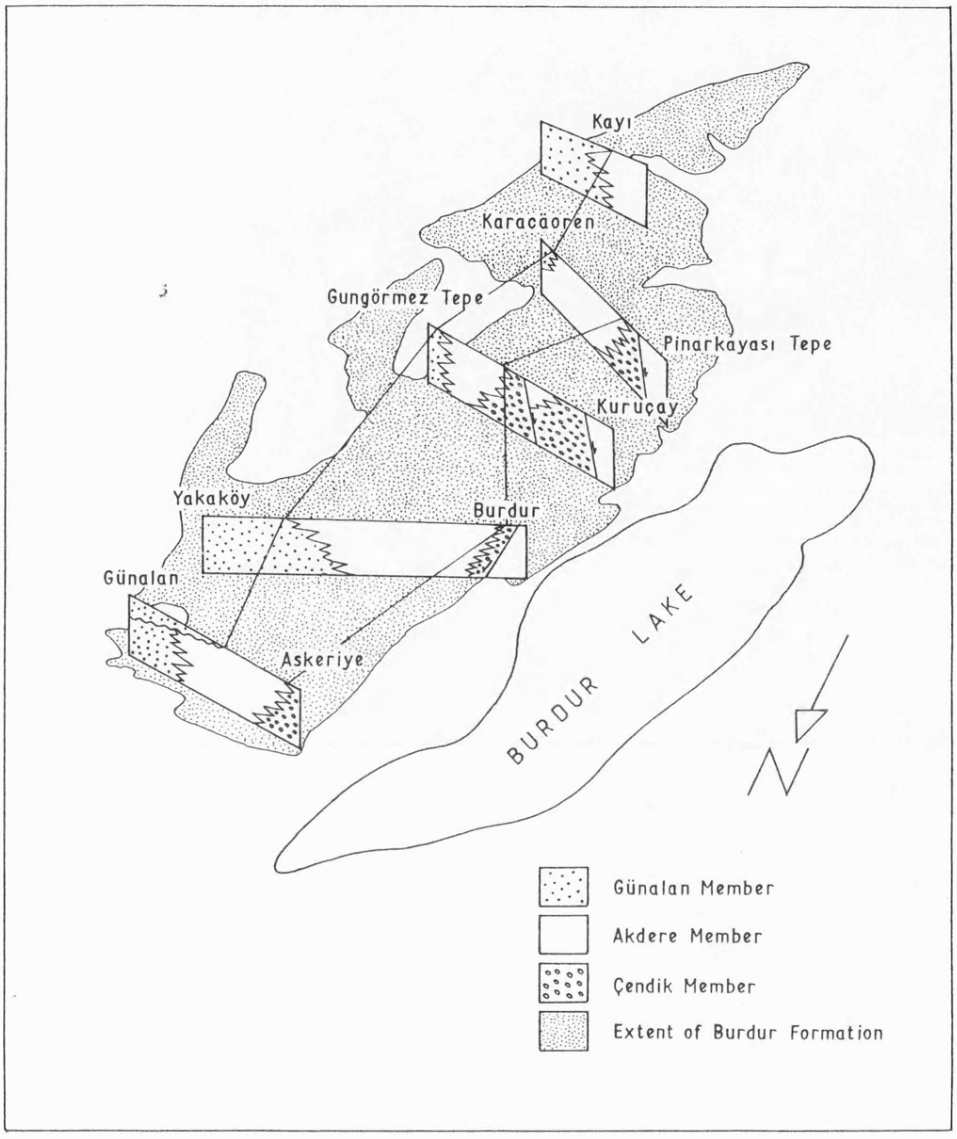

Fig.2.2b. Fence diagram showing the approximate geographical distribution of the summary stratigraphic logs shown in Fig.2.2a.

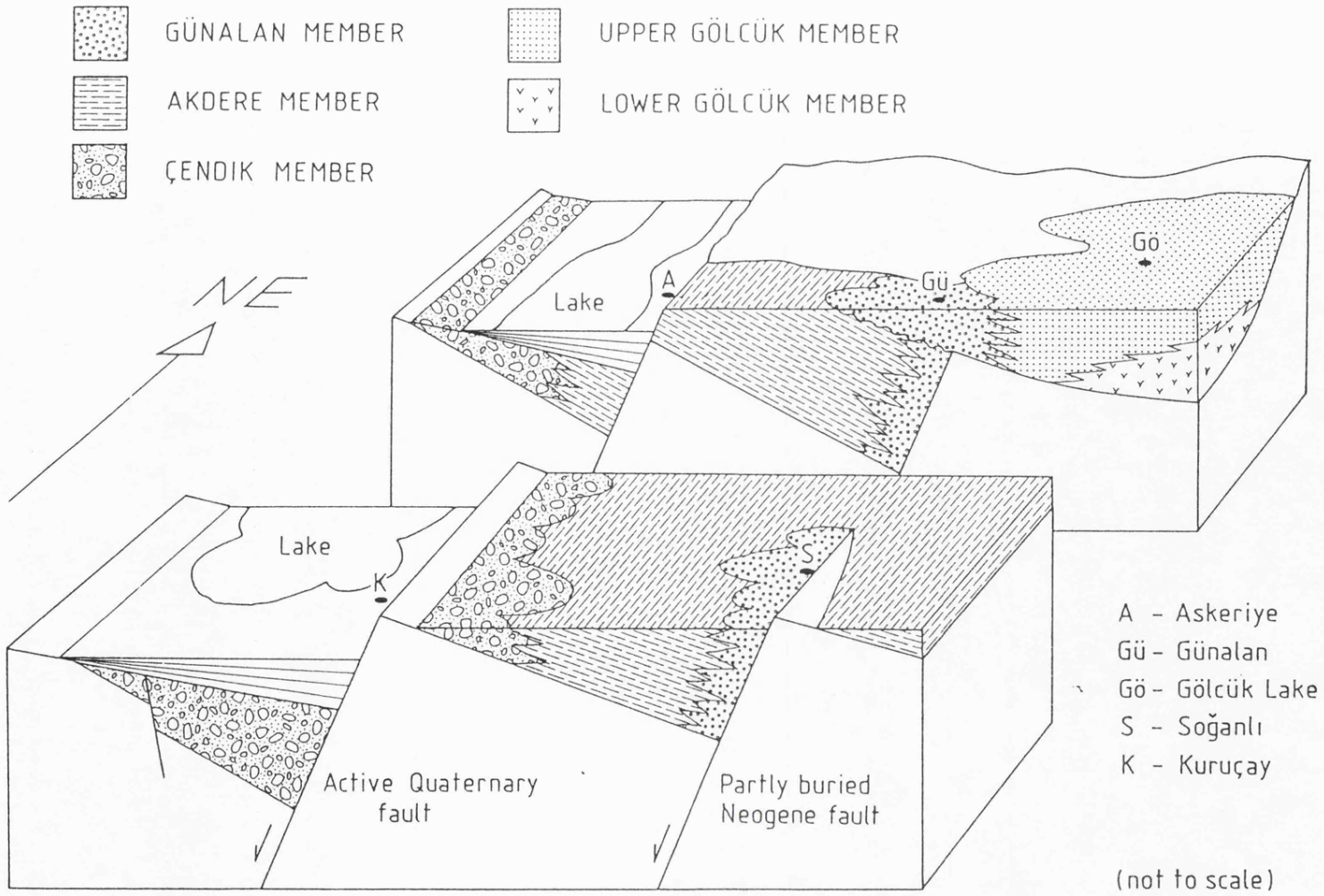

Fig.2.3. Cartoon showing the geometry of individual members of the Burdur Formation.

Geophysical and structural field data therefore indicate that the Burdur Formation was deposited in a half-graben controlled by a system of northwest dipping basement faults.

2.3.2. The individual members.

The geological map of the Burdur region (see enclosure 1) shows the spatial distribution of the individual members of the Burdur Formation. There is a clear spatial relationship between the 3 members which make up the central basinal succession. Ignoring the positions of the Burdur and Tefenni Quaternary basins (which have buried much of the earlier Burdur Formation) a northeast-southwest trend to the central basinal succession is apparent. The succession outcrops from Keçiborlu in the northeast to Tefenni in the southwest and each member forms a narrow strip along the strike length of the outcrop; the Çendik Member to the northwest (mainly exposed on the northwest side of the Quaternary basins), the Akdere Member in the centre and the Günalan Member to the southeast.

(a) Çendik Member.

The Çendik Member, as already mentioned, is dominated by fluvially deposited sediments. These sediments are characterized by laterally discontinuous alluvial fan deposits (see Chapter 3). At many localities there is a rapid transition from proximal to distal fan deposits. The Çendik Member, therefore, is unlikely to have a planar sheet geometry across the whole basin but to be the result of sedimentation on large alluvial fans. The outcrop of the Çendik Member is to the northwest, furthest from the basin-controlling fault. It is, therefore, most likely that this member was deposited on hanging wall slope alluvial fans. Palaeocurrent data from the Çendik Member (Fig.2.2a) substantiates this view, with the dominant current direction to the southeast into the basin and perpendicular to its axis.

(b) Akdere Member.

The Akdere Member is dominated by lacustrine sediments, which represent a mid-basin lateral facies change from the fan sediments, which form the basin margin Çendik and Günalan Members.

(c) Günalan Member.

The geometry of the Günalan Member is a little more problematic. It outcrops in the southeast adjacent to, and covering, the basin-controlling fault system (see enclosure 1). Price and Scott (1989) showed it to have been deposited by footwall-sourced alluvial fans and fan deltas. This is certainly the case where the member abuts the basin-controlling fault such as at Soganli (TG375682). Here fan delta deposits pass laterally into lacustrine deposits about 400m away from the edge of the basin. These sediments are shown on the Kuruçay-Güngörmez Tepe section in Fig.2.2.

The overall situation with the Çendik Member being deposited on hanging wall cones, the Günalan Member on footwall-sourced fans and the Akdere Member within a lake at the centre of the basin is similar to the Tectono-Sedimentary Facies Model A of Leeder and Gawthorpe (1987). However, the Günalan Member at the northern end of the basin has a rather different geometry. Here it is separated from the Akdere Member by an angular unconformity (Plate 2.1b) and contains abundant tuff and agglomerate units, which are rare in the lacustrine Akdere Member sediments beneath the unconformity (see, for example, Fig.2.7). The outcrop width of the member increases substantially to about 5km in this region (see enclosure 1). The reason for this unconformity and the sudden change from lacustrine to alluvial sedimentation was the beginning of the break up of the Neogene basinal succession into the basin geometry seen today. This break up occurred when the basin-controlling fault migrated in to the hanging wall. A possible reason for this is outlined in Chapter 7 (section 4.). Associated with this change in tectonics was a change in volcanism at the Gölcük volcanic centre from andesite lava flows (the Lower Gölcük Member) to volcaniclastic air fall agglomerate and base surge deposition (the Upper Gölcük Member). Within the basin most of the Burdur Formation became uplifted in the footwall of the newly formed fault and rapid erosion occurred, producing a wide braidplain, on which the Günalan Member was deposited. Palaeocurrents from the Günalan Member at the northern end of the basin (the Askeriye-Günalan and Burdur-Yakaköy section on Fig.2.2) are polymodal, possibly indicating relatively high sinuosity streams. The central part of the basin was still subsiding at this time as there is no unconformity between the Akdere and Günalan Members.

In the southwest the Günalan Member is thicker and has a wide outcrop (see enclosure 1 and Kayi section on Fig.2.2). Here palaeocurrents show

flow to the southwest, parallel to the basin. This axial flow is probably the result of fans being sourced in the relay structures between en echelon basement faults as described by Leeder et al. (1988). A southwest-facing slope would form in the relay structure between faults stepping to the left. This fits with the outcrop pattern of the edge of the Günalan Member, which also steps to the left and presumably approximates to the deeper structure (see enclosure 1).

2.4. DATING THE BURDUR FORMATION

2.4.1. Biostratigraphy.

Being deposited in an isolated continental intramontane basin, the Burdur Formation cannot accurately be dated using invertebrate fossils. Although pollen and ostracode zones have been established for the Neogene of Turkey (i.e. Benda 1971), they are not sufficiently reliable for accurate dating. Correlations cannot be made between the Anatolian Neogene continental successions and the well established Paratethyan and Mediterranean successions to the northwest and southwest respectively. As already mentioned, the Burdur Formation comprises a central basinal fluvio-lacustrine succession and a volcanic succession at the northeast end of the basin (Fig.2.1). The central basinal succession contains an abundant low-diversity freshwater ostracode fauna. Bering (1971b) gives a summary of biostratigraphic ages deduced for various horizons of the Burdur Formation at various localities from this fauna. He concludes that deposition began in the Burdur region in the Lower Pliocene and continued until Upper Pliocene-Lower Pleistocene times. He also states that the Burdur Formation is diachronous and becomes progressively younger to the southwest, where a considerable thickness of the succession is Pleistocene in age. Karaman (1986b) states that palynomorphs from lignite horizons within the Burdur Formation indicate a Pliocene age to the succession.

Ostracode-bearing horizons from the Burdur Formation sampled during this study were examined by Nuran Gökçen at Dokuz Eylül University, Izmir. The sample numbers are shown on the relevant stratigraphic logs and a full list of identified species given in Appendix 1. The following ostracode species are believed to be of Upper Miocene (Pontian) age (Gökçen pers.comm.):

Cyprideis seminulum (REUSS, 1850)
Cyprideis pontica KRSTIC, 1970
Candona (Pontoniella) loczyi (ZALANYI, 1929)
Candona (Pontoniella) acuminata (ZALANYI, 1929)
Candona (Caspiocypris) erzerumensis FREELS, 1980
Candona (?) namanganica (SNEJDER, 1959)
Candona (Typhlocypris) fossulata POKORNY, 1952

The onset of sedimentation of the Burdur Formation may, therefore, have began in the Pontian earlier, than previously thought. However, because of the facies dependency and longevity of Neogene freshwater ostracode species from Turkey, this new age estimate is speculative. This uncertainty is highlighted by the fact that the travertine, which unconformably overlies the Burdur Formation and is of Upper Pliocene / Lower Quaternary age (see below), contains both Candona (Pontoniella) acuminata and Candona (Pontoniella) loczyi.

Vertebrate fossil remains were found and provide potentially useful biostratigraphic indicators. These were, however, expropriated by the museum curatorial staff at Burdur. One sample, collected from a lignite seam at Kemer (TG424406), was identified by Alan Gentry at the British Museum (Natural History) as the astragalus (talus) from the hind foot of a pecoran ruminant. Gentry (pers.comm.) believes the bone belonged to a Miocene giraffid or a deer of later age, with the former being more likely. Identification of molar and premolar teeth will provide a more definite identification. The following localities, to which the reader is directed, yielded mammalian vertebrate remains;

Kemer lignite seams (TG424406)
Tuffs and agglomerates at TG654756
Tuffaceous sandstones directly below the 16m thick air fall tuff near Yakaköy (TG669759)

The cessation of sedimentation of the Burdur Formation is less well constrained. Deposition was interrupted when the subsiding basin was broken up by faults which controlled (and are still controlling) the Quaternary Burdur basin. This caused uplift of the thickest part of the Burdur Formation on the footwalls of these faults and subsidence of the shallower part of the half-graben prism of sediment in their hanging walls (Fig.2.3). Bering (1971a, 1971b) believed the downfaulting of the

present lake basins to have occurred towards the end of the Lower Pleistocene. Wedding and Inque (1967) place their upper pebble member (the Günalan Member of this study) in the Upper Pliocene and the unconformably overlying travertines (Fig.2.1) at the base of the Pleistocene. According to de Planhol (1956), however, the faulting occurred after the last Würm Glacial, based on a dating of floras within the travertine deposit near the village of Yakaköy on the Burdur-Antalya road. However, Erol (1978) states that the travertine at this locality is the youngest of a series of travertines deposited from the Upper Pliocene onwards and therefore this date is an underestimate. From a study of the erosional surfaces in the region he concludes that the formation of the Quaternary basin and hence the cessation of sedimentation of the Burdur Formation was due to several stages of tectonism, which occurred over a relatively long interval covering the main parts of the Upper Pliocene and Lower Pleistocene (Erol 1978). This latter interpretation, in which the subsidence of the Quaternary basin began in the Upper Pliocene is more likely as the boundary between the p_3 and p_4 horizons of Wedding (1966) (the Akdere and Günalan Members of this study) is unconformable in places.

2.4.2. Chronostratigraphy.

The volcanic succession consists of a 150m thickness of trachyandesitic lava flows and trachytic ignimbrites (the Lower Gölcük Member) overlain by approximately the same thickness of volcaniclastic surge and fall deposits (the Upper Gölcük Member). The Upper Gölcük Member interfingers with the upper part of the central basinal succession (exposed as the Günalan Member) (Fig.2.1, Plate 2.1c). It is therefore not unreasonable to assume that the Lower Gölcük Member is synchronous with the lower part of the central basinal succession as there would appear to be some connection between the onset of basin subsidence and volcanism. Indeed, volcanism in the Gölcük region was controlled by extensional faults (Lefèvre et al. 1983). (Wernicke et al. (1987) show that intraplate volcanism in much of the North American Cordillera was synchronous with the onset of extension). Lefèvre et al. (1983) published K-Ar radiometric dates of 4.0 to 4.6 Ma (Lower Pliocene) for the Lower Gölcük Member based on whole rock analyses of ignimbrite flows and lavas in the Isparta region. K-Ar dating of biotites from lavas at the volcanic centre (Gölcük Lake) were undertaken in this study. These are the oldest lavas from this centre (the regional dip is away from it) and can be seen to rest upon

basement limestones at the caldera edge. They give an age of 4.6Ma ± 0.2 Ma.

It would therefore appear that basin subsidence and deposition of the Burdur Formation began at the start of the Pliocene in the Burdur region.

2.5. A REVISED LITHOSTRATIGRAPHY

The most important lithostratigraphical studies concerning the Neogene sediments in the Burdur region, which have been undertaken in the past are those of Wedding (1966), Wedding and Inque (1967), Bering (1971b) and Karaman (1986b). The revised version of these earlier studies, presented here, follows guidelines set by the Stratigraphy Committee of the Geological Society of London (1978). The Burdur Formation comprises a central basinal succession and a volcanic succession in the northeast (see enclosure 1). The former is entirely sub-divided into 3 stratigraphical members, the latter into 2 as shown in Fig.2.1. The 5 lithostratigraphical members are described below. Their relationships to the eleven facies associations, which are described in Chapter 3 are also given. Fig.2.3 shows the relationships between the individual members of the Burdur Formation and the localities of the type sections is shown in Fig.2.4. The type locality given for each member is a location at which there is good exposure of a section, which is representative of the member as a whole. Due to the large stratigraphical thicknesses of the members, it is not always possible to give a single location for each member at which its upper and lower contacts are exposed. Wherever possible, the localities, at which such contacts can be observed, are given.

2.5.1. Central Basinal Succession

(a) Çendik Member

Outcrop Pattern This member outcrops along the northwestern edge of the Burdur Formation. It can be found to the northwest and the southeast of the present day Burdur-Tefenni basin system, stretching from Keçiborlu to Tefenni.

Type Locality The type locality for the Çendik Member is 1km

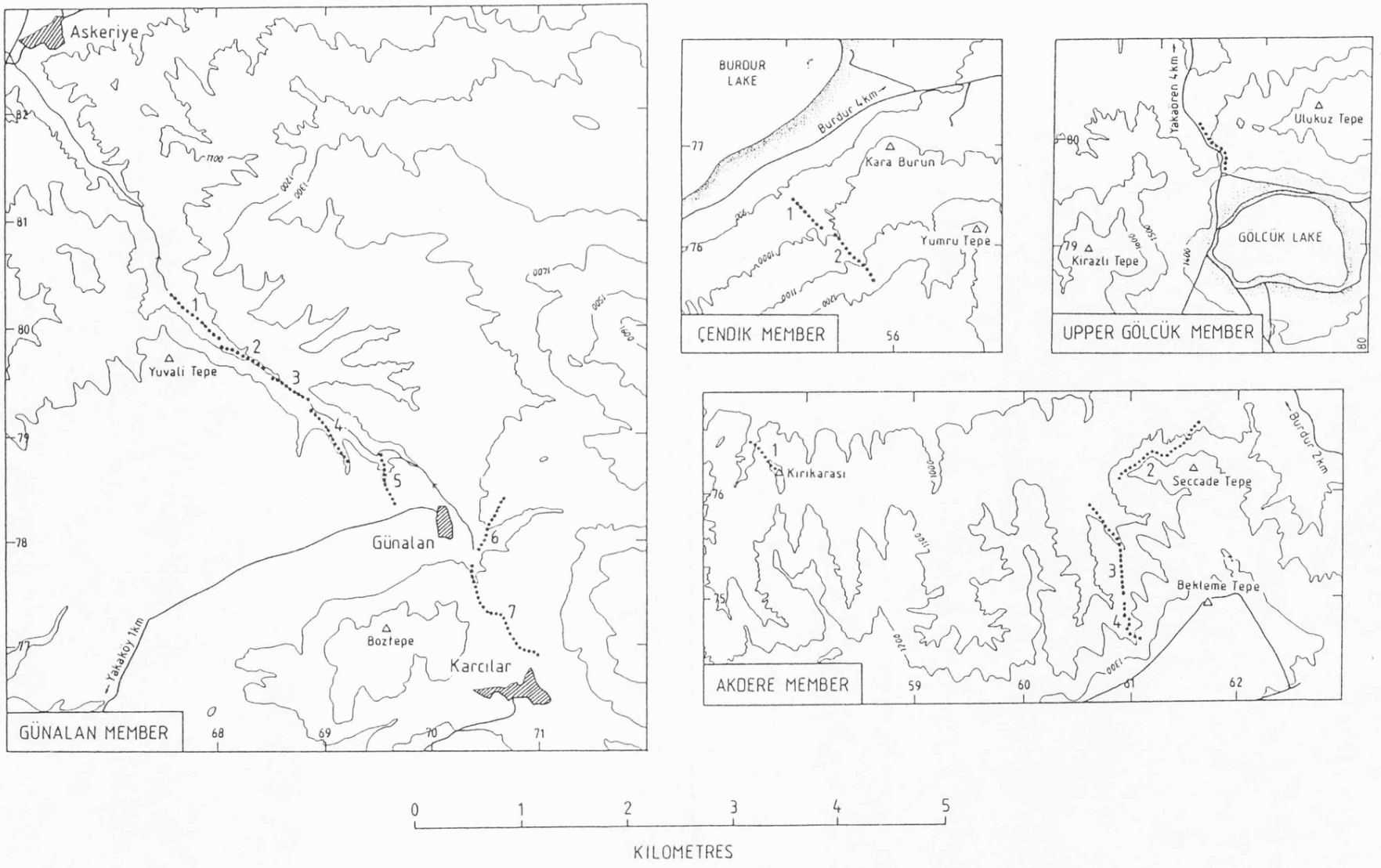

Fig.2.4. Maps showing where the type localities of individual members of the Burdur Formation are situated. These are dotted. Numbers become higher in progressively younger sections. The grids refer to the standard Turkish grid reference system. (For grid references prefix TG).

LITHOLOGY


clast-supported conglomerate


matrix-supported conglomerate


sandstone


siltstone / mudstone


organic-rich marl


organic-poor marl


limestone


dolomite


breccia


volcanic tuff / agglomerate


lignite

SEDIMENTARY STRUCTURES


planar cross-bedding


trough cross-bedding


symmetrical ripples


parallel lamination


ripple lamination


desiccation cracks


volcanic bomb sags

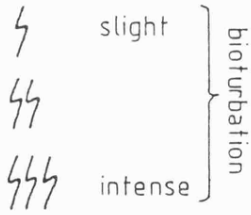

Bed Contacts:

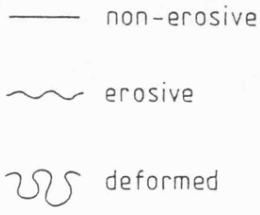

FOSSILS


plant fragments


planispiral gastropods


helical gastropods


ostracodes


rootlets


burrows

OTHERS


gypsum nodules


lenticular chert

EXPLANATION OF TYPE LOCALITIES

southwest of Kara Burun near to Çendik beach. The type section starts at the unconformity above basement serpentinite (TG551764) and the contact with the Akdere Member occurs near the topmost erosion surface (D_{III} after Erol (1981)). There are approximately 20m missing from the section at this locality, but the section is resumed at TG558755 (Fig.2.5).

Thickness

At the type locality the member is 140m thick. The thickness varies across the basin from 0m to more than 170m. The maximum thickness occurs in the Kuruçay region (Fig.2.2a), where a thick succession of alluvial conglomerate and siltstone is overlain by cross-bedded fan delta sandstones. The base of the member is not exposed in this region. There is no trend in thickness variation as the member covers an irregular basement topography and is thicker in palaeovalleys. These palaeovalleys are often preserved as topographic features to the present day, such as the valley north of Karamanli, which contains alluvial Çendik Member sediments resting directly upon basement serpentinite (Plate 2.2a). The member is absent where the margin of the palaeolake is coincident with the edge of the basin and no alluvial plain is developed.

Sedimentary Facies

The Çendik Member is dominated by conglomerates and sandstones of Facies association A but in places such as at Kuyuçak (TG588955) wave-rippled sandstones and marls of Facies association B are present. At the type locality the member fines upwards over 140m from a proximal fan facies at the base to a distal fan facies at the top (Fig.2.5).

Previous Work

Previous authors have placed the Çendik Member in the Oligocene (Penck 1918) and the Miocene (Wedding 1966). Bering (1971b) recognised it as a basin-edge facies, related it to the p_1 horizon of Wedding (1966) and called it the Bassisschichten. Karaman (1986b) does not treat it as a separate litho-stratigraphical unit but includes it with the Akdere Member.

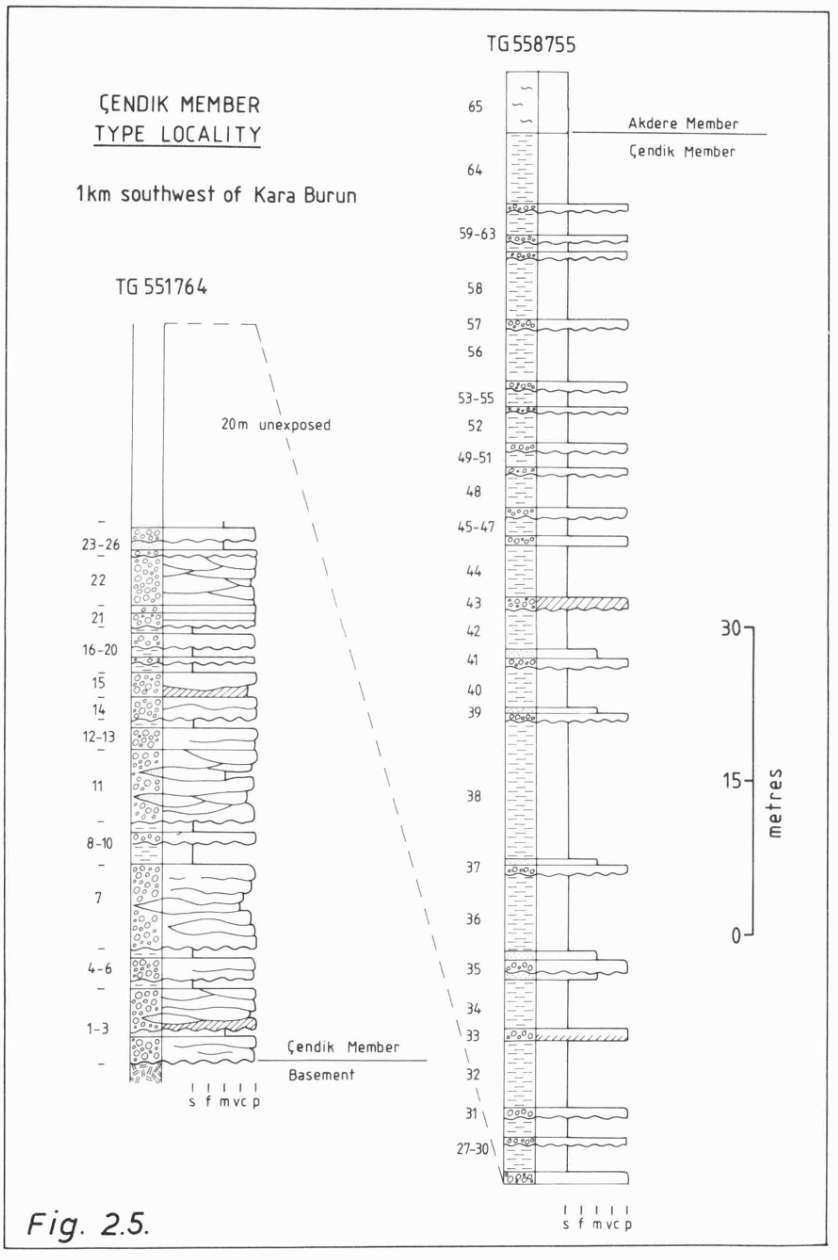
ÇENDIK MEMBER
TYPE LOCALITY
1km southwest of Kara Burun
TG 551764
20m unexposed
23-26
22
21
16-20
15
14
12-13
11
8-10
7
4-6
1-3
Çendik Member
Basement
s f m vc p
TG 558755
65
64
59-63
58
57
56
53-55
52
49-51
48
45-47
44
43
42
41
40
39
38
37
36
35
34
33
32
31
27-30
Akdere Member
Çendik Member
30
15
0
metres
s f m vc p

Fig. 2.5.

(b) Akdere Member

Outcrop Pattern This member outcrops on the southeast side of the present-day Burdur-Tefenni basin system in a 10km wide zone from near to Askeriye (TG665825) to Kayali (QB607332) in the southwest.

Type Locality There is no single locality where the whole of the Akdere Member outcrops. For this reason, four type localities are proposed, which together comprise a complete type section with both the base and the top of the member exposed. The Kirikarasi Hill Section (TG575765) is the lowermost section. Here the lower contact of the member is a syn-depositional fault contact with the underlying basement limestones. This is a coincident type lake margin (Plate 2.2b). The top of this section can be traced around the hillside behind Burdur to the approximate position of the base of the Seccade Tepe Road Section (TG609761), which starts at a slump fault. The top of this section is easily correlated with the base of the nearby Lower Akdere Road Section, which starts at TG607759. The rest of the Akdere Member outcrops along this road and the contact between this and the overlying Günalan Member outcrops just before the exposure dies out at the D_{III} erosion surface (after Erol (1981)).

Thickness Fig.2.6 shows the total thickness of the Akdere Member to be 620m at the type localities. Fig.2.2 shows the variation in thickness of the member throughout the basin. It is thinnest in the Kuruçay region (approximately 250m) and thickens northeastwards to 620m in the Burdur Region and southwestwards to 850m in the region between Pinarkayasi Tepe and Karacaören. Bering (1971b) indicates a 400-500m thickness in the Burdur region, whereas Karaman (1986b) suggests 1000m. A value somewhere between these 2 estimates is indicated in Fig.2.6, but since neither of these authors published logged sections nor defined member boundaries, direct comparisons are not possible.

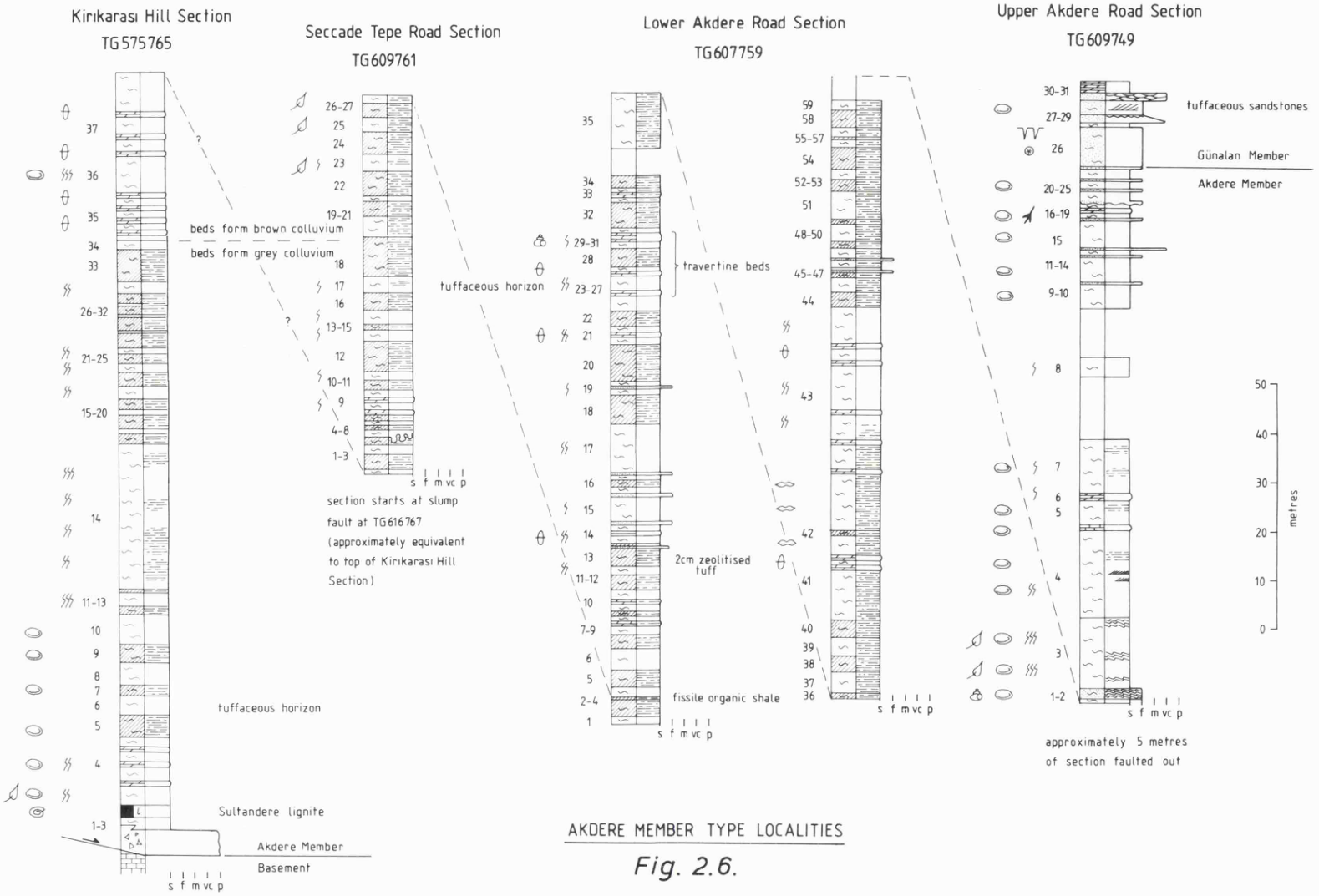

AKDERE MEMBER TYPE LOCALITIES

Fig. 2.6.

Sedimentary Facies The Akdere Member is the most lithologically varied stratigraphic unit of the Burdur Formation. It is dominated by laminated marls of Facies association G, which makes up most of the member at the type locality (Fig.2.6). Other facies within the Akdere Member are, in decreasing order of abundance, Facies associations F, E, C, B, D and H.

Previous Work The name Akdere Member is adopted from Karaman (1986b), but here is restricted to the strata described by Bering (1971b) as Limnische Schichten. The Akdere Member is equivalent to the p_2 and p_3 horizons of Wedding (1966).

(c) Günalan Member

Outcrop Pattern This member outcrops to the southeast of the Akdere Member in a zone about 5km wide running from Günalan (TG702782) southwestwards to near Kemer (TG430383). There is a break near to Bereket, where basement highs (such as Besparmak Dag) prevented sedimentation.

Type Locality As with the Akdere Member, there is no single uninterrupted section through the Günalan Member. Therefore five sections are proposed, which together show the complete member (Fig.2.7). The lowermost section at Yuvali Tepe (TG680798 and TG684796) shows the boundary between the Günalan Member and the underlying Akdere Member. At this locality the boundary is a shallow angular unconformity, best observed by standing on the valley side at TG680800 and looking southwestwards towards Yuvali Tepe. Further westwards this unconformity has marked angularity (Plate 2.1b). The other sections occur in the valley running SE from this locality and these are easily and accurately correlated. Stratigraphically, the highest beds found in the Günalan Member are the tuffs and agglomerates near Karcilar (Fig.2.7). The upper contact is defined by unconformably overlying travertines and this unconformity is well-exposed in

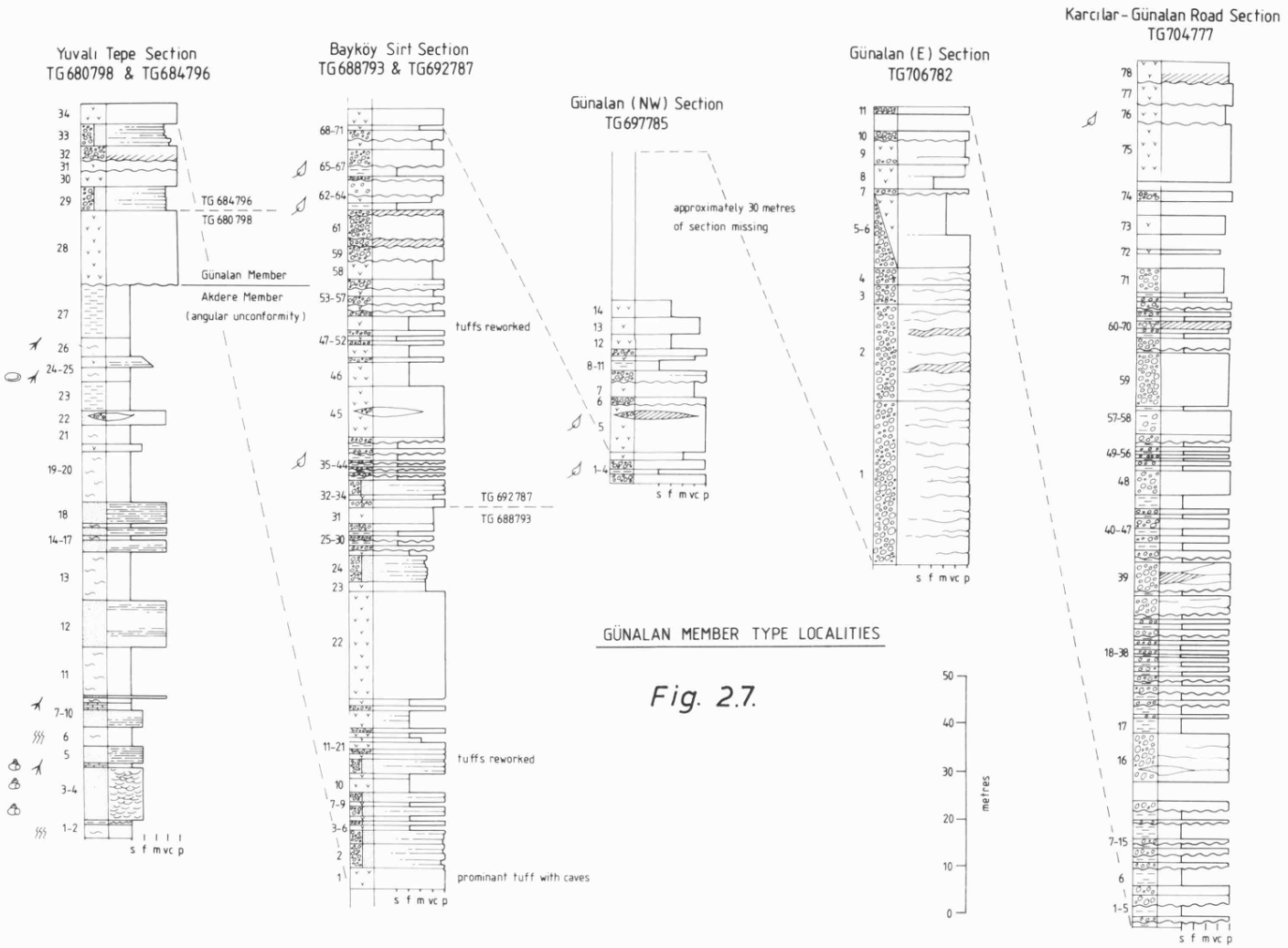

GÜNALAN MEMBER TYPE LOCALITIES

Fig. 2.7.

the valley 2km east of Yakaköy (TG660760)(Plate 2.2c).

Thickness The Günalan Member is partly a basin-edge facies and therefore is mostly in the subsurface (see Fig.2.3), being, in part, laterally equivalent to the Akdere Member. It overlaps onto basement to the southeast. Its true maximum stratigraphical thickness is therefore comparable to that of the Akdere Member. However, locally the Günalan Member unconformably overlies the Akdere Member (as well as being stratigraphically equivalent to it in the subsurface). This is the case at the type localities, where it has a total thickness of 650m. According to Bering (1971b) it is only 50-60m thick adjacent to the present-day Tefenni basin. However, Fig.2.2 shows the thickness in the SW to be 600m.

Sedimentary Facies The Günalan Member is dominated by siltstones, sandstones and conglomerates of Facies association A. Because the conglomerates form lenticular bodies within the siltstones and sandstones, the bed numbers shown in Fig.2.7 cannot be used for correlation purposes. The thick tuff and agglomerate beds of Facies association I, which interfinger with the alluvial sediments at the northeast end of the basin (Plate 2.1c), are used instead. Facies associations B and C are also present, but to a lesser extent, within this member.

Previous Work The Günalan Member is equivalent to the p_4 horizon of Wedding (1966) and the Hangende Klastische Schichten of Bering (1971b).

2.5.2. Volcanic Succession

(a) Lower Gölcük Member

Outcrop Pattern This member outcrops at Gölcük Crater Lake (TG790790), the volcanic centre, west of Isparta. There are also

exposures south of Isparta, near Buçak, which is outside the study area. These are described by Lefèvre et al. (1983).

Type Locality The Lower Gölcük Member is best exposed on the eastern edge of the Gölcük Lake caldera (TG790790), where it is seen to consist of several lava flows with brecciated contacts.

Thickness The maximum thickness of the Lower Gölcük Member is 150m. This is seen at Pilav Tepe (TG787782), 1km south of Gölcük Lake.

Sedimentary Facies There are no sediments in this member.

Previous Work K-Ar dating of the Lower Gölcük Member was done by Lefèvre et al. (1983). Karaman (1986b) used the term Gölcük Member but did not differentiate between upper and lower members. The Vulkanite von Isparta of Bering (1971b) is again an undifferentiated unit, representing both the upper and lower members.

(b) Upper Gölcük Member

Outcrop Pattern This member outcrops around the volcanic centre at Gölcük Lake. It covers an area of about 100km^2 with Isparta on its western edge (see enclosure 1).

Type Locality Although not a complete section through the Upper Gölcük Member, the best section is along the Gölcük-Isparta road, starting at TG783802. Here its lower contact is observed to unconformably overlie basement limestones, showing that the Upper Gölcük Member overlaps the Lower Gölcük Member. The presence of numerous faults in the lower part of this section renders its true stratigraphic thickness uncertain (Fig.2.8).

Thickness The thickness of the Upper Gölcük Member is at a maximum of 300m in the Gölcük area and thins rapidly

Fig. 2.8.

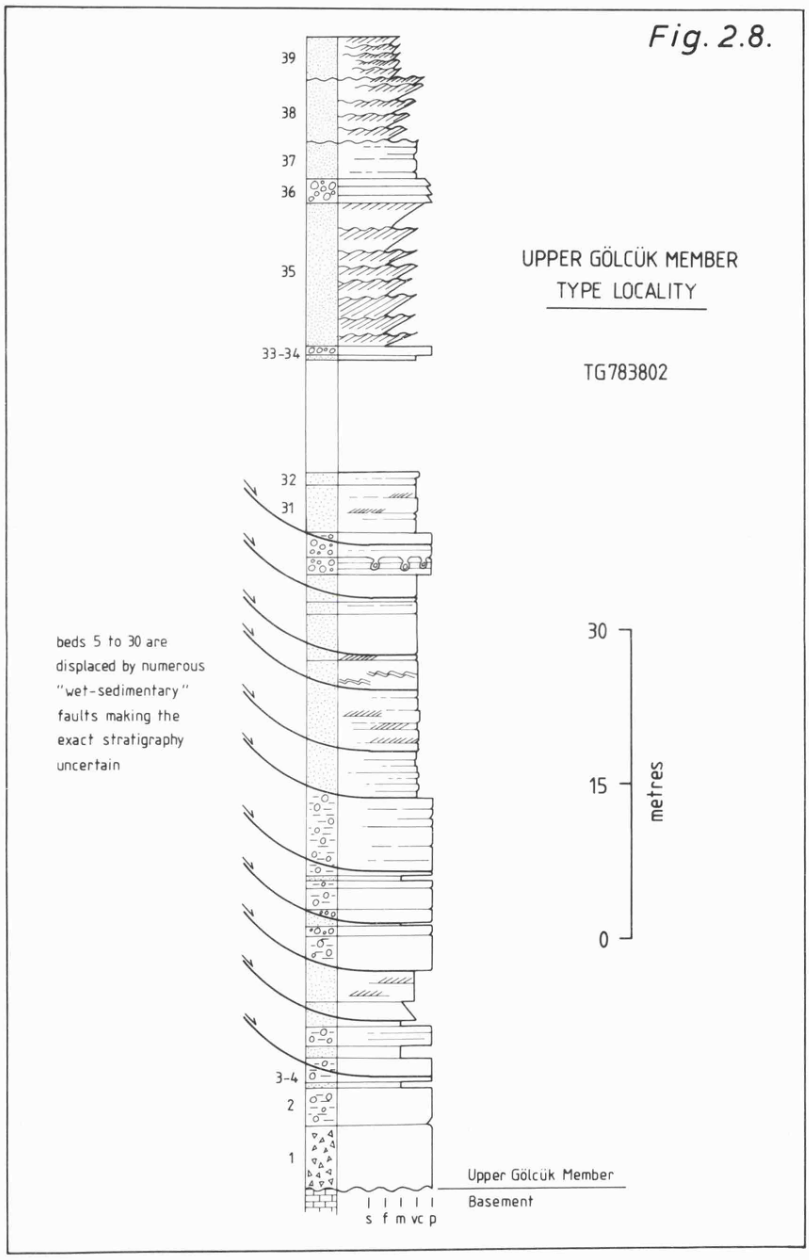
UPPER GÖLCÜK MEMBER
TYPE LOCALITY
TG783802
beds 5 to 30 are displaced by numerous "wet-sedimentary" faults making the exact stratigraphy uncertain
39
38
37
36
35
33-34
32
31
3-4
2
1
30
15
0
metres
Upper Gölcük Member
Basement
s f m vc p

away in all directions. This estimate is taken from the relief caused by this member around the crater rim. Away from the volcanic centre, to the SW, tuffs and agglomerates are interbedded with alluvial conglomerates of the Günalan Member (Plate 2.1c) showing the Lower Gölcük Member and the Günalan Member to be lateral equivalents. A single air fall agglomerate can be traced as far as Lake Egridir, about 30km to the northeast, where it has thinned to a thin 20cm thick bed.

Sedimentary Facies The Upper Gölcük Member is dominated by Facies association J. Facies associations I and J are also present. On the section in Fig.2.8 conventional clastic symbols are used rather than the volcaniclastic hatch. This is so as not to mask changes such as the distinction between clast-supported and matrix-supported lithologies.

Previous Work See Lower Gölcük Member.

2.6. CONCLUSIONS

Previous lithostratigraphic interpretations of the Burdur Formation have done little to highlight the 3-dimensional geometry of the individual members. A consideration of available structural, geophysical and sedimentological data rejects the simple 'layer-cake' stratigraphical model. Instead a half-graben sedimentation model is proposed, where the individual members approximate to laterally equivalent facies units, with hanging wall slope alluvial fans passing laterally into lake sediments, which in turn pass into footwall-sourced alluvial fans. The break up of the basin caused by the basin-controlling fault migrating into the hanging wall succession is also shown by the development of a several kilometre wide braidplain eroding the uplifted lacustrine succession.

2.7. REFERENCES

Becker-Platen, J.D. 1971. Stratigraphic Division of the Neogene and oldest Pleistocene in Southwest Anatolia. Newsletter on Stratigraphy, v.1, p.19-22.

Benda, L. 1971. Principles of the palynological subdivision of the Turkish Neogene. Newsletter on Stratigraphy, v.1, p.23-26.

Bering, D. 1971a. The developement of the Neogene and Quaternary intramontane basins within the Pisidic lake district in S. Anatolia. Newsletter on Stratigraphy, v.1, p.27-32.

Bering, D. 1971b. Lithostratigraphie, tektonische Entwicklung und Seengeschichte der neogenen und quatäran intramontanen Becken der Pisidischen Seenregion (Südanatolien) (Känozoikum und Braunkohlen der Türkei. 5.). Beihefte zum Geolischen Jahrbuch, v.101, 150pp.

Erinç, S., Bener, M., Sungur, K. and Göçmen, K. 1971. 12 Mayis 1971 Burdur Depremi. Istanbul Üniversitesi Cografya Enstitüsü Yayinlari, No.66, 27pp.

Erol, O. 1975. Quaternary deposits of the Burdur Lake Basin. Congress of Earth Sciences 50th Anniversary of the Turkish Republic, Ankara, p.386-391.

Erol, O. 1978. The Quaternary History of the Lake Basins of Southern and Central Anatolia. In Brice, W.C. (ed) The Environmental History of the Near and Middle East Since the Last Ice Age, Academic Press, p.111-139.

Erol, O. 1981. Neotectonic and Geomorphological Evolution of Turkey. Zeitschrift für Geomorphologie N.F., v.40, p.193-211.

Holland, C.H., Audley-Charles, M.G., Basset, M.G., Cowie, J.W., Curry, D., Fitch, F.J., Hancock, J.M., House, M.R., Ingham, J.K., Kent, P.E., Morton, N., Ramsbottom, W.H.C., Rawson, P.F., Smith, D.B., Stubblefield, C.J., Torrens, H.S., Wallace, P. and Woodland, A.W. 1978. A guide to stratigraphical procedure. Geological Society of

London Special Report, No.10.

Karaman, M.E. 1986a. Burdur ili ve çevresindeki yerlesim alanlarinin depremselligi. Mühendislik Jeolojisi Bülteni, No.8, p.23-30.

Karaman, M.E. 1986b. Burdur Dolayinin Genel Stratigrafisi. Akdeniz Üniversitesi Isparta Mühendislik Fakültesi Dergisi, v.2, p.23-36.

Leeder, M.R. and Gawthorpe, R.L. 1987. Sedimentary Models for extensional tilt-block/half-graben basins. In: Coward, M.P., Dewey, J.F. and Hancock, P.L. (eds) Continental Extensional Tectonics, Geological Society of London Special Publication, No.28, p.139-154.

Leeder, M.R., Ord, D.M. and Collier, R. 1988. Developement of alluvial fans and fan deltas in neotectonic extensional settings: implications for the interpretation of basin-fills. In: Nemec, W. and Steel, R.J. (eds) Fan Deltas: Sedimentology and Tectonic Settings, Blackie and Son, Glasgow and London, p.173-185.

Lefèvre, C., Bellon, H. and Poisson, A. 1983. Présence de leucitites dans le volcanisme pliocène de la région d'Isparta (Taurides occidentales, Turquie). Comptes Rendus Académie des Sciences Paris, v.297(II-10), p.369-372.

Myers, J.S. and Hamilton, W. 1964. Deformation asociated with the Hebgen Lake earthquake of August 17, 1959. United States Geological Survey Professional Paper, No.435, p.55-98.

Penck, W. 1918. Die tektonische Grundzüge Westkleinasiens, Stuttgart.

Planhol, X de. 1956. Contribution à l'Etude Géomorphologique du Taurus occidental et de ses plaines bordières. Revue Géographique Alpine, v.44, p.1-86.

Price, S. and Scott, B. 1989. A revised lithostratigraphy and sedimentology of the Burdur Formation, SW Turkey. Bulletin of the Technical University of Istanbul, v.42, p.1-27.

Sungur, K.A. 1978. Burdur, Acigöl Depresyonlari ve Tefenni Ovasinin Fizikî Cografyasi. Istanbul Üniversitesi Cografya Enstitüsü

Yayinlari, No.95, p.36-126.

Wedding, H. 1966. Burdurun güneyindeki Kömür zuhurlari. Die Kohlenvorkommen südlich Burdur. M.T.A. Report (unpublished), Ankara.

Wedding, H. and Inque, E. 1967. Report on the lignite bearing Pliocene strata around Burdur city. M.T.A. Report 1-11 (unpublished), Ankara.

Wernicke, B.P., Christiansen, R.L., England, P.C. and Sonder, L.J. 1987. Tectonomagmatic evolution of Cenozoic extension in the North American Cordillera. In: Coward, M.P., Dewey, J.F. and Hancock, P.L. (eds) Continental Extensional Tectonics, Geological Society of London Special Publication, No.28, p.203-211.

Plate 2.1. (a) Unconformity between horizontal Yakaköy travertines and faulted marls of the Burdur Formation. Photograph taken on Antalya road 4km from Burdur (TG646756).

(b) Tilted conglomerates of the Akdere Member unconformably overlain by near horizontal agglomerate (lowermost bed of the Günalan Member). The agglomerate bed is approximately 15m thick. View is towards the southwest from TG680833.

(c) 2 air fall agglomerate beds, each approximately 10m thick. The poorly exposed sediments above the lower agglomerate are fluvial sediments of the Günalan Member. The sediments below the lower agglomerate are lacustrine marls of the Akdere Member. The lower agglomerate is a product of the same eruption that deposited the agglomerate in (b). Here, there is no unconformity between the Akdere and Günalan Members. Photograph taken at TG671757.

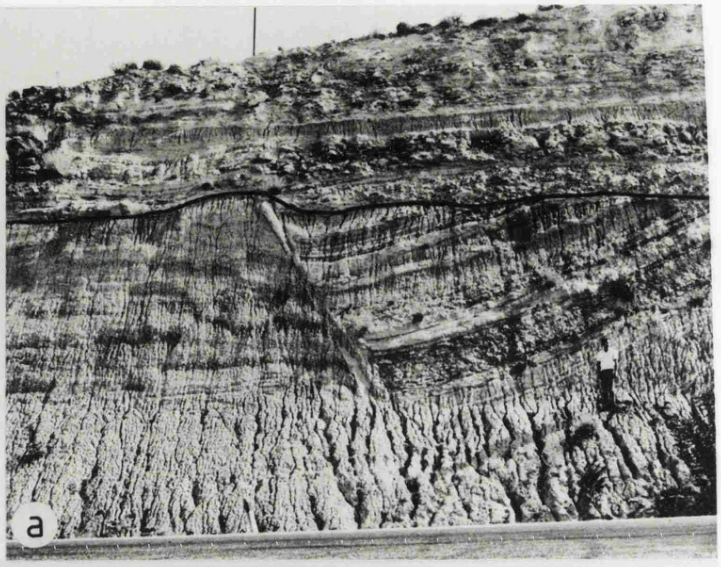

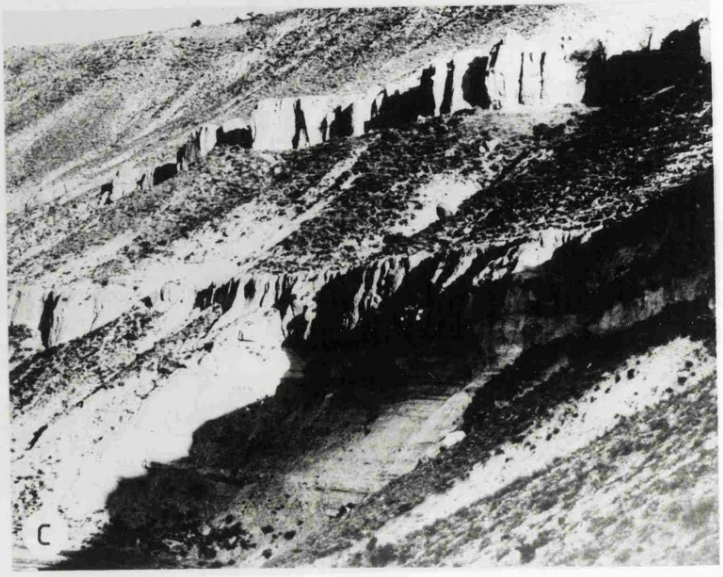

Plate 2.1.

Plate 2.2. (a) Alluvial conglomerates of the Çendik Member unconformably overlying basement serpentinite in road cutting 2km northeast of Karamanli at TG506436.

(b) Lacustrine marls of the Akdere Member lying directly against basement Mesozoic limestone at the base of the Akdere Member type locality (Kirikarasi Hill Section; TG575765). Here the edge of the lake coincided with the basin margin with no alluvial plain or fan developed.

(c) Unconformity between reworked volcaniclastic sediments of the Günalan Member and the Yakaköy travertine 2km east of Yakaköy at TG678760.

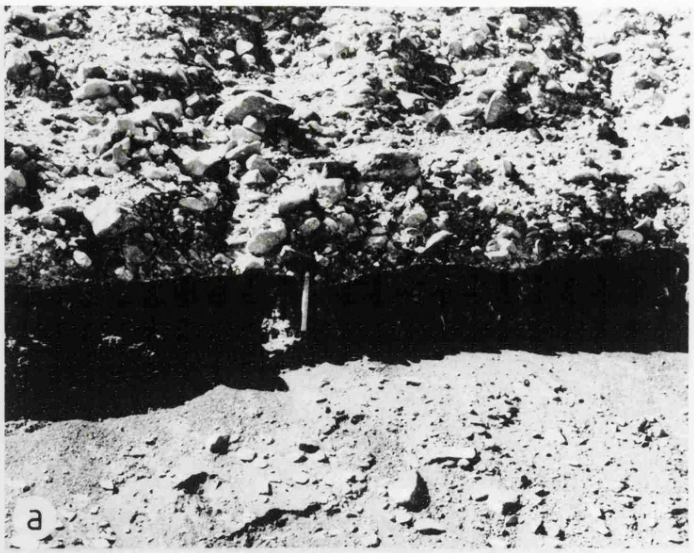

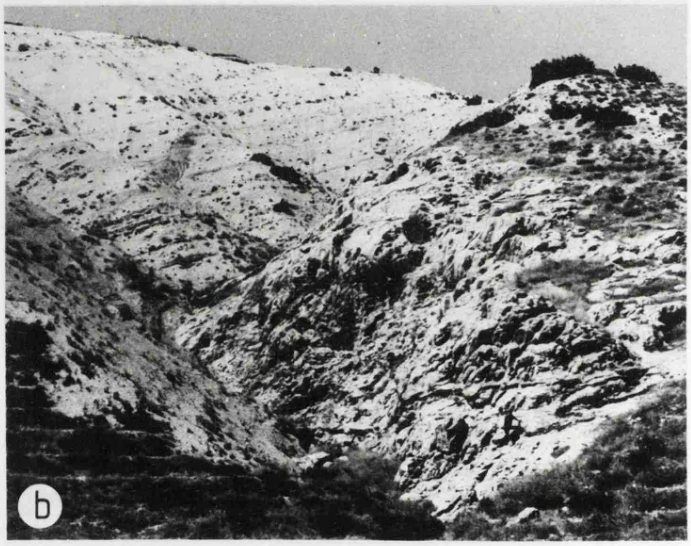

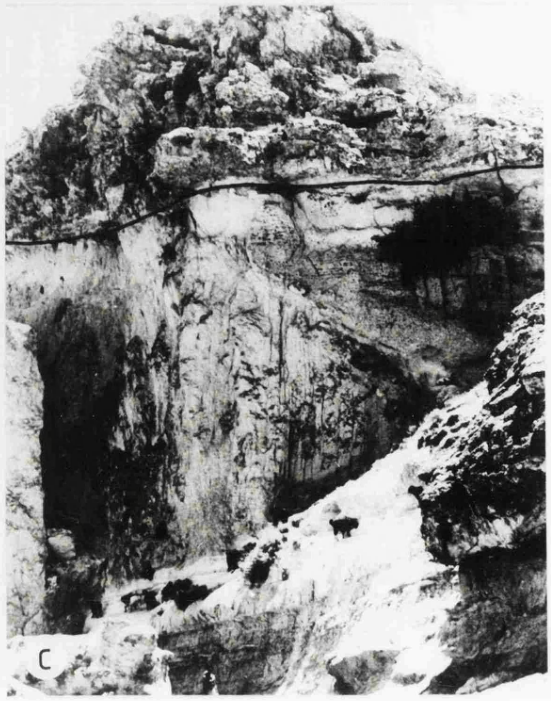

unconformity

Plate 2.2.

CHAPTER THREE.

SEDIMENTOLOGY OF THE BURDUR FORMATION, SW TURKEY.

3.1. INTRODUCTION.

The purpose of this chapter is to describe in detail the sedimentology of the Burdur Formation in terms of a facies analysis. The geometries of individual members of the Burdur Formation were described in Chapter 2. The half-graben sedimentological model proposed in Chapter 2 (see Chapter 2; Fig.2.3) is also described in more detail. Frequent cross-references to type sections figured in Chapter 2 occur in this chapter.

Bering (1971) and Karaman (1986) both gave brief lithological descriptions of the Burdur Formation. Neither of these authors considered the relationship between sedimentation and tectonics, highlighted in this chapter.

3.2. SEDIMENTARY FACIES.

The Burdur Formation can be divided into a number of members of distinct facies, each defined predominantly on lithology and sedimentary structures. The term "facies" is used here in an interpretive rather than a descriptive sense. Such a use requires a thorough knowledge of the rock body described. Therefore, this facies analysis is based on observations accumulated over 3 field seasons. Because of the wide range of depositional environments represented in the Burdur Formation the scale of sub-division of facies is low. For this reason the facies analysis is based on the recognition of 11 facies associations, most of which are characterised by a number of distinct lithologies. Each individual member of the formation has sediments representative of one or more of these facies associations (see Chapter 2). They are described below.

3.2.1. Facies Association A: Alluvial fan-fluvial deposits.

Description.

The alluvial fan-fluvial facies association dominates the Çendik and

Günalan Members. A continuum of lithofacies types representing proximal through to distal (proximal braidplain) fan environments can easily be recognised.

This facies is present as fining-upward units between 0.5 and 4m thick (Plate 3.1a). Individual units start with basal conglomerate on an erosive base and pass upwards into red sandstones, siltstones or mudstones before the next unit. The contact between the 2 lithologies is welded. Conglomerate bodies may have scoured or planar erosive bases and are lenticular with a length/thickness ratio less than 20. Less commonly, conglomerates fill channels up to 2m thick, 10m wide, with erosive concave-up bases. Most conglomerate bodies are clast-supported, although matrix-supported tabular bodies (generally with erosive bases) also occur. The conglomerates are poorly-sorted with rounded clasts of maximum clast-size between 10 and 100cm. All basement lithologies occur as clasts and intraformational tuff clasts occur at the NE end of the basin. Clasts are generally equant although imbricated tabular clasts of flaggy Miocene sandstone dominate at the SW end of the basin (Plate 3.1b). Internally the conglomerate bodies are structureless or poorly-stratified, commonly with planar or trough cross-bedded bases and they often contain small lenticular trough cross-bedded sandstones.

The conglomerates pass upwards into red sandstones, siltstones and mudstones, which are also lenticular. The finer units contain abundant plant debris, and the siltstones, which are the commonest of the 3 finer-grained lithologies, and mudstones often contain rhizocretions (Plate 3.1c). Isolated rounded extraformational clasts are common within these sediments. Sandstone horizons are often cross-laminated with asymmetrical ripples (Ripple Index = 7). Marly laminations are common. Planorbis sp. occurs in these sediments.

Interpretation.

In sediments interpreted as proximal fan deposits, such as those exposed in road cuttings near Karamanli (QB500400), conglomerate and coarse sandstone make up the whole succession. These proximal fan deposits represent both sheetflood and stream channel deposits. They appear structureless due to the thickness of bedding and the textural uniformity of the sediments. They are laterally inextensive and usually lie in palaeovalleys, resting directly upon basement lithologies, with no soil

horizon preserved, possibly indicating an arid environment (e.g. see Chapter 2; Plate 2.2a).

Distal fan (proximal braidplain) deposits are composed mainly of imbricated clast-supported conglomerates. Although usually structureless, the conglomerates are occasionally planar cross-bedded, representing longitudinal and transverse bars respectively (Miall 1985). These were accreted at a high flood stage and during times of inactive deposition (low water level) finer sediments were deposited on top giving the small-scale fining-upward sequences observed (Hayward 1983). Erosion surfaces within accreting bar sequences are usually planar. Channel margins are rarely seen, partly because channels tend to be minor parts of a gravelly fluvial landscape and also because they are difficult to recognise in lithologically homogeneous sequences. The red colouration of finer sediments and the minor developement of pedogenic calcrete attest to prolonged periods of subaerial exposure, possibly in an arid/semi-arid environment (Williams 1973). The percentage of fines within the succession varies. Parts of the succession dominated by sandstone are presumed to represent braidplain type sedimentation, where the gradient of the fan is diminished and finer sediments in suspension have been deposited. The exposed part of the Günalan Member often shows a marked reduction in grain-size, characterising this type of sedimentation, with abundant deposits of ripple-laminated and cross-bedded sandstones. This is a consequence of the lack of relief at the time of deposition of the upper part of the Günalan Member, due to the burial of the main basin-controlling basement faults at the end of the Pliocene.

In summary, it would appear that sedimentation of the conglomerate -siltstone association took place mainly upon arid-type fans. However, this type of fan is usually characterised by an abundance of matrix-supported debris flow deposits (especially on the proximal reaches of the fan). These are noticeably absent from the succession. This may be due to the lack of good exposure of this facies association and the fact that they simply have not been recognised but it seems more likely that the lack of fine-grained sediment in the basement source area (which is composed mainly of crystalline limestone) is not condusive to initiation of mudflows.

3.2.2. Facies Association B: Fan delta plain deposits.

Description.

This facies consists of planar-bedded silty marl and fine sandstone. Beds are generally less than 10cm thick with gradational bedding contacts. The silty marls are olive green and composed predominantly of pellets. They contain abundant leaves and occasional wood fragments. Rootlet horizons are common, each generally 1-2cm thick, and these are often regularly spaced. The sediments may be laminated but are more commonly burrowed or intensely bioturbated to give them a mottled appearance. Fine sandstones interbedded with the silty marls are often flaser bedded. Scott and Price (1988) described ball-and-pillow structures within sediments of this facies caused by rapid loading of an air fall tuff.

A rare occurence within marls of this facies are nodules of magnesite ($MgCO_3$) and huntite ($CaMg_3(CO_3)_4$). Both minerals are found at TG532733 (on the old mountain road NE of Çendik) and huntite alone, in the valley north of Soganli at TG564625. Both minerals occur within marl deposits, which are interbedded with travertine, silty marl, sandy marl and conglomerate. Magnesite occurs in a 5m thick marl horizon and forms resistant spherical nodules to 3cm in diameter. Huntite occurs in horizons of similar thickness and forms soft white amorphous nodules between 0.1 and 10cm in diameter. These grew displacively within the sediment and smaller nodules grew along bedding parallel horizons. Nodules are flattened parallel to bedding (Plate 3.2a).

Interpretation.

Deposition of this facies occurred within interdistributory bays on a delta plain. The dominant style of sedimentation in these bays was overbank flooding resulting in deposition from suspension of fine-grained clastic sediment (silt, fine sand). This subsequently became bioturbated. Between flooding events inorganic carbonate precipitation dominated. Ripple laminated horizons are probably the result of locally-generated wind-waves inducing mild agitation of the sediment (Coleman and Gagliano 1965). Abundant rootlets within the finer horizons throughout this facies indicate repeated emergence or near emergence of the sediment. Periodic dessication of non-vegetated areas is indicated by the presence of intraformational marl rip-up clasts. Although overbank flooding is

believed to be the dominant sedimentation mechanism, cross-bedded and rippled medium-grained sandstones represent the deposits of crevasse splays. These units have sheet geometry and formed lobes covering a large part of the distributory bay area.

The presence of huntite and magnesite nodules within sediments of this facies attests to high evaporation rates. Both huntite and magnesite are secondary carbonates and replace dolomite, which already existed within the sediment, at Mg/Ca ratios greater than about 40 (Müller et al. 1972). Such ratios are brought about by intense evaporation. Secondary huntite and magnesite is found within the sediments of modern Anatolian playa lakes such as Tuz Lake and Acigöl (Müller et al. 1972).

The presence of marshes and/or ponds supporting a low-diversity fauna for extended periods and the abundance of vegetation (shown by rootlet horizons) suggest a temperate climate at the time of sedimentation. However, the occasional dessication of non-vegetated areas (rip-up clasts) and the formation of huntite and magnesite nodules indicate periodic aridity.

3.2.3. Facies Association C: Fan-delta front deposits.

Description.

This facies is found within the Akdere Member and to a lesser extent, the Günalan Member. It is associated with the silty marls and laminated marls of the fan delta plain and offshore lacustrine facies respectively. Medium to coarse-grained sandstone units dominate this facies. These form cosets of tangentially-based tabular foresets with coset thicknesses up to 16m. Individual sets vary from 0.5 to 3.0m in thickness and coarsen upwards. The length/thickness ratio of the individual sets is about 12. This facies is best observed in the valley east of Kuruçay, on the side of Afyonluk, by standing on the hill at TG680535 and looking ENE onto the opposite side of the valley. Here a several metre thick unit, with bottomset, foreset and topset beds preserved, is seen to thin to the NW over a distance of 400m. Bottomset and topset thickness is 5-10% that of the foreset. Bottomset beds are generally represented by planar bedded fine sandy marl. Foresets commonly show asymmetrical ripples and intraformational clasts (often as reworked caliche). Against the basement fault near Soganli at TG570625 this facies coarsens upwards (over a

thickness of 12m) and towards the basement to conglomerates and laterally fines to sandstone over a distance of 300m away from the basement. Wet-sediment deformation is abundant within this facies with overturned cross-bedding (Plate 3.2b) and small syn-sedimentary faults within the sediment.

Interpretation.

Sediments of this facies are interpreted as the deposits of a delta front. Individual foresets were deposited by prograding mouth bars. The high angle of dip of the foresets suggests that these were Gilbert-style deltas fed by bed-load streams (Ayers 1986). The deltas prograded by the avalanche of sediment gravity flows down the foresets with the preservation of topset and bottomset beds. This progradation was most intense following large flood events. The sandstones occur mostly as series of stacked sets forming cosets of considerable thickness. Similar stacking of deltaic mouth bars was observed by Kazanci (1988) in a Pleistocene fluvio-deltaic complex from the opposite side of the Burdur Basin. She attributed this stacking to tectonic subsidence of the basin floor.

3.2.4. Facies Association D: Coastal plain deposits.

Description.

This facies association is restricted to the Akdere Member. It is represented by lignites, which occur at 4 localities in the study area. At Sultandere is a 120cm thick lignite horizon (bed 3 of the Kirirkasi Hill Section, TG575765) (see Chapter 2; Fig.2.6) associated with ostracodal marls. At the Kemer lignite mine (TG424406) there are 12 lignite horizons varying in thickness from 4 to 135cm. Lignite also outcrops at 2 localities along the track from Akören to Pinarbasi (TG404475 and TG408472). These deposits may be lateral equivalents to those at the Kemer lignite mine, which have been repeated by faulting. Lignite horizons are interbedded with gastropodal mudstones, siltstones, fine sandstones and fine sandy marls and themselves commonly contain lenticular siltstone horizons. They often contain clasts, broken gastropod fragments and rarely have a rootlet bed at the base, suggesting that many horizons were redeposited. Crushed specimens of Planorbis sp., abundant within the lignite horizons, are perfectly preserved in the

interbedded siltstones and marls. Rare mammalian vertebrate remains have been found in the lignites at Kemer lignite mine.

Due to the poor exposure, little is known about the geometry of individual lignite horizons. The thickest lignite horizon at Kemer lignite mine has been worked underground and although no plans exist for the mine, the horizon is laterally persistent for at least 50m, with no change in thickness over this distance (Plate 3.2c).

Interpretation.

Although lignite-forming environments have traditionally been interpreted as deltaic, McCabe (1984) and Haszeldine (1989) point out the importance of fluvially dominated freshwater environments upstream of deltas. Lignites from the study area are interbedded with silty ostracodal marls, interpreted as nearshore lacustrine deposits. Although the 3-dimensional geometry of individual lignite horizons is not known, their association with nearshore lacustrine sediments may indicate a coastal plain environment. Eutrophic marshes along lake margins may be subjected to periodic submergence by the lake, giving the vertical facies sequence observed. A similar environment was proposed by Ayers (1986) for Palaeocene coals from the Powder River Basin of Wyoming and Montana. This author postulated broad coastal plains between elongate deltas prograding into a lake. Such an environment is isolated from major clastic influx and if accumulation of peat keeps pace with basin subsidence, thick coals can be formed. A lake margin environment can also account for the reworking of many of the lignite horizons upon lake transgression and the introduction of clastic material into them. However, the presence of planispiral gastropods in the lignite and the intervening silty marls suggest that transportation was restricted. If this interpretation is correct, then the lignite horizons should be laterally persistent along depositional strike and future prospects are therefore most likely to be situated to the NE and SW of present outcrops.

3.2.5. Facies Association E: Interdeltaic shoreline deposits.

Description.

This facies is restricted to the Akdere Member. It is dominated by poorly-cemented fine grained sandstones with sheet-like geometries. These

have symmetrical ripples (Ripple Index ≈ 12) with wavelengths of up to 40cm (Plate 3.3a). Marl is commonly preserved in ripple troughs. The sandstones occur in horizons with gradational bases from a few centimetres to a few metres thick. The sandstones are often calcareous (with intraformational marl grains) or tuffaceous (especially at the NE end of the basin) and have sub-angular to sub-rounded, well-sorted grains. Intraformational conglomerate horizons are occasionally present within the sandstone horizons. Gastropods and plant debris are common throughout this facies and, more rarely, vertebrate remains can be found. Other sedimentary structures exhibited by sediments of this facies are planar and trough cross-bedding (e.g. bed 30 of the Upper Akdere Road Section, TG609749) and small sub-spherical gypsum nodules and mudcracks (e.g. bed 25 of the Upper Akdere Road Section, TG609749). In the more structureless units, normal-graded units are commonly interbedded with silty marls, siltstones and wavy laminated intrabiomicrites.

Interpretation.

The abundance of symmetrical ripples within this facies indicates the action of free gravity waves, which generally give rise to ripples with indices between 6 and 7. The measured average value of 12, due to long wavelengths, is a feature of ripples forming in deeper water (Collinson and Thompson 1984) indicative of a submerged shoreline. The paucity of dessication features and of interference ripples (usually formed by modification of the current direction on an exposed sandflat) indicates that the shoreline rarely became emergent. Trough and planar cross-bedding represent dunes and sandwaves respectively.

3.2.6. Facies Association F: Nearshore lacustrine deposits.

Interpretation.

This facies is found mainly within the Akdere Member although is present within the Günalan Member at TG674760. It is usually associated with sediments of the offshore lacustrine facies. The dominant lithology within this facies is silty ostracodal marl. Sandstone laminae and beds are also occasionally present. This lithological association is similar to that of the fan delta plain facies. It is often difficult to distinguish between them if no other criteria are available.

Marl beds may be several metres thick and clay-rich laminae are often preserved. However, intense bioturbation is common, destroying any internal structures. Ostracodes are common within the marl and these are generally disarticulated and have random orientation. However, in plan view they are concentrated along symmetrical linear horizons suggesting low-amplitude ripples from wave reworking. The marls also contain gastropods and, more rarely, charaphyte oogonia. Thin oolitic horizons (to 3cm), with burrowed bases although rare, can be found interbedded with the marl. Plant stems, encrusted with calcite are also common within this facies at Bereket (TG595595).

Travertines are unique to this facies. These form hummocky beds varying in thickness between 0.5 and 4m. Although these beds are lenticular and thin out along strike over several tens of metres, they form thick "travertine-rich" units, interbedded with marl and cross-bedded sandstone (the latter of the fan delta front facies), which are traceable over large distances. Such a unit, which is 85m thick at Doganlaya Tepe (TG542665) can be traced to Adikivan (TG505625) 6km to the SW. The travertines are composed of low-Mg calcite. They are best described as clastic travertines (after Julia 1983) as they consist of calcite accumulations on marl clasts, caliche clasts, pellets and ooids. They also encrust helical gastropods. Surprisingly, many of the travertines show well-developed low-angle planar cross-bedding. Foresets are picked out by dense and porous laminae where set thickness is between 0.5 and 1m.

Interpretation.

Ostracodal marl containing a large proportion of clastic material is indicative of a littoral lacustrine environment (Dean and Fouch 1983). This is the part of the lake populated by rooted aquatic vegetation. Vegetation and algae within this zone promote the precipitation of calcite by the removal of CO_2. This is evidenced by the encrusted plant stems observed at Bereket (TG595595). However, calcareous algae and vegetation characteristic of this type of environment are rare within the Burdur Formation. Isotopic evidence (see Chapter 4; section 4.5.) suggests that the dominant mechanism for calcite precipitation was the mixing of meteoric water with highly-alkaline lake water. The presence of ooids is further indication of a marginal lacustrine environment as seen in Higgins Lake, Michigan (Wilkinson et al. 1980). The marl-bench

environment of North American hardwater lakes (e.g. Murphy and Wilkinson 1980) provides the best modern analogy to marls of this facies.

The travertines associated with this facies are amalgamated to form sheet geometries covering several km². For this reason it is unlikely that they formed in laterally inextensive travertine forming environments such as around springs (e.g. Irion and Müller 1968) or in stream channels (e.g. Marker 1971). Also, none of the features characteristic of these environments, such as vertical and overhanging laminae, are exhibited. Above the "travertine-rich" unit at Adikivan, at TG506619, laminated marls of the offshore lacustrine facies association directly overlie travertine, strongly suggesting that the latter formed in a nearshore lacustrine environment. Such a suggestion is confirmed by the close association of travertine with silty ostracodal marl. Travertine may form in the littoral zone of a lake, where vegetation favours the precipitation of calcite (Julia 1983). This would give rise to laterally extensive travertine horizons as observed in the Burdur Formation. Cross-bedded travertine units may represent recemented deltaic mouth bars. This is especially the case where intraclasts are abundant. However, where intraclasts are absent and the foresets are picked out by dense and porous laminae the "cross-bedding" is probably a primary feature such as a drape structure, common in travertines formed in stream channels (Julia 1983). This requires these travertines to have formed subaerially. In a lake of fluctuating volume, as geochemical evidence suggest for Palaeolake Burdur (see Chapter 4), it is possible for subaerially precipitated travertine to be interbedded with marl from the littoral lacustrine zone.

3.2.7. Facies Association G: Offshore lacustrine deposits.

Description.

This facies forms a major part of the Akdere Member. The sediments are interbedded organic-rich and organic-poor marls, with each individual organic-rich/organic-poor couplet ranging in thickness from 3 to 15m. The organic-poor horizons are generally bioturbated and structureless, whereas the organic-rich horizons are mostly well laminated (Plate 3.3b). Each organic-rich horizon can be further divided into organic-rich / organic-poor units on a decimetre scale. Individual laminations are less than 1mm in thickness and can be traced for several metres in good

outcrops. Birdseye structures are fairly common and have an early calcite fill around which the lamination wraps upon compaction of the sediment. These are probably caused by gas entrapment of decaying organic matter. At many horizons wet-sedimentary microfaults displace the laminations. Although leaves and plant debris are often preserved on the laminations, other fossils are rare within this facies. Ostracodes, when present, are generally found within the organic laminated organic-rich marls and are represented by Ilyocypris sp.. Thin (<15cm) planar beds of micrite and dolomicrite commonly occur within this facies. These may be laminated or bioturbated and commonly have the dwelling burrow Arinicolites protruding from the base (Plate 3.3c). Occasional thin (<2cm) horizons of zeolitised tuff also occcur within this facies. These have been completely replaced by heulandite. Finally, thin (<0.5cm) nodular chert horizons are found within this facies. These are most common in the upper part of the Lower Akdere Road Section (TG607759) and are often internally laminated.

Interpretation.

This facies is dealt with in detail in Chapter 4 and is only considered briefly here. Carbonate sedimentation giving rise to this facies is believed to have occurred by the mixing of different water bodies in a lake. This phenomena is the cause of carbonate sedimentation in modern Lake Burdur (Müller et al. 1972). The facies forms a thick, uninterrupted succession (e.g. see Akdere Member type localities in Chapter 2; Fig.2.6) suggesting that the lake was deep. Organic-poor units are bioturbated and indicate an oxygenated hypolimnion. Geochemical evidence (Chapter 4) suggests that these were deposited during relatively arid periods when surface runoff was low and evaporation high. Organic-rich units are laminated and indicate anoxic bottom waters. These were deposited at times of increased surface runoff and reduced evaporation. The climatic change, giving rise to alternating organic-rich/organic-poor carbonate sedimentation was probably orbitally-driven as spectral analysis of logged sections reveals a dominant periodicity equivalent to that of the Earth's precessional cycle (see Chapter 4).

3.2.8. Facies Association H: Offshore Turbidite deposits.

Description.

This facies, associated with the offshore and nearshore lacustrine

facies, consists of thin (to 7cm) isolated beds of normally-graded sandstone, each generally with a layer of coarse biotite fragments on the top. It is best represented in the Upper Akdere Road Section (TG609749) (see Chapter 2; Fig.2.6). In this section beds 10, 12, 16 and 25 each form a couplet with a lower tuff horizon. Plate 3.4a shows bed 12 in which a tuff with ripple lamination at the base is overlain by 2 normally-graded fine to medium sandstone units, each with a crude internal lamination. These are overlain by a parallel laminated siltstone horizon. The contact between the tuff unit and the graded sandstone units is deformed indicating rapid deposition of the latter.

Interpretation.

The graded sandstone beds show a marked similarity with sandstone beds in Lake Brienz, Switzerland, believed by Sturm and Matter (1978) to have been deposited by turbidity currents. These beds vary from 2 to 150cm in thickness and, like the graded beds from the study area, do not exhibit a complete Bouma sequence, possibly due to rapid deceleration of the turbidity current as shown in experimental studies (Banerjee 1977). The turbidity currents are probably related to rapid flooding of rivers flowing into the basin with water flowing into the lake as a dense underflow.

In many of the horizons there appears to be a link between volcanic tuff and graded sandstone deposition. Immediately following the settling of an air fall tuff through the water column, a turbidite is usually deposited. A likely explanation for this phenomenon is the sudden release or breakthrough of water ponded by pyroclastic air fall deposits on the fan-delta plain or the alluvial fan causing a dense underflow of sediment-laden water into the lake.

3.2.9. Facies Association I: Air fall tuff/agglomerate deposits.

Description

This facies is mainly associated with the alluvial fan-fluvial facies and the base surge facies, although it is also interbedded with the fan delta plain facies at TG671757. It forms beds averaging 5m in thickness but reaching 22.5m (bed 22 of the Bayköy Sirt Section, TG688793) (see Chapter 2; Fig.2.7). The facies is restricted to the Upper Gölcük Member, the

Günalan Member and the upper part of the Akdere Member at the NE end of the basinal succession outcrop. Both tuffs and agglomerates are represented with clasts in the agglomerates between 0.2 and 45cm in diameter. The finer-grained units are often welded and columnar-jointed. At Gölcük lake, which occupies the collapsed caldera of the volcano which gave rise to these deposits, the deposits are coarser and consist mainly of pumice fragments. Here, however, individual horizons do not exceed 8m in thickness and can be seen to mantle the topography. These horizons have a crude internal stratification, with up to 3 finer ash bands separating the coarser lapilli horizons. Clasts occur as angular blocks of andesite or tuff or, more rarely, Mesozoic limestone, serpentinite, Oligocene conglomerate or wood. Semi-vesicular andesite and pumice bombs also occur (Plate 3.4b), the former usually as dumbbells with flattened undersurfaces. The units are generally structureless although reverse grading is commonly seen at the top, and normal grading and laminations at the bottom of some beds. Also rare low-angle cross-bedding has been observed (e.g. bed 78 of the Karcilar-Günalan Road Section, TG704777) (see Chapter 2; Fig.2.7). The thicker units are occasionally separated by lenticular conglomerate horizons suggesting they are composite units representing 2 or more depositional events, each separated by an erosional event. The units themselves have sheet like geometries and can be traced for several hundred metres although bed 5 in the Günalan (East) Section (TG706782) (see Chapter 2; Fig.2.7), which is about 15m thick, thins out laterally over a distance of 50m. The base of each unit is planar and non-erosive and at the base of bed 23 in the Bayköy Sirt Section (TG688793) (see Chapter 2; Fig.2.7) flattened and aligned grass casts are observed. Prolonged periods of subaerial exposure of these units is shown by the weathered nature of the top 50-100cm of most units and the conglomerates containing reworked clasts (in channeled bodies up to 3m wide) of some.

Rapid sedimentation is indicated by ball-and-pillow style deformation which is always observed where units of this facies have been deposited on sandstones and silty marls (Plate 3.4c). An example of this is discussed in Scott and Price (1988). Deformation in fine-grained lithologies (siltstone to fine sandstone) occurs to a depth of about 2m below the base of the tuff unit (Fig.3.1), although in coarse-grained units (medium to coarse sandstone) the increased pore fluid pressure associated with sediment loading is dissipated more rapidly, resulting in a narrower zone of deformation (Fig.3.2).

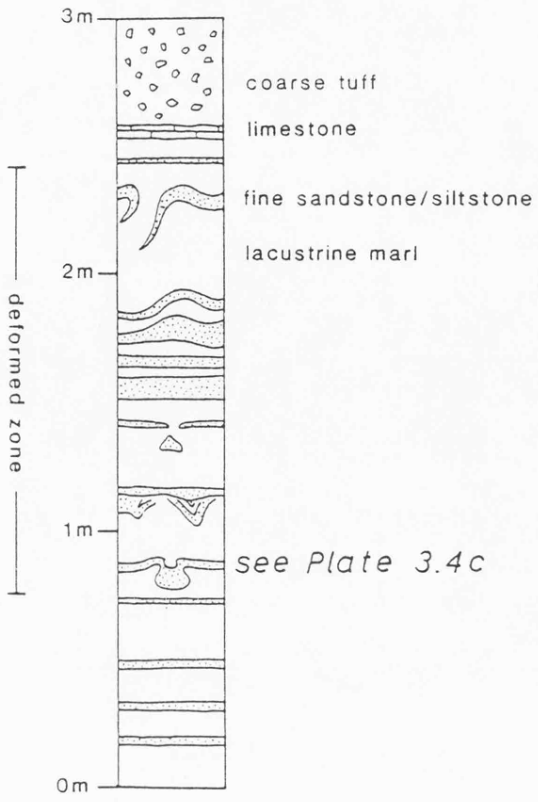

Fig.3.1. Sequence showing the relationship between deformed sediments and an overlying air fall tuff unit in the Akdere Member 1.5km east of Yakaköy (TG671757) (from Scott and Price 1988).

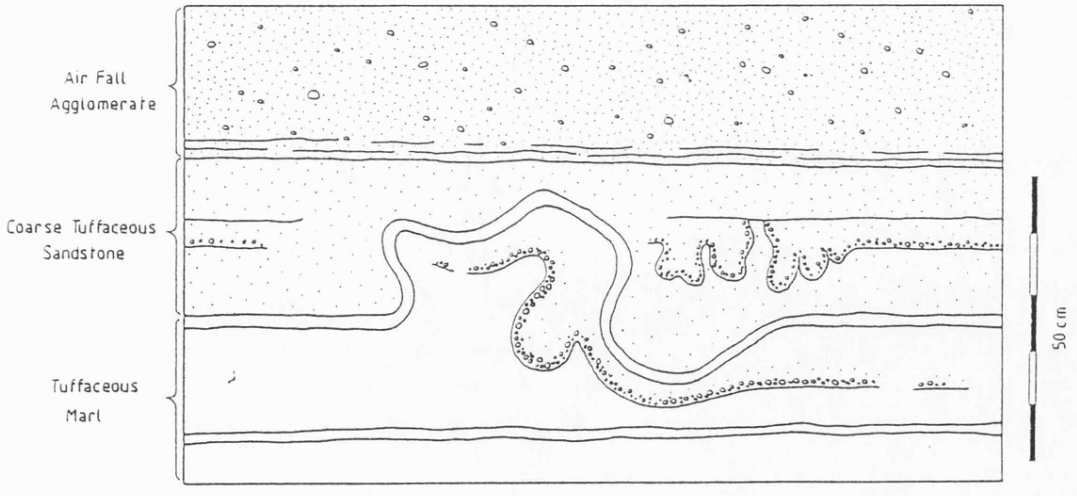

Fig.3.2. Field sketch showing deformation in coarse sandstones beneath an air fall agglomerate unit in the Akdere Member 1.5km east of Yakaköy (TG671757). Note the thickness of the deformed zone (<50cm) compared with Fig.3.1.

Rare mammalian vertebrate remains have been found within sediments of this facies.

Interpretation.

Sediments of this facies are interpreted as air-fall deposits. Evidence for this include their non-erosive bases, generally structureless appearance, decrease in grain-size away from the vent and sheet-like geometries, which mantle a hummocky topography. The homogeneous nature of these deposits is indicative of continual fall-out from a down-wind plume, which is continually being fed by a continuous gas blast. The scale of these deposits, with 22.5m thick horizons being deposited 10km from the vent (at Gölcük) is suggestive of highly explosive Plinean-type activity. Reverse grading, observed towards the top of many units (Plate 3.5a), is a common feature in fall deposits several kilometres from the vent (e.g. Bond and Sparks 1976; Bloomfield et al. 1977). Wilson et al. (1980) suggested that reverse grading in Plinean-type fall deposits is a result of vent-widening by wall erosion during an eruption, giving an increase in the mass discharge rate which causes the eruptive column to grow and coarser material to be deposited further downwind.

Internal stratification is observed in the coarser deposits near to the vent (Plate 3.5b). This can be attributed to the pulse-like nature of a single eruption, where temporary ceasing of volcanic activity (or diminution of the muzzle velocity and discharge rate) causes a break in the deposition of coarse material as the column reduces in size and finer ash particles settle out. Such a halt in volcanic activity could be brought about by blocking of the conduit by collapse of the vent. Such a collapse also explains the increased concentration of lithic fragments in the sediments.

Welding of the thicker air-fall deposits shows that ejecta remained hot and were compacted and welded under their own weight. Rapid sedimentation is required to retain the heat of the pyroclasts and evidence for this comes from the wet-sediment deformation in all potentially-liquefiable sediments beneath the fall deposits. The thicker welded deposits occur several kilometres from the vent. This may be due to the non-preservation of many deposits near to the vent away from the subsiding basin but this seems unlikely as nearly all of the air-fall tuffs within the basinal succession are thicker. It is more likely that deposition occurred from

an extremely high eruptive column such as those associated with Ultraplinean eruptions, whose columns exceed 50km in height (Walker 1980). In such a situation the thickest deposits will occur several kilometres downwind.

3.2.10. Facies Association J: Base surge deposits.

Description

This facies is restricted to the immediate vicinity of Gölcük crater lake. It is interbedded with deposits of the air fall tuff/agglomerate facies. Both planar and pyroclastic rocks are represented in this facies.

Planar-bedded units form horizons from 1 to 4m thick (Plate 3.5c). Bed thickness within a unit is generally 10 to 20cm and grain size varies from coarse ash (>0.063mm) to lapilli (<64mm). There is a great deal of variation in grain-size between successive beds indicating a possible pulse-like nature to the depositional process. In places the boundary between planar-bedded and cross-bedded units is gradational with low-angle truncations occuring within the intervening strata. These low-angle erosional surfaces help to distinguish this facies from stratified air fall deposits, which tend to be coarser nearer to the volcanic centre. Bedding sags caused by the impact of blocks into wet, unconsolidated sediment are common within the planar-bedded tuffs and agglomerates (Plate 3.6a). These are often seen to impact the sediment at an angle away from the rim of the volcanic centre. Basement lithologies are not represented in these blocks, which are dominantly of andesite lava indicating that explosive activity occurred at shallow depths.

Cross-bedded units form horizons up to 10m thick (e.g. bed 35 of the Upper Gölcük Member Type Section, TG783802) (see Chapter 2; Fig.2.8). Climbing-dune and sandwave bedforms (depending on size) are characteristic of these sediments, with individual sets being lenticular and up to 1m in thickness. Bedding sags and single clast-thick conglomerates are commonly found between sets, which generally have erosive bases and are reverse graded. Grain size variations within the cross-bedded units are the same as those of the planar-bedded units. Bedforms are stationary or regessive (Plate 3.6b).

Interpretation.

Both planar- and cross-bedded sediments are interpreted as volcanic base surge deposits, where surges transport pyroclasts along the surface as an expanded, turbulent, low-particle concentration gas-solid dispersion (Cas and Wright 1987). These surges are formed when the thermal energy of rising magma is translated to groundwater above this magma, giving explosive volcanic activity. Surge deposits form a proximal facies close to the vent of a volcano (Wohletz and Sheridan 1979). Some authors attempted to relate the structures seen within surge deposits to changing flow conditions with time, with cross-bedded units resulting from turbulent and fluidized flow and planar-bedded units resulting from laminar grain flow (Wohletz and Sheridan 1979; Suthren 1985). However, the complexities of surge mechanism led Cas and Wright (1987) to suggest that base surge facies models are premature. Allen (1982) believed that analogies of base surge mechanisms with those of subaqueous sedimentary environments are not valid.

The stationary and regressive bedforms of the deposits from the study area indicate wet, three-phase surges (gas-solid-water) at, or below, the boiling point of water (Allen 1982). Therefore there can be no analogy with normal sedimentary systems which is further highlighted by the rapid changes in grain size between successive beds, suggesting pulsatory, non-equilibrium flow conditions.

3.2.11. Facies Association K: Lahar deposits.

Description.

This facies forms a minor part of the succession of the Upper Gölcük Member at Gölcük lake and is represented by several beds at the lower part of the of the Upper Gölcük Member Type Section (TG783802) (see Chapter 2; Fig.2.8). The facies consists of matrix-supported conglomerates containing sub-angular clasts of Mesozoic limestone, trachyte and tuff. Clasts are poorly-sorted and vary in size from 0.5 to 40cm. The matrix is mud to silt-grade and tuffaceous. Internally the deposits are usually structureless (Plate 3.6c), although occasionally crudely stratified. They form horizons from about 0.4 to 7m thick. Although the upper contacts of individual horizons are planar and sharp, clasts commonly protrude into the horizon above. Lower contacts are nowhere well-exposed. Most outcrops of this poorly-exposed facies are affected by wet-sediment faulting, so nothing can be said about the

3-dimensional geometry of individual units.

Interpretation.

Sediments of this facies are interpreted as lahars. These are viscous mass gravity flows with a high matrix strength containing contemporaneous volcanic debris. The apparent buoyancy of many of the larger clasts within these deposits attests to the high matrix strength of the flow. A mechanism of grain dominant debris flow (after Cas and Wright 1987) is proposed due to the low mud-content of the matrix.

3.3. A SEDIMENTARY MODEL.

The spatial distribution of sedimentary facies in the Burdur Formation is picked out by the spatial distribution of its constituent members (e.g. see enclosure 1). The temporal distribution of facies can only be obtained from high-resolution seismic data and borehole data, neither of which are available for this area. The depth of erosion within the Burdur Formation is generally less than 100m, which is not enough to gain an insight into the vertical distribution of facies in a succession over 1km thick. Because of the SE tilt on the Burdur Formation, sedimentary logs of the succession can be made by traversing across the basin. These, however, give more information on the lateral, rather than the vertical facies changes. This problem is outlined in Chapter 2 (section 3), where it was concluded that the Burdur Formation was a half-graben basin fill consisting of the deposits of footwall-sourced fans passing laterally away from the footwall into lake sediments and finally hangingwall -sourced fans (see Chapter 2; Fig.2.3). Leeder and Gawthorpe (1987) proposed sedimentary models for extensional half-grabens. Their model of a continental basin with interior drainage (tectono-sedimentary facies model A; Leeder and Gawthorpe 1987) closely approximates to the situation at the time of deposition of the Burdur Formation. This model is now discussed in more detail, and deviations from it are highlighted.

3.3.1. Hangingwall-sourced fans.

The deposits of hangingwall-sourced fans form a NE-SW trending belt along the NW side of the Burdur Formation outcrop (i.e. the Çendik Member in enclosure 1). This belt spans the entire basin length from Keçiborlu in

the NE to Tefenni in the SW. Alluvial fan deposits of Facies association A, which lie directly upon basement lithologies, pass laterally into fan delta deposits of Facies associations B and C. The morphology of the fans is difficult to assess. Topography exerted a strong control on fan shape as seen on the northern side of the present-day Tefenni Basin, where alluvial fan deposits are confined to karstic depressions within the basement limestone. The best example of this occurs in the N-S trending depression N of Karamanli (QB500400). Here, the fan was 2-dimensional and constricted; the valley sandur delta-type of Nemec and Steel (1988).

Upon leaving the confines of the basement, the fan geometry is less certain. Fig.3.3 shows logged sections through an alluvial fan/fan-delta complex exposed in the valley SE of Kuruçay (TG508700), which is approximately in the centre of the basin. This is the only exposed hangingwall-sourced fan-delta complex in the Burdur Formation. Here, the fans were not confined by basement topography. A 220m thick alluvial fan succession is overlain by a 150m thick fan-delta complex, which is in turn overlain by nearshore and offshore lacustrine deposits of Facies associations F and G respectively. The fan-delta complex thins towards the SE (Fig.3.3). Neither alluvial fan nor fan-delta deposits are seen in the valley leading east from Suludere (TG510713), 2km north of the Kuruçay valley. 2km to the south both types of deposit abut the basement lithologies, which form Manastir düzü (TG525675). The alluvial fan/fan-delta complex is therefore less than 4km across depositional strike, which palaeocurrent data indicate to be approximately NE-SW trending (Fig.3.3). Palaeocurrents from the alluvial fan/fan-delta complex indicate flow to the SE, perpendicular to the basin axis (see Chapter 2; Fig.2.2). However, Fig.3.3 indicates a wide variation in current direction with flow to the S, through E, to NE in the alluvial fan sediments and to the SW, through E, to NE in the fan-delta sediments. This variable current direction is indicative of sedimentation on stacked fan-delta lobes, each with a 3-dimensional "ideal" fan geometry (Nemec and Steel 1988). At least 3 such lobes are seen in the succession of the Kuruçay valley. These overprint the general transgressive signature of the lake (Fig.3.3). The strong southward component of flow was perhaps due to a structural control in the hangingwall of the basin margin such as en echelon antithetic faulting. This would also explain how such a thick succession of fan sediments can build out in one place. This hypothesis cannot, however, be confirmed as the hanging wall basin margin is now buried beneath the present-day Burdur Basin.

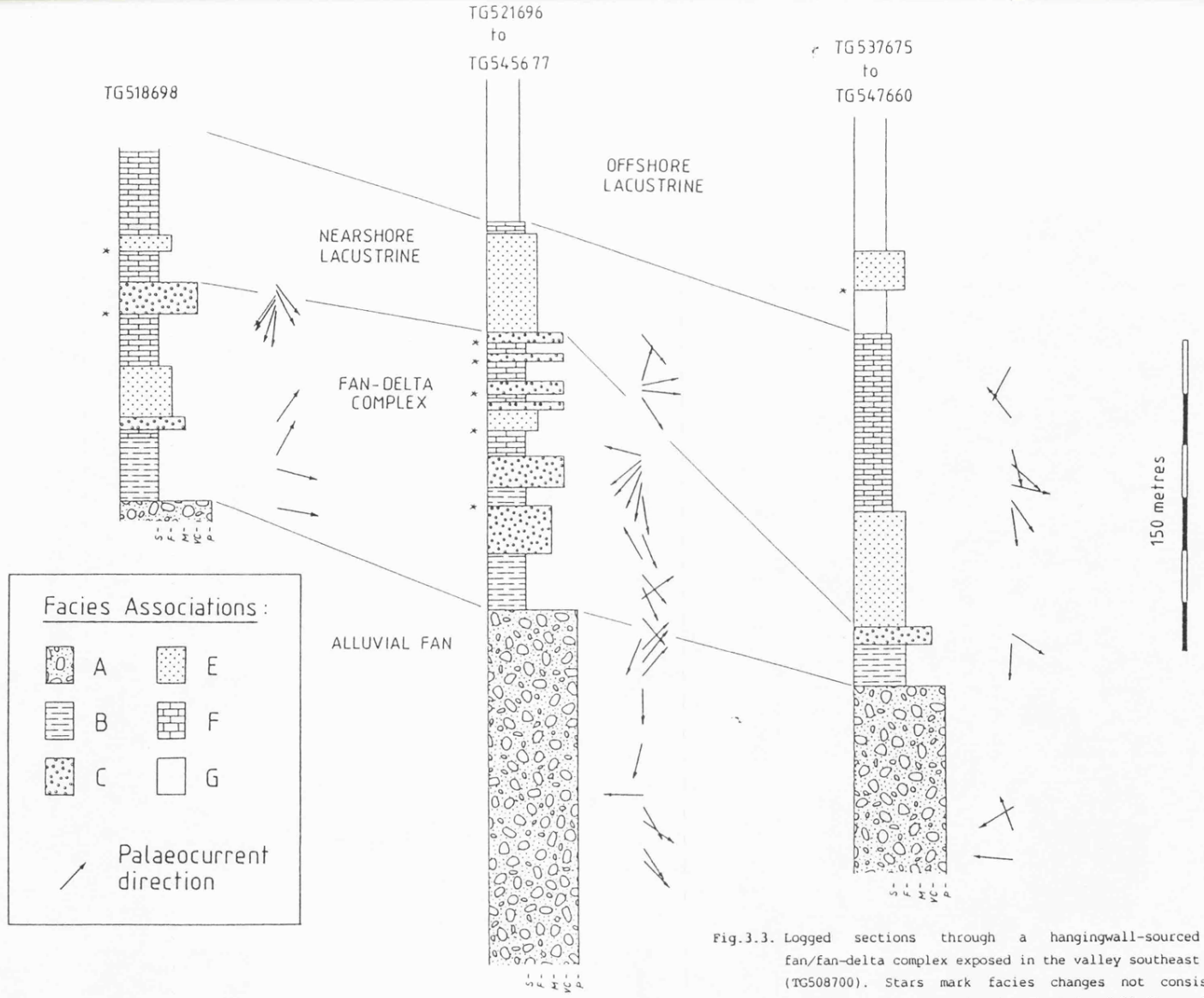

Fig.3.3. Logged sections through a hangingwall-sourced alluvial fan/fan-delta complex exposed in the valley southeast of Kuruçay (TG508700). Stars mark facies changes not consistent with overall lake transgression (see text for full discussion).

3.3.2. Footwall-sourced fans.

The deposits of footwall-sourced fans form a NE-SW trending belt along the SE edge of the Burdur Formation outcrop (e.g. the Günalan Member on enclosure 1). This belt is widest in the northern and central southern parts of the basin, where fan deposits overlap the fault-bounded basin margin. In the central part of the basin, near Soganli (TG575625) the belt is only a few hundred metres wide.

In the N, alluvial fan deposits of Facies asociation A are interbedded with air fall tuffs and agglomerates of Facies association I. This succession is approximately 650m thick and unconformably oversteps lacustrine strata (see Chapter 2; Plate 2.1b) due to uplift of the hangingwall succession by fault migration into the hangingwall (see Section 3.4.).

In the central part of the basin, near Soganli, the basin-boundary fault is exposed. Against the fault plane are fan-delta front, interdeltaic shoreline and nearshore lacustrine sediments of Facies associations C, E and F respectively. A coarsening-upward sequence representing regression of the lake margin due to the building out of fan-deltas can be recognised (Fig.3.4). These fan-delta front conglomerates and sandstones overlap the basin-boundary fault and die out laterally away from the fault (basinwards) over a distance of 400m. There is no evidence for emergence of the fan-deltas. The fan-delta succession thins to the SW along depositional strike until, at Karacäoren (TG537584), which is 5km to the SW, nearshore lacustrine deposits lie directly against the basin-boundary fault. Here, the lake margin coincided with the basin margin (this was termed a "coincident-type" margin by Donovan 1975). Sedimentation along the footwall basin margin in the central part of the basin therefore took place on a narrow belt of coalescing fan-deltas, forming a bajada. Palaeocurrents indicate flow to the NW, directly away from the basin margin and perpendicular to the basin axis (Fig.3.4).

At the southern end of the Burdur Formation, in the region of Kayi (TG457473), 600m of alluvial fan sediments of facies association A overlie lacustrine strata of facies associations E, F and G. Although there appears to be no fan-delta succession, the exposure in this area is poor and the contact between alluvial fan and lacustrine sediments is not observed. There is a greater percentage of conglomerate in the upper part

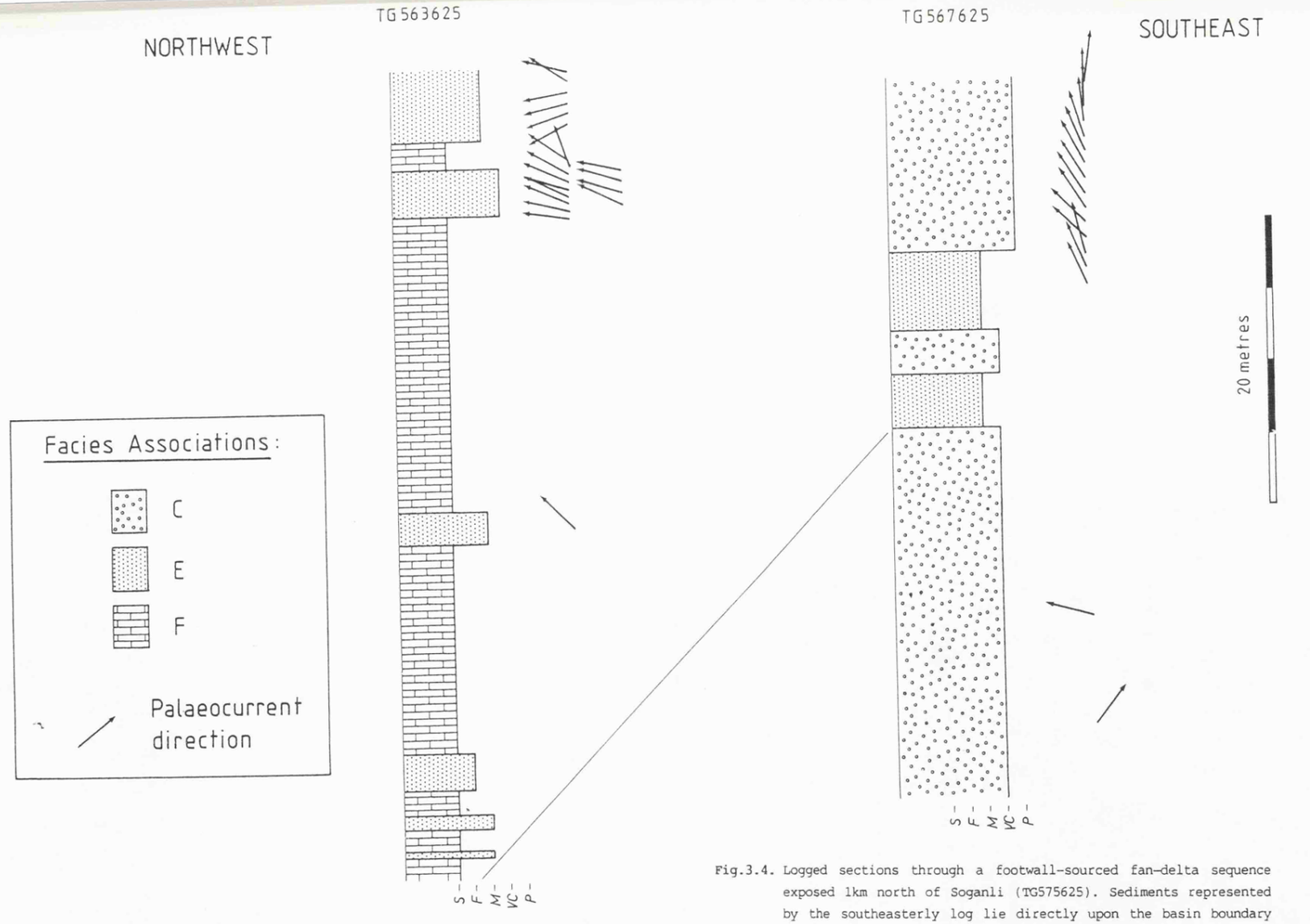

Fig.3.4. Logged sections through a footwall-sourced fan-delta sequence exposed 1km north of Soganli (TG575625). Sediments represented by the southeasterly log lie directly upon the basin boundary fault plane.

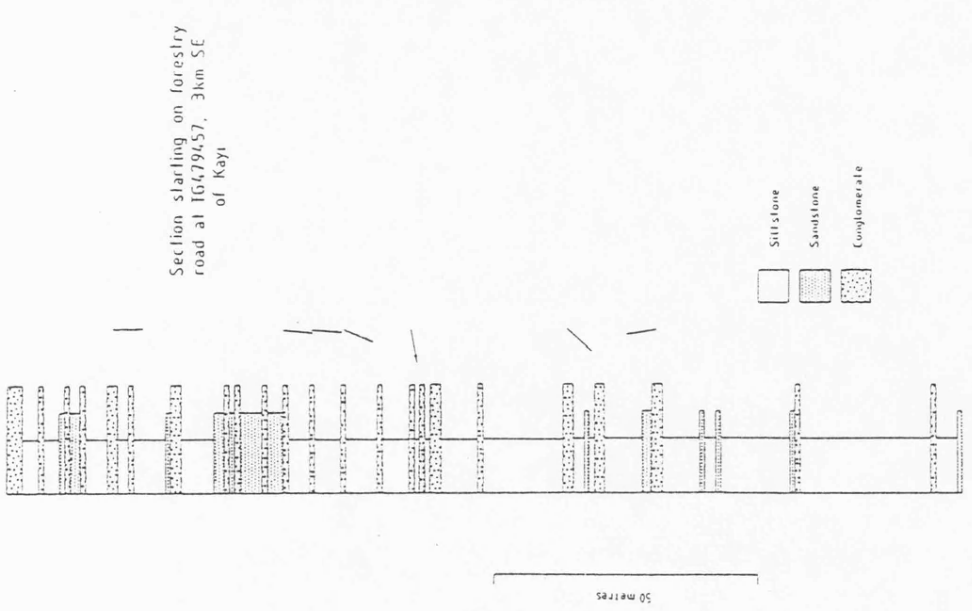

Fig.3.5. Logged section of part of a footwall-sourced alluvial fan sequence exposed on the forestry road 3km southeast of Kayi (TG479457).

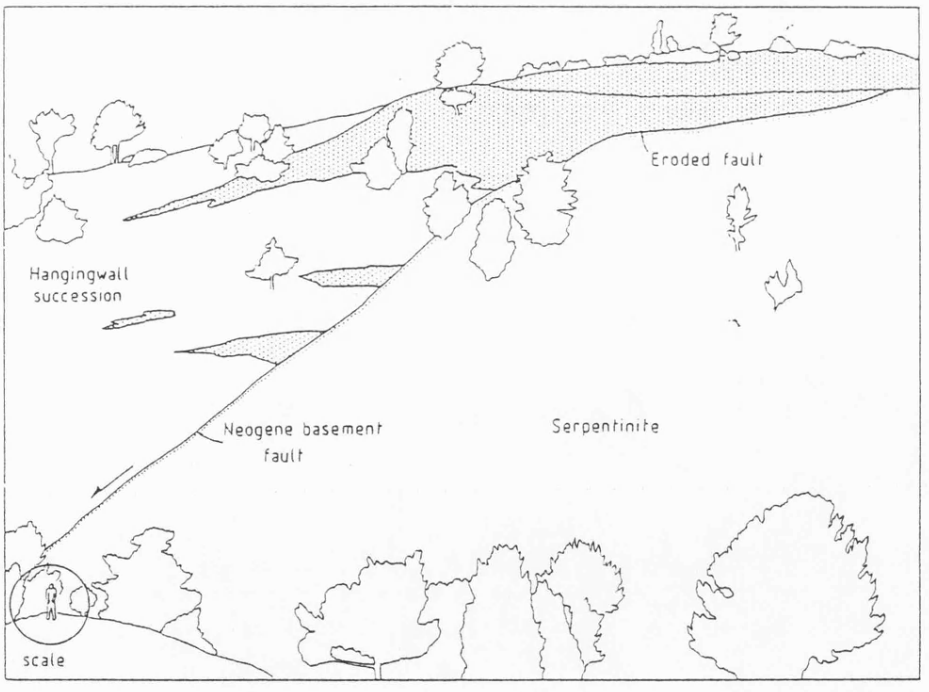

Fig.3.6. The Neogene basin-boundary fault as exposed in the valley 1km north of Soganli (TG575625). The upper part of the fault became eroded when fault activity ceased towards the end of the Neogene. Shaded areas represent the coarsest (conglomeratic) fan deposits. Note that these prodgraded into the basin when the fault became inactive.

of the alluvial fan succession, suggesting overall progradation of the fan system (Fig.3.5). Palaeocurrents (see Chapter 2; Fig.2.2 and this chapter; Fig.3.5) indicate flow to the S and SW. This is due to the fan being sourced in the relay structure between 2 en echelon fault segments as discussed in Chapter 2 (section 3.2.). Relay structures between fault segments allow larger-than-average drainage systems to exploit the area between the fault terminations (Crossley 1984, Leeder and Gawthorpe 1987). This explains how such a thick fan succession can accummulate against the footwall, when elsewhere (i.e. the central part of the basin), only a narrow bajada forms.

3.3.3. Fan-lake interactions.

The transgressive sequence of environments from hangingwall-sourced alluvial fan, through fan-delta, to marginal lacustrine seen in Kuruçay valley (Fig.3.3) is not unique to this region. At the type locality of the Çendik Member of the Burdur Formation (Chapter 2; Fig.2.5) lacustrine strata overlie a fining-upward sequence of alluvial fan deposits. These fan deposits contain clasts of Eo-Oligocene conglomerates derived from the basement to the NW and therefore represent hangingwall-sourced fans. In both cases the transgressive sequence occurs over more than 100m. Transgression of a lake over hangingwall-sourced fans is caused by the migration of the hangingwall pivot (the line of zero uplift or subsidence) away from the footwall. This causes onlap of the sediments in the half-graben up the hangingwall (Alexander and Leeder 1987). Once the lake is established it will deepen, depending on the rate of extension of the basin, climate and sediment input. Throughout the Burdur Formation a thick succession of offshore lacustrine strata of Facies association G is developed. At the type locality of the Akdere Member (Chapter 2; Fig.2.6) a 450m thick succession of offshore lacustrine marl was deposited, indicating very little sediment input into a rapidly extending and subsiding basin.

The geometries of both hangingwall- and footwall-sourced fans have already been described. Discounting the large fan complex sourced in the footwall between en echelon fault segments at the southern end of the basin, footwall-sourced fans were much smaller than their counterparts on the opposite side of the basin. Also in the areas exposed the fans do not appear to have been emergent. (It must be emphasized that the small radii of footwall-sourced fans is only representative of the upper 100m or so

of sediment exposed against the basin-boundary fault. The geometry of footwall-sourced fans in the sub-surface is unknown). Death Valley, California, provides a reasonable modern analogue for the Burdur Formation, although the absence of a lake in the former prevents a complete comparison from being made. In Death Valley, the hangingwall is drained by a number of large coalescent fans whereas fans sourced in the footwall have radii less than 1km and are isolated. Hooke (1972) ascribes this discrepency in size to backward tilting of the footwall-sourced fans during subsidence and lower sediment yields from the drier watersheds in the footwall. Although nothing is known about the size of the drainage basins of the Burdur Formation fans, basement lithology is not thought to have strongly influenced fan area. The footwall- and hangingwall-sourced fans both drained a basement of predominantly Mesozoic limestone and serpentinite. Tectonic tilting of the basin floor probably had the strongest influence on fan area as described below.

Cyclothems of coarse-grained fan deposits and fine-grained marine, lacustrine or longitudinal fluvial deposits are a common feature against the faulted margins of half-grabens and many examples exist in the literature (e.g. Beerbower 1964; Blair 1985, 1987; LeTourneau 1985; Steel et al. 1977; Vondra and Burggraf 1978). Coarse-grained deposits in these cyclothems have traditionally been ascribed to periods of tectonic activity with fine-grained lithologies being deposited at times of tectonic quiescence (Barrell 1917). However, Blair and Bilodeau (1988) argue that during a period of tectonic activity a lake will respond more quickly than a fan in filling the tectonic depression in the hangingwall next to the fault. Therefore during such periods the footwall basin margin will be occupied by a lake. During a period of tectonic quiescence fans will prograde out over the lake sediments. If lake sediments were to cover the fans during quiescent periods as predicted in the traditional model, the lake level would be required to rise in order to cover the fans along the basin margin, which, topographically, would form the highest part of the basin fill.

It is proposed that the absence of large footwall-sourced fans in the exposed part of the Burdur Formation is a feature of the rapid subsidence rate in the hangingwall adjacent to the basin-boundary fault. This is partly substantiated by the fact that the coarsest fan deposits observed in the sequence at Soganli (Fig.3.4) occur at the top of the section, where sediments clearly overlap the basin-boundary fault (Fig.3.6).

Therefore, at this locality, the greatest influx of sediment occurred at a time of tectonic quiescence, when the fault became inactive.

The large-scale change in facies from alluvial fan, through fan delta, to lacustrine seen within Kuruçay valley (Fig.3.3) can be explained by lake onlap due to the migration of the hangingwall pivot away from the basin-boundary fault. Smaller-scale variations in facies occuring within the succession require explanation. Facies changes not consistent with overall lake transgression are shown on Fig.3.3. Most of these occur at the bases of fan-delta front deposits of Facies Association C and represent progradation of these fan-deltas over the lake floor. 2 opposing processes therefore appear to be causing this small-scale facies variation. On the one hand is tectonically-driven lake transgression and on the other is fan-delta progradation. On at least 3 occasions the latter effect outweighs the former (Fig.3.3). In Chapter 4 it is demonstrated that orbitally-driven changes in precipitation rate occurred during the Neogene in the study area. These had a frequency of approximately 20 ka, equivalent to the Earth's precessional cycle. It is proposed that fan delta progradation occurred during periods of increased surface run-off on this time-scale.

3.3.4. Effect of fault migration.

Towards the end of the Neogene, the basin-boundary fault migrated northwestwards into the basin. (A possible reason for this is outlined in Chapter 7 (Section 4.)). The effects of this fault migration were most marked at the northern end of the basin. Here, there is a marked unconformity above that part of the basinal succession which was uplifted in the footwall of the newly formed fault. The angularity of this unconformity increases northwestwards towards the fault as the amount of footwall uplift (by elastic rebound and isostatic unloading) increased. Above the unconformity is a 650m thick succession of alluvial fan deposits and air fall tuffs and agglomerates of Facies associations A and I respectively. This is the type section of the Günalan Member of the Burdur Formation (see Chapter 2; Fig.2.7). The effects of this basinward migration of fault activity were dramatic. Footwall-sourced alluvial fans were uplifted and eroded. The older parts of these footwall sourced fan sequences are now buried beneath the unconformity which developed (see Chapter 2; Fig.2.3). The scarp of unconsolidated sediment in the footwall of the newly-formed fault would have rapidly retreated southeastwards.

Above this eroded surface the thick succession of alluvial fan and volcaniclastic sediments were deposited. These were fed by the same streams as those which fed the footwall-sourced fans beneath the unconformity. Palaeocurrent data (Chapter 2; Fig.2.2) is scattered, indicating that these streams had developed a higher sinuosity on what would have been a lower gradient braidplain. The old basin margin was, at this time, eroded and buried, giving a much more subdued topography. With further uplift on the footwall of the newly-formed fault the braidplain became totally dissected and the consequent stream system feeding it became antecedent to the new basin (i.e. the present-day Burdur Basin).

3.4. CONCLUSIONS.

The following conclusions, summarised in Fig.3.7 concerning the sedimentological evolution of the Burdur region during the late Neogene can be made from this study:

(a) The proximal parts of hangingwall-sourced fans were confined to karstic depressions in the basement. Distally, these fans are represented by the Kuruçay fan complex, which is a 400m thick sequence of stacked alluvial fan and fan-delta lobes, up to 4km wide and with "ideal" cone-shaped fan geometry. This stacking was caused by periodic fan progradation in a subsiding basin, which, in turn, was caused by cyclic variations in surface run-off. These fans flowed to the SE into the basin and perpendicular to its axis, although a component of axial flow to the S was probably due to structural control of drainage at the basin margin by antithetic faulting.

(b) In the central part of the basin footwall-sourced fans coalesced to form a narrow bajada (less than 400m wide) with flow to the NW into the basin and perpendicular to its axis. In places the footwall margin of the basin was a coincident lake margin. At the southern end of the basin 600m of sediment was deposited by a prograding alluvial fan, on which flow was to the S and SW, axially into the basin. This axial flow was due to drainage being sourced in the relay structure between left-stepping en echelon faults.

(c) The transgressive sequence seen in Kuruçay valley shows the drowning of hangingwall-sourced fans by the lake due to migration of the

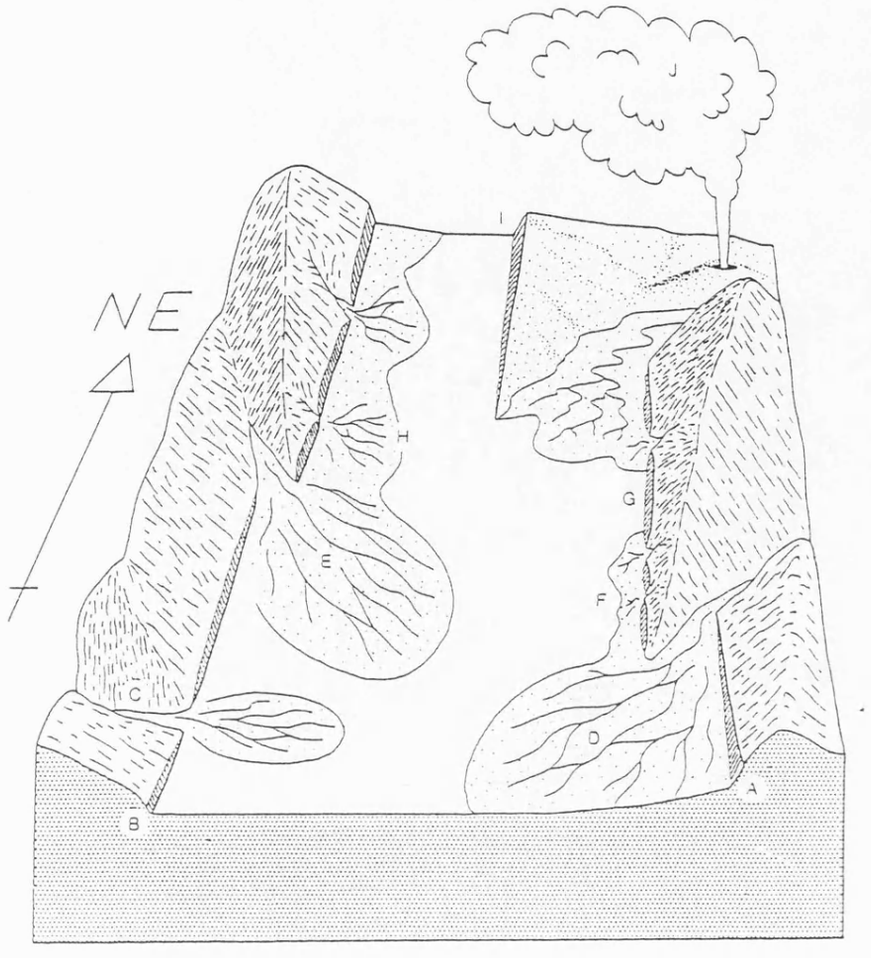

Fig.3.7. Cartoon showing the Burdur region at the time of deposition of the Burdur Formation. The following features are worthy of note: A - Main fault system; B - Antithetic fault system; C - Hangingwall-sourced fans proximally confined to karstic depressions in limestones forming the source region; D - Kayi fan sourced in the relay structure between en echelon fault segments; E - Kuruçay fan sourced in the relay structure between en echelon fault segments; F - Narrow bajada of coalesced footwall-sourced fans; G - Coincident-type lake margin; H - Tectonically-driven transgression of the lake over hangingwall-sourced fans; I - Incipient mid-basinal fault at the northern end of the basin; J - Ultraplinean eruptive column.

hangingwall pivot away from the basin-boundary fault.

(d) The small size of footwall-sourced fans compared to hangingwall-sourced fans was due to rapid subsidence of the basin floor adjacent to the basin-boundary fault. Footwall-souced fans are best developed when the fault ceased to become active as they are seen to overlap the eroded basement at the basin margin.

(e) The migration of the basin-boundary fault to the NW into the basin at the end of the Neogene caused much of the basinal succession to be uplifted and eroded. A wide braidplain with high sinuosity streams developed on this erosional surface due to a reduction in gradient at the basin margin. This was caused by the erosion and burial of the footwall crest of the older, inactive fault.

3.5. REFERENCES.

Alexander, J.A. and Leeder, M.R. 1987. Active tectonic control of alluvial architecture. In: Ethridge, F.G., Flores, R.M. and Harvey, M.D. (eds) Recent Developments in Fluvial Sedimentology. Special Publication of the Society of Economic Paleontologists and Mineralogists, No.39, p.243-252.

Allen, J.R.L. 1982. Developments in sedimentology. Vols. 30A and B: Sedimentary structures. Their character and physical basis. Amsterdam, Elsevier.

Ayers, W.B. Jr. 1986. Lacustrine and fluvial-deltaic depositional systems, Fort Union Formation (Paleocene), Powder River Basin, Wyoming and Montana. American Association of Petroleum Geologists Bulletin, v.70, p.1651-1673.

Banerjee, I. 1977. Experimental study on the effect of deceleration on the vertical sequence of sedimentary structures in silty sediments. Journal of Sedimentary Petrology, v.47, p.771-783.

Barrell, J. 1917. Rhythms and the measurement of geologic time. Bulletin of the Geological Society of America, v.28, p.745-904.

Beerbower, J.R. 1964. Cyclothems and cyclic depositional mechanisms in alluvial plain sedimentation. In: Merriam, D.F. (ed) Symposium on cyclic sedimentation. Kansas Geological Survey Bulletin, v.169, p.31-42.

Bering, D. 1971. Lithostratigraphie, tektonische Entwicklung und Seengeschichte der neogenen und quatäran intramontanen Becken der Pisidischen Seenregion (Südanatolien) (Känozoikum und Braunkohlen der Türkei. 5.). Beihefte zum Geologischen Jahrbuch, v.101, 150pp.

Blair, T.C. 1985. Sedimentological response to tectonism in nonmarine rift basins: A comparison of the Jurassic Todos Santos Formation, Chiapas, Mexico, with Quaternary deposits in Death Valley, California. Society of Economic Paleontologists and Mineralogists Mid-year Meeting Abstracts, v.2, p.11-12.

Blair, T.C. 1987. Tectonic and hydrologic controls on cyclic alluvial-fan, fluvial, and lacustrine rift-basin sedimentation, Jurassic-lowermost Cretaceous Todos Santos Formation, Chiapas, Mexico. Journal of Sedimentary Petrology, v.57, p.845-862.

Blair, T.C. and Bilodeau, W.L. 1988. Development of tectonic cyclothems in rift, pull-apart, and foreland basins: Sedimentary response to episodic tectonism. Geology, v.16, p.517-520.

Bloomfield, K., Sanchez Rubio, G. and Wilson, L. 1977. Plinean eruptions of Nevado de Toluca volcano, Mexico. Geologische Rundschau, v.66, p.120-146.

Bond, A. and Sparks, R.S.J. 1976. The Minoan eruption of Santorini, Greece. Journal of the Geological Society of London, v.132, p.1-16.

Cas, R.A.F. and Wright, J.V. 1987. Volcanic Successions: Modern and Ancient. Allen and Unwin, 528pp.

Coleman, J.M. and Gagliano, S.M. 1965. Sedimentary structures: Mississippi river deltaic plain. In: Middleton, G.V. (ed) Sedimentary Structures and their Hydrodynamic Interpretation. Special Publication of the Society of Economic Paleontologists and Mineralogists, No.12, p.133-148.

Collinson, J.D. and Thompson, D.B. 1984. Sedimentary Structures. Allen and Unwin, 194pp.

Crossley, R. 1984. Controls of sedimentation in the Malawi rift valley, Central Africa. Sedimentary Geology, v.40, p.33-50.

Dean, W.E. and Fouch, T.D. 1983. Lacustrine Environment. In: Scholle, P.A., Bebout, D.G. and Moore, C.H. (eds) Carbonate Depositional Environments. American Association of Petroleum Geologists Memoir, No.33, p.97-130.

Donovan, R.N. 1975. Devonian lacustrine limestones at the margin of the Orcadian Basin, Scotland. Journal of the Geological Society of London, v.131, p.489-510.

Haszeldine, R.S. 1989. Coal reviewed: depositional controls, modern analogues and ancient climates. In: Whateley, M.K. and Pickering, K.T. (eds) Deltas: Sites and Traps for Fossil Fuels. Geological Society of London Special Publication, No.41, p.289-308.

Hayward, A.B. 1983. Coastal alluvial fans and associated marine facies in the Miocene of SW Turkey. In: Collinson, J.D. and Lewin, J. (eds) Modern and ancient fluvial systems. Special Publication of the International Association of Sedimentologists, No.6, p.323-336.

Hooke, R.LeB. 1972. Geomorphic evidence for late-Wisconsian and Holocene tectonic deformation, Death Valley, California. Bulletin of the Geological Society of America, v.83, p.2073-2098.

Irion, G. and Müller, G. 1968. Mineralogy, petrology and chemical composition of some calcareous tufa from the Schwabische Alb, Germany. In: Müller, G. and Friedman, G.M. (eds) Recent developements in carbonate sedimentology in central Europe. Springer-Verlag, p.157-171.

Julia, R. 1983. Travertines. In: Scholle, P.A., Bebout, D.G. and Moore, C.H. (eds) Carbonate Depositional Environments. American Association of Petroleum Geologists Memoir, No.33, p.64-72.

Karaman, M.E. 1986. Burdur Dolayinin Genel Stratigrafisi. Akdeniz Üniversitesi Isparta Mühendislik Fakültesi Dergisi, v.2, p.23-36.

Kazanci, N. 1988. Repetitive deposition of alluvial fan and fan-delta wedges at a fault-controlled margin of the Pleistocene-Holocene Burdur Lake graben, southwestern Anatolia, Turkey. In: Nemec, W. and Steel, R.J. (eds) Fan Deltas: Sedimentology and Tectonic Settings. Blackie and Son, p.186-196.

Leeder, M.R. and Gawthorpe, R.L. 1987. Sedimentary models for extensional tilt-block/half graben basins. In: Hancock, P.L., Coward, M.P. and Dewey, J.F. (eds) Continental Extensional Tectonics. Special Publication of the Geological Society of London, No.28, p.139-152.

LeTourneau, P.M. 1985. Alluvial fan development in the Lower Jurassic Portland Formation, central Connecticut-Implications for tectonics

and climate. United States Geological Survey Circular, No.946, p.17-26.

McCabe, P.J. 1984. Depositional environments of coal and coal-bearing strata. In: Rahmani, R.A. and Flores, R.M. (eds) Sedimentology of Coal and Coal-bearing Sequences. Blackwell Scientific Publications, Oxford, p.13-42.

Marker, M.E. 1971. Waterfall tufas: a facet of karst geomorphology. Zeitschrift für Geomorphologie, v.12, p.138-152.

Miall, A.D. 1985. Architectural-element analysis: a new method of facies analysis applied to fluvial deposits. Earth Science Reviews, v.22, p.261-308.

Müller, G., Irion, G. and Förstner, U. 1972. Formation and diagenesis of inorganic Ca-Mg carbonates in the lacustrine environment. Naturwissenschaften, v.59, p.158-164.

Murphy, D.M. and Wilkinson, B.H. 1980. Carbonate deposition and facies distribution in a central Michigan marl lake. Sedimentology, v.27, p.123-135.

Nemec, W. and Steel, R.J. 1988. What is a fan delta and how do we recognise it? In: Nemec, W. and Steel, R.J. (eds) Fan Deltas, Sedimentology and Tectonic Settings, Blackie, p.3-13.

Scott, B. and Price, S. 1988. Earthquake-induced structures in young sediments. Tectonophysics, v.147, p.165-170.

Steel, R.J., Maehle, S., Nilsen, H., Roe, S.L. and Spinnangr, A. 1977. Coarsening-upward cycles in the alluvium of Hornelen Basin (Devonian), Norway: Sedimentary rsponse to tectonic events. Bulletin of the Geological Society of America, v.88, p.1124-1134.

Sturm, M. and Matter, A. 1978. Turbidites and varves in Lake Brienz (Switzerland): deposition of clastic detritus by density currents. In: Matter, A. and Tucker, M. (eds) Modern and Ancient Lake Sediments. Special Publication of the International Association of Sedimentologists, No.2, p.147-168.

Suthren, R.J. 1985. Facies analysis of volcaniclastic sediments: a review. In: Brenchley, P.J. and Williams, B.P.J. (eds) Sedimentology: Recent developments and applied aspects. Blackwell Scientific Publications, p.123-146.

Vondra, C.F. and Burggraf, D.R. 1978. Fluvial facies of the Plio-Pleistocene Koobi Fora Formation, Karari Ridge, East Lake Turkana, Kenya. In: Miall, A.D. (ed) Fluvial sedimentology. Canadian Society of Petroleum Geologists Memoir, No.5, p.511-529.

Walker, G.P.L. 1980. The Taupo pumice: product of the most powerful known (ultraplinean) eruption? Journal of Volcanological and Geothermal Research, v.8, p.69-94.

Wilkinson, B.H., Pope, B.N. and Owen, R.M. 1980. Nearshore ooid formation in a modern temperate region marl lake. Journal of Geology, v.88, p.697-704.

Williams, G.E. 1973. Late Quaternary piedmont sedimentation, soil formation and paleoclimates in arid South Australia. Zeitschrift für Geomorphologie N.F., v.17, p.102-125.

Wilson, L., Sparks, R.S.J. and Walker, G.P.L. 1980. Explosive volcanic eruptions-IV. The control of magma properties and conduit geometry on eruption column behaviour. Geophysical Journal of the Royal Astronomical Society, v.63, p.117-148.

Wohletz, K.H. and Sheridan, M.F. 1979. A model of pyroclastic surge. Geological Society of America Special Paper, No.180, p.177-194.

Plate 3.1. (a) Facies Association A: 2 fining-upward units with planar, erosive bases (although note the scour at the base of the upper unit). These represent the deposition of fine sediment over gravelly bars during waning flood events. The photograph was taken 2km east of Palet Çendik Motel (at TG545757).

(b) Facies Association A: Imbricated clasts of flaggy Miocene sandstone in conglomerates, 2km southwest of Kayi (TG439459).

(c) Facies Association A: Rhizocretions in red mudstone deposited on a fluviatile floodplain. Note the clinometer at the centre of the photograph for scale. The photograph was taken 3km southeast of Kayi (at TG479457).

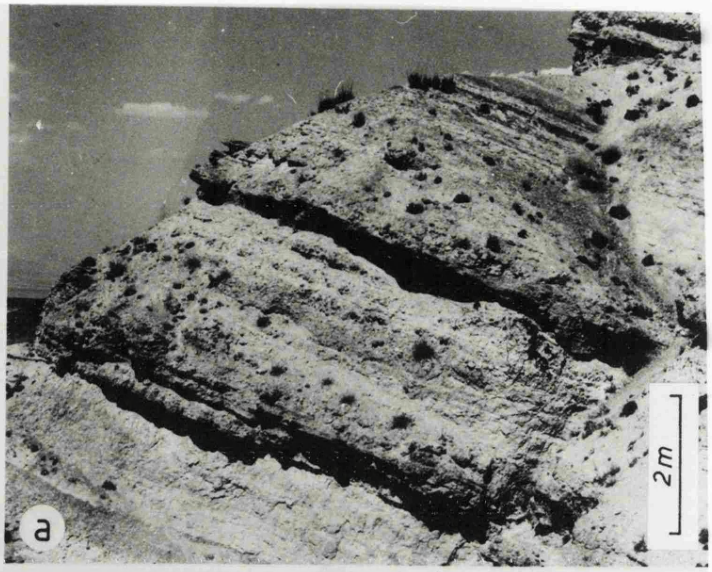

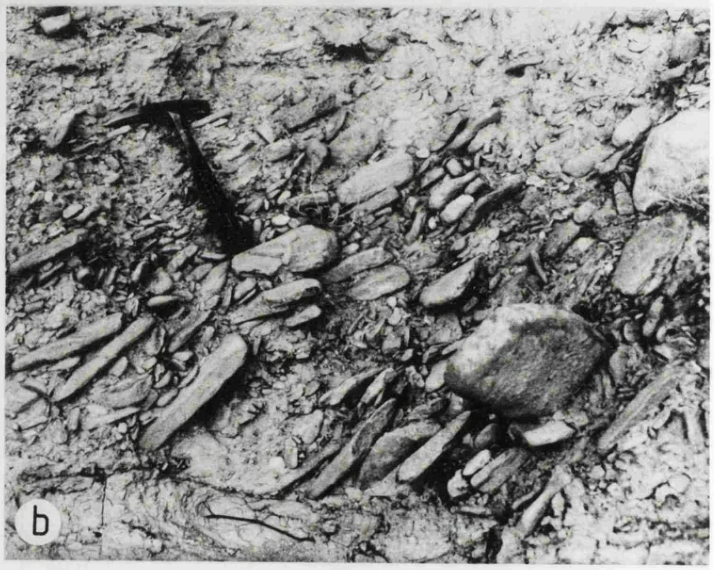

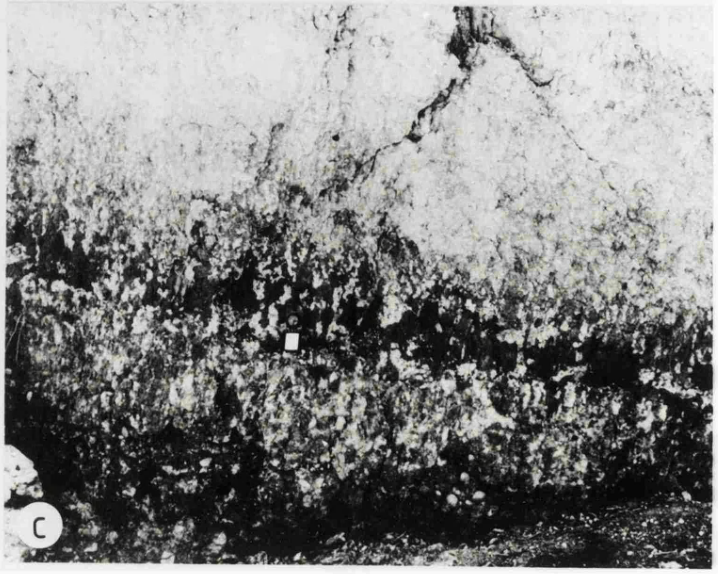

Plate 3.1.

Plate 3.2. (a) Facies Association B: Sub-spherical nodules of huntite ($CaMg_3(CO_3)_4$) in silty marls of the fan-delta plain environment. Note the slight flattening of the nodules parallel to bedding, which is horizontal. Huntite is a secondary carbonate, replacing dolomite, in freshwater environments. Its presence attests to high evaporation rates. The photograph was taken in the valley north of Soganli (at TG564625).

(b) Facies Association C: Inclined fan-delta foresets representing prograding mouth bars. Note the rapid grain-size transitions from fine sandstone (lighter) to coarse sandstone/conglomerate (darker). The latter probably represent the avalanche of coarse material down the foreset during flood events. The wet-sediment deformation is probably earthquake-induced. The photograph was taken 3km southeast of Kuruçay (at TG537677).

(c) Facies Association D: Opencast lignite mine near Kemer (TG424406). Lignites are interbedded with silty ostracodal marls.

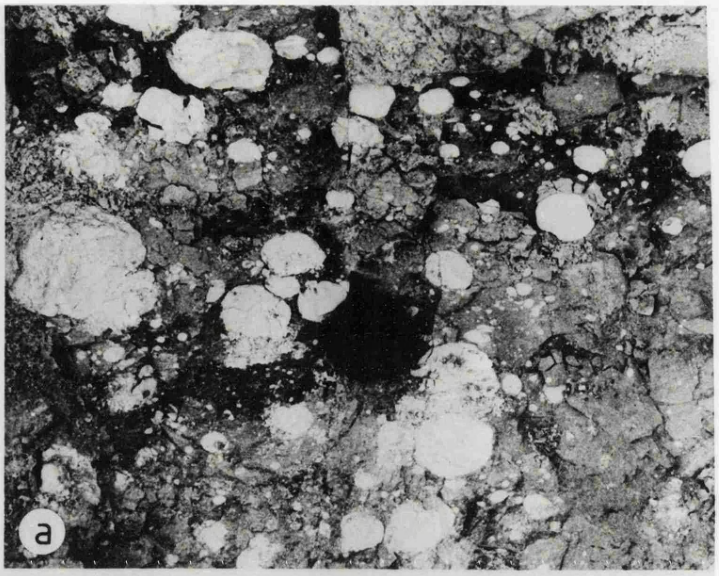

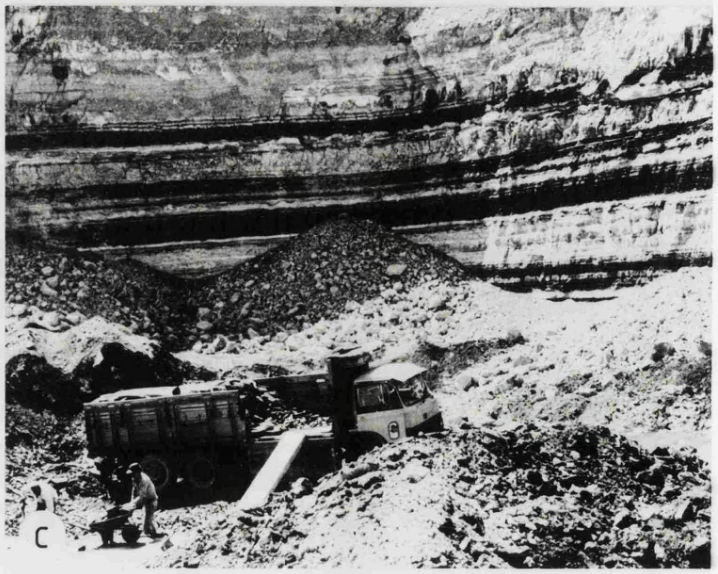

Plate 3.2.

Plate 3.3. (a) Facies Association E: Fine-grained sandstone with symmetrical ripples, indicating the action of free gravity waves. The high ripple index (≈12) suggests fairly deep water, indicating a submerged shoreline. The photograph was taken 3km southeast of Askeriye (at TG677802).

(b) Facies Association G: Lacustrine marl with organic-rich and organic-poor laminations. The organic-rich horizon above 5.5cm on the ruler has well developed internal laminations indicating an anoxic hypolimnion. Below this the organic-poor horizon is bioturbated indicating an oxic hypolimnion. The photograph was taken 2km south of Burdur (at TG609761).

(c) Facies Association G: The underside of a thin dolomicrite bed (not in situ) showing troughs of the dwelling burrow Arenicolites. The sample was collected 2.5km south of Burdur (at TG608755).

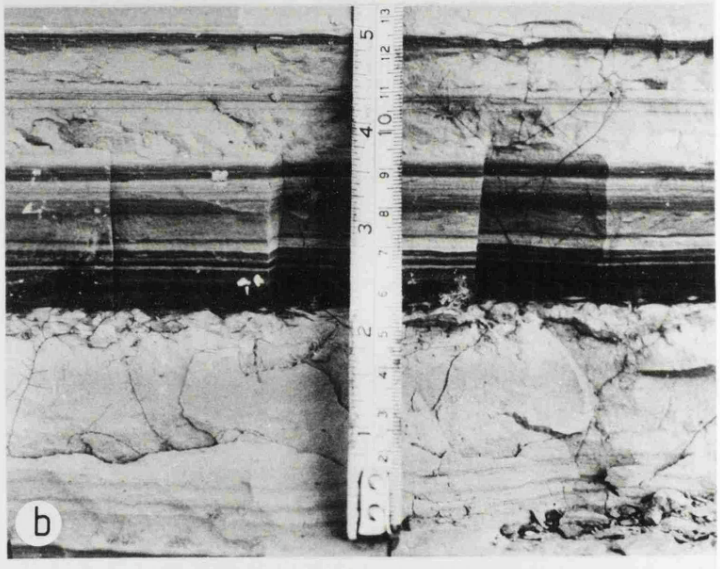

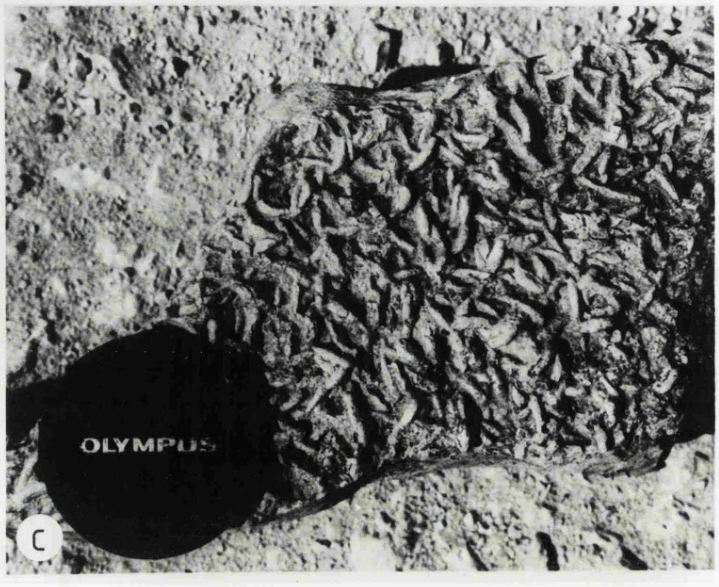

Plate 3.3.

Plate 3.4. (a) Facies Association H: A tuff/sandstone couplet within lacustrine marl. The contact between the lower tuff (light) and upper sandstone (dark) is deformed. The sandstone is composed of 2 medium to fine-grained fining-upward units. The contact between the sandstone and the overlying marl is gradational. The sandstones probably represent small turbidity currents into the lake caused by the sudden release of sediment-laden water ponded by air fall tuffs and agglomerates. These were deposited by the same eruption that produced the lower tuff unit. The photograph was taken 3.5km south of Burdur (at TG609748).

(b) Facies Association I: Sub-spherical pumice bombs within an air fall agglomerate 0.5km east of Yakaköy (at TG665759).

(c) Wet-sediment deformation caused by the loading of an air fall agglomerate (see Fig.3.1). Fine-grained sandstone (dark) has downwarped into silty marl (light) during sediment failure caused by increased pore fluid pressure. The photograph was taken 1.5km east of Yakaköy at TG674758.

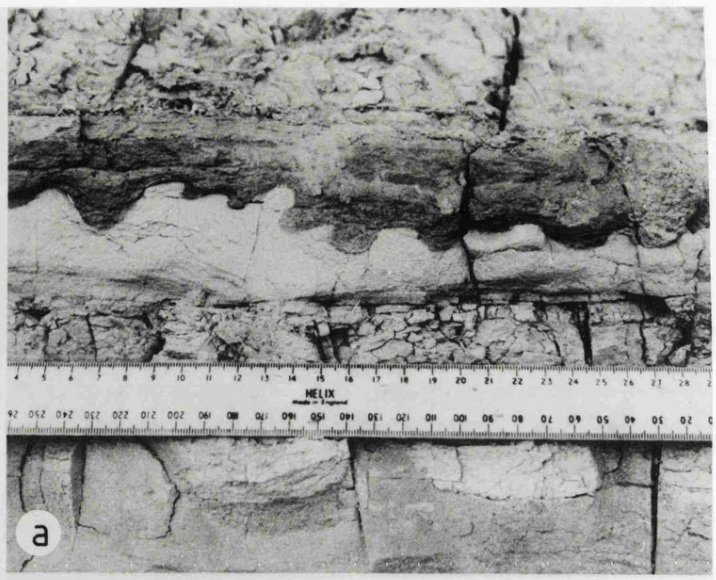

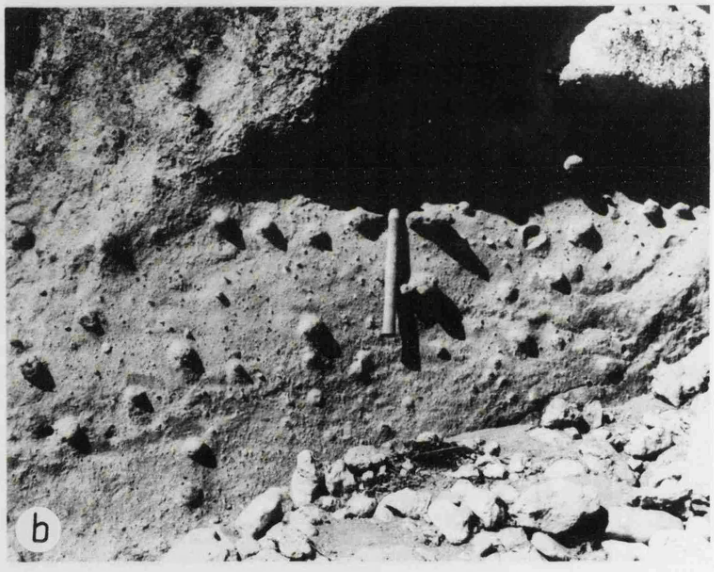

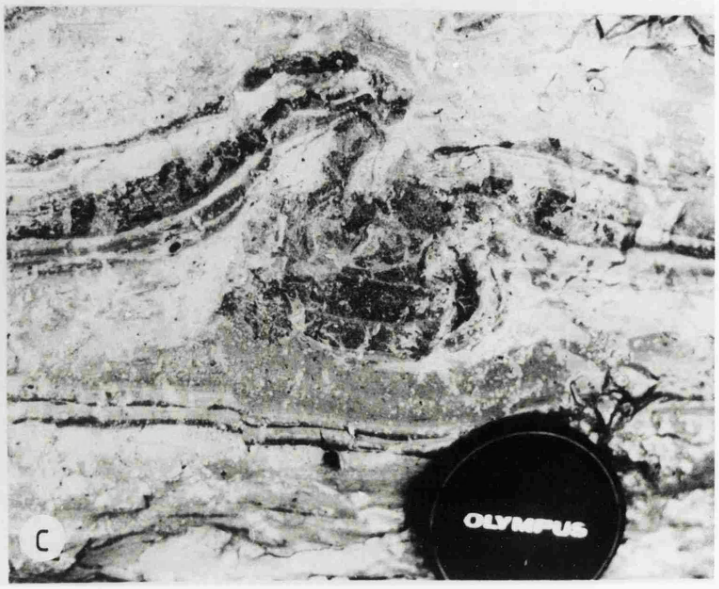

Plate 3.4.

Plate 3.5. (a) Facies Association I: Reverse-grading within an air fall agglomerate, possibly caused by vent widening during eruption, giving rise to a higher eruptive column. Note the compass for scale at the centre of the photograph. The photograph was taken 2km southwest of Yakaören at TG778838.

(b) Facies Association I: Proximal air fall agglomerate containing blocks to 40cm. The poorly-developed internal stratification indicates a pulse-like nature to the eruptive column. The photograph was taken 0.5km northeast of Gölcük lake (the volcanic centre) at TG801799.

(c) Facies Association J: Above the shoulders and below the shins of the geologist are planar-bedded base surge deposits. The lowermost of these are slightly gradational between sandwave and planar deposits (note the low-angle truncation to the right of the geologist's head). Between these 2 horizons is a 1.2m thick sequence of regularly alternating coarse ash and lapilli horizons possibly representing the settling of surges through a standing body of water. Short-lived isolated lakes were probably ponded against earlier surge and fall deposits. The 2 blocks which have impacted the sediment do not noticeably truncate laminae (compare with Plate 3.6a). This may be due to decceleration of the falling block through a water column. The photograph was taken 0.5km northeast of Gölcük lake (at TG797798).

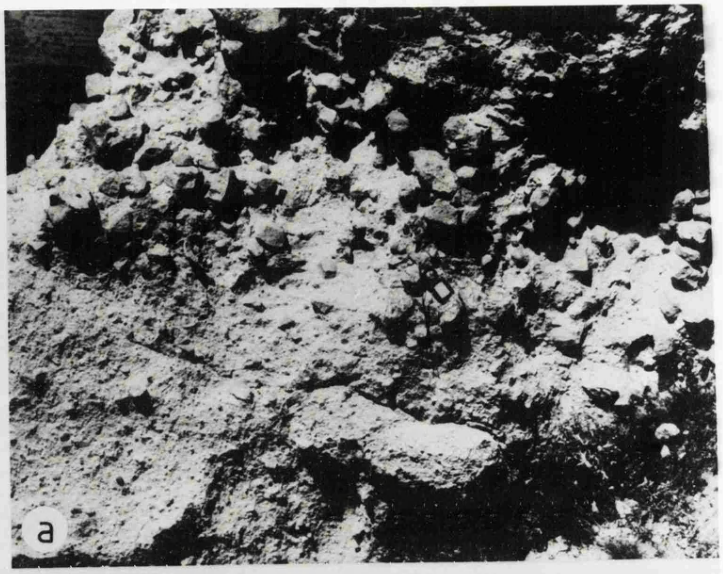

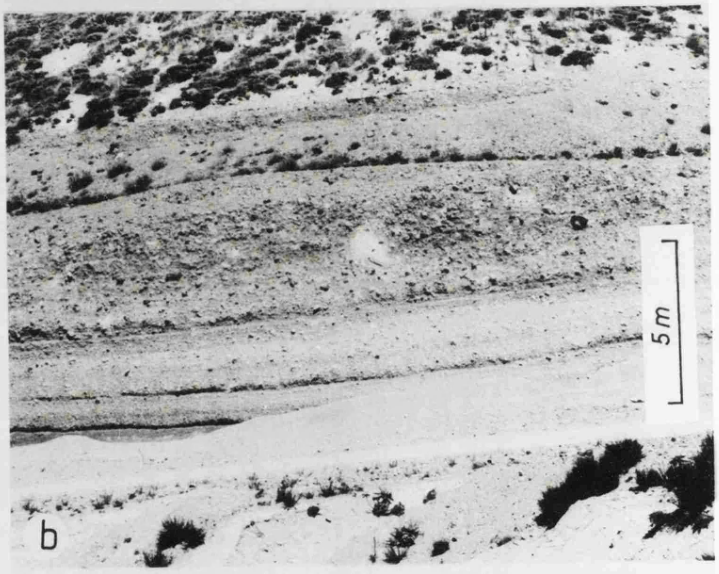

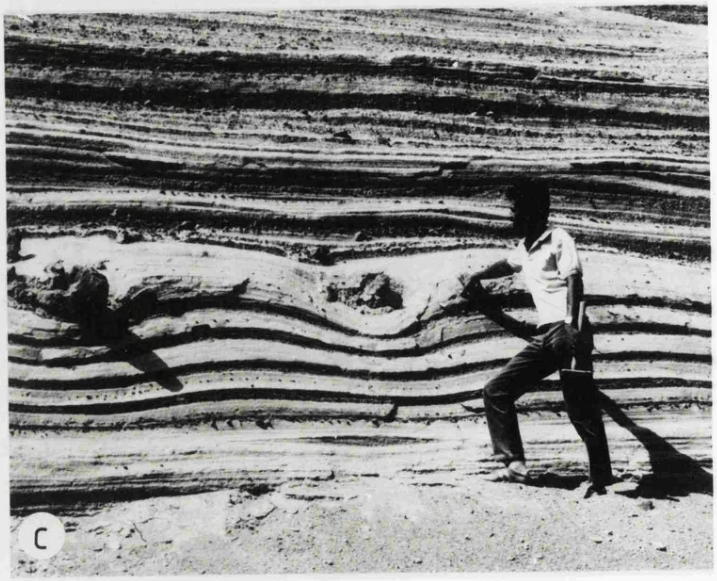

Plate 3.5.

Plate 3.6. (a) Facies Association J: A bedding sag caused by the impact of a balistically ejected andesite block into wet sediment, in this case a planar-bedded surge deposit. The photograph was taken 0.5km northeast of Gölcük lake (at TG800796).

(b) Facies Association J: Sandwaves within a base surge deposit. Flow was from the right of the photograph (the volcanic centre is 0.2km away in this direction). The bedforms are therefore slightly regressive indicating a relatively wet and cool flow. The photograph was taken at TG786798.

(c) Facies Association K: A matrix-supported massive conglomerate deposited by debris flow. Photograph taken 0.8km northwest of Gölcük lake at TG784801.

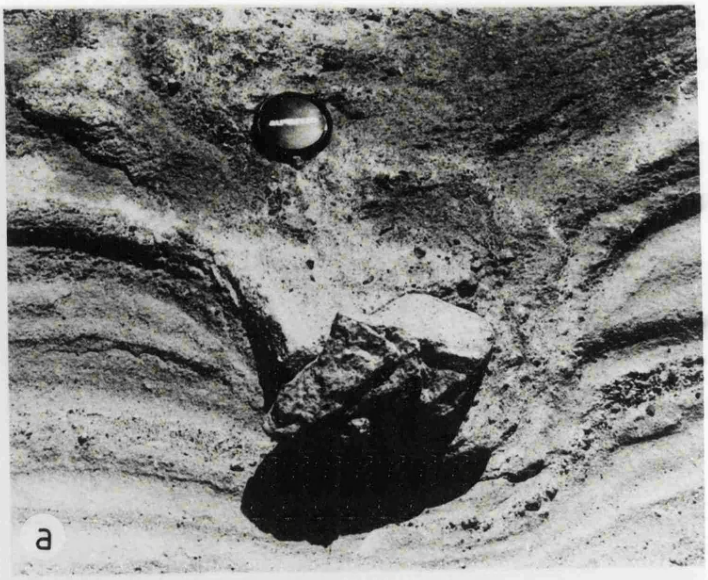

Plate 3.6.

CHAPTER FOUR.

A SPECTRAL AND GEOCHEMICAL STUDY OF CYCLIC SEDIMENTATION IN NEOGENE LAKE BURDUR, SW TURKEY.

4.1. INTRODUCTION

During the late Neogene the Burdur region was covered by a large lake occupying an area of about 400km² (Fig.4.1). This lake was contained within a half-graben with the boundary fault along its southeastern edge. Towards the end of the Pliocene the basin was dissected by renewed faulting, which uplifted the Neogene basinal succession in the footwall of faults, which now control the present day Burdur basin, containing modern Lake Burdur. The maximum thickness of the Neogene basin fill (the Burdur Formation) is 1200m, of which up to 850m was deposited in Pliocene Lake Burdur and forms the Akdere Member (Fig.4.2). The basin system is entirely continental and, according to the altitude curve for Anatolia published by Sengör et al. (1985), has been at an altitude of about 800 to 1000m since its formation in the Neogene. The present altitude of Lake Burdur is 854m.

The lacustrine sediments comprising the Akdere Member are dominantly fine-grained carbonates, believed to be inorganically precipitated with variable clay and organic carbon contents. These can be sub-divided into a nearshore lacustrine facies association, containing abundant cross-bedded sandstone units, travertines and organic-poor ostracodal marls, and an offshore lacustrine facies association containing interbedded organic-rich and organic-poor unfossiliferous marls. Organic-rich/organic-poor cycles in this latter group are well-developed and have a periodicity of a few metres. The laminated (but occasionally bioturbated) organic-rich horizons are of similar thickness to the intensely bioturbated organic-poor horizons. These cycles overprint smaller scale cycles between organic-rich and organic-poor marl, which are preserved in the organic-rich horizons. These small-scale cycles have a periodicity of a few centimetres (Fig.4.3, Plate 4.1) and the organic-rich marls are laminated.

The purpose of this study is firstly, using Walsh Power spectra analysis, to detect the periodicity of the large-scale cyclicity observed within

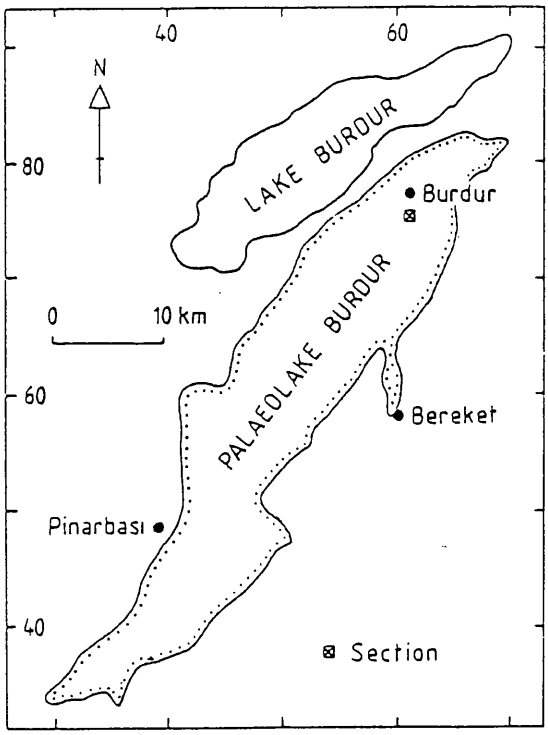

Fig.4.1. Map showing the approximate position of Palaeolake Burdur compared with modern Lake Burdur. The cross south of Burdur shows the position of the sampled locality.

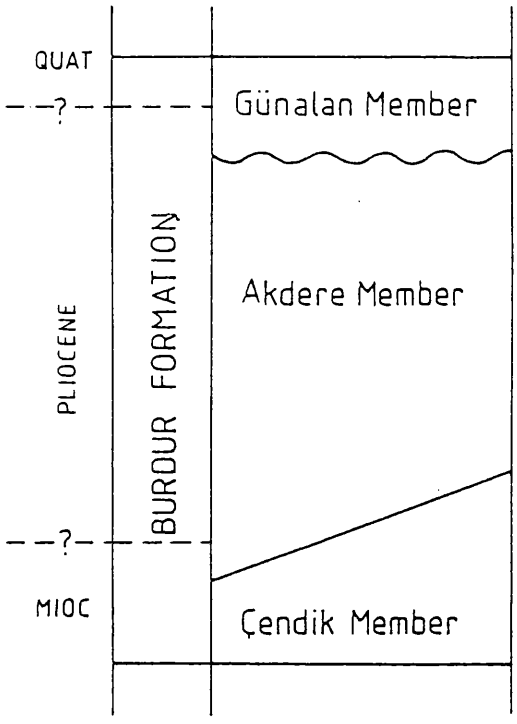

Fig.4.2. Stratigraphic units of the Burdur Formation.

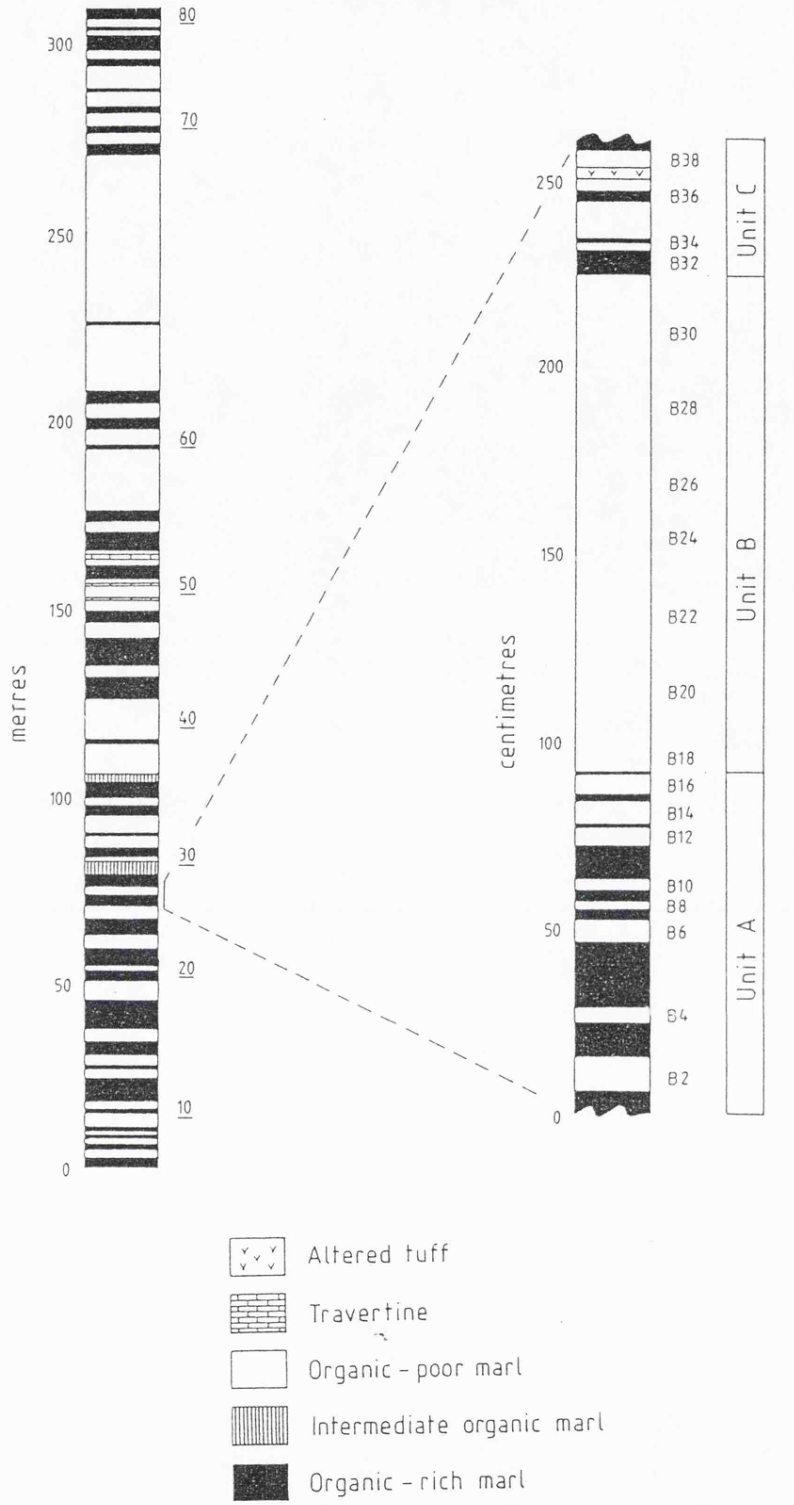

Fig.4.3. The left-hand column shows the Akdere Member succession 1km south of Burdur. There is a cyclicity of organic-rich / organic-poor marl of the order of a few metres. (Bed numbers are shown on the right-hand side of this column). The right-hand column is an expanded view of beds 25, 26 and 27 (units A, B and C respectively). An organic-rich/organic-poor marl cyclicity of the order of tens of centimetres is apparent at this scale. (Sample numbers are shown on the right-hand side of this column).

the offshore lacustrine facies association and, secondly, by studying a single couplet, to determine the nature of the cyclicity geochemically. Finally, a comparison is made with the palaeolake system at the time of ostracodal marl deposition.

4.2. SAMPLE ACQUISITION AND TREATMENT.

4.2.1. Field Sampling and Sample Preparation.

The samples were collected from the well-exposed section along the mountain road, 2km south of Burdur. This is the type section for the Akdere Member and ostracodes from the section indicate a possible late Miocene age (Gökçen, N. pers. comm., 1988). Organic-rich, organic-poor cycles on the scale of a few metres are well-developed in the lower part of the section and sampling was undertaken across one of these cycles in beds 25, 26 and 27 (throughout this study, called unit A, unit B and unit C respectively) at TG607759 (Fig.4.3). Unit A and unit C are both dark grey organic-rich units, characterized by organic-rich / organic-poor couplets on the scale of a few centimetres. Unit B is organic-poor and well-bioturbated (Plate 4.1). After making a detailed graphic sedimentary log across units A, B and C, samples were collected from organic-rich and organic-poor horizons. After removing weathered surface material, an orientated sample weighing about 0.2kg was cut loose and placed in a sealed plastic bag to avoid deterioration due to desiccation. Ostracode samples were taken from horizons stratigraphically higher in the Akdere Member, along the same road. For each sample about 1kg of rock was taken and transported to the laboratory in a sealed plastic bag, where it was broken into smaller fragments and immersed in H_2O_2 solution to break down the marl. After wet-sieving of the residue, the 125μm fraction was taken and ostracodes were separated from the calcium carbonate matrix using a vacuum syringe.

4.2.2 Analytical Techniques.

(a) X-Ray Diffraction.

Finely ground powders were mixed with acetone on a glass slide and analysed on a Philips PW-1050/25 diffractometer with a Philips PW-1729 generator using Cu K-alpha radiation. Each sample was scanned in the

range 25° to 32° 2θ and the major reflections of calcite, aragonite and dolomite were compared with mixtures of known composition to calculate the bulk percentage of each of the carbonate constituents (Royse et al. 1971). Calibration mixtures were made from standard laboratory analytical calcite, skeletal aragonite (prepared from a Pinctada shell) and sample B-2, whose only carbonate component was dolomite. The degree of ordering within the dolomites was determined by examining XRD reflections between 2θ values of 32 and 40° and 66 and 72°. These were compared with reflections from well-ordered "ideal" dolomites from Gabbs, Nevada and Binnental, Switzerland (Goldsmith and Graf 1958a, p.684-5). The stoichiometry of the dolomites was determined using the relationship of Ca-content to d_{104} spacing (Goldsmith and Graf 1958b).

(b) Trace Elements.

After leaching each sample with 25% HCl in a 50°C bath for 12 hours, elemental concentrations were determined using a Philips PV-8050 emission spectrometer with a PV-8490 inductively coupled plasma (ICP) source attached. This was calibrated for carbonates with an analytical calcium carbonate standard. Ca, Mg, Sr and Na elemental concentrations were measured for each sample.

(c) Stable Isotopes.

Carbonate samples were analysed for carbon and oxygen isotope compositions on a VG Isogas mass spectrometer at the Department of Geology, University of Liverpool. Organic material was first removed by treating the samples in a plasma asher for 2 hours. Then 3mg of sample was reacted with 4ml of 100% phosphoric acid to liberate CO_2. The isotopic composition of the CO_2 was then measured relative to an internal laboratory standard of Lincolnshire Limestone and corrections were made according to Craig (1965). The results are expressed in the standard δ notation relative to the Peedee Belemnite (PDB). The instrumental precision of the results is 0.2 permil. The samples analysed from the section are multi-mineralic and were therefore reacted with phosphoric acid at different temperatures, depending on the bulk percentage of dolomite. All samples containing more than 10% dolomite were reacted at 50°C and their isotope ratios calculated using the known phosphoric acid fractionation factor for dolomite at 50°C (1.01011). For samples containing 100% dolomite, the value given will obviously be correct.

However, for those which contain less than 100% dolomite, which were run as dolomites (e.g. at 50°C using the phosphoric acid fractionation factor for dolomite at 50°C), their compositions must be recalculated using a fractionation factor for calcite at 50°C to give 2 end-members (and hence an error bar). The phosphoric acid fractionation factor for calcite at 50°C is determined experimentally by running a Lincolnshire Limestone laboratory standard at 25°C and 50°C. The difference in the δ^{46} value for the standard run at 25°C and 50°C is 1.225 permil (see Table 1), so the newly calculated fractionation factor for calcite at 50°C will be 1.008885, resulting in a depletion in $\delta^{18}O$ of 1.22 permil for a sample which is 100% calcite/aragonite and which was initially run at 50°C using the fractionation factor for dolomite at 50°C. The dilution of dolomite by calcite and/or aragonite, will decide the size of the error bar.

4.3. DOLOMITE ORDERING AND STOICHIOMETRY.

Fig.4.4 (B-10) shows the typical pattern for dolomite from the studied section. The (0012) reflection is slightly attenuated and displaced from the position of the well-ordered dolomite and is also more depressed than the (030) reflection of the same sample. The ratio of the integrated intensity of (015), one of the principal ordering reflections, to (110) is lower than that for the well-ordered dolomite. These changes are due to replacement of Mg in the lattice by Ca and the weak reflections observed indicate a less-ordered structure than the ideal dolomite.

The stoichiometry of the dolomites was determined using the relationship of Ca-content to d_{104} spacing (Goldsmith and Graf 1958b). The following equation relating these two factors (from Lumsden 1979), was used to determine the molar percentage of CaCO3 within the dolomite:

$$N_{CaCO3} = M\,d + B \qquad \text{(eq.1)}$$

where N_{CaCO3} is the molar percentage of CaCO3 in the dolomite lattice, d is the observed d spacing in Å units (from the XRD trace) and M and B are constants (333.33 and -911.99 respectively). The results (Table 2) show that the dolomite is non-stoichiometric, containing 51.06 to 61.80 Mol% CaCO3. Previous studies of dolomitic limestones have shown that the degree of Ca-enrichment in the dolomite correlates with the abundance of a separate calcite phase (Füchtbauer and Goldschmidt 1965, Schmidt 1965,

Phosphoric Acid Fractionation Factors

Calcite @ 25°C 1.01025
Dolomite @ 50°C 1.01011

Lincolnshire Limestone (calcite) standard

$\delta^{46}_{25°C}$ +0.362
$\delta^{46}_{25°C}$ −0.863
1.225 permil

So, Calcite @ 50°C = (1.010250 − 0.001225)
= 1.008885

Therefore, there will be a DEPLETION in $\delta^{18}O$ of (1.01011 − 1.008885) or 1.22 permil for a 100% calcite sample initially run as a dolomite at 50°C.

Table 1. Table showing errors incurred in a $\delta^{18}O$ analysis by running a calcite sample at 50°C using the dolomite phosphoric acid fractionation factor.

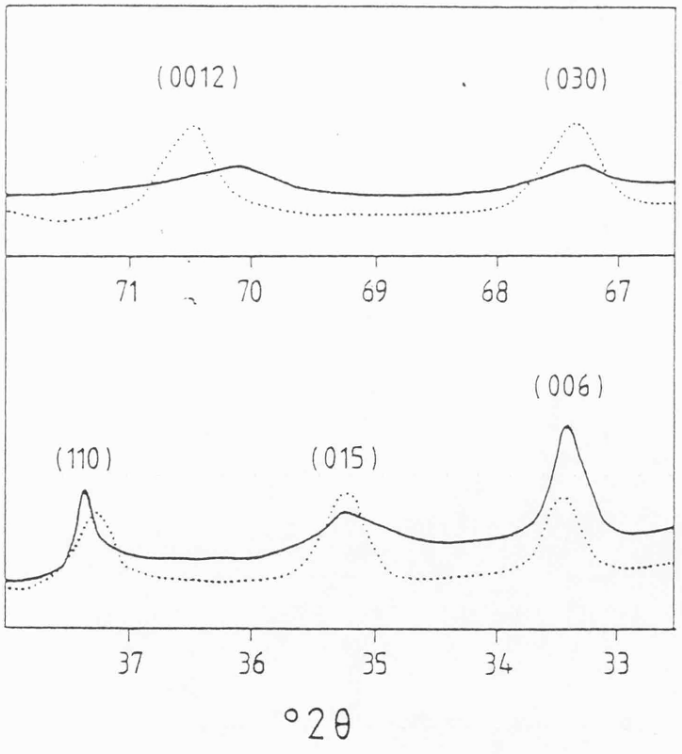

Fig.4.4. XRD trace of 100% dolomite sample B-10 (solid line) compared with that of a well-ordered "ideal" dolomite from Binnental, Switzerland (dotted line) (after Goldsmith and Graf 1958b). The y-axis indicates relative intensity.

Table 2. Geochemical Results.

Sample No.	Bulk % Dolomite	Bulk % Calcite	Bulk % Aragonite	Mol % $CaCO_3$ in Dolomite	%I.R.	$\delta^{18}O$	$\delta^{13}C$	Wt.% Ca	Mg	$x10^3$ ppm Na	Sr
Sampled Section at TG607759											
B1	31	38	31	56.57	65.4	-2.482	0.955	9.96	3.94	3.96	0.327
B2	100	-	-	57.50	22.2	2.946	1.154	17.80	10.15	1.49	0.805
B3	30	35	35	56.87	69.6	-3.683	0.147	8.14	3.78	3.83	0.239
B4	97	3	-	55.63	20.6	2.851	1.360	18.39	9.95	2.00	0.763
B5	58	42	-	56.87	67.4	-2.459	1.624	9.10	4.16	2.47	0.301
B6	100	-	-	52.27	18.6	3.639	-0.701	20.32	11.60	2.02	0.925
B7	52	48	-	59.33	67.4	-4.617	-0.319	6.00	3.83	1.07	0.181
B8	100	-	-	55.93	17.2	-	-	21.43	11.24	1.90	0.937
B9	37	40	23	59.03	76.0	-4.835	-0.656	6.70	4.06	0.86	0.207
B10	100	-	-	53.50	28.2	4.133	-0.715	19.11	10.72	1.53	0.907
B11	21	32	47	55.03	65.6	-2.466	1.923	12.80	4.54	1.70	0.591
B12	92	8	-	55.33	23.2	3.255	-0.197	19.95	9.87	1.62	0.860
B13	79	21	-	60.57	56.0	0.986	0.688	11.71	6.79	0.26	0.469
B14	92	8	-	56.27	28.4	2.213	2.195	20.53	9.32	1.53	0.893
B15	28	43	29	56.57	35.0	-2.552	2.430	12.69	5.29	1.25	0.534
B16	7	18	75	57.50	39.6	-1.198	4.053	18.78	4.36	2.68	1.084
B17	50	11	39	58.73	25.4	-0.744	3.258	17.26	6.81	2.13	0.822
B18	84	6	10	55.33	26.6	2.309	2.933	19.53	9.06	1.52	0.818
B19	10	14	76	59.33	30.2	-0.247	4.283	23.26	4.83	2.78	1.220
B20	11	13	76	55.63	36.4	-	-	23.54	4.53	2.93	1.190
B21	17	11	72	58.10	37.4	-0.742	3.441	21.63	5.59	2.14	1.142
B22	59	28	17	55.93	34.8	-0.418	4.145	18.50	6.96	0.84	0.745
B23	8	23	69	58.40	21.2	-0.715	3.958	23.00	3.90	1.89	1.103
B24	13	16	71	57.80	31.8	-1.071	4.136	22.19	4.58	2.25	1.148
B25	7	18	76	56.27	11.8	-0.871	4.261	24.35	3.78	2.53	1.248
B26	5	22	73	56.27	38.8	-1.321	4.017	23.86	3.70	2.60	1.183
B27	11	18	71	58.40	39.4	-2.143	3.730	24.90	4.86	3.41	1.320
B28	10	4	86	60.57	36.4	1.302	4.064	24.18	5.70	3.81	1.336
B29	10	10	80	56.57	38.6	0.680	4.058	24.56	5.33	3.48	1.339
B30	7	13	80	57.50	42.8	0.374	4.324	25.00	4.70	4.17	1.287
B31	7	11	81	58.10	37.6	0.989	4.057	21.24	4.31	2.79	1.120
B32	36	23	41	56.57	58.2	-0.560	2.985	12.95	4.46	0.42	0.641
B33	92	8	-	55.33	26.2	3.251	2.258	18.47	9.40	1.12	0.688
B34	63	37	-	55.03	67.0	-	-	7.64	4.47	-	0.283
B35	100	-	-	51.06	18.8	4.414	1.015	21.28	11.78	1.84	0.820
B36	32	40	28	59.33	49.6	-1.071	1.831	12.69	3.92	0.81	0.460
B37	51	34	15	58.10	44.2	0.070	1.928	17.30	5.14	1.16	0.613
B38	82	18	-	61.80	25.0	-	-	17.42	7.55	1.98	0.560
B39	49	31	19	54.43	49.8	-0.388	1.076	14.23	5.41	2.26	0.457
Ostracodes at TG607759											
MP4	-	100	-	-	-	1.487	-1.210	-	-	-	-
MP5	-	100	-	-	-	0.809	1.182	-	-	-	-
MP8	-	100	-	-	-	-0.890	-0.700	-	-	-	-
MP13	-	100	-	-	-	-1.723	0.381	-	-	-	-
MP18	-	100	-	-	-	-1.319	0.081	-	-	-	-
MP19	-	100	-	-	-	2.720	0.076	-	-	-	-
MP107	-	100	-	-	-	2.819	-1.346	-	-	-	-
(Matrix)	-	100	-	-	-	-5.291	2.315	-	-	-	-
MP108	-	100	-	-	-	0.055	0.065	-	-	-	-
(Matrix)	-	100	-	-	-	-4.514	2.904	-	-	-	-

Shinn et al. 1969, Andrews et al. 1987). Although there appears to be no clear relationship in the dolomites from the studied area, samples consisting of 100% dolomite have the lowest Ca-content (Fig.4.5). This suggests that complete dolomitization was accompanied by the formation of near-stoichiometric dolomite.

The lack of a well-ordered structure and the non-stoichiometry of the dolomite from the studied section indicates that they are metastable non-ideal calcian dolomites. Their presence in the samples suggests that the rock has undergone little, if any, alteration since the Upper Miocene / Lower Pliocene. All Recent lacustrine dolomites described in the literature are poorly-ordered calcian dolomite (e.g. Peterson and Bien 1963, Alderman and Skinner 1957).

4.4. CYCLIC SEDIMENTATION.

4.4.1. Periodicity of Cycles.

(a) Technique

Stratigraphic sections in which a few lithologies alternate can easily be digitized to produce a discontinuous time series (e.g. a sequence of parameter values occupying only a few states obtained at a constant time interval). Walsh power analysis can be used to analyse such discontinuous time series in order to detect the periodicity of regular sedimentary cycles (Weedon 1989). To perform a Walsh power analysis on a given stratigraphic section it must have sharp lithological transitions, each lithology should have planar geometry, the thickness of each bed must be related to the time taken to deposit it and exposure must be continuous (Weedon 1989). All but the last condition are satisfied by the measured section in Fig.4.3. In this section there is a non-exposed horizon at 175-180m (below bed 58). The section was therefore split into 2 time series, each analysed separately. The Walsh technique restricts the data set to 2^k points, where k is an integer, so that an upper section of 8192cm and a lower section of 16384cm was analysed. To reduce computing time a point every 2cm was taken reducing the upper section to 4096 points and the lower section to 8192 points. To check for consistency the lower section was also divided into 2 equal sections of 4096 points which were analysed separately (Fig.4.6).

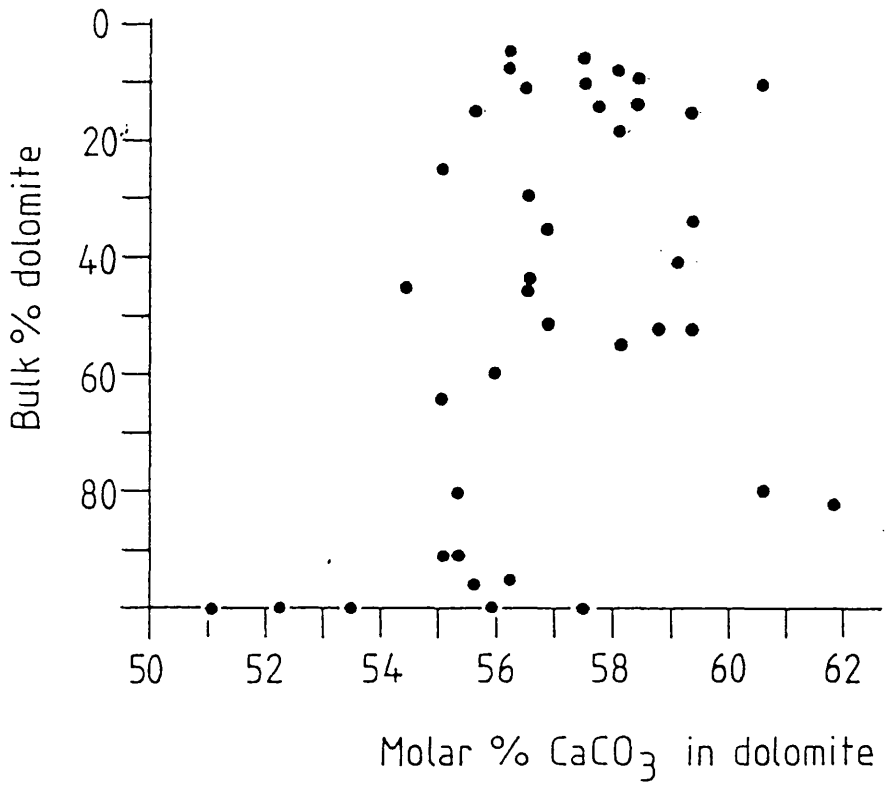

Fig.4.5. The relationship between the bulk % dolomite and the molar % $CaCO_3$ in dolomite of samples from the studied section.

Mg/Ca ratio	Primary carbonate	Secondary carbonate
<2	low-Mg calcite	none
2-7	high-Mg calcite	none
7-12	high-Mg calcite	dolomite
>12	aragonite	none
v.high	hydrous Mg carbonates	

Table 3. Table showing the carbonate phase precipitating from waters of varying Mg/Ca ratio (after Müller et al. 1972).

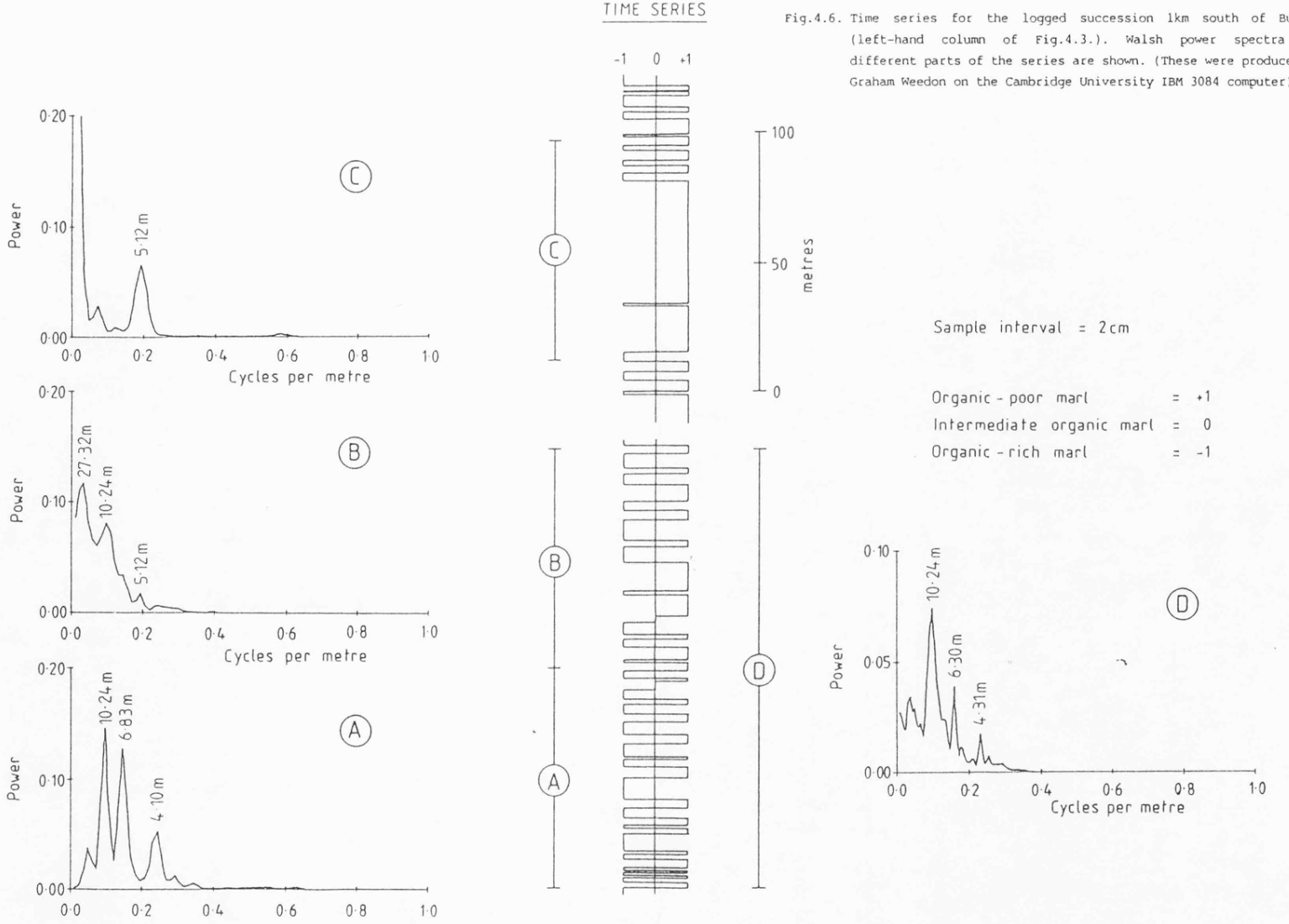

Fig.4.6. Time series for the logged succession 1km south of Burdur (left-hand column of Fig.4.3.). Walsh power spectra for different parts of the series are shown. (These were produced by Graham Weedon on the Cambridge University IBM 3084 computer).

Graham Weedon performed the analyses on the Cambridge University IBM 3084 computer. (For a full account of the technique see Beauchamp 1984).

(b) Results

The spectra produced by the Walsh analysis are shown in Fig.4.6. The complete lower spectrum shows 3 peaks with cycles of 10.24m, 6.30m and 4.31m in thickness. These peaks are distinct from the background noise levels. However, the data does not appear to be stationary as can be seen when the section is divided in 2 to give an upper and a lower spectrum. A general shift in the spectra (in terms of background noise) towards lower frequencies is seen going up section. This shift may be related to an increase in sedimentation rate with time. However, the position of the peak at 10.24m does not change suggesting otherwise.

Actual sedimentation rates can be calculated for the sediments in the section by measuring the thickness of lamination couplets assumed to be lacustrine "non-glacial varves" (i.e. Kelts and Hsü 1978). These vary from 0.46 to 0.70mm (average 0.55mm with 2σ of 0.26mm) suggesting an average sedimentation rate of 55cm/ka. Preliminary varve thickness studies do not indicate changing sedimentation rates through the section. Also there is no change in the lithological character of the sediments throughout the section (below the non-exposed horizon). This, together with the constancy of the 10.24m peak suggest constant sedimentation rates. Applying the 0.55cm/ka sedimentation rate to this 10.24m cycle gives a periodicity of 18.62ka.

The spectrum for the section above the non-exposed horizon (Fig.4.6) shows a peak corresponding to a cycle of 5.12m thickness and another corresponding to a low-frequency cycle. The low-frequency cycle is a consequence of the homogenization of horizons by intense bioturbation. Interestingly, there is no peak at 10.24m in this section. It is unlikely that such a low-frequency peak has been removed by bioturbation. A possible explanation for its absence is the fact that the sediments from this section were deposited in a slightly different environment, perhaps less sensitive to the driving-force of this frequency. This change in environment is seen by the gradual introduction of ostracodes.

4.4.2. Geochemical Results and Discussion.

(a) Sediment Texture.

Several samples from the section were examined under the Scanning Electron Microscope. Carbonate grains dominate each sample. These are idiomorphic to hypidiomorphic and of fairly uniform grain-size, ranging from 3 to 15μm. Clay content is variable.

Samples from the organic-poor horizons consist mainly of idiomorphic dolomite rhombs with well-defined crystal edges. These are in contact with allotriomorphic dissolution surfaces (Plate 4.2a) on other carbonate grains. Clay content is generally low, although occasional undisturbed laminae exist. In these, clay grains are unflocculated and aligned (Plate 4.2b).

Samples from the organic-rich horizons consist of idiomorphic aragonite needles to 20μm in length and blocky calcite and/or dolomite grains (Plate 4.2c). The aragonite grains always have well-defined fresh crystal edges, whereas although idiomorphic, the more blocky dolomite grains appear to show some signs of dissolution, with some crystal faces being slightly etched. Clay is generally common and evenly distributed throughout the samples as small flakes generally less than 3μm in diameter. In some samples well-rounded, spherical quartz grains to 10μm across are present and the clays wrap around these detrital grains, showing their primary origin (Plate 4.2d).

(b) Mineralogy.

Calibration of X-Ray Diffraction reflections against those of known mixtures shows regular variations in bulk carbonate composition throughout the section (Table 2). In units A and C, the organic-poor horizons are generally purely dolomitic, whereas the organic-rich horizons contain less dolomite with varying amounts of low-Mg calcite and aragonite (on average 43% dolomite, 36% low-Mg calcite and 21% aragonite). Unit B, with the exception of sample B-22, is dominated by aragonite, containing on average 76% aragonite, 14% low-Mg calcite and 10% dolomite (Fig.4.7).

By studying the water chemistry and mineralogy of modern lakes Müller et al. (1972) showed that the mineralogy of inorganic lacustrine Ca-Mg carbonates is related to the Mg/Ca ratio of the lake waters from which

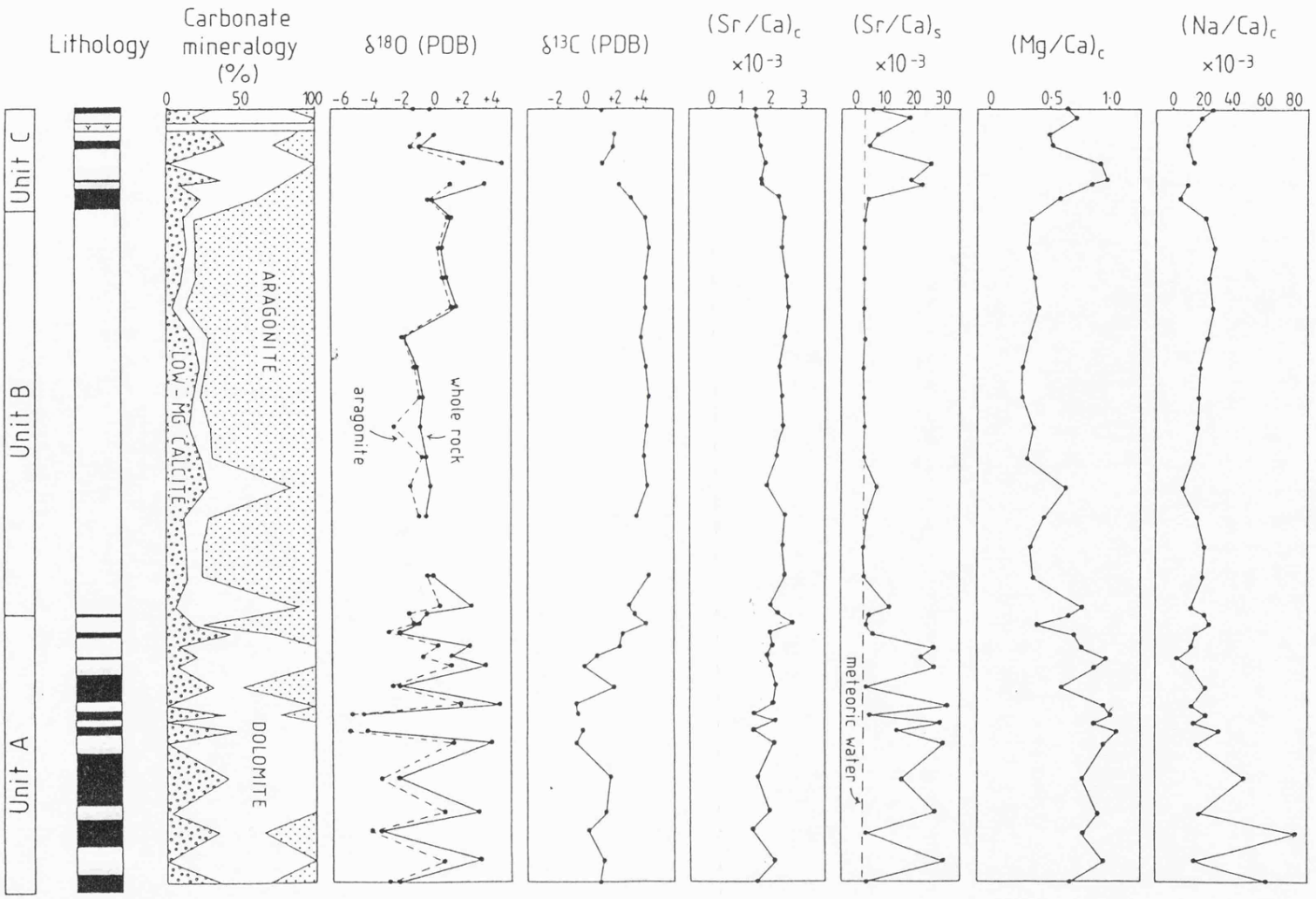

Fig.4.7. Mineralogical and geochemical results for the sampled section (right-hand column of Fig.4.3.).

they precipitated or the pore waters with which they are in contact. General water chemistry, salinity, pH and Eh do not seem to affect this relationship. At low Mg/Ca ratios (less than 2) low-Mg calcite precipitates with high-Mg calcite forming in the range of 2-12 and aragonite forming at values of greater than 12. Lacustrine dolomite, according to Müller et al. (1972), forms by the early diagenetic replacement of high-Mg calcite at elevated Mg/Ca ratios (in the range 7-15). At very high Mg/Ca ratios hydrous Mg-carbonates can be expected. (These observations are summarized in Table 3). Therefore, in "stationary" lakes with minor fluctuations in water volume, only one of the above carbonate phases will be found, whereas in "dynamic" lakes with major fluctuations, 2 phases, and in extreme cases, 3 phases will be found. So, the following main groups of carbonate assemblages within a lacustrine sediment are possible, depending on the Mg/Ca ratio of the lake and its annual variation:

(i) Low-Mg calcite and/or high-Mg calcite (e.g. Lake Constance, Switzerland; Lake Manyara, Tanzania).

(ii) High-Mg calcite, aragonite, dolomite, huntite and magnesite (e.g. Tuz Lake and Acigöl, Turkey).

(iii) Aragonite (e.g. Lake Burdur and Lake Van, Turkey).

Sediments from the studied section contain low-Mg calcite, aragonite and dolomite in varying amounts. Any primary high-Mg calcite has presumably been completely replaced by dolomite. This is not surprising as these sediments would have sat below the water table and been surrounded by pore waters of varying Mg/Ca ratio until they were uplifted in late Pliocene/early Quaternary times, about 3Ma after their initial formation. However XRD traces of the organic-rich samples B-5, B-15 and B-36 show very small reflections at 30.1° 2θ, indicating the presence of minor, unquantifiable high-Mg calcite. The presence of both low-Mg calcite and aragonite in the same sediment sample would require a major change in the Mg/Ca ratio of the lake water and, therefore, probably the lake volume, during the time taken to deposit it (probably a few hundred years). However, the thickness of the offshore lacustrine sequence in the Burdur Formation (approximately 250m) and the lack of any evidence of subaerial exposure (desiccation cracks, rootlet horizons etc.) indicate a fairly deep lake with little variation in water volume. The studied section near

to Burdur is situated near to the footwall margin of the asymmetrical half-graben and therefore near to the deepest part of the lake. Therefore only complete desiccation of the lake would result in the presence of desiccation features in the section and it is not surprising that they do not exist. In the studied section, an increase in the dolomite content of the sediment is generally at the expense of aragonite, with the low-Mg calcite content remaining fairly static. This may indicate that the low-Mg calcite is allochthonous and was introduced to the lake by wind. In Holocene sediments from Lake Balaton, Hungary, low-Mg calcite is believed to be allochthonous (Müller and Wagner 1978). However in these sediments most of the allochthonous grains are of sand grade, whereas in the studied section sand grains are rare. If low-Mg calcite is allochthonous, then its absence in organic-poor horizons units A and C has to be explained.

Ignoring considerations about the origin of low-Mg calcite, it is thought, based on Müller et al. (1972), that unit B, which is dominated by aragonite, formed at times of increased lake water Mg/Ca ratio (generally greater than 12) and units A and C, with increased dolomite (and hence precursor high-Mg calcite), formed when the lake had lower Mg/Ca ratios (generally less than 12).

(c) Minor Elements.

(i) Strontium.

The variation in Sr content throughout the studied section is shown in Table 2. There is a wide variation in Sr throughout the section with values varying from 181ppm to 1339ppm. The maximum Sr values (>1200ppm) occur towards the top of unit B. The variations observed are largely a mineralogical effect, caused by the preferential incorporation of Sr into the large cell of orthorhombic aragonite compared with dolomite and aragonite (Veizer 1983). The Sr content of horizons in which the carbonate is entirely dolomite (B-6, B-8 and B-10) is just above 900ppm.

The distribution coefficients ($\underline{D}$) for $Sr_{dolomite}$, $Sr_{calcite}$ and $Sr_{aragonite}$ are poorly understood. Temperature and kinetic factors (in particular rate of precipitation) will influence $\underline{D}$ values and any quoted value must therefore be considered at best an order of magnitude estimate (Veizer 1983). However, for our purposes, trends outweigh absolute values

in importance and therefore only a crude estimate of initial lake water composition is required. Veizer (1983) gives a summary of reported $\underline{D}$ values for trace elements in the common carbonate minerals. The $\underline{D}^{Sr}_{dolomite}$ values he cites vary between 0.025 (Katz and Matthews 1977) and 0.07 (Jacobson and Usdowski 1976), the latter best fitting the observed range of Sr in early diagenetic dolomite. Sr substitutes mostly in the Ca positions of the dolomite lattice, so $\underline{D}^{Sr}_{dolomite}$ should be about half the value of $\underline{D}^{Sr}_{calcite}$ (Behrens and Land 1972, Kretz 1982). Therefore $\underline{D}^{Sr}_{calcite}$ is taken as 0.13 (Veizer 1983). The $\underline{D}^{Sr}_{aragonite}$ values cited by Veizer (1983) vary between 0.9 and 1.2, so an average value of 1.05 was taken. Using these values ($\underline{D}^{Sr}_{dolomite}$=0.07; $\underline{D}^{Sr}_{calcite}$=0.13; $\underline{D}^{Sr}_{aragonite}$=1.05) and the expression:

$$\left(\frac{m_M}{m_{Ca}}e\text{-}\right)_c = D^M{}_e \left(\frac{m_M}{m_{Ca}}e\text{-}\right)_s \qquad \text{(eq.2)}$$

where M_e is the trace element under consideration, m is the molar concentration and "c" and "s" represent the solid carbonate mineral and the solution respectively, the approximate Sr/Ca ratios of the precipitating lake waters can be calculated. These values were obtained by calculating the relative contribution of each of the three carbonate phases in each sample to the overall Sr/Ca ratio of the sample. This method assumes that the three phases in each sample were co-precipitated from the same lake water body with the same Sr/Ca ratio. This is not the case, but the ratio calculated is an average value for the lake and/or diagenetic fluids in the time interval represented by the sample.

The Sr/Ca ratio of sediments in the section varies between $1.34\text{x}10^{-3}$ and $2.64\text{x}10^{-3}$. Sr/Ca values of the water show a more marked variation within the section (Fig.4.7), being constant at about $3\text{x}10^{-3}$ in unit B and varying between about $3\text{x}10^{-3}$ and $31\text{x}10^{-3}$ in units A and C, the higher values occurring in the dolomitized organic-poor horizons. These values can be compared with values for typical Recent meteoric water ($^{m}Sr/^{m}Ca = 2\text{x}10^{-3}$; Andrews et al. 1987) and seawater ($^{m}Sr/^{m}Ca = 9\text{x}10^{-3}$; Veizer 1983). The aragonite-rich horizons were, therefore, precipitated from water with a comparable $^{m}Sr/^{m}Ca$ ratio to Recent meteoric water, whereas the water from which dolomite was precipitated had a $^{m}Sr/^{m}Ca$ ratio enriched relative to seawater.

(ii) Magnesium.

Mg within the studied section varies from 3.70% to 11.78% (Table 2). The variation in Mg throughout the section closely follows the variation in bulk percentage dolomite in the sample. The Mg/Ca ratio also follows this trend with values from 0.26 to 1.05 (Fig.4.7). The Sr/Ca and Mg/Ca ratios have the same trend in unit A. However, the organic-rich dolomite-poor horizons represented by samples B-7 and B-9 have increased Mg/Ca ratios, which is opposite to the expected trend. This is probably due to the nature of the acid extraction process, where whole rock samples are reacted with 10% HCl in a 50°C bath for 12 hours to remove all of the dolomite. Any magnesium-rich clays within the sample may be broken down to form an amorphous silica gel and Mg, Fe and Mn dissolved, giving erroneously high carbonate values. This accounts for the Mg/Ca ratio of 1.05 in B-7, which is a mixture of calcite, aragonite and calcian dolomite. So, apart from the 2 anomalous results there is an increase in Mg/Ca ratio with Sr/Ca ratio in the lower laminated organic-rich unit. This relationship is unusual in that Sr substitutes mostly in the Ca lattice positions and is therefore usually depleted in dolomite relative to calcite (Behrens and Land 1972, Kretz 1982).

However, Andrews et al. (1987) noticed a positive correlation in Mg/Ca and Sr/Ca ratios in Jurassic dolostones from NW Scotland. They accounted for this by the early diagenetic dolomitization of a Sr-poor calcite in a freshwater closed lagoon. In a closed-system dolomitization model a Sr-poor, Mg-rich calcite precursor to dolomite would result in the positively covarying Mg/Ca and Sr/Ca ratios observed. This is because high-Mg calcite dissolution releases few Sr^{2+} but relatively few Mg^{2+} ions compared with aragonite dissolution (Andrews et al. 1987).

(iii) Sodium.

The distribution coefficient, $\underline{D}$, for $Na_{calcite}$, $Na_{dolomite}$ and $Na_{aragonite}$ is salinity dependent, which has enabled some authors in the past to use Na as a palaeosalinity indicator. However, because $\underline{D}<<1$ for all carbonate phases, the sodium content is drastically reduced in the precipitating carbonate (Veizer et al. 1977). This is further complicated by the presence of Na (usually as NaCl) in fluid inclusions within the minerals precipitating, although Land and Hoops (1973) analysed "typical marine carbonate sediments" and showed that Na not balanced by Cl (i.e. co-precipitated Na) exceeds that found balancing Cl on a molar basis by at least a factor of 6.

Halite does not occur in sediments of the Burdur Formation so Na^+ can be treated as a conservative ion in Palaeolake Burdur being removed from it, in trace amounts only, by co-precipitation in carbonates. The Na/Ca profile for the studied section is shown in Fig.4.7. Approximate estimates for the salinity of palaeolake Burdur can be obtained given:

(a) The relationship between the $\underline{D}$ value for Na in the carbonate phases and salinity.

(b) The Na/Ca ratio of the carbonate phases.

(c) The Na/Ca ratio of the lake water.

Katz et al. (1977) experimentally determined the relationship between $\underline{D}^{Na}_{aragonite}$ and Dead Sea water of varying dilution. Their results are summarized in Fig.4.8. This relationship is largely temperature independent. It can be seen that with increasing salinity, Na is more easily incorporated into the aragonite lattice structure. Katz et al. (1977) give relative, not absolute, salinity values, so a value of Dead Sea salinity of 27‰ was taken from Bentor (1961). As aragonite in the Dead Sea precipitates as "whitings" in surface waters during high summer (Neev and Emery 1967), surface water salinity values were taken.

Fig.4.7 shows the Na/Ca ratios of the carbonate phases in the section. Only the relationship between $\underline{D}^{Na}_{aragonite}$ and salinity is known, so only information concerning aragonite need be extracted from these results. Fortunately the $\underline{D}$ value for aragonite is 3 to 4 times greater for aragonite than for calcite and dolomite (White 1977, 1978; Veizer 1983), so Na/Ca values for units containing aragonite will tend to reflect aragonite values rather than calcite or dolomite values. To illustrate this, the carbonate fraction of unit B contains, on average, about 80% aragonite and 20% calcite and dolomite. Using approximate low salinity $\underline{D}$ values ($\underline{D}^{Na}_{aragonite} \simeq 0.00014$, $\underline{D}^{Na}_{calcite/dolomite} \simeq 0.000025$; Veizer 1983), it can be seen that the contribution from aragonite to the Na/Ca ratio of the total carbonate is about 22 times that of calcite and dolomite. Even for horizons containing as little as 30% aragonite (such as B-3, from unit A) the contribution from aragonite is about 2.5 that of calcite and dolomite. So, readjusting the Na/Ca ratios to give us values more indicative of aragonite gives us 20×10^{-3} (no change) for unit B and 40×10^{-3} for B-3.

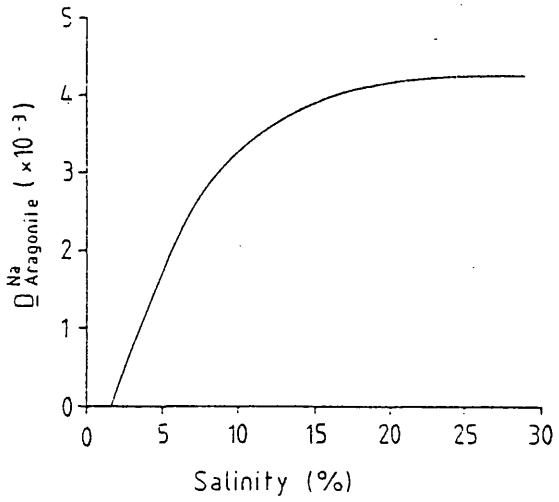

Fig.4.8. The relationship between $D^{Na}_{aragonite}$ and salinity determined experimentally for Dead Sea water by Katz et al. (1977). Absolute salinity values are taken from Bentor (1961).

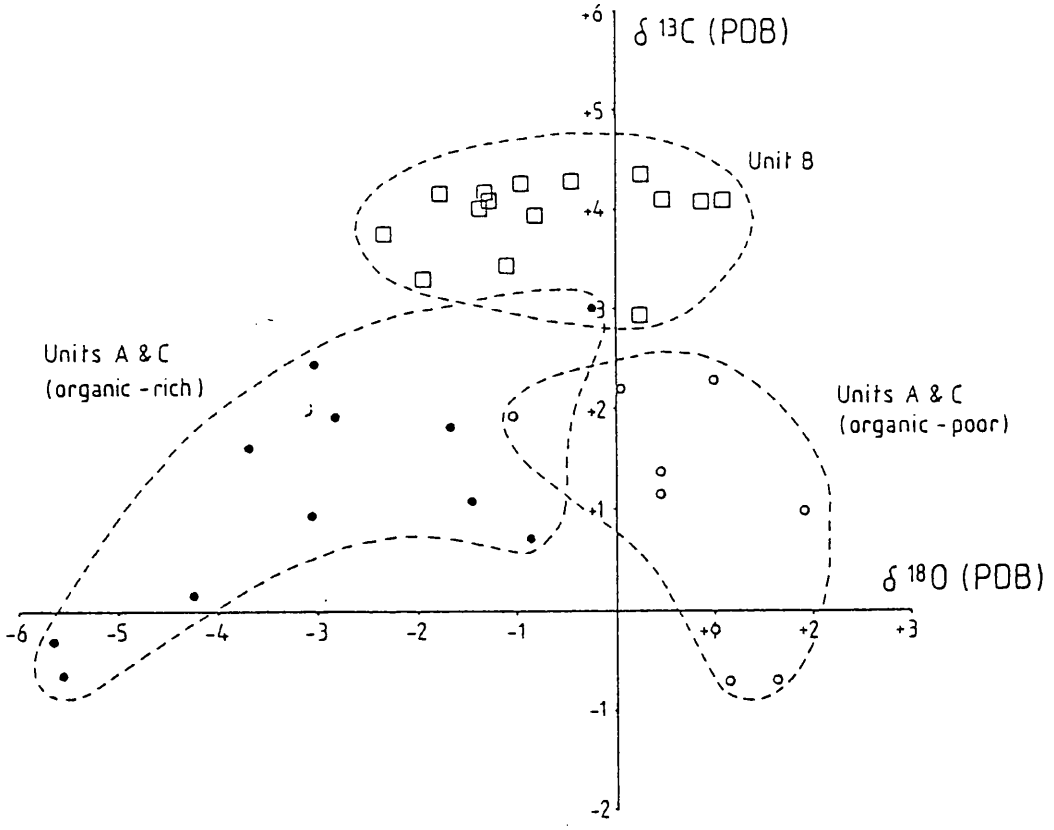

Fig.4.9. $\delta^{13}C$ (PDB) - $\delta^{18}O$ (PDB) cross-plot for samples from the studied section.

The present-day Na/Ca ratio of Burdur Lake water is 450 (Irion 1973). The effect of river waters flowing into the lake is small due to their low salinities. Although the present-day lake is smaller than Palaeolake Burdur, no precipitation of NaCl occurred during shrinkage. Burdur lake brine is still at an early stage in its evolution as aragonite is the only mineral precipitating at present. Pliocene Lake Burdur had reached a similar stage with aragonite and high-mg calcite precipitation dominating. (Gypsum found in small amounts in parts of the Burdur Formation may be due to post-uplift desiccation). Therefore, it is reasonable to take the present day Burdur Lake water Na/Ca ratio to be approximately the same as that of Pliocene Lake Burdur.

Substituting into eq.(2) the Na/Ca ratios for the aragonite and the assumed palaeolake water, the $D^{Na}_{aragonite}$ values 2.7×10^{-5}, for unit B, and 5.3×10^{-5}, for sample B-3, are obtained. These values are extremely low and correspond to the lowest salinities experimentally measured by Katz et al. (1977). Fig.4.8 indicates values of about 19‰(or 19 g/l) for the calculated $\underline{D}$ values. Although the estimated salinity of 19‰ is only a crude estimate, due to the fact that the Na/Ca ratio of Pliocene Lake Burdur cannot be accurately determined, it is interesting to note that if the estimate is an order of magnitude too great, then the salinity calculated will only change to 27‰. A value of about 19‰ shows that Pliocene Lake Burdur had a similar salinity to the present day Burdur Lake, which has a value of 14‰ (Müller et al. 1972) or 17‰ (Irion 1973).

(d) Oxygen Isotopes.

Table 2, Fig.4.7 and Fig.4.9 show the wide range of $\delta^{18}O$ values throughout the section. Units A and C both have $\delta^{18}O$ values fluctuating between about -5 and +4, the heavier values occurring in the dolomitic organic-poor horizons. $\delta^{18}O$ values from unit B show no systematic variation, being fairly constant at -1 (Fig.4.7). Fig.4.10 shows graphically the relationship between $\delta^{18}O$ of lake water, $\delta^{18}O$ of aragonite precipitated from it and precipitation temperature from the following palaeotemperature equation, produced by Grossman and Ku (1981):

$$t(°C) = 19.00 - 3.52\ (\delta_c - \delta_w) + 0.03\ (\delta_c - \delta_w)^2 \qquad \text{(eq.3)}$$

where δ_c is the $\delta^{18}O$ of CO_2 generated from carbonate at 25°C (relative to PDB) and δ_w is the $\delta^{18}O$ of CO_2 generated in equilibrium with water at

25°C (relative to SMOW). Knowing the $\delta^{18}O$ of aragonite precipitated, and estimating the temperature of the lake at the time of precipitation, we can calculate a value for the $\delta^{18}O$ of the lake water.

(i) $\delta^{18}O$ of aragonite.

The palaeotemperature equations for both calcite and aragonite are both well-known. Grossman and Ku (1981) showed that aragonite is enriched in ^{18}O relative to calcite by 0.5 permil at 20°C. However, because well-ordered dolomite has not been synthesized at low temperatures, the oxygen isotopic fractionation between sedimentary dolomite and water is not reliably known. Extrapolation of high-temperature exchange experiments show that dolomite should be enriched in ^{18}O relative to syngenetic calcite by about 6 permil at 25°C (Northrop and Clayton 1966; O'Neil and Epstein 1966). However, naturally coexisting dolomite and calcite often have very similar $\delta^{18}O$ values, and this, according to Degens and Epstein (1964), is due to the non-exchange of CO_3^{2-} during dolomitization. This closed (to anions) system of dolomitization means that the $\delta^{18}O$ value of dolomite is purely dependent on that of the precursor calcite. Land (1980), on the other hand, believed that if cations are imported and exported during dolomitization, then so are anions and he suggested that water composition and temperature are the controlling factors of $\delta^{18}O$ in dolomite in an open system. Studies of Holocene dolomites (for a summary see Land 1980) show that there may be no unique value of $\delta^{18}O$ enrichment in dolomite at 25°C, with values varying between +2 and +4 permil. Land (1980) suggests a working value of +3 permil. This is the value used in this study. Therefore, knowing the mineralogical composition of our samples and the enrichment of ^{18}O in dolomite and aragonite relative to calcite at sedimentary temperatures, we can normalize the $\delta^{18}O$ data. For our purposes all values are normalised to represent an aragonite composition. We will, therefore, obtain a $\delta^{18}O$ value for each sample, which is the value that sample would have, if it were completely aragonitic. So, if

$$\delta^{18}O_{aragonite} = \delta^{18}O_{calcite} + 0.5 \text{ (Grossman and Ku 1981)} \quad \text{and,}$$

$$\delta^{18}O_{dolomite} = \delta^{18}O_{calcite} + 3.0 \text{ (Land 1980)}$$

then,

$$\delta^{18}O_{aragonite} = \delta^{18}O_{total} + (0.5x/100) - (2.5y/100) \quad \text{(eq.4)}$$

where $\delta^{18}O_{total}$ is the isotopic composition measured for the total carbonate fraction and x and y are the bulk percentages of total carbonate for calcite and dolomite respectively. The recalculated $\delta^{18}O$ values are shown in Fig.4.7. The recalculated values show a depletion in ^{18}O as the effect of dolomite, which concentrates the heavier isotope relative to the other carbonate minerals, has been removed. Obviously the greatest depletion is observed in the most dolomitic samples. The initial trends in $\delta^{18}O$ have been retained with unit A now having $\delta^{18}O$ values of +1 to about -6, for the organic-poor and organic-rich horizons respectively. There is less isotopic variation in unit B, with values of around -1 to -2, switching to +1 towards the top.

(ii) Lake water temperature.

A reasonable estimate of Neogene lake water temperature can be obtained by considering the climate at the time. Zubakov and Borzenkova (1988) believed that world climates during the Pliocene were very similar to present-day climates. The present-day Mediterranean has a sub-tropical dry summer climate although mountainous areas are more temperate due to decreased winter temperatures, which may result in snowfall for several weeks. Palynological studies show that, during the Pliocene, the Black Sea was surrounded by a subtropical flora (Koreneva and Kartashova 1978). At this time the Mediterranean was also experiencing a warm climate with the tropical foram Globorotalia margaritae being found in cores from the Tyrrhenian basin (Ciaranfi and Cita 1973). Evidence for a cooler, more temperate climate around parts of the Mediterranean during the early Pliocene, however, is indicated by palynological studies in the Ionian basin (Marchetti and Accorsi 1978). Erol (1979) stated that the climate in SW Turkey at the end of the Miocene was hot and arid and progressively cooled to a more temperate climate by the beginning of the Quaternary. Fig.4.11 shows mean monthly temperatures for Isparta, near to the study area. Isparta is at an altitude of about 900m, has a mean annual temperature of 12.2°C and a range of about 20°C. The summer maximum temperature is 23°C.

The thermal behaviour of lakes is a complex problem (for a good summary see Ragotzkie 1978). A moderately deep temperate lake will become thermally stratified in the spring and summer with warm surface waters

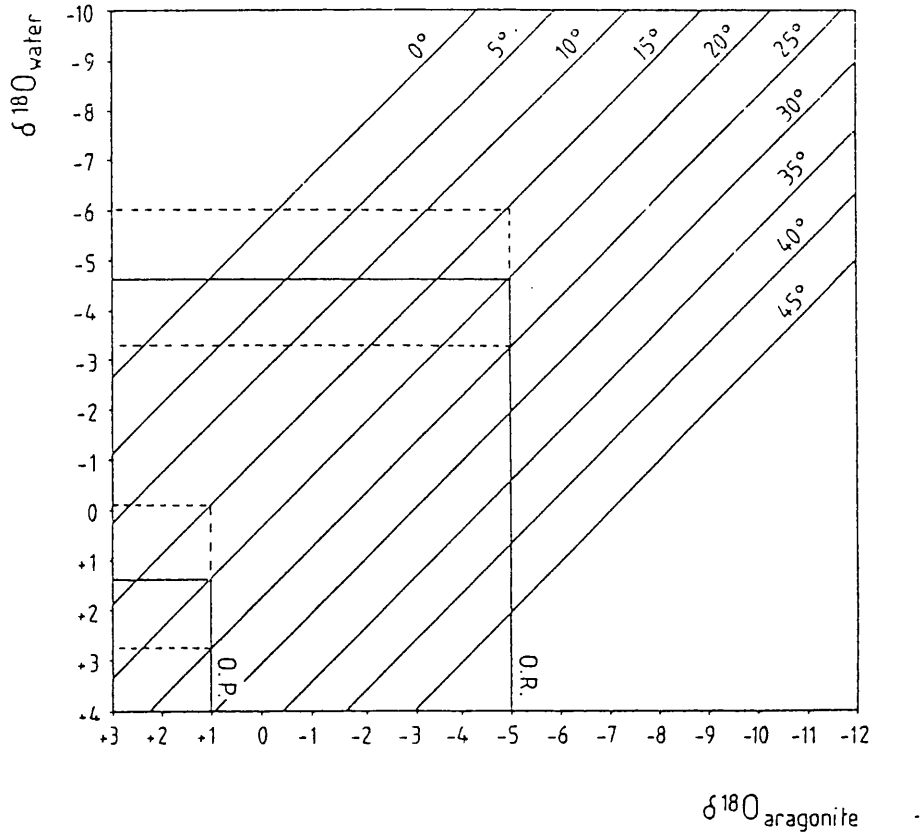

Fig.4.10. The relationship between $\delta^{18}O$ of water, $\delta^{18}O$ of aragonite and precipitation temperature from the palaeotemperature equation $t(°C) = 19.00 - 3.52\ (\delta_c - \delta_w) + 0.03\ (\delta_c - \delta_w)^2$ (after Grossman and Ku 1981). Assuming a Pliocene lake water temperature of 20°C (±5°C) (see discussion in text) the range of $\delta^{18}O_{water}$ is shown for organic-rich (O.R.) and organic-poor (O.P.) sediments from the studied section.

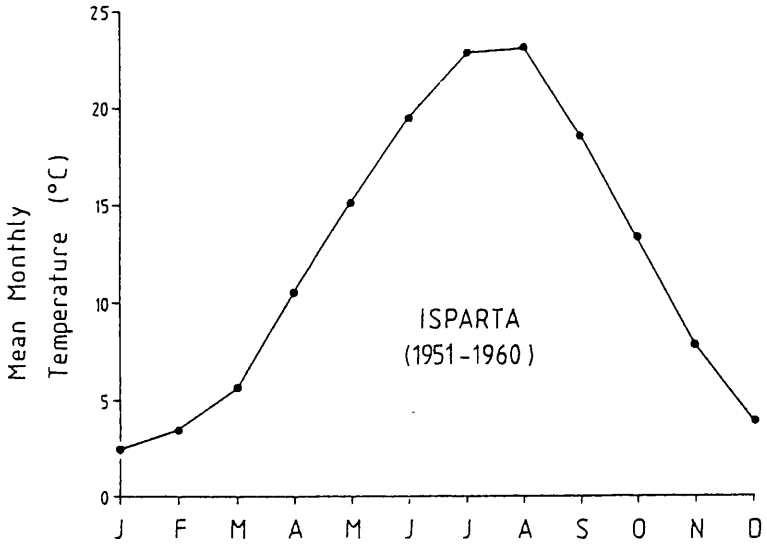

Fig.4.11. Mean monthly temperatures for Isparta, SW Turkey, for the period 1951-1960.

(the epilimnion) being separated from cooler water at depth by (the hypolimnion) by a thermocline. The epilimnion is mixed by wind action and acts as a thermal trap. It therefore attains its maximum temperature in the late summer, after which it cools and is mixed with the hypolimnion.

As a working hypothesis a maximum summer temperature of 20°C for Pliocene Lake Burdur will be assumed.

(iii) Meteoric Water Composition.

Variations in the mean annual isotopic composition of meteoric water around the globe can be interpreted by a continuous (Rayleigh) process of cooling of an air mass (Anderson and Arthur 1983; Gat (1980) points out some problems with this model). $\delta^{18}O$ of meteoric water varies as a function of temperature (which can be sub-divided into changes due to latitude and changes due to altitude) (Dansgaard 1964). Yurtsever (1975) showed that for North America at the present day changes in latitude had the effect of decreasing $\delta^{18}O$ by approximately 0.5 permil/degree northwards. The altitude effect depends on local climate and topography but a change of 0.15 to 0.5 permil $\delta^{18}O$/100m was found by Gat (1980). δD and $\delta^{18}O$ of meteoric water are related by the equation (Craig 1961):

$$\delta D = 8\ \delta^{18}O + 10 \text{ in permil} \qquad \text{(eq.5)}$$

This relationship describes the meteoric water line (MWL) which is offset from mean ocean water and closed basin waters due to the kinetic effects of evaporation.

The global variation in the isotopic composition of present day meteoric waters is well known from the IAEA station network. There is no published data available for isotopic compositions of meteoric waters from the Neogene of Turkey. The present day mean $\delta^{18}O$ precipitation value for Turkey from the IAEA network is approximately -6 (Yurtsever 1975). This value can probably reasonably be extrapolated back to the Neogene. The general present-day plate tectonic configuration of the earth's surface was already developed by the early Pliocene and Sengör et al. (1985) showed that the elevation of SW Turkey was, at this time, the same as at present. Therefore it would appear that the present day $\delta^{18}O$ value of -6 is a good working value. Sheppard (1986) showed that Tertiary $\delta^{18}O$ meteoric water values for North America were almost identical to those of

the present day. Anderson and Arthur (1983) published a curve relating mean monthly surface temperature to mean monthly $\delta^{18}O$. By estimating the mean monthly surface temperature during the late Miocene / early Pliocene a value can therefore be obtained for the mean monthly $\delta^{18}O$ for meteoric waters feeding the lake at the time of sedimentation. The early Pliocene climate of the eastern Mediterranean was similar to that of the present day. A reasonable estimate for the mean monthly temperature in the early Pliocene of the mountainous parts of SW Turkey is, therefore, about 10-15°C. On the curve of Anderson and Arthur (1983) (Fig.4.12) this corresponds to a $\delta^{18}O$ value of -5. This compares well with the value of -6 proposed above.

Using the palaeotemperature equation of Grossman and Ku (1981), the isotopic composition of Pliocene Lake Burdur water can now be calculated. The $\delta^{18}O$ values for unit A are +1 permil, for the organic-poor horizons and -5 permil for the organic-rich horizons (Fig.4.7). So, assuming a water temperature of 20°C (± 5°C), a $\delta^{18}O$ value of +1.3 (± 1.4) permil for lake water precipitating carbonate in the organic-poor horizons and -4.7 (± 1.4) permil for the organic-rich horizons is calculated. Unit B, having a $\delta^{18}O$ variation from -1 permil to +1 permil will have been precipitated in water of composition -0.7 (± 1.4) permil to +1.3 (± 1.4) permil. The organic-rich horizons were therefore precipitated in water which was close to meteoric water in composition, whereas the organic-poor horizons were deposited in evaporated meteoric water. Likewise, unit B was precipitated in evaporated meteoric water. The variations in the $\delta^{18}O$ of the lake carbonates may also be due to changes in water temperature at the time of precipitation. Fig.4.10 shows that to develop the variation of +1 to -5 permil observed, a temperature range of about 24°C is required. Although this may be a reasonable seasonal temperature range for the epilimnion of a temperate lake, it is too high to represent variations in the average yearly temperature over the relatively short period represented by a single couplet in unit A (each being about 100 to 500 years in duration). Therefore, lake temperature changes cannot solely account for the changes in the $\delta^{18}O$ of the lake carbonates.

(e) Carbon Isotopes.

Table 2 and Fig.4.7. show the variation in $\delta^{13}C$ throughout the section. There is a clear distribution with heavier values occurring in the

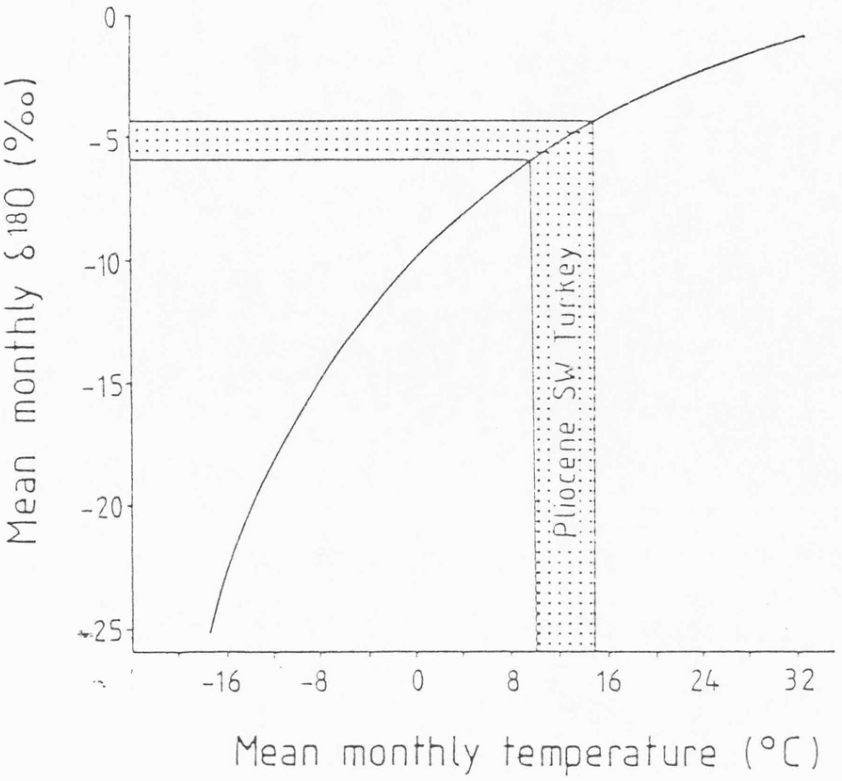

Fig.4.12. Mean monthly $\delta^{18}O_{water}$ versus mean monthly temperature (from Anderson and Arthur 1983).

Ostracode	Salinity (‰)
Candona candida	0.1 - 5.7
Heterocypris salina	1.1 - 20+
Ilyocypris bradyi	0.4 - 4.5

Table 4: Ostracodes from the Akdere Member, with salinity ranges taken from recent European faunas (after De Deckker 1981).

organic-poor unit B, which has values of about +4 permil. Units A and C have values of -1 to +2 permil for both organic-rich and organic-poor beds. The $\delta^{13}C$ of total dissolved carbonate in lake water can vary substantially, as it comes from a variety of sources with $\delta^{13}C$ values varying from about +1 permil (marine limestone in the source area) to about -25 permil (dissolved CO_2 from plant respiration and decay). The values of -1 to +4 for carbonates from the section are therefore very high. "Average" lacustrine carbonates have $\delta^{13}C$ values in the range -7 to -2 permil (Stuiver 1975, McKenzie 1982). The high $\delta^{13}C$ values of the sediments in the section indicate that CO_2 from plant respiration and decay was a minor constituent of the total dissolved lake water carbonate. Dissolution of preexisting carbonate rocks, in this case Tethyan basement limestones, although diluting the vegetation effect, by supplying heavy carbon to the lake waters cannot account for values of greater than about +1 permil. Equilibration of the lake water mass with atmospheric CO_2 will tend to result in water with a composition of +1 to +2 permil at 25°C (Veizer 1983), which again cannot account for values of up to +4.5 permil observed in unit B.

Some authors (e.g. Hsü and Kelts 1978, McKenzie 1982) have noticed a shift towards heavier $\delta^{13}C$ values in sediments during periods of lake water stagnation, brought about by an increase in lake productivity. During these periods the hypolimnion becomes anoxic and organic plankton, which is depleted in $\delta^{13}C$, is stored in the sediment, resulting in an enrichment of HCO_3^- and hence carbonates precipitating in surface waters. This is not the case for Pliocene Lake Burdur, as the heavier $\delta^{13}C$ values are associated with unit B, which was precipitated when the lake's hypolimnion was oxic, seen by the lack of organic matter and the bioturbated nature of the sediment. In fact, the uniformly high $\delta^{13}C$ value for unit B is probably a result of intense bioturbation, which will tend to destroy any smaller-scale variation. Organic-rich horizons within units A and C do not have heavier $\delta^{13}C$ values than organic-poor horizons (Fig.4.7), indicating that the storing of organic matter in the sediment had little effect on the $\delta^{13}C$ of the lake HCO_3^-. However, the high $\delta^{13}C$ values relative to "average" lacustrine carbonate in the organic-rich units A and C may be due to this effect.

Heavy $\delta^{13}C$ values have been reported in saline lakes from arid regions. For example, lake Lisan, the Pleistocene precursor of the Dead Sea, has $\delta^{13}C$ values up to +3.5 permil (Katz et al. 1977). These higher values

were not believed to be related to biogenic activity, but due to the fractionation between HCO_3^- and slowly released CO_2. If the loss of CO_2 is rapid, a kinetic fractionation will occur between HCO_3^- and CO_2(aq) and the $CaCO_3$ precipitated will show a simultaneous enrichment in ^{13}C and ^{18}O (Hendy 1971). However, there is no correlation between $\delta^{13}C$ and $\delta^{18}O$ in the sampled section minimizing the importance of this kinetic fractionation. So, neglecting the equilibrium between carbon species in solution and atmospheric CO_2, the process dominating the composition of carbon species in solution is an equilibrium "Rayleigh distillation" caused mainly by the fractionation between HCO_3^- and slowly released gaseous CO_2 (Katz et al. 1977). The fractionation for this reaction is +8.38 permil at 20°C (Emrich et al. 1970). This will result in heavier dissolved carbon as CO_2 is released prior to the precipitation of $CaCO_3$. This enrichment is approximately halved as soon as $CaCO_3$ begins to precipitate (Katz et al. 1977). The isotopic composition of $CaCO_3$ therefore reflects the efficiency of the slow CO_2-degassing process, which will be related to evaporation from the lake surface. So, if $CaCO_3$ precipitation is delayed, as is seen in the modern Dead Sea (Neev and Emery 1967), then saline, ^{13}C-enriched waters will result. A correlation between the Na/Ca ratio and $\delta^{13}C$ of $CaCO_3$ would therefore be expected. There is little variation in $\delta^{13}C$ or Na/Ca ratio in unit B (Fig.4.7), so the effectiveness of the slow CO_2-degassing process during its deposition can neither be demonstrated nor dismissed. In units A and C, whose high $\delta^{13}C$ values have already been explained by the storing of organic matter in the sediment, there is no correlation (Fig.4.7). This suggests that the CO_2-degassing process did not influence $\delta^{13}C$ values in these units.

It is proposed that the high $\delta^{13}C$ values of unit B, relative to units A and C, are a result of the slow degassing of CO_2 from surface lake waters with delayed $CaCO_3$ precipitation.

4.5. OSTRACODAL SEDIMENTS.

To complement the above study of cyclic sedimentation, samples were taken from stratigraphically higher in the section, representing Palaeolake Burdur at a later stage in its evolution. Higher in the section the organic-rich/organic-poor cyclicity of the sediments diminishes and ostracodes become abundant. The ostracodes are disarticulated and occur in small patches, often having linear trends, suggestive of some current

reworking.

Ostracodes from the Akdere Member are dominated by Candona sp.. Table 4 shows salinity ranges, taken from De Deckker (1981) for ostracodes collected from the Akdere Member. Candona sp., the dominant genus, is found in waters of low salinity (generally less than 0.5%). So, an initial presumption is that during the deposition of the ostracodal marls, Palaeolake Burdur was a relatively low-salinity water body.

Chivas et al. (1986a,b) showed that trace element concentrations in adult non-marine ostracode shells can be useful indicators of palaeosalinity and palaeotemperature. Ostracodes moult their bivalved shells up to 9 times before adulthood, building new ones from elements in the host water obtained only at the time of formation. The Mg and Sr content of an individual ostracode shell is a function of the growth stage of the ostracode and the temperature, salinity and Sr or Mg content of the host water. However, the Mg and Sr content is also species dependent and Chivas et al. (1986b) published D_{Sr} and D_{Mg} values for various ostracode species. D_{Sr} values varied from 0.176 for Cypronotus sp. to 0.474 for Cyprideis sp.. D_{Mg} was only reported for Cyprideis sp. at 25°C (0.0046) since Mg-partitioning is temperature dependent , requiring growth tests to be undertaken in a controlled environment. Full calcification of the shell is required otherwise the Mg/Ca ratio is too high. This is difficult to achieve when the ostracode is under stress. Because of the species-dependancy of the distribution coefficients, little can be said about the trace element concentrations in the shells of ostracodes from the Akdere Member.

The oxygen isotopic ratios of ostracodes are useful indicators of lacustrine palaeoenvironment. Fig.4.13 and Table 2 shows the $\delta^{18}O$ and $\delta^{13}C$ values for ostracodes from the upper part of the section. $\delta^{18}O$ values vary from -2 to +3 permil, the wide range possibly being due to the rapid calcification of an ostracode shell, taking only a few days, and therefore not smoothing out rapid (seasonal?) fluctuations in lake water isotopic composition. Whole rock $\delta^{18}O$ values are, however, much lighter. Although only 2 results are available they are consistent at -5 permil. These samples represent inorganically precipitated low-Mg calcite with minor ostracode. Therefore, due to dilution effects, the true value of the calcite matrix will be a little lower. Using the palaeotemperature equation, produced by Craig (1965)

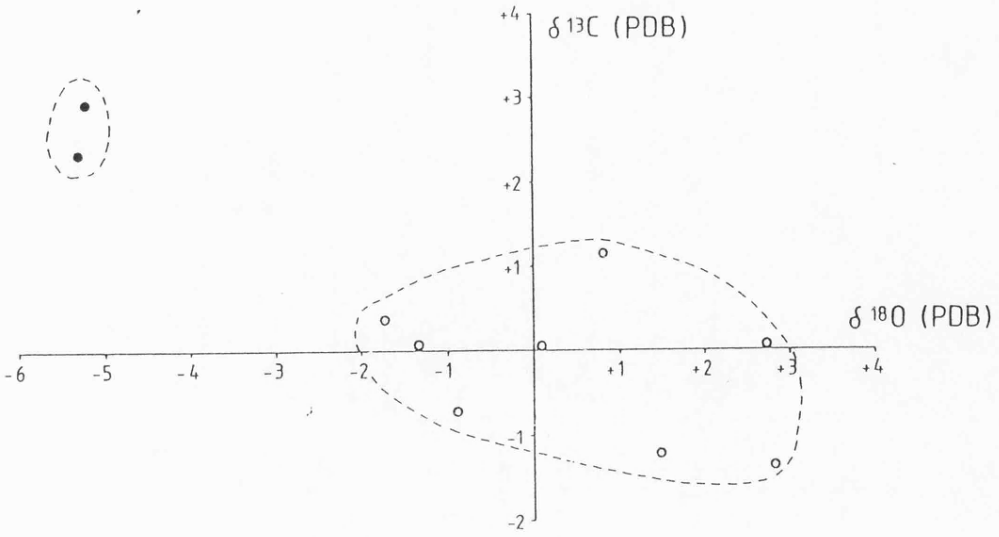

Fig.4.13. $\delta^{13}C$ (PDB) - $\delta^{18}O$ (PDB) cross-plot for ostracodes (open circles) and sediment (closed circles) from the upper part of the section.

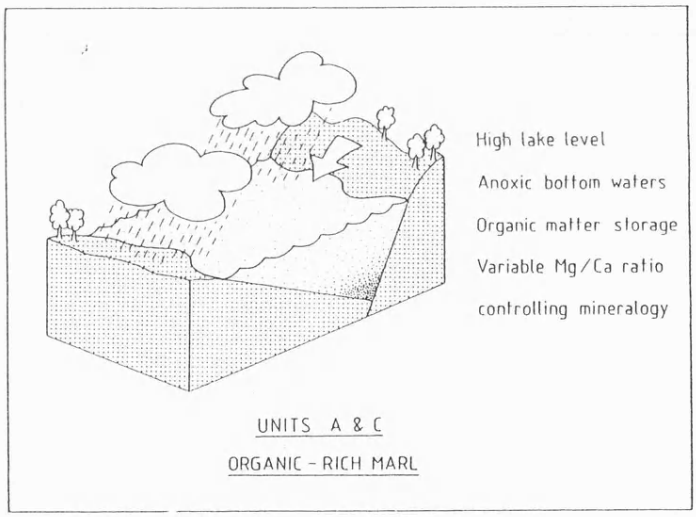

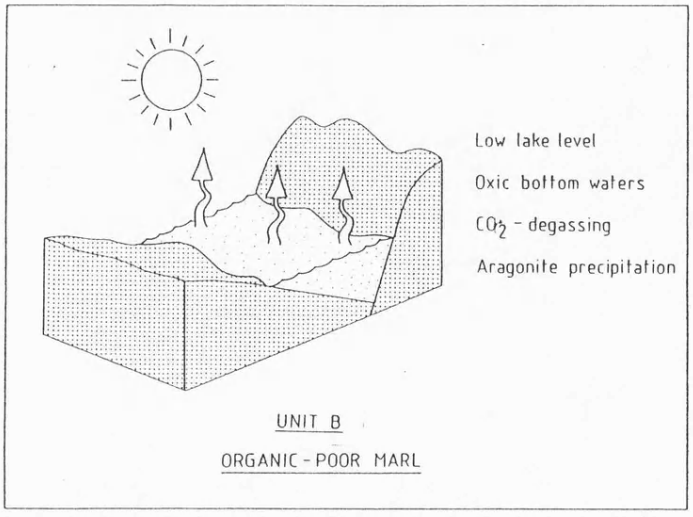

Fig.4.14. Block models summarising environments operating in Palaeolake Burdur.

$$t(°C) = 16.90 - 4.20\ (\delta_c - \delta_w) + 0.13\ (\delta_c - \delta_w)^2 \qquad \text{(eq.6)}$$

and assuming lake water temperatures of about 20°C, it can be seen that the calcite matrix was precipitated in waters with $\delta^{18}O$ values of about -4.5 permil, whereas the ostracodes lived in waters of about -1 to +4 permil. This supports an idea of carbonate being precipitated in the mixing zone between incoming meteoric waters and alkaline lake waters, as seen in present day Anatolian lakes (Müller et al. 1972). The lighter values for the carbonate show a strong meteoric water influence, whereas the heavier values are representative of the lake bottom (as ostracodes are benthic), indicating that here the lake water has the isotopic composition of evaporated meteoric water. The wide range in the lake bottom values is probably seasonal, due to the mixing of isotopically heavier evaporated surface waters with lighter bottom waters during the autumn. It is possible that some of the difference between the $\delta^{18}O$ values of ostracodes and those of the calcite matrix are due to temperature, with ostracodes living in colder waters than those in which the calcite sediment precipitated.

4.6. DISCUSSION.

4.6.1. Nature of Cyclic Sedimentation.

The cyclic sediments of the Akdere Member were deposited in a lake in a closed intramontane basin. This basin was fed by river and/or groundwater-derived meteoric water, draining a basin of Mesozoic Tethyan limestone and serpentinite. The Mg/Ca and Sr/Ca ratios of the lake were controlled by the balance between ionic supply, evaporation of the lake and mineral precipitation. The exact mechanism of precipitation is unknown. Loss of CO_2 giving rise to carbonate precipitation as a result of planktonic algal blooms is thought to be unlikely due to the lack of any algae preserved within the succession. Therefore either evaporative concentration of lake water or mixing of different water types can be invoked as possible causes of precipitation. Present day Anatolian lakes, which are precipitating aragonite, do this by the latter process, where river water with a pH of about 7.5 enters highly alkaline lake waters, thus promoting calcium carbonate precipitation in the mixing zone (Müller et al. 1972; Irion 1973). Assuming a Pliocene climate similar to that of the present and also unchanged basement lithologies, this process was

probably the major contributor to precipitation in Palaeolake Burdur.

The geological and geochemical information discussed above can be put together in the following model for the formation of lacustrine sedimentary cycles in Palaeolake Burdur. This model is summarized in Fig.4.14. An individual cycle is a few metres thick and consists of an organic-rich/organic-poor couplet. The organic-rich unit can be further sub-divided into smaller organic-rich/organic-poor couplets on the scale of a few centimetres.

Firstly, consider the larger scale organic-poor cycles. These are intensely bioturbated indicating an oxygenated hypolimnion. Aragonite is the dominant carbonate phase, and this was precipitated in lake water of increased Mg/Ca ratio (probably greater than 12). Aragonite acts as a sink for Sr, resulting in low Sr/Ca lake water ratios, similar to those of present-day meteoric water. High rates of evaporation and relatively low rainfall resulted in the low clay content of these sediments (due to reduced surface run-off) and an enrichment in ^{18}O. These high evaporation rates increased the effect of degassing of CO_2 from the lake waters. The fractionation between HCO_3^- in the lake water and this slowly degassing ^{13}C-depleted CO_2 gave rise to increased $\delta^{13}C$ values. These high values (up to 4.5 permil) suggest that there was also reduced respiration and decay of vegetation in and around the lake.

Following deposition of an organic-poor horizon, organic-rich sediments were deposited in the lake. These are generally laminated, indicating anoxic bottom waters. During periods of increased rainfall and reduced evaporation, indicated by reduced $\delta^{18}O$ values (similar to meteoric water) and increased clay content, a mixture of carbonate phases was precipitated. This can be related to a highly variable Mg/Ca ratio of the lake, probably caused by short term variations in surface runoff. Sr/Ca ratios are low, having similar values to present day meteoric water, again, partly due to the presence of minor aragonite in these sediments. $\delta^{13}C$ values during the deposition of the organic-rich horizons are relatively low due to the reduction of CO_2 degassing from the lake. However, at about -1 to +2 permil, values are still higher than "average freshwater limestone" values. This may be because ^{13}C-depleted organic matter is preserved in the sediment during anoxia, resulting in heavier carbon in HCO_3^- in the surface lake waters, and hence heavier carbonate precipitating. Minor burrowing within these laminated organic-rich

sediments was probably caused by annelid worms similar to the genus Nereis, which is present in the Caspian Sea today (Zenkevich 1957) and was also present in the late Neogene Black Sea (Hsü and Kelts 1978). Nereis can live successfully in poorly circulated waters and can withstand short periods of anoxia.

Within the organic-rich horizons are interbedded organic-poor dolomites. The high $\delta^{18}O$ values associated with these indicate evaporated lake waters. These also had high Mg/Ca and Sr/Ca ratios. The increased Sr/Ca ratios of the dolomite is possibly a result of the dissolution of a high-Mg calcite as a Sr-rich aragonite precursor would produce an antipathetic relationship between Mg/Ca and Sr/Ca in the dolomite (Andrews et al. 1987). However, this assumes closed-system dolomitization; most likely since the lake was closed. Obviously, if the system was open to the exchange of ions, then no information can be gained from the trace elements as to the dolomite precursor.

At a later stage in its evolution, Palaeolake Burdur developed into a relatively low-salinity water body, supporting an abundant low-diversity ostracode fauna. High $\delta^{18}O$ values for the calcite of these ostracode shells compared with low values for the calcite sedimentary matrix support a model where calcite precipitation took place in a mixing zone between lake waters and incoming meteoric water.

4.6.2 Cause of Cyclic Sedimentation.

A periodicity of lacustrine cycles of approximately 18.6ka has been detected in sediments from Palaeolake Burdur. Due to the variability of sediment varve thickness this figure may lie anywhere between 12.6 and 35.3ka. This periodicity is reflected in the large-scale change from organic-rich to organic-poor marl deposition within the succession. Geochemical data suggests that this change was climatically-driven with organic-rich marls representing times of relatively high rainfall and low evaporation with high lake productivity and organic-poor marls representing times of reduced rainfall with a corresponding increase in evaporation and lower levels of productivity.

Climatic changes over periods of the order postulated above have commonly been attributed to changes in the Earth's orbit, which lead to variations in the amount of insolation received by the Earth. The refined

Pleistocene time-scale has meant that most studies concerning climatic variation in the geological record have concentrated on this epoch (e.g. Hays et al. 1976). Berger (1984) showed that the dominant orbital periods have not deteriorated over the last 5Ma so that extrapolations back to the Pleistocene are valid. Several authors have, in the past, related cyclic lacustrine sedimentation to these orbital periods. By counting varves, Bradley (1929) demonstrated the record of the Earth's precessional cycle in lacustrine sediments of the Eocene Green River Formation. A similar approach was adopted by Olsen (1984) who showed that cyclic sedimentation in the Triassic Lockatong Formation of New Jersey and Pennsylvania recorded the change from a deep clastic-dominated lake to a shallow playa lake over a time scale equivalent to the Earth's precessional cycle. Kanari et al. (1984) showed that late Pleistocene - Holocene sedimentation in Lake Biwa, Japan, was affected by eccentricity, obliquity and precession orbital cycles.

The Earth's precessional cycle has 2 components, one at 23ka and the other at 19ka. The periodicity of lacustrine cycles in Palaeolake Burdur, at approximately 18.6ka, correlates well with this cycle. This, along with the fact that the precessional cycle is becoming increasingly recognised in lacustrine settings, suggests that this is the external driving force of the large-scale lacustrine cycles in Palaeolake Burdur.

The smaller-scale cycles observed within the organic-rich units represent changes from periods of relatively low evaporation to periods of increased evaporation and dolomitization. These cycles have an average length of 2.1ka (calculated by dividing average cycle thickness by average varve thickness). Their frequency is too high to represent orbital cycles. They may instead be related to solar cycles. However, although relatively short term cycles have been recognised based on historical sunspot records (e.g. Cohen and Lintz 1974), the largest cycle so far recognised is 180 years (Sleeper 1972). This is due to the relatively short observational period (since 1750).

Another possible driving force for cyclic sedimentation within a syn-faulting sedimentary succession is cyclic shear stress loading of the fault controlling sedimentation. Sibson (1989) showed that displacements on a fault occur at regular time intervals due to the build up of shear stress on the fault plane, which drops during rupture. However, this would cause perturbations to the clastic input of the basin and is

therefore unlikely to be the cause of cyclic sedimentation in Palaeolake Burdur as sedimentation was almost entirely by inorganic precipitation.

4.7. CONCLUSIONS.

The following list of conclusions can be drawn from this study:

(a) Palaeolake Burdur was a deep water body in which sedimentation was dominated by the inorganic precipitation of carbonate in a mixing zone between the lake water body and incoming meteoric water. The Na/Ca ratio of aragonite suggests a lake with salinity approximately equivalent that of modern Lake Burdur (1.9 to 2.7‰).

(b) Organic-poor marl deposition occurred during periods of relatively high evaporation and low rainfall (shown by the enrichment of ^{18}O and ^{13}C, the latter caused by the effect of degassing of CO_2 from the lake).

(c) Organic-rich marl deposition occurred during periods of increased rainfall and reduced evaporation (shown by the low $\delta^{18}O$ values), when the bottom waters of the lake became anoxic. Short term periods of evaporation (of the order of a few thousand years and possibly related to the solar cycle) gave rise to dolomitization, probably of a high-Mg calcite precursor.

(d) Organic-rich and organic-poor units are interbedded and form cycles with a dominant periodicity of about 19ka. This cyclicity may be the result of climatic change related to the Earth's precessional cycle.

4.8. REFERENCES.

Alderman, A.R. and Skinner, H.C.W. 1957. Dolomite sedimentation in the southeast of South Australia. American Journal of Science, v.255, p.561-567.

Andrews, J.E., Hamilton, P.J. and Fallick, A.E. 1987. The geochemistry of early diagenetic dolostones from a low-salinity Jurassic lagoon. Journal of the Geological Society, London, v.144, p.687-698.

Beauchamp, K.G. 1984. Application of Walsh and Related Functions, with an Introduction to Sequence Theory. Academic Press.

Behrens, R.W. and Land, L.S. 1972. Subtidal holocene dolomite, Baffin Bay, Texas. Journal of Sedimentary Petrology, v.42, p.155-161.

Bentor, Y.K. 1961. Some geochemical aspects of the Dead Sea and the question of its age. Geochimica et Cosmochimica Acta, v.25, p.238-260.

Berger, A. 1984. Accuracy and frequency stability of the Earth's orbital elements during the Quaternary. In. Berger, A., Imbrie, J., Hays, J., Kukla, G. and Saltzman, B. (eds) Milankovitch and Climate, Part 1, Reidel Publishing Company, p.3-39.

Bertolani Marchetti, D. and Accorsi, C. 1978. Palynological studies on samples from DSDP Leg 42A. In: Hsü, K.J., Montadert, L. et al. (eds) Initial Reports of the Deep Sea Drilling Project, XLII. U.S. Government Printing Office, Washington D.C., p.789-804.

Bradley, W.H. 1929. The varves and climate of the Green River Epoch. United States Geological Survey Professional Paper, No.158, p.87-110.

Chivas, A.R., De Deckker, P. and Shelley, J.M.G. 1986a. Magnesium content of non-marine ostracod shells: a new palaeosalinometer and palaeothermometer. Palaeogeography, Palaeoclimatology, Palaeoecology, v.54, p.43-61.

Chivas, A.R., De Deckker, P. and Shelley, J.M.G. 1986b. Magnesium and strontium in non-marine ostracod shells as indicators of

palaeosalinity and palaeotemperature. Hydrobiologia, v.143, p.135-142.

Ciaranfi, N. and Cita, M.B. 1973. Palaeontological evidence of changes in the Pliocene climates. In: Ryan, W.B.F., Hsü, K.J. et al. (eds) Initial Reports of the Deep Sea Drilling Project, XIII. U.S. Government Printing Office, Washington D.C., p.1387-1399.

Cohen, T.J. and Lintz, P.R. 1974. Long term periodicities in the sunspot cycle. Nature, v.250, p.398.

Craig, H. 1965. The measurement of oxygen isotope paleotemperature. Proceedings of the Spoleto Conference on Stable Isotopes in Oceanographic Studies and Palaeotemperature, p.161-182.

Dansgaard, W. 1964. Stable isotopes in precipitation. Tellus, v.16, p.436-468.

De Deckker, P. 1981. Ostracods of athalassic saline lakes. Hydrobiologia, v.81, p.131-144.

Degens, E.T. and Epstein, S. 1964. Oxygen and carbon isotope ratios in coexisting calcites and dolomites from recent and ancient sediments. Geochimica et Cosmochimica Acta, v.28, p.23-44.

Emrich, K., Ehhalt, D.H. and Vogel, J.C. 1970. Carbon isotope fractionation during the precipitation of calcium carbonate. Earth and Planetry Science Letters, v.8, p.363-371.

Epstein, S. Buchsbaum, R., Lowenstam, H.A. and Urey, H.C. 1953. Revised carbonate-water temperature scale. Bulletin of the Geological Society of America, v.64, p.1315-1326.

Füchtbauer, H. and Goldschmidt, H. 1965. Beziehungen zwischen Calciumgehalt und Bildungsbedingungen der Dolomite. Geologische Rundschau, v.55, p.29-40.

Gat, J.R. 1980. The isotopes of hydrogen and oxygen in precipitation. In: Fritz, P. and Fontes, J.C. (eds) Handbook of Environmental Geochemistry, Elsevier, p.21-47.

Goldsmith, J.R. and Graf, D.L. 1958a. Structural and compositional variations in some natural dolomites. Journal of Geology, v.66, p.678-693.

Goldsmith, J.R. and Graf, D.L. 1958b. Relation between lattice constants and composition of the Ca-Mg carbonates. American Mineralogist, v.43, p.84-101.

Grossman, E.T. and Ku, T.L. 1981. Aragonite and water isotopic paleotemperature scale based on the benthic foraminifera Hoeglundia elegans. Geological Society of America Annual Meeting (Abstract with Programs), p.464.

Hays, J.D., Imbrie, J. and Shackleton, N.J. 1976. Variations in Earth's orbit: pacemaker of the ice ages. Science, v.194, p.1121-32.

Hendy, C.H. 1971. The isotopic geochemistry of speleothems-I. The calculation of the effects of different modes of formation on the isotopic composition of speleothems and their applicability as palaeoclimatic indicators. Geochimica et Cosmochimica Acta, v.35, p.801-824.

Hsü, K.J. and Kelts, K. 1978. Late Neogene chemical sedimentation in the Black Sea. In: Matter, A. and Tucker, M.E. (eds) Modern and ancient lake sediments, Special Publication of the International Association of Sedimentologists, Blackwell Scientific Publications, Oxford, No.2, p.129-145.

Irion, G. 1973. Die anatolischen Salzeen, ihr Chemismus und die Enstehung ihrer chemischen Sedimente. Archiv für Hydrobiologie, v.71, p.517-557.

Jacobson, R.L. and Usdowski, H.E. 1976. Partitioning of strontium between calcite, dolomite and liquids. Contributions to Mineralogy and Petrology, v.59, p.171-185.

Kanari, S., Fuji, N. and Horie, S. 1984. The paleoclimatological constituents of paleotemperature in lake Biwa. In. Berger, A., Imbrie, J., Hays, J., Kukla, G. and Saltzman, B. (eds) Milankovitch and Climate, Part 1, Reidel Publishing Company, p.405-414.

Katz, A. and Matthews, A. 1977. The dolomitization of $CaCO_3$: an experimental study at 252-295°. Geochimica et Cosmochimica Acta, v.41, p.297-308.

Katz, A., Kolodny, Y. and Nissenbaum, A. 1977. The geochemical evolution of the Pleistocene Lake Lissan - Dead Sea system. Geochimica et Cosmochimica Acta, v.41, p.1609-1626.

Keltz, K. and Hsü, K.J. 1978. Freshwater Carbonate Sedimentation. In: Lerman, A. (ed) Lakes; Chemistry, Geology, Physics. Springer-Verlag, p.295-324.

Kretz, R. 1982. A model for the distribution of trace elements between calcite and dolomite. Geochimica et Cosmochimica Acta, v.46, p.1979-1981.

Land, L.S. 1980. The isotopic and trace element geochemistry of dolomite: the state of the art. In: Zenger, D.H., Dunham, J.B. and Ethington, R.L. (eds) Concepts and Models of Dolomitization, Special Publication of the Society of Economic Paleontologists and Mineralogists, No.28, p.87-110.

Lumsden, D.N. 1979. Discrepancy betwee thin section and X-ray estimates of dolomite in limestones. Journal of Sedimentary Petrology, v.49, p.429-436.

McKenzie, J.A. 1982. Carbon-13 cycle in Lake Greifen: a model for restricted ocean basins. In: Schlanger, S.O. and Cita, M.B. (eds) Nature and Origin of Cretaceous Carbon-rich Facies, Academic Press, New York, p.197-208.

Müller, G., Irion, G. and Förstner, U. 1972. Formation and diagenesis of inorganic Ca-Mg carbonates in the lacustrine environment. Naturwissenschaften, v.59, p.158-164.

Müller, G. and Wagner, F. 1978. Holocene carbonate evolution in Lake Balaton (Hungary): a response to climate and the impact of man. In: Matter, A. and Tucker, M.E. (eds) Modern and ancient lake sediments, Special Publication of the International Association of Sedimentologists, Blackwell Scientific Publications, Oxford, No.2,

p.57-81.

Neev, D. and Emery, K.O. 1967. The Dead Sea, depositional processes and environments of evaporites. Bulletin of the Geological Survey of Israel, v.41, 147pp.

Northrop, D.A. and Clayton, R.N. 1966. Oxygen isotope fractionation in systems containing dolomite. Journal of Geology, v.74, p.174-196.

Olsen, P.E. 1984. Periodicity of lake-level cycles in the late Triassic Lockatong formation of the Newark basin (Newark supergroup, New Jersey and Pennsylvania). In. Berger, A., Imbrie, J., Hays, J., Kukla, G. and Saltzman, B. (eds) Milankovitch and Climate, Part 1, Reidel Publishing Company, p.129-146.

O'Neil, J.R. and Epstein, S. 1966. Oxygen isotope fractionation in the system dolomite-calcite-carbon dioxide. Science, v.152, p.198-201.

Peterson, M.N.A. and Bien, G.S. 1963. Radiocarbon age determinations of Recent dolomite from Deep Springs Lake, California. Transactions of the American Geophysical Union, v.44, p.108 (abstract).

Ragotzkie, R.A. 1978. Heat Budgets of Lakes. In: Lerman, A. (ed) Lakes; Chemistry, Geology, Physics. Springer-Verlag, p.1-18.

Royse, C.F., Wadell, J.S. and Petersen, L.F. 1971. X-ray determination of calcite-dolomite: an evaluation. Journal of Sedimentary Petrology, v.41, p.483-488.

Schmidt, V. 1965. Facies, diagenesis and related reservoir properties in the Gigas Beds (Upper Jurassic) northwestern Germany. In: Pray, L.C. and Murray, R.C. (eds) Dolomitization and Limestone Diagenesis. Special Publication of the Society of Economic Paleontologists and Mineralogists, No.13, p.124-168.

Sengör, A.M.C., Görür, N. and Saroglu, F. 1985. Strike-slip faulting and related basin formation in zones of tectonic escape: Turkey as a case study. In: Biddle, K.T. and Christie-Blick, N. (eds) Strike-slip deformation basin formation and sedimentation. Special Publication of the Society of Economic Paleontologists and Mineralogists, No.37,

p.227-264.

Shinn, E.A., Lloyd, R.M. and Ginsberg, R.N. 1969. Anatomy of a modern tidal-flat, Andros Island, Bahamas. Journal of Sedimentary Petrology, V.39, p.1202-1228.

Sibson, R.H. 1989. Earthquake faulting as a structural process. Journal of Structural Geology, v.11, p.1-14.

Sleeper, H.P. 1972. Planetary resonances, bi-stable oscillation modes and solar activity cycles. National Aeronautics and Space Administration Contractor Report CR-2035, Washington, D.C.

Veizer, J. 1983. Chemical diagenesis of carbonates: theory and application of the trace element technique. In: Arthur, M.A., Anderson, T.F., Kaplan, I.R., Veizer, J. and Land, L.S. Stable Isotopes in Sedimentary Geology. Society of Economic Paleontologists and Mineralogists Short Course Notes No.10, Tulsa, Oklahoma, p.3.1-3.100.

Weedon, G.P. 1989. The detection and illustration of regular sedimentary cycles using Walsh power spectra and filtering, with examples from the Lias of Switzerland. Journal of the Geological Society of London, v.146, p.133-144.

White, A.F. 1977. Sodium and potassium coprecipitation in aragonite. Geochimica et Cosmochimica Acta, v.41, p.613-625.

White, A.F. 1978. Sodium coprecipitation in calcite and dolomite. Chemical Geology, v.26, p.65-72.

Yurtsever, Y. 1975. Worldwide survey of stable isotopes in precipitation. Report of the Isotope Hydrology Section, IAEA, 40pp.

Zenkevich, L.A. 1957. Caspian and Aral Seas. In: Hedgpeth, J.W. (ed) Treatise on Marine Ecology and Palaeoecology. Memoir of the Geological Society of America, No.67, p.891-916.

Zubakov, V.A. and Borzenkova, I.I. 1988. Pliocene palaeoclimates: past climates as possible analogues of mid-twenty-first century climate.

Palaeogeography, Palaeoclimatology, Palaeoecology, v.65, p.35-49.

Plate 4.1. Gradational contact between the organic-rich unit A and organic-poor unit B. Note the development of decimetre-scale organic-rich/organic-poor couplets preserved within unit A.

Plate 4.1.

Plate 4.2. Scanning Electron Microscope photographs:

(a) Organic-poor marl showing idiomorphic dolomite rhombs (sample B-8).

(b) Organic-poor marl with aligned clay fabric wrapping around dolomite rhombs (sample B-6).

(c) Organic-rich marl containing elongate aragonite needles and blocky low-Mg calcite and dolomite grains (sample B-32).

(d) Organic-rich marl, here composed almost entirely of clay flakes, which wrap around a single rounded detrital grain, possibly of aeolian origin (sample B-1).

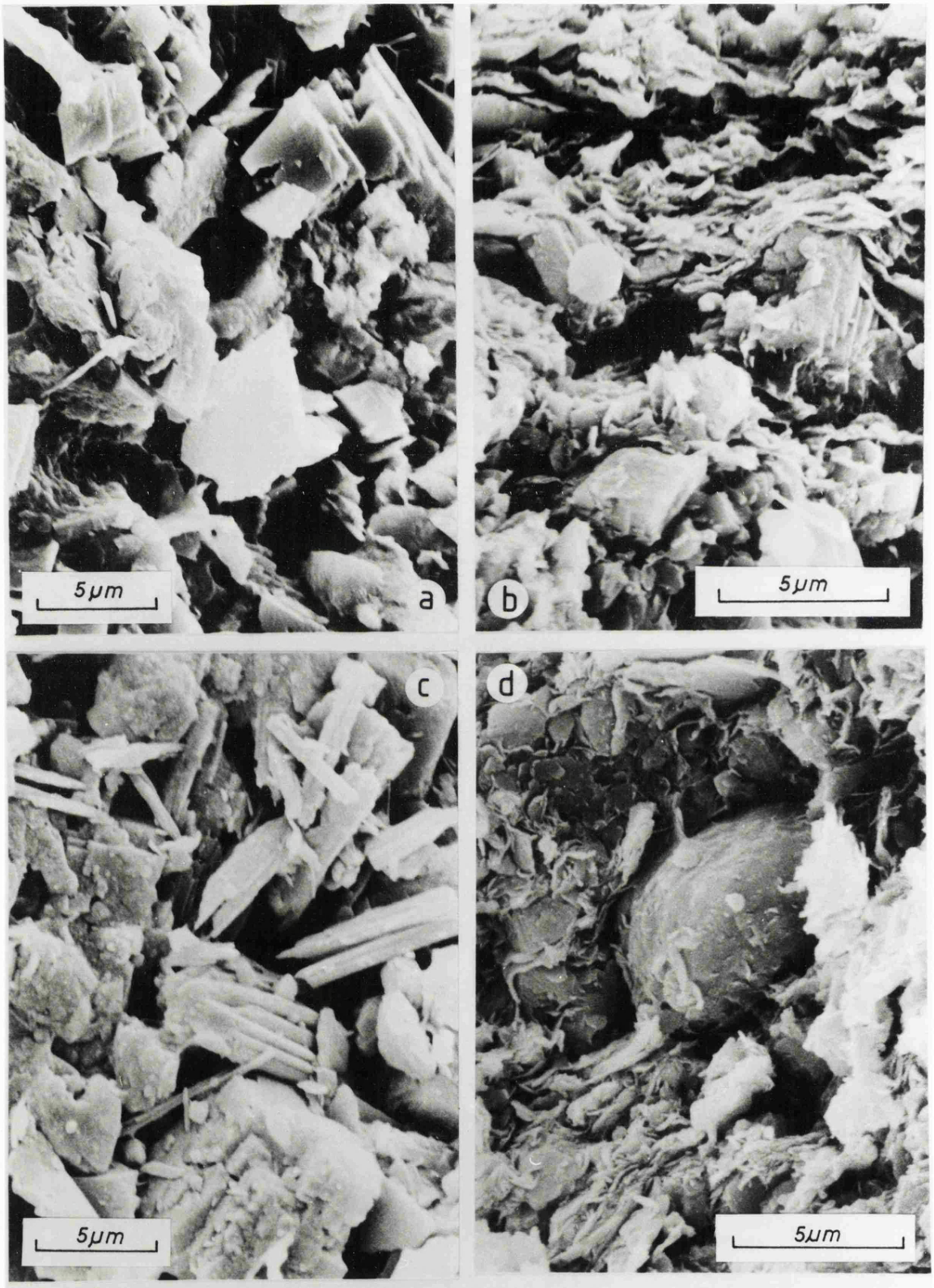

Plate 4.2.

CHAPTER FIVE.

THE STRUCTURE OF THE BURDUR-ACIGÖL-BAKLAN BASIN SYSTEM, SW TURKEY.

5.1. INTRODUCTION.

Many maps have been published showing the main neotectonic structures of western Turkey (e.g. Koçyigit 1984; McKenzie 1978; Sengör 1987; Sengör et al. 1985). Although these correctly show the trends of the major basins, there is an inconsistency in the location of the surface breaks of major faults controlling these basins, especially in the study area, which comprises the Burdur, Acigöl and Baklan Basins (see enclosure 2). This is partly due to the lack of detailed fieldwork in many of the regions and also because on many maps only fault breaks associated with recent large earthquakes are shown.

Previous studies in the Burdur region have done little to highlight the deep structure of the neotectonic basins. Penck (1918) believed the Burdur Basin to have formed in a downwarp caused by a late Tertiary syncline. Wedding and Inque (1967) and, later, Karaman (1986) recognised the importance of the topographic break on the SE side of Lake Burdur and both related this to faulting. Erinç (1967) showed that the Acigöl Basin was controlled on both sides by large-scale faults and both Bering (1971) and Koçyigit (1984) produced block diagrams of the region showing the basins to be symmetrical grabens. More recently, sedimentological studies on a basin margin fan delta sequence led Kazanci (1988) and Kazanci and Erol (1987) to propose that the Burdur Basin is a symmetrical graben with movement on the boundary faults occurring alternately to create a "see-saw" motion.

This chapter describes the surface geometry of faults in the Burdur-Acigöl-Baklan system and also the deep structure of this system. Extension magnitudes and directions are also described.

5.2. BASEMENT FAULTS.

The topography of the study area is dominated by the linear NE-SW

trending basement highs of Besparmak Mountain, the Sogut Mountains, the Yan Mountains and Maymun Mountain (enclosure 2). These are structurally-controlled fault-bounded tilt blocks. Syn-depositional faults affecting the basement (basin-boundary faults) control the topography in the region. For the purposes of this study, basement faults are subdivided into those of Neogene and those of Quaternary age. This subdivision is in view of the fact that the Neogene and Quaternary basins in the study area do not coincide and are geographically unrelated. The dating of the basement faults into either Neogene or Quaternary is based primarily on the age of the sediments in the basins which they control. Quaternary basement faults control the basins which contain Quaternary sediments (and are presently active). Because these faults are generally still active, they control the topography and their slip planes are well-exposed and easily studied. Neogene basement faults are those which form the boundaries to the now inactive Neogene basins. Most of these faults became buried at the end of the Neogene and are poorly-exposed.

5.2.1. Quaternary Basement Faults.

A detailed description of each locality where Quaternary basement faults can be observed would prove rather laborious and unnecessary, so the following is a more concise description of such faults in the study area picking out some of their main features, in particular their surface expression. Enclosure 2 shows the distribution of Quaternary faults in the study area.

(a) The Burdur basin.

Quaternary basement faults bounding the Burdur basin are mostly on its SE side at Suludere, Yassigume, Hacilar and Pinarbasi, all developed in basement Mesozoic limestone. At each of these localities a slip plane up to 20m high is developed. These slip planes overlie compact breccia sheets and are overlain by incoherent breccia up to a metre in thickness. The slip planes themselves are slickensided (often with more than one generation of striation) and corrugated with a wavelength of about a metre. Often more than one slip plane is developed. Striae on clasts within fault breccias is common and shows that not all of the shear is taken up on slip planes. Quaternary debris is seen to overlie slip planes at most localities and, in each case, the contact is an unconformity. This is the type 2 contact of Stewart and Hancock (1988). The only

basement faulting observed on the NW side of the basin is at Kubur (TG584925), where a large fault displaces a recent erosion surface by about 15m. Tension gashes are well-developed on the slip plane of this fault. Most of the faults controlling the Burdur Basin cannot be traced for more than 1km. This is because the Quaternary Burdur Basin formed by dissecting an earlier Neogene Basin. Therefore much of the footwall of Quaternary faults is composed of rapidly eroding Neogene sediment, which gives no surface topographic expression (Fig.5.1). It is only where topographic highs in the basement occur (such as at Suludere, Yassigume, Hacilar and Pinarbasi) that the faults can be observed at the surface (Plate 5.1a). The city of Burdur is situated at the edge of a 20km long scarp of Neogene and Oligocene sediments which trends NE-SW. Although there is no evidence for faulting in these sediment it is seen to be a fault by the small basement high of Eo-Oligocene conglomerate at Karaburun, 3km NE of Burdur. Here, on the NW side of this inlier is a well-developed slip plane. Further evidence for faulting continuing between the basement highs at depth is the position of surface fault breaks associated with recent large earthquakes. These occur in recent sediments on the SE side of the lake basin between the basement highs (Erinç et al. 1971; Ambraseys 1988).

(b) The Acigöl basin.

The longest continuous fault in the study area is the fault on the SE side of the Acigöl Basin (the Acigöl Fault), having an uninterrupted length of 15km and producing the most marked topography, with a footwall relief of 1100m. This fault has a poorly-exposed slip plane, against which is a 10-15m thick incoherent breccia. A wide fracture zone, up to 2km wide at the NE end of the fault, is developed in the footwall. Aerial photographs show this fracture zone to have a strong fabric parallel to the fault. The fault scarp is degraded with a slope angle of 35° (Plate 5.1b). Not all of the faults in the study area have a straight surface expression. The Maymundag Fault on the NW side of the Acigöl Basin trends 095 in the W and bends northward to 050 in the E (see enclosure 2).

(c) The Baklan basin.

The fault on the SE side of the Baklan Basin (the Baklan Fault) shows up on the enhanced Landsat 5 image of the study area (see Chapter 7; Plate 7.2) as a strong 47km long lineament trending approximately 020. However,

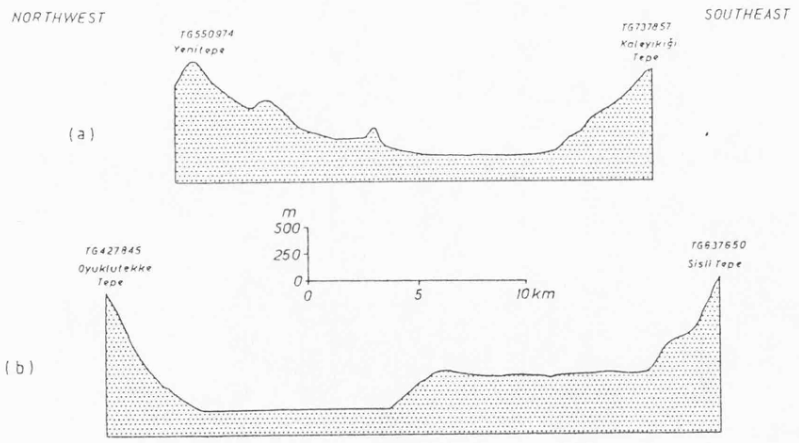

Fig.5.1. (a) Topographic profile across the northern end of the Burdur basin. Note the steeper slope of the southeast basin margin. Both basin margins are composed of Eo–Oligocene flysch sediments. (b) Topographic profile across the southern end of the Burdur basin. The shallow slope of the southeast basin margin is due to the rapid erosion of Neogene marl. The increase in slope towards Sisli Tepe marks the contact between Neogene marl and more resistant Mesozoic limestone. (For the exact positions of both profiles see enclosure 1).

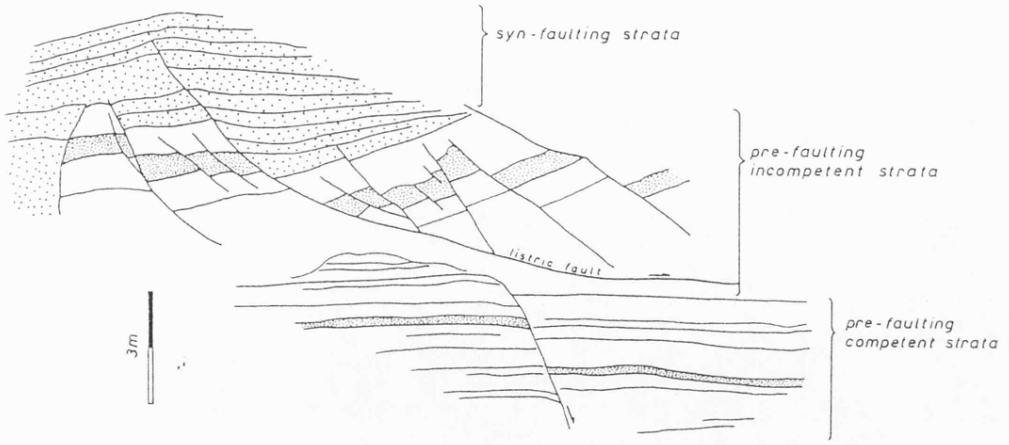

Fig.5.2. Sketch of the listric syn-depositional growth fault within lacustrine marls and siltstones 3km ENE of Suludere (TG542719) (see Plate 5.3a). Bedding has been restored to horizontal. The listric fault displaced relatively unconsolidated sediments as a response to block faulting in the more competent strata beneath.

in the field it can be seen to be a broken scarp composed of 8-9km long segments. The only place where a slip plane can be observed on this fault is at Besparmak Dag near to Baklan. S of this locality the fault cannot be traced in the field as it passes through soft easily erodible and poorly exposed Neogene sediments and therefore has no surface topographic expression. The Baklan Fault is interesting in that, at its northern end, it crosscuts an earlier fault trending 055 near to the village of Tokça. Although no slip plane exists for this fault, 3 erosion surfaces in the uplifted footwall tilt away from the fault towards the SE, showing its polarity (i.e. dip to the NW).

The lack of continuity along strike is a feature of active normal fault zones with apparently large surface ruptures associated with earthquakes being composed of smaller (always less than 25km) ruptures (see, for example, Jackson and White 1989; their Fig.2). Jackson and White (1989) points out the apparent relationship between the length of surface fault segments and the thickness of the upper seismogenic layer of the crust. This segmentation extends to depth as seismograms from earthquakes giving rise to segmented surface faulting show that slip occurred in discrete "sub-events" separated by a few seconds (Doser 1985, Eyidogan and Jackson 1985, Yielding 1985). The break up of a fault zone into smaller blocks, which continue at depth, is a geometrical requirement of blocks rotating both on horizontal and vertical axes (Jackson and White 1989).

5.2.2. Neogene Basement Faults.

Basement faults of undoubted Neogene age are rare in the study region. Many of the Quaternary faults may represent older reactivated structures. Two faults which are definitely Neogene in age are the fault S of Kayaalti, described below, and the boundary fault to the Neogene Burdur Basin.

The Kayaalti Fault is sub-vertical and even has a reverse sense of displacement along part of its length (Plate 5.2a). This orientation indicates a rotation of at least 30° since its formation (assuming Andersonian fault mechanics). Since Quaternary rotations in the region are of the order of only a few degrees (see below), the structure must be Pre-Quaternary in age.

The boundary fault of the Neogene Burdur Basin is exposed at only 2

localities; 1km NE of Soganli and 1km N of Karacaören. At both localities Neogene fluvio-lacustrine sediments are in contact with basement serpentinite. At Karacaören the fault is exposed in a road cutting. Although masked in part by a landslip, Neogene travertines and marls can be seen to dip away from the fault plane which has a shallow dip of 47° to the NW. At Soganli a valley has eroded through the buried fault to give an excellent exposure of the basin boundary (Plate 5.2b). Neogene fan delta sediments dip away from the fault plane which here has a dip of 47° to the NW. In detail the fault is a 4m wide zone. Moving from the hanging wall into the footwall the following sequence is observed:

(i) Neogene hanging wall sediments. Well-cemented next to fault plane.

(ii) A 1m wide zone of broken marl (Neogene) with chert blocks (basement) to 1m.

(iii) A 3m wide zone of highly sheared serpentinite.

(iv) Heavily jointed in situ basement serpentinite and chert.

The dip of the sediments away from the fault plane at both localities is not "drag folding" but the increasing effect of compaction in a thickening sediment pile moving away from the fault (see Chapter 6).

5.3. FAULTS WITHIN THE NEOGENE SUCCESSION.

Faults within the Neogene sedimentary cover fall into 5 categories.

5.3.1. Syn-depositional tectonic faults.

These are meso- and macro-scale structures (Hancock 1985). Faults belonging to this category are mainly normal although reverse faults do occur. The growth geometry of the normal faults is usually confirmed by thickening of the sedimentary sequence in the hanging wall. Although planar in outcrop scale they do occasionally show listric geometry (Fig.5.2, Plate 5.3a). Reverse faults also occur in some areas and these break through the penecontemporaneous sediment surface as seen in Plate 5.3b where the fault has broken the surface to form a topographic scarp, over which a brittle travertine horizon has draped.

5.3.2. Post-depositional tectonic faults.

These are often impossible to distinguish from syn-depositional faults. They are most commonly mesofaults in the sedimentary pile above a buried basement fault such as at Kubur and Soganli. This shows that movement occurred on the basement faults after their burial. Faults within the sedimentary succession often have a reverse orientation as a result of progressive rotation of a normal fault (Plate 5.3c) (Jackson et al. 1982). Mesofaults are much more common than macrofaults (which have measured displacements up to 50m). All faults within this category are generally planar in outcrop, forming conjugate sets with well-developed frictional wear striations, which can easily be confused with plumose markings on joint surfaces. These striae are often accompanied by asymmetric incongruous steps perpendicular to them. The fault surfaces are well-polished in clay-rich lithologies. The age of these faults is not always easy to determine.

5.3.3. Landslips.

Recent landslips are extremely common due to the unconsolidated nature of the Neogene sediments. They should not be confused with tectonic faults, with which they share many characteristics (e.g. displacements up to several tens of metres, faults antithetic to the main listric profile, striated surfaces). They can be recognised by the fact that they often displace Recent colluvium and they involve much larger rotations than the tectonic faults, with near vertical beds often sitting above a near horizontal detachment. The best examples of this latter phenomenon can be found in road cuttings on the Antalya road just outside Burdur. Neogene landslips and slumps are common next to the buried Neogene basement fault at Soganli.

5.3.4. Liquefaction-related faults.

These are normal microfaults associated with ball-and-pillow type liquefaction. They can be found within a centimetre or so of the sediment downwarp, formed by liquefaction and they represent the brittle rearrangement of sediment as the pore-fluid pressure diminishes after the shock has passed. Also, laminated lacustrine sediments contain many normal microfaults, which often stop abruptly at "fluidized" detachment surfaces.

5.3.5. Compaction-related faults.

This is an unimportant group of normal microfaults commonly observed in fluvial siltstones and sandstones which compact around conglomerate lenses.

5.4. PALAEOSTRESS ANALYSIS.

5.4.1. The method

Determination of the principal stress axes of a region can be undertaken from a study of the faults and their associated striae, which formed under the stress regime in question. There are several methods of determining principal palaeostress axes from such a data set, all sharing the basic assumption that the direction of maximum resolved shear stress on the fault plane is shown by the striation. Methods range from simple graphical methods, such as the "right-dihedra method" of Angelier and Mechler (1977) to more complex methods, where a mean stress tensor is computed (e.g. Angelier 1979). The method used in this study is a version of the "right-dihedra" method, which has been improved by Lisle (1987). The necessary software to perform this analysis is given in Lisle (1988).

A fault plane and perpendicular auxiliary plane, where striae on the fault plane are normal to the auxiliary plane, will define a pair of compressional dihedra (containing σ_1, the maximum compressive principal stress axis) and a pair of extensional dihedra (containing σ_3, the minimum principal stress axis). Knowing the sense of slip on the fault allows it to be deduced which pair of dihedra contain σ_1 and which σ_3 (Fig.5.3). Stereographically combining data from several faults by overlapping the dihedra confines σ_1 and σ_3. This is the "right-dihedra method" of Angelier and Mechler (1977). Lisle's (1987) method further constrains σ_1 and σ_3 because, for any given fault, admissible slip directions lie in a sector bounded firstly by the line which is the orthogonal projection of σ_1 and secondly by the line which is the orthogonal projection of σ_3 (Fig.5.3). Disadvantages of these simple graphical methods are that no distinction is made between the fault plane and the auxiliary plane and Φ, the ratio of principle stress differences (defined by Angelier 1989) is not determined.

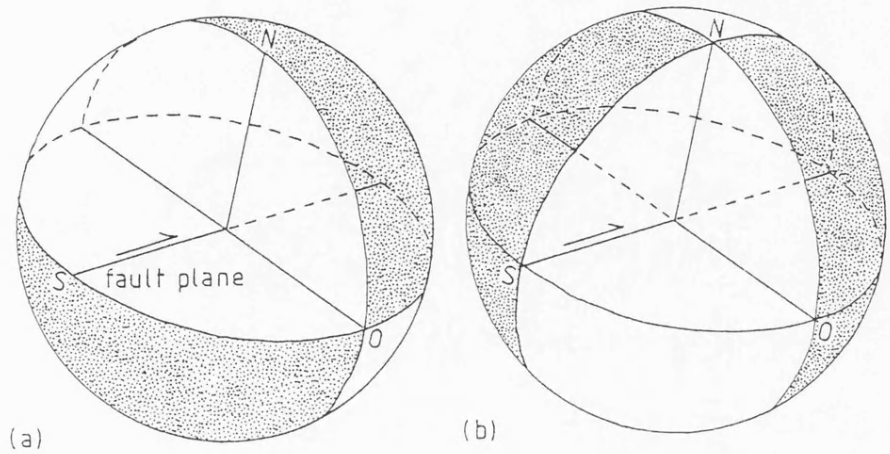

Fig.5.3. (a) σ_1 and σ_3 defined by fault plane (plane containing slip direction S and O) and "auxiliary plane" (plane containing O and N). σ_1 dihedra are unshaded; σ_3 dihedra are shaded. (b) Right dihedra (so-called "A and B dihedra") bounded by planes SN and ON. A dihedra are shaded and B dihedra are unshaded. Lisle (1987) showed that σ_1 and σ_3 are located in different pairs of dihedra, that is if σ_1 lies in A pair, σ_3 must lie in B pair, and vice versa (after Lisle 1988).

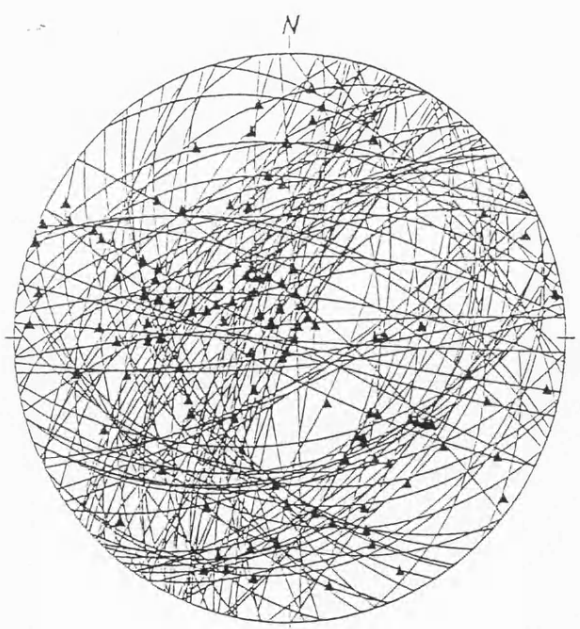

Fig.5.4. Lower hemisphere stereographic projection of faults which displace basement lithologies in the Burdur region.

5.4.2. Data and results

Fault plane and striae data are available for both Quaternary basement faults and faults within the Neogene succession in the study area. The majority of data are from the Burdur Basin and its associated uplifted Neogene sediments (the Burdur Formation) due to the better developed slip planes of Quaternary basement faults and better exposures of Neogene sediments.

Basement fault slip data are available for 4 major fault systems in the study area and are grouped accordingly. These fault systems are, from NW to SE, the Besparmak Dag Fault, the Maymundag Fault, the Acigöl Fault and the Burdur Fault system. All available data for the first 3 faults are used due to the poorer exposure of slip planes on these faults. A combination of fewer readings and possible confusion with palaeotectonic slip planes and striae make the results from these 3 faults less reliable. Many readings are available for the faults surrounding the Burdur Basin. Fig.5.4 shows all of these faults. Obviously the picture is rather complicated so to avoid contamination of data by palaeotectonic faults only selected faults were used. Two criteria were used for selection. Faults chosen must be seen to be basin-bounding (i.e. not well into the footwall) and they must affect the topography. Consequently, the results for the Burdur fault system are more reliable.

Fig.5.5 shows, for each fault, the orientation of slip planes and striae and the orientation of the principal stress axes, calculated using Lisle's method. The direction of least compression, σ_3, for the Burdur, Maymundag and Besparmak Dag Fault is NW-SE. Although little data are available for the latter 2, it can be seen that the faults have a fairly regular orientation. In particular, the Andersonian pattern of faulting at Burdur (Fig.5.5) shows that most measured faults dip to the NW with some dipping to the SE. This latter group are faults measured on the NW side of the basin at Kubur. Striae are generally steep, but with a minor sinistral strike-slip component. The significance of this is discussed in Chapter 7. The calculated principal stress axes for the Acigöl Fault show it to be extending in a NE-SW direction. This is erroneous as such extension (with σ_1 vertical) cannot be achieved on a NE-SW trending fault. Fig.5.5 shows the random distribution of slip planes and striae measured on the Acigöl Fault. The majority of these are minor (possibly palaeotectonic) faults within the footwall. The only reliable slip plane

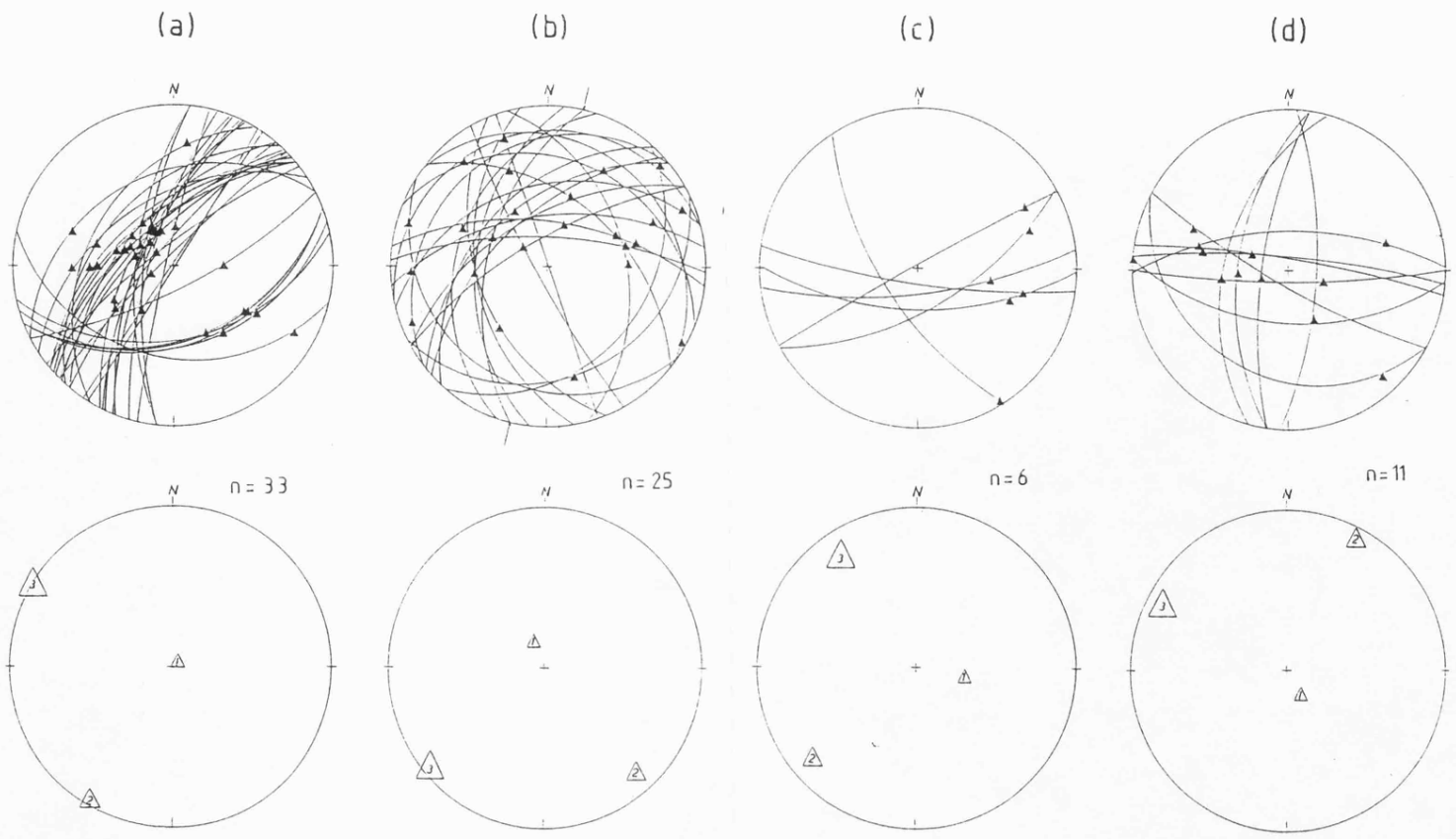

Fig.5.5. Orientation of slip planes and striae for the major fault systems of the study area (a - Burdur Fault; b - Acigöl Fault; c - Maymundag Fault; d - Besparmak Dag Fault). The orientation of the principal stress axes, calculated using the method of Lisle (1987), is also shown (triangles) for each system. The arrows mark the only reliable slip plane measurement on the Acigöl Fault.

found on the Acigöl Fault (at QB602917) is marked on Fig.5.5. This, taken alone, shows a WNW-plunging slip vector, in agreement with the stretching directions of the other major faults in the study area.

The Burdur Formation is grouped into 7 sub-areas and slip plane and striae data from each area combined to determine palaeostress axes. Fig.5.6 shows the fault data and palaeostress axes determinations for each sub-area. The direction of least compression, σ_3, varies in orientation from NNE-SSW (area 7) to WSW-ENE (area 4) averaging approximately NW-SE (Fig.5.6). This large spread of σ_3 is perhaps a combination of the low population of faults in each area and irregular hanging-wall deformation. The former, however, cannot account for the difference in σ_3 orientation of areas 2 and 4 both of which contain a reasonably large number of faults. It would therefore seem that irregular hanging-wall deformation causes most of the variation. One other important factor is the age of the fault. Faults within the Neogene sediment may be either Neogene or Quaternary (or both) in age. It is usually not possible to differentiate between the various possibilities in the field apart from using orientation (i.e. faults conjugate about the horizontal are more recent than those about the bedding in a tilted sequence). This however is not reliable enough to subdivide faults in the sub-areas in terms of their age. Angelier et al. (1981) sub-divided late Tertiary faults in SW Turkey into age groupings, based largely on "earlier stratigraphic studies and tectonic consistency" (Angelier et al. 1981, p.T3). Their theory, which was based on these groupings, has subsequently been invalidated (e.g. Jackson et al. 1982). Therefore the variation in σ_3 orientation may be a result of sampling of a changing stress field.

5.5. STRUCTURE OF THE BURDUR BASIN.

5.5.1. Seismic structure.

Plate 5.4 shows an unmigrated seismic line from the southern part of the Burdur Basin, stretching from Soganli (TG375682) in the NW to Karacaören (TG515557) in the SE. It runs across the Quaternary graben, perpendicular to its axis, in the NW and across the uplifted Neogene sediments in the SE. The line was interpreted using 2-D line migration of the dominant reflectors by Ray Trace Migration with the 'AIMS' computer package at

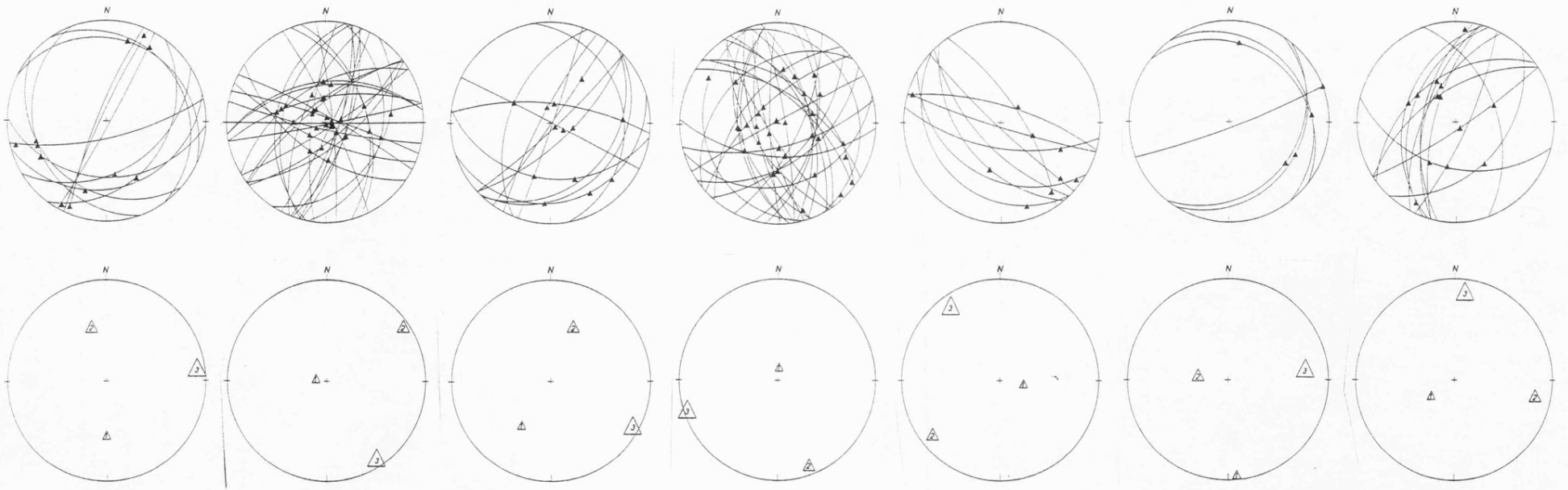

Fig.5.6. Orientation of slip planes and striae for faults within the Burdur Formation. The formation is divided into 7 sub-areas, each with a measured population of faults. The orientation of the principal stress axes, calculated using the method of Lisle (1987), is also given (triangles) for each of these sub-areas.

Leicester University (Tongue 1988). Features of note on this section are the strong reflectors at its NW end. These represent the basinal fill beneath the present day Burdur Basin and are inclined to the SE, terminating near to station number 400, where a large basement fault is observed at the surface, in the field. The continuation of this fault at depth is shown by the presence of a series of diffraction hyperbolae and a line, representing the fault, can be drawn through the apices of these. On this part of the section the deepest reflector correlates with a velocity boundary between internal velocities of 3.3 km/s and 5.0 km/s. This horizon is represented on the sections by a number of curved diffractions off the basement topography, which condense back to their point sources upon migration. There are no major reflectors below 2 seconds two-way-time (which corresponds to a depth of about 2 km) because at this depth basement limestones are reached and these are fairly massive with no large velocity contrasts. Above 1 second two-way-time on this part of the section are four sub-parallel reflectors. There are many internal discontinuities of these reflectors, including curved refractions representing probable small grabens defined by synthetic and antithetic faults within the basinal succession. These are not considered to be of major structural importance and are not discussed further. Also a larger antithetic fault affecting basement and with a throw of about 150 metres can be easily identified.

The SE end of this section represents the uplifted Neogene basinal succession, outcropping to the SE of the present-day Burdur Basin. Here, large hyperbolic diffractions define a normal fault dipping to the NW, against which a series of SE-dipping reflectors terminate. These can be correlated, using their character and pattern, with reflections seen in the NW present-day Burdur Basin (see above), suggesting the presence of Neogene sediments beneath the Quaternary sediments in this basin. Also, not only do reflectors dip to the SE in this part of the section but their separation increases southeastwards as well. Against the presumed fault plane the reflectors clearly dip northwestwards forming a shallow syncline with its axis approximately above the intersection of the fault with the deepest reflector on the section. This syncline is probably a result of dynamic compaction in the thickening sediment pile away from the fault.

Before the section could be migrated, internal velocities were calculated using the Dix Formula (Dix 1955), which gave an accuracy of +/- 10%. This

corresponds to a +/- 50 metre error on the depth section. The general effect of migration is to steepen reflectors and move them up dip. The resulting depth section is shown in Fig.5.7. Residual gravity profiles along the same lines as the seismic sections were modelled using the Talwani 2-D method to produce a depth density model, constrained by the seismic interpretation (see Fig.5.7 and Tongue 1988).

5.5.2. Neogene-Quaternary boundary.

The depth of the Neogene-Quaternary boundary beneath the present day Burdur Basin was calculated to be at a depth of approximately 450m from seismic data (Fig.5.7). This boundary was chosen as it appears to mark a slight unconformity, which may be associated with the end-Neogene tectonic event. The absence of borehole data prevents an accurate determination of the boundary depth but an independent estimate of this depth can be made by considering the volume of material contained within the Quaternary basin. The Burdur and Tefenni Basins form a closed system and all of the sediment eroded from the uplifted Neogene sediments will be deposited in these 2 basins. Therefore by estimating the volume of eroded sediment and knowing the area of the Quaternary basins, their depth can be calculated. Fig.5.8a shows the approximate aerial extent of the uplifted Neogene sediments and the Quaternary basins. The dip of the Neogene next to the Neogene boundary fault is required to calculate the missing volume and a reasonable value for this is 7°. This dip is taken from dip profiles across the Neogene succession (Chapter 6; Fig.6.7b), away from the effect of the hanging wall compaction syncline. The volume of eroded sediment is calculated to be 292km^3 in the Burdur region and 61km^3 in the Tefenni region, giving a total of 353km^3. This was deposited in 2 basins of total length 90.6km and weighted average width 10.23km. The thickness of sediment perpendicular to the dip of the base of the basinal succession, t, is given by the quadratic form

$$0 = t^4 - t^2 l^2 + (2A)^2 \qquad \text{(eq.1)}$$

where l is the width of the basin and A is the cross-sectional area of the basin-fill calculated from the basin volume and length (Fig.5.8b). So substituting the above values into equation (1) a value of 0.76km is obtained for t. This can be considered a minimum estimate for the following reasons:-

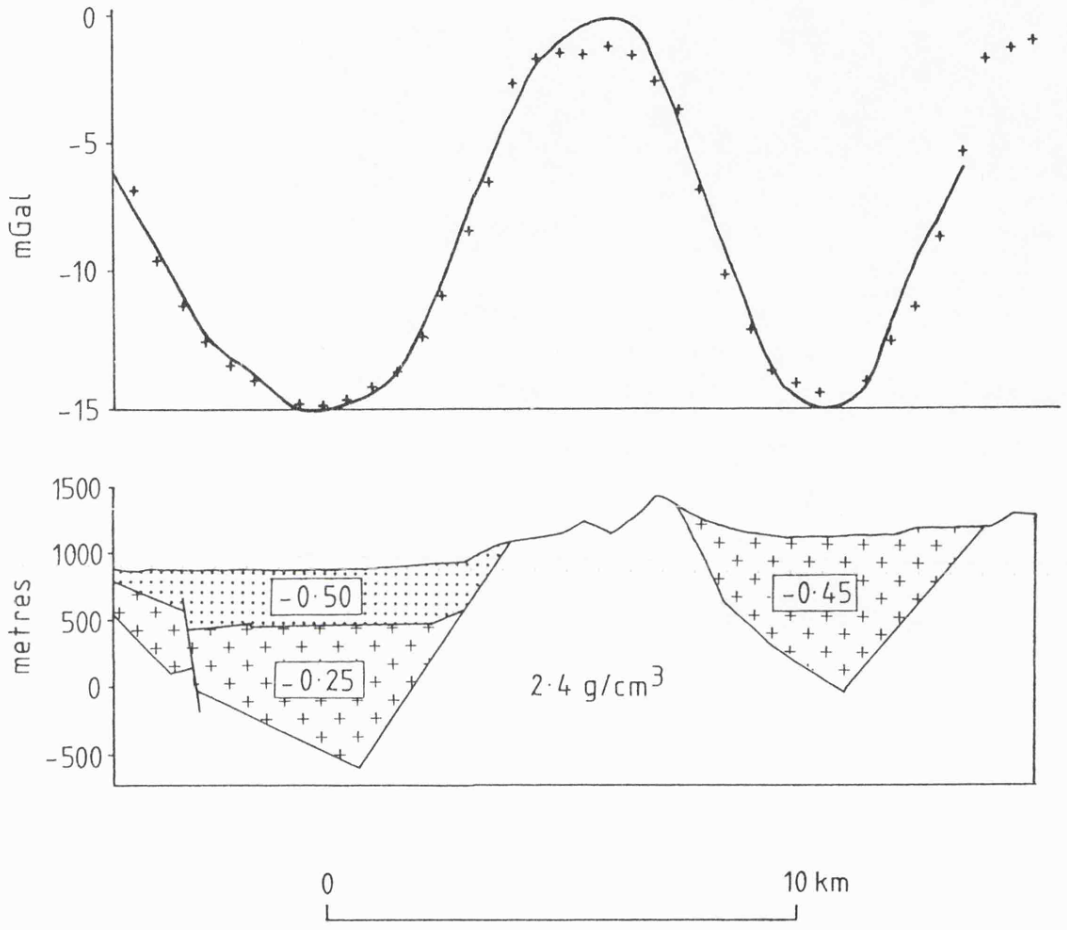

Fig.5.7. Migrated depth-density model of the seismic section shown in Plate 5.4. The dotted and crossed areas are interpreted to be Quaternary and Neogene sediments respectively. The 2 are separated by a slight unconformity, which is the only criterion available for positioning the boundary (after Tongue 1988).

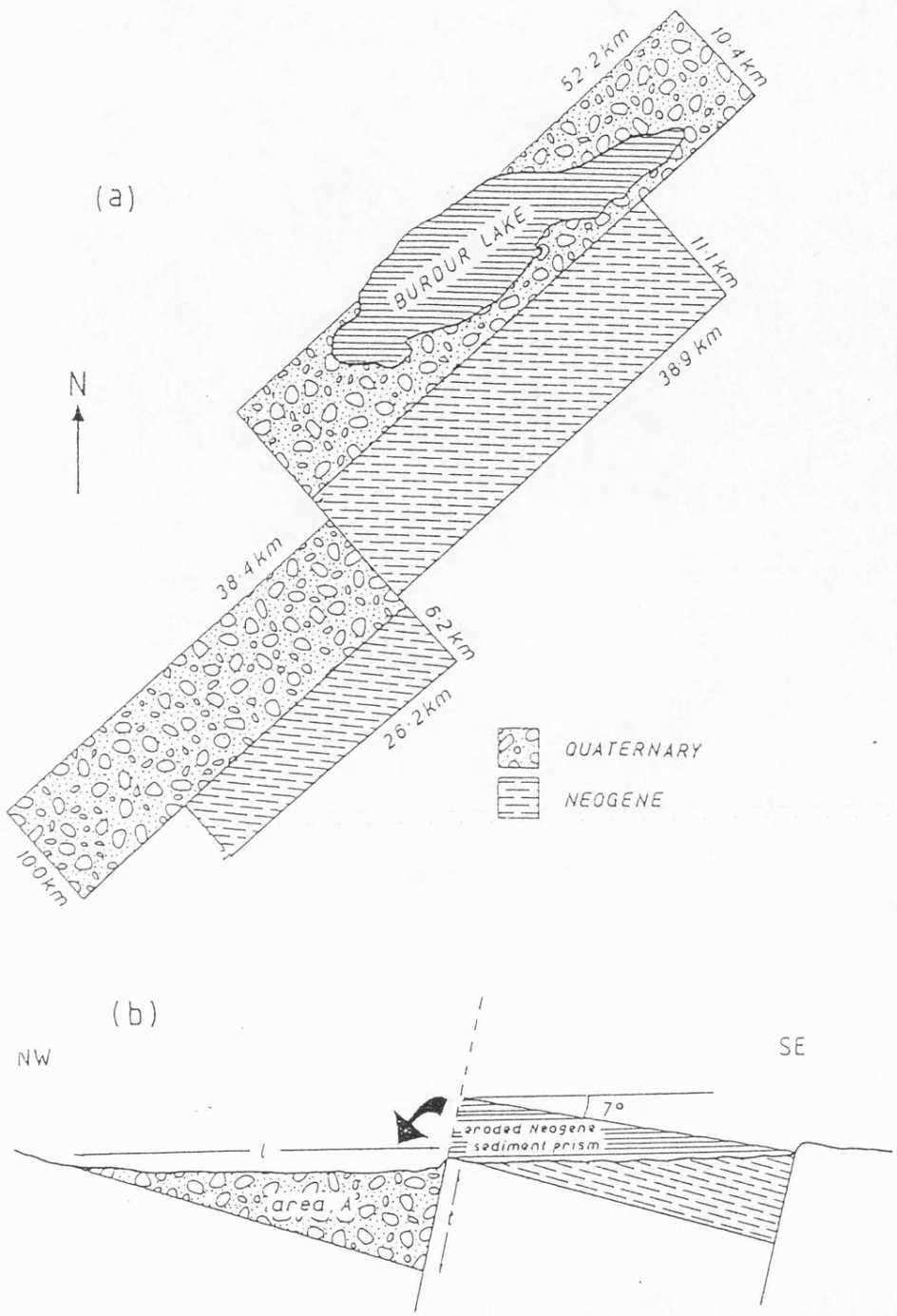

Fig.5.8. (a) Cartoon showing the approximate aerial extent of the uplifted Neogene sediments (dashed hatch) and the Quaternary basins into which they were deposited (conglomerate hatch).
(b) Cross-section through the Neogene and Quaternary basins showing the Quaternary basin width and maximum thickness, l and t respectively, and the cross-sectional area of the Quaternary basin, A. These are related by equation (1).

(a) Although the Neogene sediments are unconsolidated and rapidly eroding they do not provide all of the Quaternary basin-fill.

(b) Both clastic erosion-deposition and chemical dissolution-precipitation styles of sedimentation are operating. The basin is closed so dissolution of the surrounding basement limestones will provide sediment to the Quaternary basin.

(c) The value estimated is an average for both the Tefenni and Burdur Basins. Topographic basement highs protrude through the floor of the Tefenni Basin but not the Burdur Basin, suggesting the former to be shallower.

So, the Neogene-Quaternary boundary is at a depth of 450m or more than 760m according to seismic data and sediment volume considerations respectively. The following geometrical reasoning can be used to decide which of these 2 estimates is more likely.

If a ground surface at an altitude of N_0 is offset by a normal fault then the hanging wall will subside to an altitude N_1 and the footwall uplift to an altitude N_2. Jackson and McKenzie (1983) showed that the hanging wall subsidence will be approximately ten times greater than the footwall uplift.

On the SE side of Lake Burdur in the footwall of the Burdur Fault the contact between basement serpentinite and basal Neogene conglomerates occurs at an altitude of 925m. This boundary is at a depth of 1500m (altitude of -646m) in the hanging wall beneath the Burdur Basin (Fig.5.7). Fig.5.9 shows predicted altitudes for N_0 (assuming footwall uplift to be 10% of hanging wall subsidence) and N_2 assuming values for N_1 of 404m (450m depth) and 94m (760m depth). The lower the thickness of the Quaternary succession, the lower the altitude of N_0, the end-Neogene base level. The present day lake surface is at an altitude of 854m so a drop in base level of 978m and 668m is required to achieve Quaternary thicknesses of 450m and 760m respectively (Figs.5.9a and b). There is no reason to suspect such large drops in base levels throughout the Quaternary. Smaller fluctuations of the order of tens of metres are documented by Erol (1978). A thicker Quaternary succession is therefore favourable. Fig.5.9c shows the predicted Quaternary thickness assuming that N_0 is unchanged (i.e. no drop in base level). Here, most of the

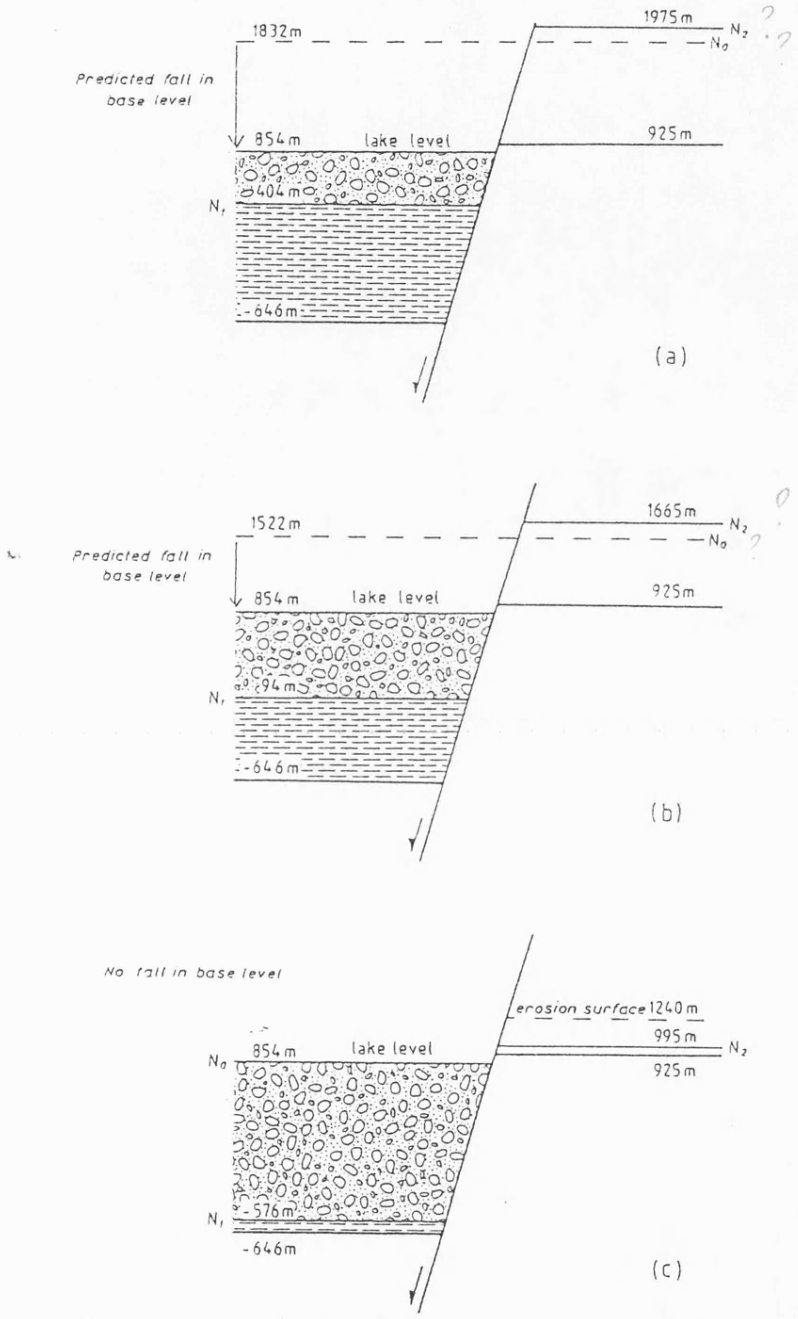

Fig.5.9. Estimation of the depth of the Neogene–Quaternary boundary in the Burdur basin from simple uplift–subsidence considerations (see text for full discussion and definition of symbols).
(a) Position of N_0, N_1 and N_2 assuming the Quaternary succession to be 450m thick as suggested by seismic studies. (b) Position of N_0, N_1 and N_2 assuming the Quaternary succession to be 760m thick as suggested by simple geometrical considerations). (c) Position of N_0, N_1 and N_2 assuming that N_0 is unchanged (i.e. no drop in base level).

basin-fill is Quaternary. For this geometry the top of the Neogene in the footwall must be at an altitude of 995m. However, Neogene sediments are found to an altitude of 1240m in the footwall, where they are crosscut by the D_{III} erosion surface of Erol (1981). This problem can be resolved by considering that the footwall altitude of the basement-Neogene boundary (taken at 925m) was measured on a basement high. In most of the footwall (i.e. in the vicinity of Burdur) it is in the subsurface.

Because of variations in the altitude of the basement-Neogene boundary in the footwall and the unknown base level changes throughout the Quaternary the exact thickness of the Quaternary succession in the Burdur Basin cannot be calculated. However, a thickness of >760m is favourable for the reasons outlined above. The altitudes calculated for N_0 should not be interpreted as absolute heights above Neogene sea-level as regional uplift or subsidence has not been taken into account. For our purposes only the differential movement between hanging wall and footwall is important.

The above reasoning only holds if the fault controlling the Burdur Basin was initiated in the Quaternary and dissected a single Neogene basin. The basin geometry shown in Fig.5.7 could equally be brought about if 2 half-grabens had existed during the Neogene and progressively deepened until, at the end of the Neogene, the southeasterly one became inactive and was uplifted in the footwall of the northwesterly one. A single Neogene half-graben is favoured for 2 reasons. Firstly, along most of the footwall of the Quaternary fault there is no exposed basement showing that Neogene sedimentation was continuous and uninterrupted across the basin. Secondly, basal Neogene conglomerates sitting unconformably upon serpentinite basement in the footwall of the Quaternary fault 1km SW of Kara Burun (TG553761), and therefore in the southeastern basin, contain clasts of Eo-Oligocene conglomerates which are exposed on the NW side of the Quaternary graben. This, again, implies continuous sedimentation across a single Neogene basin.

5.6. EXTENSION.

Tectonic tilts taken from the migrated seismic line (Fig.5.7) can be combined with surface fault dips measured in the field to obtain an estimate of the amount of neotectonic extension which has occurred in the

Burdur region. Because of the uncertainty of the exact position of the Neogene–Quaternary boundary on Fig.5.7, extension is not sub–divided into Neogene and Quaternary. The basal Neogene reflector beneath the Quaternary graben dips at 13° and the Neogene boundary fault, exposed at Soganli, dips at 47°. The geometrical relationship of Thompson (1960) relates the amount of extension, β, to the dip of the faults, θ, and the tilt of the fault blocks, Θ, so that:

$$\beta = \sin(\Theta+\theta) \,/\, \sin\theta \qquad \text{(eq.2)}$$

Substituting the values from the southern Burdur Basin gives a β value of 1.18 since the onset of extension. Although the fault dip is reliable in that it was measured directly in the field, the tilt taken from Fig.5.7 needs confirmation. Fig.5.10 shows poles to bedding for the Burdur Formation (the uplifted Neogene succession on the SE side of Fig.5.7). The centre of the cluster indicates an average tilt of 8° to the SE, which is slightly lower than the true maximum tilt required in equation (2) due to the fact that in an uplifted hanging–wall succession, the dip will change away from the fault due to the shape of the fault in the subsurface (see Chapter 6). So, to a first approximation 13° seems a reasonable value to use.

Equation (2) assumes that the faults are planar at depth . However, a listric fault curvature of up to 10–15° cannot usually be ruled out on seismological grounds (e.g. Nabalek in press). Indeed, it is shown in Chapter 6 that a curvature of up to 40° is possible on the basin–boundary fault of the Burdur basin. White (1988) showed that assuming faults to be planar will underestimate the amount of extension and that β can be estimated for listric faults if the amount of curvature is known, so that:

$$\beta \sin\psi_0 = \sin\psi_1 \qquad \text{(eq.3)}$$

where the tilt of the strata, $\Theta = \psi_0 - \psi_1$, ψ_0 and ψ_1 being the initial and final dip of the fault at depth. If the Quaternary fault at Burdur has a curvature of 15° the value of β increases to 1.33.

In the Acigöl and Baklan Basins there are no subsurface data and β values must be determined from surface tilts and fault dips. Fig.5.11 shows poles to bedding for the Acigöl Formation (the Neogene sediments of the

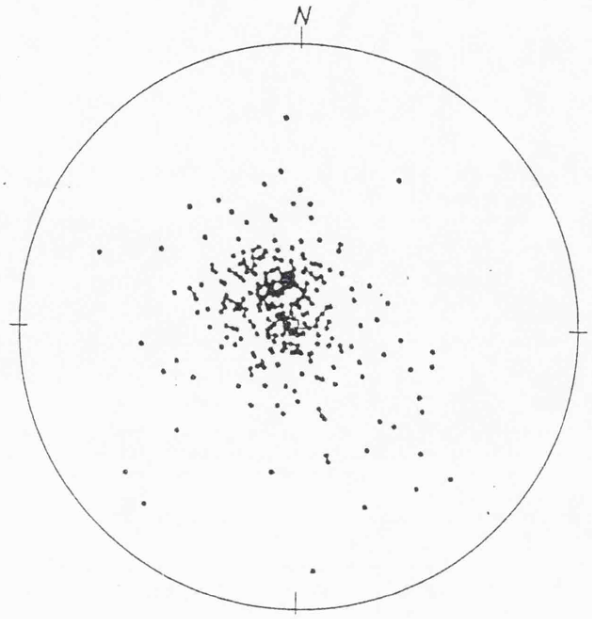

Fig.5.10. Lower hemisphere stereographic projection of poles to bedding for the Burdur Formation.

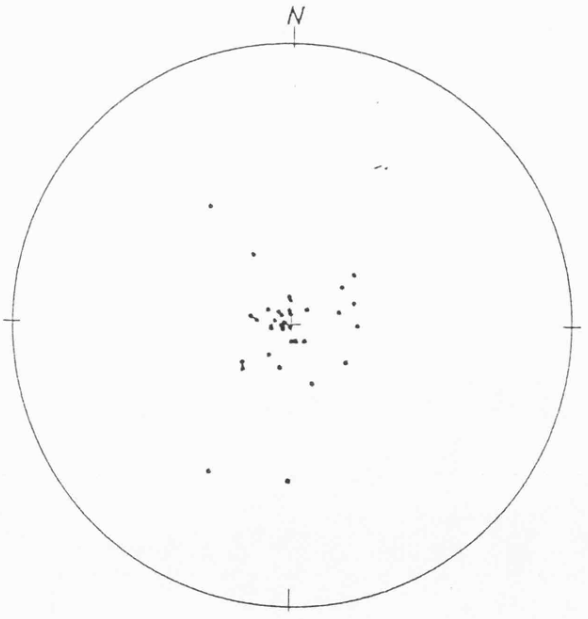

Fig.5.11. Lower hemisphere stereographic projection of poles to bedding for the Acigöl Formation.

Acigöl region) (see enclosure 2). These sediments are near horizontal with an average tilt of about 3° to the ESE. They have not been uplifted to the extent of the Burdur Formation as there is no major fault dissecting them as at Burdur. Therefore, tilts from these sediments should not be used to estimate β. The large degraded fault scarps of Yandagi and Maymundagi attest to large vertical motions associated with extension (e.g. Jackson et al. 1988) in this region in the past.

5.7. DISCUSSION.

The parallel nature and equidistance of the Burdur, Acigöl and Baklan Basins (enclosure 2) suggests that they are deforming in a manner similar to the domino model first proposed by Ransome et al. (1910). This model essentially involves rigid crustal blocks bounded by planar faults. As the crust extends both the blocks and the faults extend to form half-grabens. Each of the 3 studied basins, however, has faulted margins on both sides.

Most of the faults identified around the Burdur Basin outcrop on its SE side and the regional tilt of the Neogene strata, together with seismic data, show that the major faults (i.e. those with the greatest displacements) are on the S side of both the Neogene and Quaternary basins. The lack of seismic data and basin-fill outcrop in the Acigöl and Baklan Basins makes any statements regarding their polarity somewhat circumstantial. However, the size of the fault scarp on the SE margin of the Acigöl Basin (length 15km; relief 1100m) compared with that on the NW margin (length 6km; relief 780m) strongly suggests a greater displacement on the former since as a rule of thumb, assuming a constant base level, uplift is about 10% of subsidence (Jackson and McKenzie 1983). Also, the limited bedding tilt data for the region (Fig.5.11) shows a shallow dip to the ESE, supporting this view. The Baklan Basin is fault-controlled on both sides. No information is available, concerning the tilts of the Neogene sediments outcropping to the NW of the basin but geomorphological data presented in Chapter 7 (section 3) suggest that the fault on the SE side has been more active in the last few hundred thousand years. Also, as Fig.5.12 shows, the Büyük Menderes river occupies an asymmetrical meander belt in the Baklan basin with the abandoned part to the NW of the active channel. The channels of meandering rivers in half-grabens commonly move laterally towards the major basin-boundary fault (e.g. the

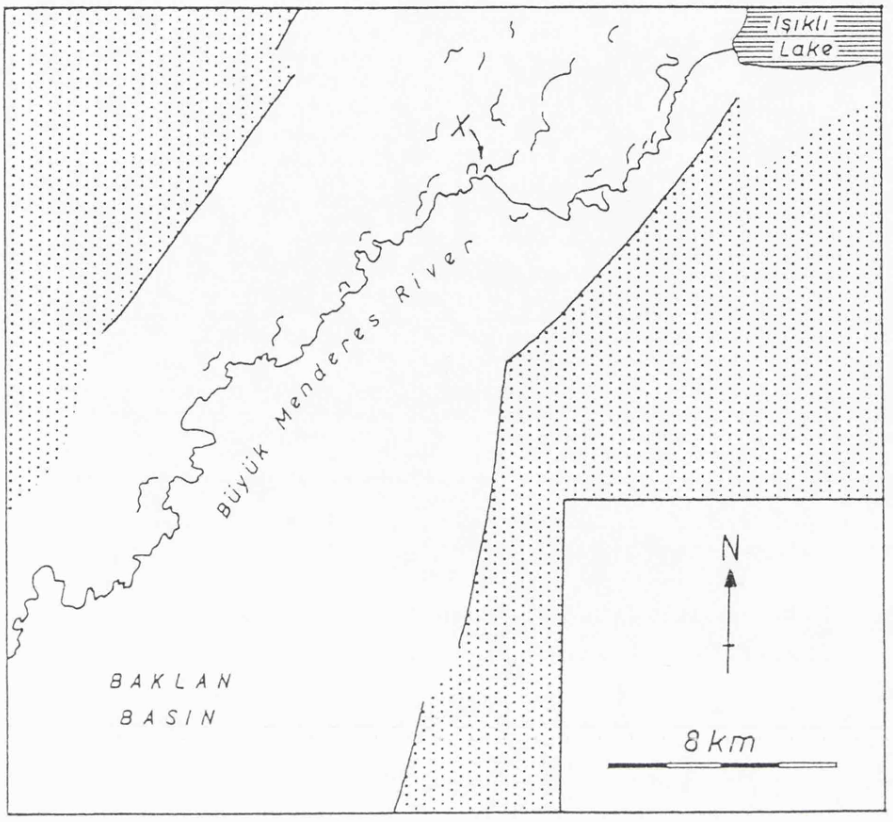

Fig.5.12. The meander belt of the Büyük Menderes river in the Baklan basin. Solid black lines represent basin-bounding faults with the footwalls shaded. The asymetry of the meander belt and the rapid change in course of the channel at X suggest that the major fault is on the southeast side of the basin.

area of maximum subsidence) (Alexander and Leeder 1987). This further suggests that the major fault is on the SE side of the Baklan basin. This process of downslope channel migration is generally slow although at one locality (shown on Fig.5.12) avulsion appears to have occurred instantaneously, probably during a single tectonic event. Here, bank breaching has caused the river to occupy a new, gravitationally advantageous course.

Each of the 3 basins seems to have the same tectonic polarity but the simple domino-model does not apply because the blocks are not behaving rigidly, but are being broken up by antithetic faults (see Chapter 7; Fig.7.2). A possible explanation for this is the instability of the topography formed by the rotating blocks. This is further discussed in Chapter 7.

β values of 1.18 for the Burdur region are at the lower end of the range of β values calculated for faults in central Greece. Roberts (1988) showed a range of β values from 1.2-1.3. Various estimates have been put forward for extension in the Aegean region. Jackson and McKenzie (1988) assumed a constant vertical strain rate for the last 5Ma in the Aegean to come up with a β value of 1.8. This value, they argue accounts for the crustal thinning in the Aegean from an unstretched 40-50km to a stretched 22-32km (Makris 1976; Makris and Vees 1977). Sengör (1978) argued for a minimum β value of 2 for the whole of western Turkey. The discrepancy between extension in the Burdur region and that for the whole of western Turkey is explained by the fact that most of the extension in western Turkey is taken up on the major E-W trending Gediz and Büyük Menderes Grabens, where tilts associated with extension are up to 40° (Sengör 1978; Sengör et al. 1985). As Sengör (1987) points out, caution should be adopted when interpreting β values due to complexities in basin geometry. Such complexities are the subject of Chapter 7.

5.8. REFERENCES.

Alexander, J.A. and Leeder, M.R. 1987. Active tectonic control of alluvial architecture. In: Ethridge, F.G., Flores, R.M. and Harvey, M.D. (eds) Recent Developments in Fluvial Sedimentology. Special Publication of the Society of Economic Paleontologists and Mineralogists, No.39, p.243-252.

Ambraseys, N.N. 1988. Engineering Seismology. Earthquake Engineering and Structural Dynamics, v.17, p.1-105.

Anderson, E.M. 1951. The Dynamics of Faulting, 2nd edition, Oliver and Boyd, Edinburgh, 206pp.

Angelier, J. 1979. Determination of the mean principal stresses for a given fault population. Tectonophysics, v.56, p.T17-T26.

Angelier, J. 1989. From orientation to magnitudes in paleostress determinations using fault slip data. Journal of Structural Geology, v.11, p.37-50.

Angelier, J. and Mechler, P. 1977. Sur une méthode graphique de recherche des contraintes priniples également utilisable en tectonique et en séismologie: la méthode des dièdres droits. Bulletin de la Société Géologique de France, v.19, p.1309-1318.

Dix, C.H. 1955. Seismic velocities from surface measurements. Geophysics, v.20, p.68-86.

Doser, D. 1985. Source parameters and faulting processes of the 1959 Hebgen Lake, Montana, earthquake sequence. Journal of Geophysical Research, v.90, p.4537-4555.

Erinç, S., Bener, M., Sungur, K. and Göçmen, K. 1971. 12 Mayis 1971 Burdur Depremi. Istanbul Üniversitesi Cografya Enstitüsü Yayinlari, No.66, 27pp.

Erinç, S. 1967. Acigöl'un Pleistosendeki Seviyesi Hakkinda. Istanbul Üniversitesi Enstitüsü Dergi, v.16, p.141-143.

Erol, O. 1975. Quaternary deposits of the Burdur Lake Basin. Congress of Earth Science 50th Anniversary of the Turkish Republic, Ankara, p.386-391.

Erol, O. 1978. The Quaternary History of the Lake Basins of Southern and Central Anatolia. In: Brice, W.C. (ed) The Environmental History of the Near and Middle East since the Last Ice Age, Academic Press, p.111-139.

Erol, O. 1981. Neotectonic and Geomorphological Evolution of Turkey. Zeitschrift für Geomorphologie N.F., v.40, p.193-211.

Eyidogan, H. and Jackson, J.A. 1985. A seismological study of normal faulting in the Demirci, Alasehir and Gediz earthquakesof 1969 in western Turkey: implications for the nature and geometry of deformation in the continental crust. Geophysical Journal of the Royal Astronomical Society, v.81, p.569-607.

Hancock, P.L. 1985. Brittle microtectonics: principles and practise. Journal of Structural Geology, v.3, p.437-457.

Jackson, J.A., King, G. and Vita-Finzi, C. 1982. The neotectonics of the Aegean: an alternative view. Earth and Planetry Science Letters, v.61, p.303-318.

Jackson, J.A. and McKenzie, D.P. 1983. The geometrical evolution of normal fault systems. Journal of Structural Geology, v.5, p.471-482.

Jackson, J.A. and McKenzie, D.P. 1988. The relationship between plate motions and seismic moment tensors, and the rates of active deformation in the Mediterranean and Middle East. Geophysical Journal, v.93, p.45-73.

Jackson, J.A. and White, N.J. 1989. Normal faulting in the upper continental crust: observations from regions of active extension. Journal of Structural Geology, v.11, p.15-36.

Jackson, J.A., White, N.J., Garfunkel, Z. and Anderson, H. 1988. Relations between normal-fault geometry, tilting and vertical motions in extensional terrains: an example from the southern Gulf

of Suez. Journal of Structural Geology, v.10, p.155-170.

Karaman, M.E. Burdur ili ve çevresindeki yerlesim alanlarinin depremselligi. Mühendislik Jeolojisi Bülteni, No.8, p.23-30.

Kazanci, N. 1988. Repetitive deposition of alluvial fan-delta wedges at a fault-controlled margin of the Pleistocene-Holocene Burdur Lake graben, southwestern Anatolia, Turkey. In: Nemec, W. and Steel, R.J. (eds) Fan Deltas: Sedimentology and Tectonic Settings. Blackie and Son, p.186-196.

Kazanci, N. and Erol, O. 1987. Sedimentary characteristics of a Pleistocene fan-delta complex from Burdur basin, Turkey. Zeitschrift für Geomorphologie N.F., v.31, p.261-275.

Koçyigit, A. 1984. Güneybati Turkiye ve Yakin dolayinda levha içi yeni tektonik gelisim. Turkiye Jeoloji Kurumu Bülteni, v.27, p.1-16.

Lisle, R.J. 1987. Principal stress orientations from faults: an additional constraint. Annales Tectonicae, v.1, p.155-158.

Lisle, R.J. 1988. ROMSA: a basic program for paleostress analysis using fault striation data. Computers and Geosciences, v.14, p.255-259.

Makris, J. 1976. A dynamic model of the Hellenic arc deduced from geophysical data. Tectonophysics, v.36, p.339-346.

Makris, J. and Vees, R. 1977. Crustal structure of the central Aegean Sea and the islands of Evvia and Crete, Greece, obtained by refraction seismic experiments. Journal of Geophysics, v.42, p.329-341.

McKenzie, D.P. 1978. Active tectonics of the Alpine-Himalayan belt: The Aegean Sea and surrounding regions. Geophysical Journal of the Royal Astronomical Society, v.30, p.109-185.

Nabalek, J. In press. Planar vs listric faulting: the rupture process and fault geometry of the 1983 Borah Peak, Idaho earthquake from inversion of teleseismic body waves. Journal of Geophysical Research.

Penck, W. 1918. Die tektonische Grundzüge Westkleinasiens. Stuttgart.

Ransome, F.L., Emmons, W.H. and Garry, G.H. 1910. Geology and ore deposits of the Bullfrog district, Nevada. Bulletin of the U.S. Geological Survey, No.407, 130pp.

Roberts, S. 1988. Active normal faulting in central Greece and western Turkey. Unpublished Ph.D. thesis, University of Cambridge.

Sengör, A.M.C. 1978. Über die angebliche primäre Vertikaltektonik im Agaisraum. Neues Jahrbuch für Geologie und Palaontologie, v.11, p.698-703.

Sengör, A.M.C. 1987. Cross-faults and differential stretching of hanging walls in regions of low-angle normal faulting: examples from Western Turkey. In: Coward, M.P., Dewey, J.F. and Hancock, P.L. (eds) Continental Extensional Tectonics. Special Publication of the Geological Society of London, No.28, p.575-589.

Sengör, A.M.C., Görür, N. and Saroglu, F. 1985. Strike-slip faulting and related basin formation in zones of tectonic escape: Turkey as a case study. In: Biddle, K.T. and Christie-Blick, N. (eds) Strike-slip Faulting and Basin Formation. Special Publication of the Society of Economic Paleontologists and Mineralogists, No.37, p.227-264.

Stewart, I.S. and Hancock, P.L. 1988. Normal fault zone evolution and scarp degradation in the Aegean region. Basin Research, v.1, p.139-153.

Thompson, G.A. 1960. Problems of late Cenozoic structure of the Basin Ranges. International Geological Congress, XXI Session, Part XVIII, p.62-68.

Tongue, J. 1988. Analysis of the Tectonics of a Cenozoic Basin in SW Turkey. Unpublished B.Sc. thesis, University of Leicester.

Yielding, G. 1985. Control of rupture by fault geometry during the 1980 El Asnam (Algeria) earthquake. Geophysical Journal of the Royal Astronomical Society, v.81, p.641-670.

Wedding, H. and Inque, E. 1967. Report on the lignite bearing Pliocene strata around Burdur city. Maden Teknik Arama Unpublished Report, No.1-11, Ankara.

White, N.J. 1988. Extension and Subsidence of the Continental Lithosphere. Unpublished Ph.D. thesis, University of Cambridge.

Plate 5.1. (a) This photograph shows the view looking SE from Kelhüyük Tepe 2km northeast of Çendik (TG524739). The 3 hills in the right foreground, centre middleground and left background (at Suludere, Yassigume and Hacilar respectively) are composed of basement Mesozoic limestone. They represent topographic highs in the basement, which have been uplifted in the footwall of the Quaternary fault which controls the Burdur basin. This fault can be observed in the field as a slip plane on the NW side of each hill. (The right-hand side on the photograph). The white sediments deposited above and against these basement highs (seen on the left of the photograph) are Neogene marls. They are tilting away from the fault. These sediments have been eroded from between the more resistant basement highs but the presence of the fault between them is indicated by surface cracks associated with recent earthquakes.

(b) View southwest along the southeast margin of the Acigöl basin showing the degraded Acigöl fault scarp. In the foreground are sediments of the Acigöl playa.

Plate 5.1.

Plate 5.2. (a) The Kayaalti fault photographed 3km south of Kayaalti (at TG661655). Here the fault has a reverse sense of displacement seen by the slip plane on the lower right. This reverse orientation is a result of progressive clockwise (in this view) rotations of an originally northwest-dipping fault. (Northwest is to the right on this photograph).

(b) The boundary fault to the Neogene Burdur basin exposed in the valley 1km northeast of Soganli at TG569625. The dark lithology in the footwall is basement serpentinite. Sediments in the hangingwall dip away from the basin margin due to differential compaction in the thickening sediment pile away from the fault. The fault plane has a low dip (47° at this locality) and is eroded and overlapped by basinal sediments near to the 2 trees at the centre of the photograph.

Plate 5.2.

Plate 5.3. (a) A listric syn-depositional growth fault within lacustrine marls and siltstones 3km ENE of Suludere (TG542719). The detachment flattens out at the base of the light grey marl. The tilt of the sediments post-dates the fault, which was controlled by a "tectonic" fault below the detachment (see Fig.5.2).

(b) A low-angle reverse fault within travertines 1.5km northeast of Bogaziçi (TG422576). The fault is not a wet-sediment phenomenon as it displaces brittle travertines. This fault broke through the penecontemporaneous sediment surface, as indicated by the drape of brittle travertine above the small topographic scarp, which post-dates the faulting event.

(c) A high-angle apparent reverse fault formed by the progressive rotation of a normal fault into a reverse attitude. This fault is within the Neogene basinal succession in a road cutting 5km north of Bereket (at TG599643). It is analogous to the "reverse" Kayaalti fault (Plate 5.2a). Here, however, the large post-faulting tilt can be demonstrated by the steeply dipping strata which the fault offsets.

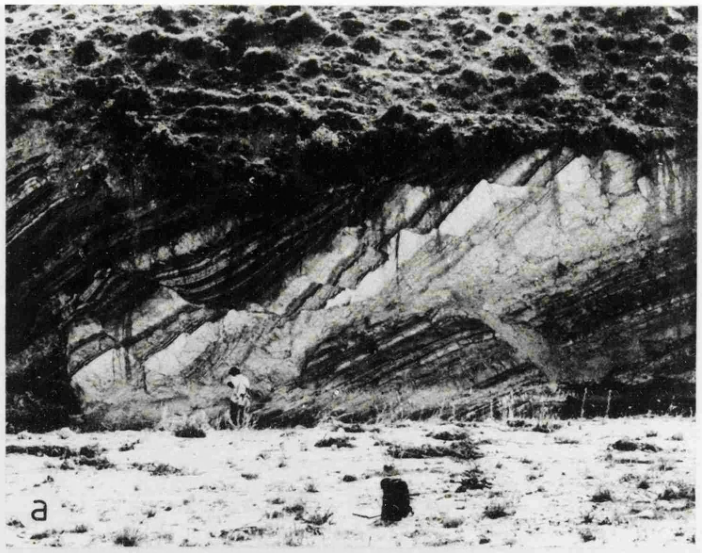

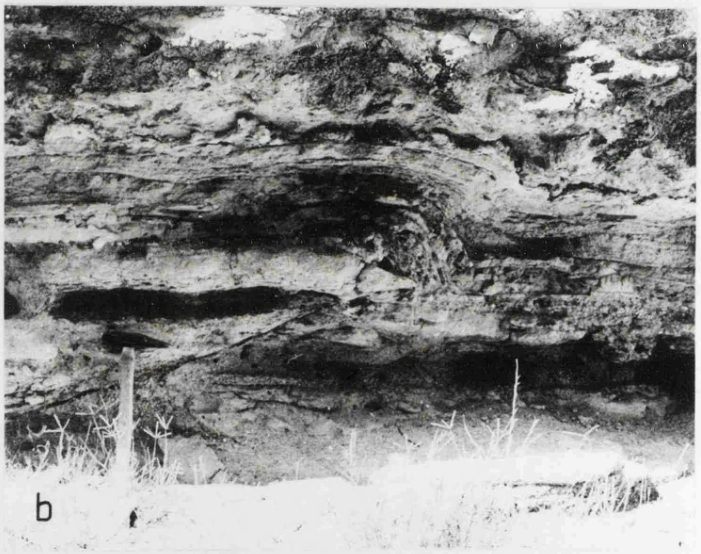

Plate 5.3.

Plate 5.4. Unmigrated seismic line showing the structure of the southern part of the Burdur basin. The exact position of the line is indicated on enclosure 1. Note the SE-dipping reflectors beneath the present-day Burdur basin in the NW and within the uplifted Burdur Formation in the SE. A depth-migrated interpretation of this line is shown in Fig.5.7. (Line courtesy of the Turkish Petroleum Corporation).

CHAPTER SIX

THE SUB-SURFACE GEOMETRY OF BASIN-CONTROLLING FAULTS FROM THE BURDUR REGION, SW TURKEY.

6.1. INTRODUCTION.

It is widely accepted that extension of the continental crust and lithosphere occurs in wide, disributed zones termed taphrogens (Krenkel 1922; Sengör 1987) and that most of the strain in these zones is taken up at shallow levels by large crustal-scale normal faults. It is these faults which usually control the deposition of thick sedimentary piles, which on burial can become viable as petroleum reservoirs. An understanding of their sub-surface geometry and of the geometry of sediments in their hangingwalls is therefore of importance. Such an understanding is best attained by studying regions which are still active, as the structures found in older regions tend to be deformed by later events unrelated to the extension which initially formed them. Jackson (1987) emphasises that although actively extending continental regions differ greatly in both scale and altitude and although the forces driving such extension may also differ between regions, the extension will always manifest itself in the same way. Movement on large crustal faults gives rise to the large (M_S>5.5) earthquakes characteristic of taphrogens (Jackson 1987). These movements account for much more strain than the cumulative effect of smaller and less regular earthquakes, which generally represent a reorganisation of the sediment pile after a large earthquake (Soufleris et al. 1982; Westaway and Jackson 1987).

The surface geometry of these faults is well-documented. There is little doubt that they are the major structures within extending zones as they tend to dominate the topography due to the large vertical movements associated with them. They generally have a strike length of about 10-15 kilometres (never exceeding 20 kilometres) and are arranged in an en echelon manner. This pattern is almost always apparent on maps showing the surface breaks for large earthquakes (e.g. Pleasant Valley, Nevada (Wallace 1984); Dixie Valley, Nevada (Tocher 1957); Hebgen Lake, Montana (Fraser et al. 1964); Bulgaria (Jankhof 1945)). Vertical displacements are greatest at the centre of each fault segment and diminish to zero at the tip. This is indicated by the vertical motions related to elastic

rebound after an earthquake event, which can be picked up on surveying networks, such as was reported by Jankhof (1945) for the April 1928 Bulgarian earthquakes. Isostatic rebound due to unloading of the footwall will amplify this pattern over a longer time period. At zero displacement the fault steps back either to the left or to the right and the pattern continues. This en echelon segmentation is believed to continue at depth as slip within a fault system occurs as discrete sub-events (Westaway and Jackson 1987; Jackson and White 1989).

The geometry of crustal-scale normal faults at depth, however, has been the subject of much debate over the past few years. Two main schools of thought have arisen; one proposing that faults are listric at depth (i.e. have a concave-upward geometry, flattening to a horizontal detachment at some depth within the crust), the other proposing that faults are planar at depth with a "rotating-domino" style of deformation as first proposed by Ransome et al. (1910).

This chapter deals with the sub-surface geometry of major basin-controlling normal faults in the Burdur region, which can be sub-divided into faults of Neogene and faults of Quaternary age. The latter group are still active, enabling fault plane solutions from major earthquakes to be compared with surface observations, giving the geometry of the fault at mid-crustal levels and at the surface. The system of faults formed during the Neogene is now inactive and its geometry can be inferred by studying the geometry of its hangingwall succession. Finally, fault dips and hangingwall bedding tilts for both sets of faults are considered in terms of simple rotations on curved surfaces. The depths of detachment for both data sets are calculated and these are compared with independent estimates to show the validity or otherwise of such a geometry.

6.2. QUATERNARY FAULT GEOMETRY.

Faults in the study area which became active during late Pliocene / early Quaternary times provide the most accurate information on the surface and sub-surface geometry of active normal faults. This is because they are still active and their surface geometries have changed little since their initiation. Also, a large earthquake occured on the Burdur Fault in 1971, enabling a fault plane solution to be produced (McKenzie 1978), which gives an indication of the sub-surface geometry of the fault.

6.2.1. Surface fault dips

Fig.6.1 shows the range of dips for basement fault planes of Quaternary age. These are dips measured at the surface in the field. Two main groups of fault, based on dip, are evident. The first represents faults dipping between 20° and 70° (with most in the range 40° to 65°). This range is representative of the range of dips for active normal faults from earthquake focal mechanisms, which range between 30° and 70° (Jackson 1987). If the domino model of faulting, first adopted by Ransome et al. (1910), applies, then the range of fault dips can be viewed in terms of progressive rotations, where faults start at about 60° and rotate through to 30°, where due to gravity they become inactive and a second generation develops. The upper dip limit is predicted by Andersonian fault mechanics (Anderson 1951). The maximum on the histogram in Fig.6.1 is at 55°-60°. It therefore seems that little rotation has occured in the study area since the faults were initiated, probably at the beginning of the Quaternary. This, of course, assumes that the faults are first generation. There is no evidence (i.e. very low-angle faults) to suggest otherwise.

The second group of faults shown in Fig.6.1 are steeply dipping (70°-90°). These represent two types of fault easily distinguished in the field:

(a) Older (i.e. Neogene) large basement faults, which have become progressively rotated into a steeper orientation. Old faults will be steepened if their dip is in the direction of downward rotation. An example of this is the long Kayaalti fault striking 025 on the western edge of Besparmak Mountain (see enclosure 1). In places this has been rotated into a reverse attitude (see Chapter 5; Plate 5.2a).

(b) Cross-faults, which are sub-vertical and perpendicular to the main fault plane. These are meso-scale structures, which probably accommodate differential movement on a fault plane. They are fairly common (e.g. at TG520676) where a sub-vertical cross-fault displaces the main fault by about 50m). In this example striations on the slip plane are dominantly strike-slip. These are not relay structures between kilometre-scale fault segments. They displace individual faults bounded by relay structures. Neither are they the same as the cross-faults of Sengör (1987), which do not displace the footwall of

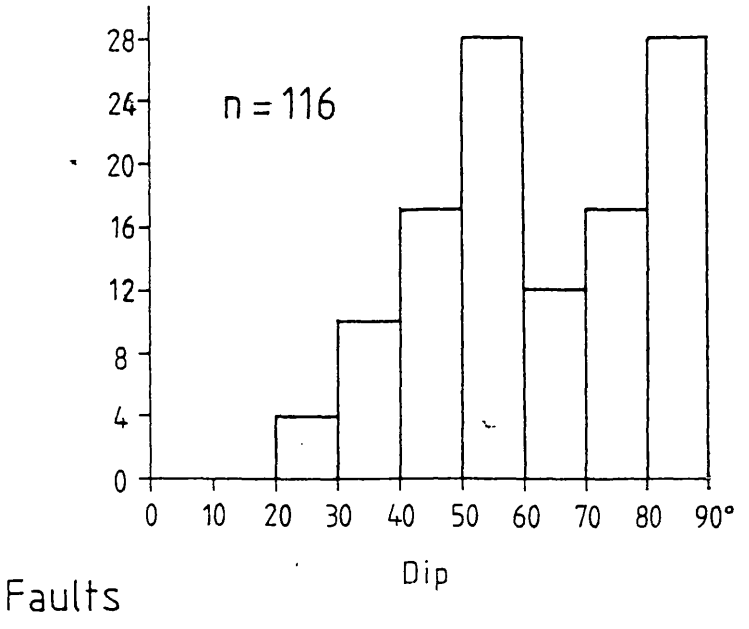

Fig.6.1. Histogram of dips of Quaternary basin-boundary faults from the study area. (Each value represents a single measurement. More than one measurement may occur on a single fault plane).

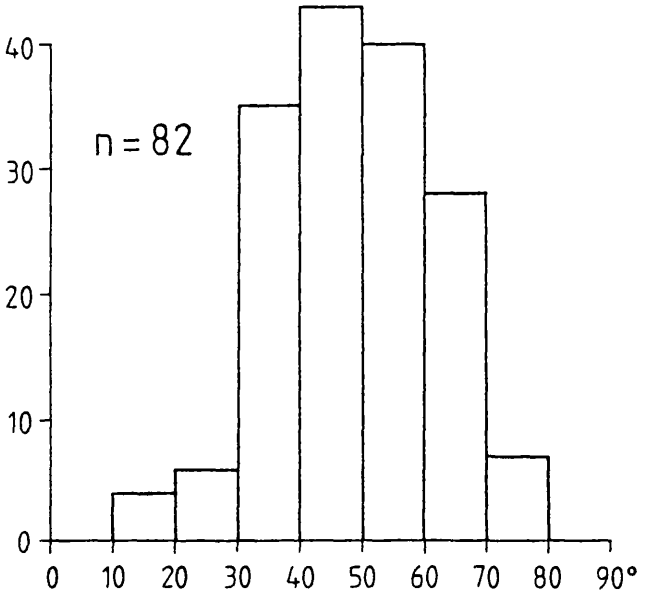

Fig.6.2. Histogram of seismogenic normal fault dips (from Jackson 1987).

the main fault.

The histogram of seismogenic fault dips shown in Jackson (1987) does not have a steeply dipping peak (Fig.6.2). This is because type (a) faults are inactive and type (b) faults would not give rise to large earthquakes.

6.2.2. Surface slip vector dips.

Fault plane solutions obtained from seismic events show the slip vector of the fault at the earthquake hypocentre. This will be the same as the fault dip for a purely dip slip normal (or reverse) fault. However, as surface observations show that most normal faults have a minor strike slip component, the slip vector measured at the surface is of importance when comparing surface observations with nodal planes taken from fault plane solutions. Striae measured on faults controlling the Quaternary Burdur Basin generally plunge in the range 40–80° (Fig.6.3). The faults chosen in Fig.6.3 are those which bound the basin (i.e. exhibit considerable topographic footwall uplift and have a strike sub-parallel to the long axis of the basin). The average surface slip vector plunge is 53° (±15°).

6.2.3. Seismological observations.

The fault plane solution for the 1971.5.12. (m_b = 5.5) event at Burdur, taken from McKenzie (1978), is shown in Fig.6.4. 2 nodal planes are indicated, one dipping at 42° towards 312 and the other at 50° towards 154. These are both well constrained and their strike is insensitive to the crustal velocity (McKenzie 1978).

McKenzie (1978) takes the southeasterly dipping nodal plane to be the main fault, the surface break of which he indicates to be on the NW side of the Burdur Basin. However, surface breaks associated with this event occured on the SE side of the basin, with none being documented from the NW side. These fault breaks were downthrown to the NW by up to 30cm (Erinç et al. 1971; Keightley 1975). This suggests that the NW-dipping nodal plane represents the fault plane with the auxiliary plane dipping to the SE. In this case, the slip vector at the hypocentre plunges at 40° towards 334 (Fig.6.4).

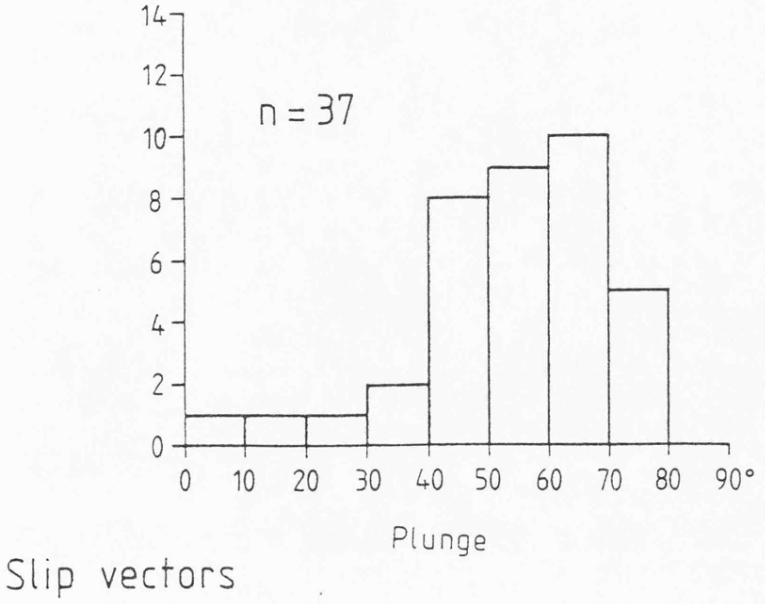

Fig.6.3. Histogram showing amount of plunge of the slip vectors measured on Quaternary faults bounding the Burdur basin. (Each value represents a single measurement. More than one measurement may occur on a single fault plane).

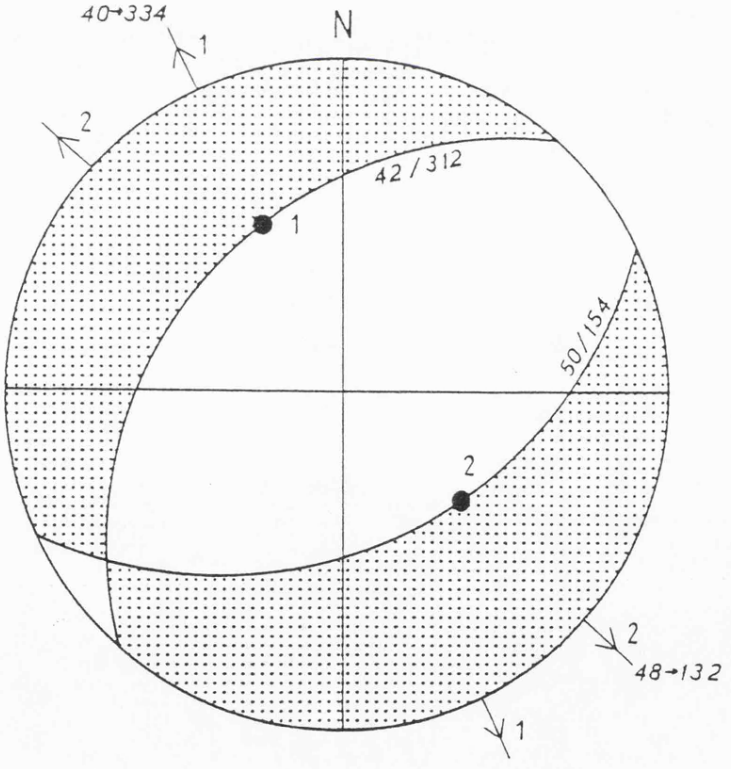

Fig.6.4. Fault plane solution for the 1971.5.12. event (m_b=5.5) at Burdur (after McKenzie 1978). Focal planes are labelled 1 and 2 arbitrarily. If plane 1 (2) is the fault plane then the slip vector is the line labelled 1 (2). Surface cracks associated with this event indicate that plane 1 is the fault plane.

The position of the hypocentre in Fig.6.4 was calculated by the National Ocean and Atmospheric Administration and is based on arrival time data. The epicentre (latitude 37.59°E; longitude 29.76°N) is situated just N of Yesilova. This determination is accurate to 10km, although according to McKenzie (1978), there may be a further northward displacement by about the same amount. The focal depth (23km) is less well constrained, having an accuracy of about ±75km. Therefore, the hypocentre is not determined accurately enough to enable a cross section to be drawn through the fault as done by Eyidogan and Jackson (1985) for the 1981.2.26. Gulf of Corinth and the 1978.6.20. Thessaloniki events.

The plunge of the slip vector at the surface is 53° (±15°) and at the hypocentre 40°. Although there are no published errors to this plunge, which is dependent upon the source velocity used, Eyidogan and Jackson (1985) indicate nodal planes to be accurate to ±5°. The variation in surface plunge is large. Fig.6.5 shows that the slip vectors measured at the surface, which have a similar plunge direction to that indicated on the fault plane solution (333), plunge in the upper end of this range at about 65-70°. Therefore, by comparing surface faulting observations with the fault plane solution for the 1971.5.12. event a reduction in dip of the fault at depth is indicated. The fault at the hypocentre (dipping at about 40°) may be as much as 30° flatter than at the surface (possibly dipping at 70°). Although the focal depth is poorly constrained it is likely that this reduction in dip is achieved by a depth of between 6 and 10km. This is the range of focal depths for earthquakes in western Turkey (Eyidogan and Jackson 1985, Jackson 1987).

6.3. NEOGENE FAULT GEOMETRY.

6.3.1. Dip profiles.

This section follows the method of Roberts (1988) which is based on the premise that where strata in the hangingwall of a normal fault are truncated by an erosion surface the variation in bedding dip away from the fault can be measured, giving a dip profile, which will yield information as to the sub-surface geometry of the fault. Roberts (1988) showed that the dip of a bed at any point in the hangingwall of a normal fault is dependent upon the shape of the fault and the amount of rotation of the fault. Other factors such as differential compaction, antithetic

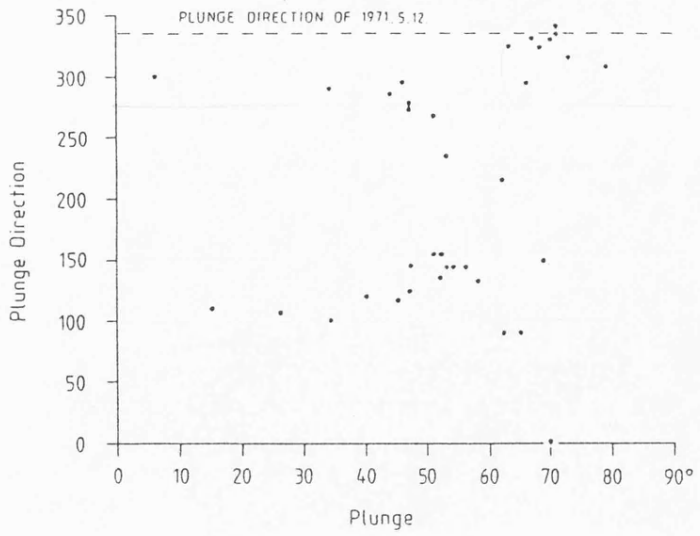

Fig.6.5. Amount versus direction of plunge of slip vectors on Quaternary faults bounding the Burdur basin. Faults sharing a plunge direction with that of the 1971.5.12. event (at its focus) dip in the range 65-70°. The cluster of readings corresponding most closely to the the plunge direction of the 1971.5.12. event (at its focus) were taken on the basin-boundary fault at Suludere (TG502716) on the southeast side of the basin. These are ringed. Much surface cracking along from this fault in recent sediments occured during the 1971.5.12. event (Erinç et al. 1971).

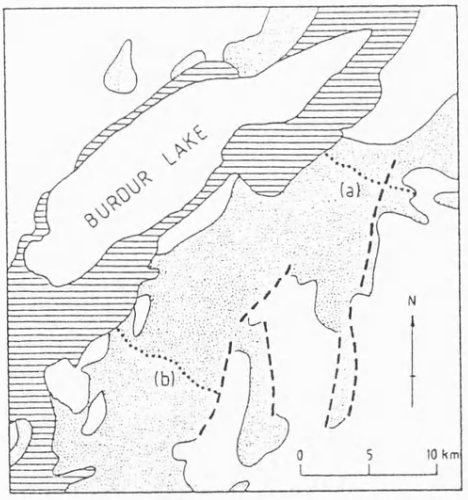

Fig.6.6. The location of dip profiles (large dots) across the Neogene hangingwall succession (shown by small dots). The Neogene basin-controlling faults are shown as thick black dashed lines . Their positions are largely inferred due to the fact that they became buried at the end of the Neogene. Horizontal lines mark the position of the present-day Burdur basin. (a) and (b) correspond to the profiles shown in Fig.6.7.

faulting and slip out of the plane of the profile will modify the observed dip at a given point.

By comparing calculated synthetic dip profiles of various fault geometries with observed dip profiles, Roberts (1988) was able to predict the sub-surface geometries of major basement normal faults. Two end-member configurations were investigated:

(a) Non-rotating listric faults.

Using a known fault shape as a starting point, synthetic dip profiles can be produced. Individual bed shapes can be calculated using the Chevron Construction (Verral 1981), but using inclined rather than vertical planes of shear as shown by White et al. (1987). The dip profile is built up by calculating the shapes of many beds of differing heave. Roberts (1988) investigated the effects of varying parameters such as the depth of the erosion surface in the hangingwall, the pre-faulting beding dip, the dip of the inclined shear planes, the compaction direction and the amount of compaction. The effects are discussed only generally here and the reader is referred to Roberts (1988) for a more detailed discussion.

A feature common to all synthetic dip profiles calculated above listric faults is that bedding dips increase towards the fault. This pattern holds for any combination of the variables such as depth of the erosion surface in the hangingwall, the dip of the inclined shear planes, the pre-faulting bedding dip and the amount of compaction.

(b) Rotating-planar faults.

By calculating incremental amounts of subsidence in a basin of known dimensions using the method of Jackson et al. (1988), which models subsidence related to rotating-planar faults, Roberts (1988) predicted the geometries of beds deposited during these incremental subsidence phases and was therefore able to produce synthetic dip profiles. This method assumes that the basin fills with sediment to a datum level (i.e. sea level) after each subsidence phase. The absence of such a fixed datum in a continental basin precludes the developement of accurate synthetic dip profiles for the hangingwall succession at Burdur.

In contrast to the dip profiles calculated for listric faults, those

calculated for rotating-planar faults show an increase in bedding dip away from the fault.

6.3.2. Burdur dip profiles.

2 dip profiles are available for the hangingwall succession of the Neogene basement fault; one from the northern end of the basin between Askeriye and Günalan and the other from the central part of the basin between Kuruçay and Güngörmez Tepe (Fig.6.6). In both cases bedding dips were measured in lacustrine marls indicating a horizontal pre-faulting attitude (Plate 6.1). In both dip profiles the spread of bedding dips at a given distance from the fault is large varying by up to 15°. Bedding dips were measured in the field to an estimated accuracy of ±2°, so, assuming that the pre-faulting dip of all beds was the same (i.e. horizontal), most of this spread can be attributed to minor faulting within the sedimentary sequence and partial slumping of the sedimentary succession. For reasons of exposure, most measurements were taken in valleys, maximising the effect of slumping.

In the Askeriye-Günalan dip profile (Fig.6.7a) the basin controlling fault has been buried and is not exposed. Its position is inferred by extrapolating the faulted basin margin observed to the S. The hangingwall succession dips towards the fault at between 5° and 35°. There is no systematic variation in bedding dip away from the fault, possibly due to the paucity of points between 0 and 3km away from it. 2 points measured in sediments above the footwall crest of the fault have greater dips, but as these represent post-faulting sediments, which bury the fault, these dips must be related to the combined effects of compaction and Quaternary tilting. A packet of more steeply dipping sediment between about 4.5 and 6km from the fault is bounded by 2 synthetic faults within the hangingwall succession, both observed in the field.

The Kuruçay-Güngörmez Tepe dip profile from the central part of the basin (Fig.6.7b) is a 10km long complete section with the fault exposed. This dip profile shows less of a spread of bedding dips than the Askeriye-Günalan dip profile (Fig.6.7a). Faults seen in the field within the succession can also be picked out on the dip profile by dragged beds dipping in the opposite direction. These faults are synthetic to the major basin-controlling fault and increase the dip the bedding (up to 50°) towards it. The uninterrupted profile between the fault and a

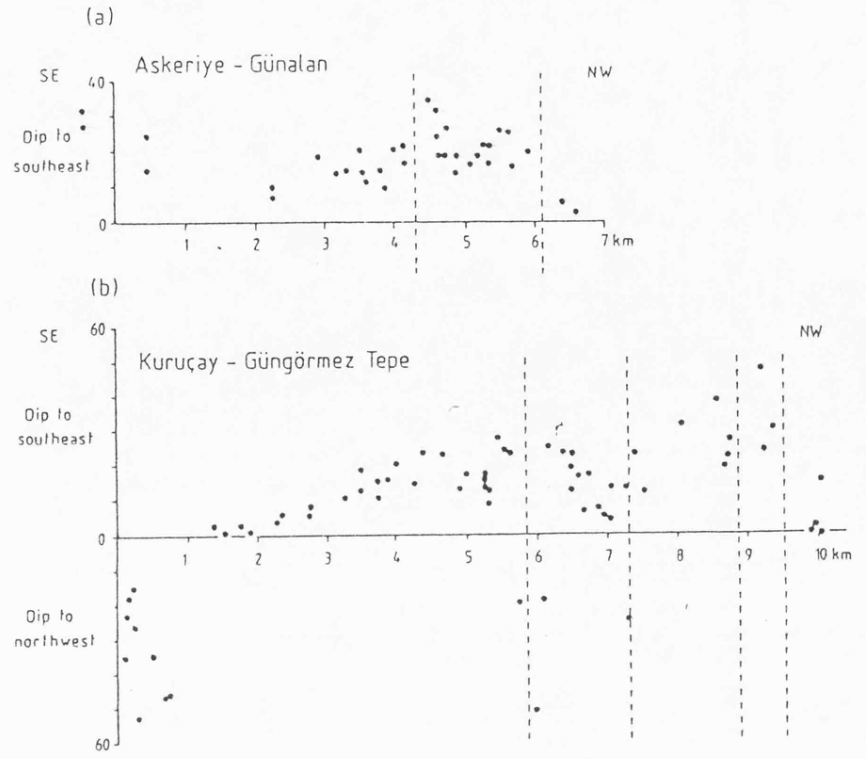

Fig.6.7. (a) The Askeriye-Günalan dip profile. The distance from the fault (now buried) is shown on the x-axis. The positions of faults within the hanging wall succession are shown as dotted lines. (b) The Kuruçay-Güngörmez Tepe dip profile. Axes as for (a). Note the increase in dip away from the fault and the effect of drag on faults within the hangingwall succession.

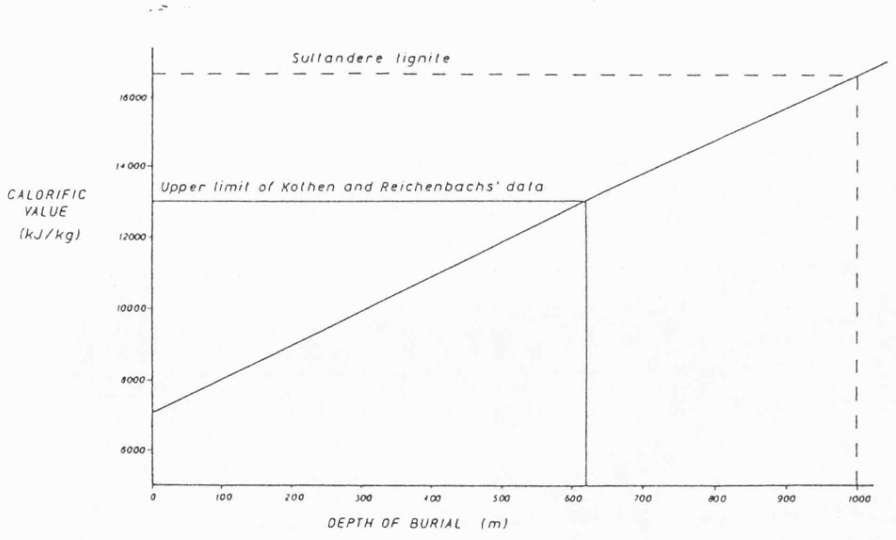

Fig.6.8. The relationship between the calorific value and the depth of burial of Miocene lignites from the Lower Rhine Embayment. The curve is extrapolated to the higher calorific value of the Sultandere lignite. (Data taken from Kothen and Reichenbach 1981).

distance 5.5km away from it shows a steady decrease of dip from 30° to 0° towards the fault until at a distance 1km away from it the beds dip in the oppposite direction by up to 55°.

6.3.3. Discussion of dip profiles.

The Askeriye-Günalan dip profile gives little information as to the geometry of the basin-controlling fault beneath the northern end of the basin for the following reasons:

(a) The measured dips at the SE end of the profile (the left-hand side of Fig.6.7a) belong to post-faulting sediments.

(b) There are not enough data points in the critical part of the dip profile between 0 and 3km from the fault.

(c) The dip profile is from the northern extremity of the basin, presumably at the end of a basement fault, where deformation is much more complex.

The Kuruçay-Güngörmez Tepe dip profile, on the other hand, contains only syn-faulting sediments, has sufficient data points and is from the central part of the basin, rendering it potentially more useful. The increase in bedding dip away from the fault in this dip profile (Fig.6.7b) is indicative of sedimentation in the hangingwall of a rotating-planar fault. As already mentioned, listric faults always show the opposite relationship with a decrease in bedding dip away from the fault.

In order to produce a synthetic dip profile for the Kuruçay-Güngörmez Tepe section the dip of the basement fault, the amount of rotation since its formation and the depth of erosion in the hangingwall must be known. The basement fault is well-exposed at the end of the section near Soganli (see Chapter 5; Plate 5.2b). Here it dips towards the NW at 47°. The basal-Neogene reflector on seismic sections from the southern part of the Burdur Basin dips towards the SE at 13° (see Chapter 5; Fig.5.7). Assuming this to be a pre-faulting horizontal datum this is the rotation (both Neogene and Quaternary), which the fault has undergone since its formation giving it an initial dip of 60°. The presence of lignite on the erosion surface in the hangingwall succession allows an approximate value

for the depth of the erosion surface in the hangingwall to be estimated. This lignite outcrops at the abandoned Sultandere mine S of Burdur (TG575765) (see Chapter 3). The approximate depth of burial of the lignite (and hence the amount of erosion of overburden) can be estimated by comparison with established coalification curves. The calorific value of the Sultandere lignite is 4000kcal/kg (16700kJ/kg) (Wedding and Inque 1967). By comparision with Miocene lignites of the Lower Rhine Embayment a burial depth of approximately 1000m seems likely for the Sultandere lignite (Fig.6.8). This value is an approximation due to compositional differences between the Sultandere lignite and those of the Lower Rhine Embayment.

Fig.6.9 shows the synthetic dip profile for a fault now dipping at 45°, which has been rotated through 15°. These figures correspond to the situation at Burdur (within field measurement error) so a comparison can be made between this synthetic dip profile and the observed dip profile (Fig.6.7b). Both dip profiles show an increase in bedding dip away from the fault but here the similarity ends. The observed dip profile shows a more rapid increase in bedding dip away from the fault than the synthetic dip profile and the former also shows that near to the fault beds dip in the opposite direction (to the NW, away from the fault). Both of these differences are compaction phenomena not modelled by Roberts (1988) and therefore not apparent on the synthetic dip profile. The hangingwall succession is dominated by lacustrine marl (see Chapter 3), which is compositionally and texturally analogous to North Sea Chalk. Sclater and Christie (1980) showed that North Sea Chalk compacts rapidly on burial losing half of its porosity by a depth of 1000m (the approximate thickness of the Neogene hangingwall succession; see Chapter 5). Therefore compaction should have a considerable effect on the hangingwall dip profile, with maximum compaction occuring above the thickest part of the basin. This will have the effect of reducing, or even reversing, the dip of the beds near to the fault plane and increasing their dip away from it. This accounts for the differences between the observed and synthetic dip profiles.

Steep reverse dips of beds next to a fault can be brought about above listric faults, especially where compaction occurs parallel to the direction of simple shear in the hangingwall (Roberts 1988; Fig.8.9). However, the increase in bedding dip away from the fault cannot be modelled in this situation.

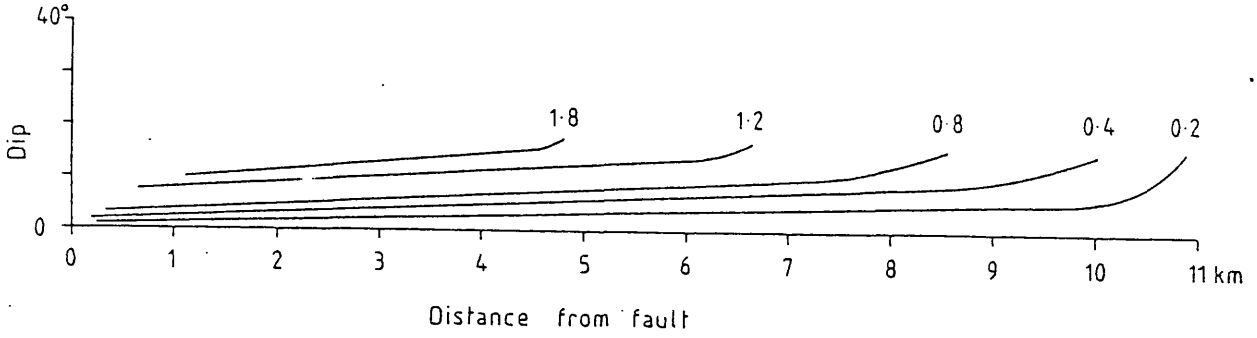

Fig.6.9. Synthetic dip profile for a fault now dipping at 45°, which has been rotated through 15°. Figures correspond to depth of erosion (in km) in the hangingwall. A figure of 1.0km is likely for Burdur (see text for discussion).

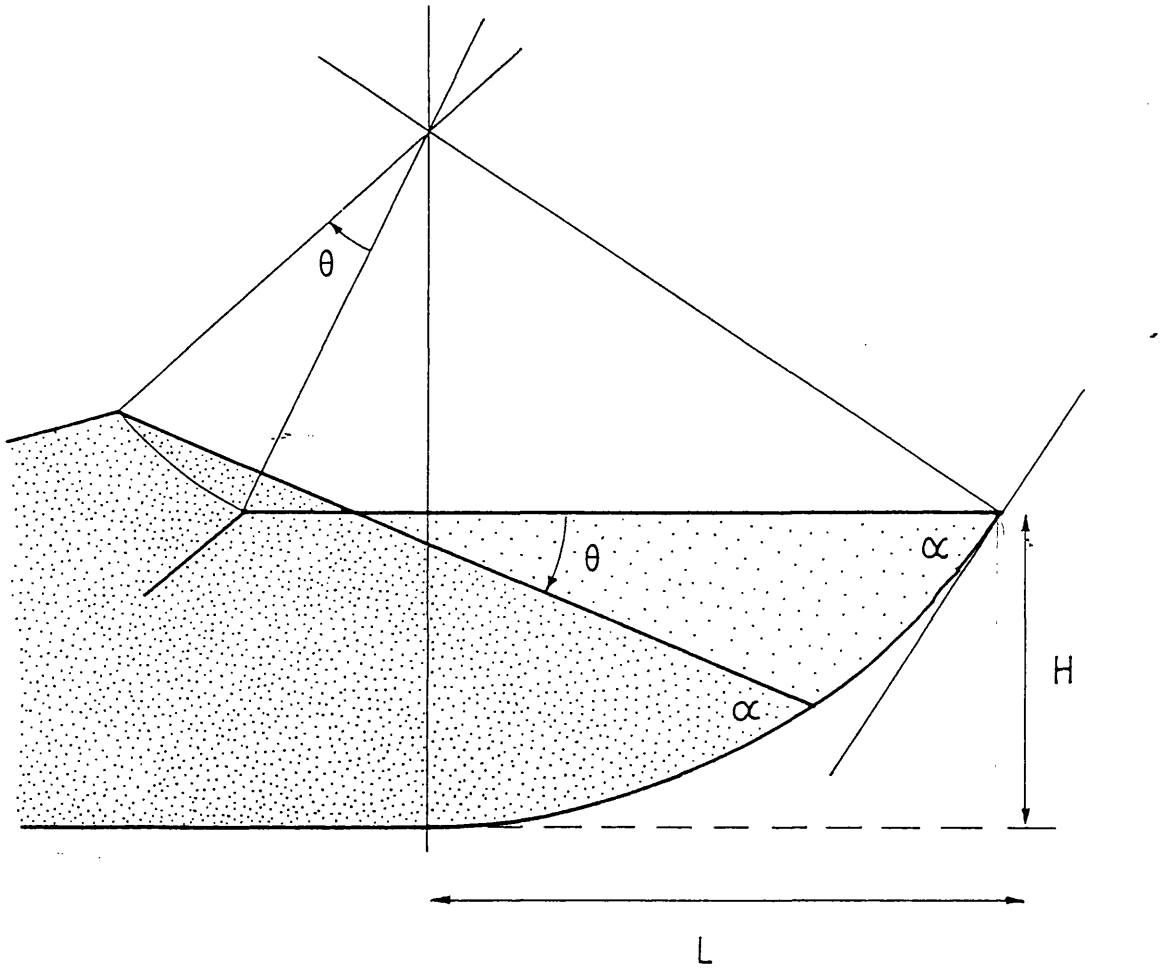

Fig.6.10. Section illustrating the symbols used in the method of Moretti et al. (1988) for studying rotations on a curved surface. H is the depth of detachment of a curved fault which has a dip of α at the surface. θ is the tilt of the fault block and L the critical position of the crest (see text for full discussion).

In summary, the modelling of bedding dip profiles in the hangingwall of the Neogene basin-controlling fault at Burdur suggest a planar-rotating fault geometry.

6.4. GEOMETRICAL CONSIDERATIONS OF ROTATIONS ON A CURVED SURFACE.

Moretti et al. (1988) produced a model for estimating the depth of detachment of a listric fault. This is the depth at which the fault becomes tangential to the horizontal. In their model, faulting is presumed to have occured on a planar surface with a circular profile. According to these authors faults are probably not perfectly circular in reality, but the vertical motions associated with such a geometry are of the same order.

Assuming the hangingwall remains rigid and the footwall is fixed, the angle between the fault and the top of the block is constant during the rotation. The crest of the block will remain on a circle with the same centre of curvature as that of the fault. Therefore, if the block is small the crest will subside and, if large, it will uplift. The critical position of the crest, L, is the downward projection of the centre of curvature of the fault on the horizontal plane (Fig.6.10), so that

$$L = H \sin \alpha / (1 - \cos \alpha) \qquad \text{(eq.1)}$$

where H is the depth of detatchment and α the dip of the fault at the surface (Moretti et al. 1988). These authors also define an inverse relationship, where the depth of detachment can be calculated from subsidence in the basin and the tilt of the hangingwall, where

$$H = h_{fault} (1 - \cos \alpha) / (\cos (\alpha - \theta) - \cos \alpha) \qquad \text{(eq.2)}$$

where h_{fault} is the subsidence and θ the tilt of the fault block. For the derivations of equations (1) and (2) see Moretti et al. (1988).

These simple geometrical relationships can be applied to both Neogene and Quaternary basement faults from the study area. Firstly, assuming a depth of detachment for the fault, a value for L can be calculated. Most present-day earthquakes in western Turkey nucleate at a depth of about 8km (Jackson 1987). This is taken as the depth of detachment for

Quaternary faults. The basement fault controlling the Quaternary Burdur Basin has a dip of 60°. This gives a value of L of 15km. The fault controlling the Neogene Burdur Basin has a dip of 47° (near Soganli). During the Neogene the upper elastic layer of the crust would have been slightly thicker than at present and a reasonable value for H is 12km. This gives a Neogene value of 28km. Assuming a constant base level, the value of L should be a minimum estimate of basinal width, as all points between the downward projection of the centre of curvature of the fault on the horizontal plane and the fault itself will be subsiding. The width of the Quaternary Burdur Basin is approximately 7km and that of the Neogene Burdur Basin approximately 18km (Fig.6.6) showing the calculated values to be overestimates.

The inverse relationship, shown in equation (2), predicts the depth of detachment from fault dips, hangingwall tilts and subsidence. The Neogene Burdur Basin has a maximum depth of 1100m and a hangingwall tilt of 13° (see Chapter 5; section 6.). Geometrical considerations show the thickness of Quaternary strata beneath the Quaternary Burdur Basin to be at least 760m predicting a Quaternary dip of about 7° (see Chapter 5; section 5.2.). In this model the footwall is fixed so Quaternary tilts will have no effect on earlier Neogene fault dips and tilts. So, substituting these values into equation (2) gives Neogene and Quaternary depths of detachment of 2.4km and 3.7km respectively. These depths are shallower than the focal depths of major normal faulting earthquakes in western Turkey. If we take the accuracy of h_{fault} to be ±200m, α to be ±5° and θ to be ±5° then the Neogene depth of detachment will lie in the range 0.8km to 3.7km and that of the Quaternary between 2.4km and 24.2km. Although the Quaternary depth of detachment is likely to fall within the calculated limits, the Neogene estimate still appears too low, particularly when one considers that the elastic upper crust was thicker in the Neogene than in the Quaternary. The fact that the model proposed by Moretti et al. (1988) cannot account for the structure of the Neogene Burdur Basin is not conclusive evidence of a lack of curvature on the fault controlling this basin. However, the notion that the hangingwall behaves rigidly is incorrect as there are many mesoscale faults within the Burdur Formation (the Neogene basinal succession of the Burdur Basin) of undoubted Neogene age, which would indicate that the hangingwall deforms by simple shear (i.e. faulting).

White et al. (1986) showed that there is a relationship between the

geometry of a bed in the hangingwall of a listric fault, the angle of simple shear in the hangingwall and the geometry of the faut at depth. They demonstrated that, when considering the inverse problem of predicting fault geometry from hangingwall data, not only does the angle of simple shear greatly influence the geometry of the fault but also the amount of estimated extension. Previous geometrical studies (i.e. Verall 1981; Gibbs 1983, 1984) had incorrectly assumed simple shear to occur by movement in vertical planes. The method of White et al. (1986) cannot be applied to the study area due to the lack of good quality migrated seismic data showing the geometry of bedding in the hangingwall and the angle of simple shear.

6.5. DISCUSSION.

6.5.1. The controversy.

The controversy over whether the faults responsible for most of the strain in a taphrogen are listric or planar has centred on the Aegean and western Turkey in recent years. Initially the concensus of opinion was in favour of listric fault geometries. McKenzie (1978) and Sengör (1978) both argued for faults in this region to be listric. Jackson et al. (1982a) accounted for the large rotations observed in the Aegean Region by movement on listric faults. Faulting in the Gulf of Corinth was also postulated by Jackson et al. (1982b) to be listric due to the nodal plane dips of 40-50° compared to near vertical dips at the surface. However, they also point out that the steep surface dips may only occur in the top few metres, where the ground fails in tension (Yielding et al. 1981). Abundant hangingwall deformation is also put forward as evidence for listric faulting (Jackson et al. 1982b). Geophysical evidence for a listric geometry for 3 faults which moved in the period 1969-70 in Demirci, Alasehir and Gediz (western Turkey) was put forward by Eyidogan and Jackson (1985). These all gave rise to large earthquakes (M_s>5.5) which nucleated at depths of 6-10 kilometres on faults dipping in the range 30-50°. Seismograms of the Alasehir and Gediz earthquakes showed them to be multiple events with later long-period signals, which were modelled by subevents with long time functions on almost flat detachment type faults. This gives rise to a model of steeply dipping faults in a brittle upper crust rapidly flattening out within a more ductile lower crust (the depth of which depends on the geothermal gradient), where

creep is the dominant style of deformation at low strain rates: in effect a "dog-leg" fault approximating to a listric geometry. Sengör et al. (1985) accepted the ideas of fault geometry put forward by Eyidogan and Jackson (1985) as a working model upon which they proposed a model to account for the perpendicular trends of grabens formed by two apparent stretching directions in western Turkey. In this model the hangingwall of a large listric fault is broken up by accommodation faults at high angles to the strike of the main fault. This gives rise to differential stretching of the hangingwall resulting in more rapid subsidence of some segments. These cross-grabens are therefore not formed by extension perpendicular to the basinal axes, but by differential axial extension (Sengör et al. 1985; Sengör 1987).

In recent years the "rotating-domino" model of continental extension has again been adopted by many authors in preference to the notion of normal faults flattening along a detachment. (Small curvatures still cannot be ruled out from studies of earthquake fault plane solutions). The modelling of hangingwall succession geometry by Roberts (1988) has demonstrated the presence of planar-rotating faults in Greece and western Turkey. The observed basin depth and subsidence of the Jeanne D'Arc basin, off eastern Canada, was modelled by Kusznir (1989) by inferring simple shear on rotating-planar faults in the upper elastic crust and plastic distributed deformation (pure shear) in the lower crust and mantle. Most authors now seem to agree that the difference between listric and planar faulting is one of scale with continents extending on rotating-planar faults and listric faults redistributing the sedimentary cover in response to vertical movements associated with block-faulting in the basement.

6.5.2. Geometry of faults at Burdur.

Dip profiles in the hangingwall of the Neogene fault system at Burdur support a planar geometry. If the Neogene bedding tilts are the result of rotations on a curved surface, then the detachment depth of this surface must be unreasonably shallow. Evidence for a planar geometry to Quaternary faults from Burdur is lacking. Indeed, a curvature of up to 40° is possible by considering the dip of the faults at the surface and the source of the 1971.5.12. event. No direct measurement of the surface breaks associated with this event was made so this figure is questionable. Quaternary fault dips, bedding tilts and subsidence can be

modelled on a curved surface with a reasonble depth of detachment but uncertainties in each of these variables leads to extremely large errors.

In summary, Neogene faults from Burdur appear to be planar at depth and Quaternary faults, slightly concave-up. As both fault systems are seperated only by age and penetrate the same crust it is reasonable to assume they will have the same 3-dimensional geometry. Therefore, I propose that basin-controlling faults from the Burdur region bound rotating domino-style blocks and are approximately planar at depth. Small curvatures are likely but no detachment at depth is envisaged.

A common problem with the "rotating-domino" style of extension is a poor understanding of the nature of the boundary of the extending zone. Deformation of the footwall at the edge of the zone as predicted by modelling (e.g. Kusznir 1989, Marsden et al. 1989) must be demonstrated but as there is generally no syn-faulting sediment preserved in the footwall this is difficult to do. The dip of pre-faulting sediments in the footwall and hangingwall can be compared. If they are the same then it can be assumed that the footwall has rotated. However, the Eo-Oligocene flysch sediments in the basement of the study area have a highly variable dip direction (see enclosure) rendering them useless in such an analysis. The individual rotating blocks have broken up internally by antithetic faulting (see Chapter 7), which partly alleviates the problem of footwall rotation. Before the "rotating-domino" model can be convincingly applied to the Burdur region footwall rotation must be demonstrated.

6.6. REFERENCES.

Anderson, E.M. 1951. The Dynamics of Faulting, 2nd edition, Oliver and Boyd, Edinburgh, 206pp.

Erinç, S., Bener, M., Sungur, K. and Göçmen, K. 1971. 12 Mayis 1971 Burdur Depremi. Istanbul Üniversitesi Cografya Enstitüsü Yayinlari, No.66, 27pp.

Eyidogan, H. and Jackson, J.A. 1985. A seismological study of normal faulting in the Demirci, Alasehir and Gediz earthquakes of 1969-1970 in western Turkey: implications for the nature and geometry of deformation in the continental crust. Geophysical Journal of the Royal Astronomical Society, v.81, p.569-607.

Fraser, G.D., Witkind, I.J. and Nelson, W.H. 1964. A geological interpretation of the epicentral area-the dual basin concept. In: The Hebgen Lake, Montana Earthquake of August 17, 1959. United States Geological Survey Professional Paper, No.435, p.99-106.

Gibbs, A.D. 1983. Balanced cross-section constructions from seismic sections in areas of extensional tectonics. Journal of Structural Geology, v.5, p.152-160.

Gibbs, A.D. 1984. Structural evolution of extensional basin margins. Journal of the Geologial Society of London, v.141, p.609-620.

Jackson, J.A. 1987. Active normal faulting and crustal extension. In: Coward, M.P., Dewey, J.F. and Hancock, P.L. (eds) Continental Extensional Tectonics. Special Publication of the Geological Society of London, No. 28, p.3-17.

Jackson, J.A. and White, N.J. 1989. Normal faulting in the upper continental crust: observations from regions of active extension. Journal of Structural Geology, v.11, p.15-36.

Jackson, J.A., King, G. and Vita-Finzi, C. 1982a. The neotectonics of the Aegean: an alternative view. Earth and Planetry Science Letters, v.61, p.303-318.

Jackson, J.A., Gagnepain, J., Houseman, G., King, G., Papadimitriou, P., Soufleris, C. and Virieux, J. 1982b. Seismicity, normal faulting and the geomorphological evolution of the Gulf of Corinth, (Greece): the Corinth earthquakes of February and March 1981. Earth and Planetry Science Letters, v.57, p.377-397.

Jackson, J.A., White, N.J., Garfunkel, Z. and Anderson, H. 1988. Relations between normal-fault geometry, tilting and vertical motions in extensional terrains: an example from the southern Gulf of Suez. Journal of Structural Geology, v.10, p.155-170.

Jankhof, K. 1945. Changes in ground level produced by the earthquakes of April 14 to 18 1928 in southern Bulgaria. In: Tremblements de Terre en Bulgarie, No.29-31, p.131-136 (in Bulgarian). Institute meteorologique central de Bulgarie, Sofia.

Keightley, W.O. 1975. Destructive earthquakes in Burdur and Bingol, Turkey: May 1971. National Research Council, Washington, D.C., 84pp.

Kothen, H. and Reichenbach, W. 1981. Teufenabhangigkiet und gegensseitige Bezielungen von Qualitätsparmeten der Braunkole der Niedewheinischen Bucht. Fortschr. Geol. Rheinland u. Westfl., v.29, p.353-380.

Krenkel, E. 1922. Die Bruchzonen Ostafrikas, Gebrüder Borntraeger, Berlin, 184pp.

Kusznir, N.J. 1989. Simple-shear/pure-shear models of extensional sedimentary basin formation: application to the Jeanne D'Arc basin, Grand Banks, Newfoundland. Terra Abstracts, v.1, p.70.

McKenzie, D.P. 1978. Active tectonics of the Alpine-Himalayan Belt: the Aegean Sea and surrounding regions. Geophysical Journal of the Royal Astronomical Society, v.55, p.217-254.

Marsden, G., Kusznir, N.J., Roberts, A. and Yielding, G. 1989. Numerical modelling of basin formation in the northern North Sea. Terra Abstracts, v.1, p.34.

Moretti, I., Colletta, B. and Vially, R. 1988. Theoretical model of block rotation along circular faults. Tectonophysics, v.153, p.313-320.

Ransome, F.L., Emmons, W.H. and Garry, G.H. 1910. Geology and ore deposits of the Bullfrog district, Nevada. Bulletin of the U.S. Geological Survey, No.407, 130pp.

Roberts, S. 1988. Active normal faulting in central Greece and western Turkey. Unpublished Ph.D. thesis, University of Cambridge.

Sclater, J.G. and Christie, P.A.F. 1980. Continental stretching: an explanation of the post mid-Cretaceous subsidence of the Central North Sea basin. Journal of Geophysical Research, v.85, p.3711-3739.

Sengör, A.M.C. 1978. Über die angebliche primäre Kertikaltektonik im Agaisraum. Neues Jahrbuch für Geologie und Palaontologie, v.11, p.698-703.

Sengör, A.M.C. 1987. Cross-faults and differential stretching of hanging walls in regions of low-angle normal faulting: examples from Western Turkey. In: Coward, M.P., Dewey, J.F. and Hancock, P.L. (eds) Continental Extensional Tectonics. Special Publication of the Geological Society of London, No.28. p.575-589.

Sengör, A.M.C., Görür, N. and Saroglu, F. 1985. Strike-slip faulting and related basin formation in zones of tectonic escape: Turkey as a case study. In: Biddle, K.T. and Chhristie-Blick, N. (eds) Strike-slip Faulting and Basin Formation. Special Publication of the Society of Economic Paleontologists and Mineralogists, No.37, p.227-264.

Soufleris, C., Jackson, J., King, G., Spencer, C. and Scholz, C. 1982. The 1978 earthquake sequence near Thessaloniki (northern Greece). Geophysical Journal of the Royal Astronomical Society, v.68, p.343-358.

Tocher, D. 1957. The Dixie Valley-Fairview Peak earthquakes of December 16th 1954. Bulletin of the Seismological Society of America, v.47, p.299-374.

Verral, P. 1981. Structural interpretation with application to North Sea problems. Joint Association for Petroleum Exploration Courses, Course Notes No.66, London, U.K.

Wallace, R.E. 1984. Faulting related to the 1915 earthquake in Pleasant Valley, Nevada, U.S.A. United States Geological Survey Professional Paper, No.1274A, 33pp.

Wedding, H. and Inque, E. 1967. Report on the lignite bearing Pliocene strata around Burdur city. M.T.A. Report 1-11 (unpublished), Ankara.

Westaway, R and Jackson, J.A. 1987. The earthquake of 23 November 1980 in Campania-Basilicata (Southern Italy). Geophysical Journal of the Royal Astronomical Society, v.90, p.373-443.

White, N.J., Jackson, J.A. and McKenzie, D.P. 1986. The relationship between the geometry of normal faults and that of the sedimentary layers in their hanging walls. Journal of Structural Geology, v.8, p.897-909.

Yielding, G., Jackson, J.A., King, G.C.P., Sinvhal, H., Vita-Finzi, C. and Wood, R.M. 1981. Relations between surface deformation, fault geometry, seismicity and rupture characteristics during the El Asnam (Algeria) earthquake of 10 October 1980. Earth and Planetry Science Letters, v.56, p.287-304.

Plate 6.1. The view north from TG529594 (1.5km NNW of Karacaören) showing the regional southeast tilt of the Burdur Formation. The sediments are lacustrine marls which are rapidly being eroded due to active uplift in the footwall of the Quaternary fault to the northwest. Individual bedding horizons within the basinal succession can be traced for many kilometres attesting to the lack of large-scale faulting within it.

Plate 6.1.

CHAPTER SEVEN.

STRUCTURAL EVOLUTION OF THE BURDUR-ACIGÖL-BAKLAN BASIN SYSTEM: THE NATURE OF THE EASTERN EDGE OF THE GRABEN SYSTEM OF WESTERN TURKEY.

7.1. INTRODUCTION.

The neotectonic history of the study area (and of much of western Turkey) can be sub-divided into Neogene and Quaternary events. During the Neogene sedimentation occurred over wide areas in structurally-controlled basins with poorly-defined fault-bounded margins. These margins became overlapped in the late Neogene. At this time the basins narrowed, giving the NE-SW trending fault-controlled grabens seen today.

The oldest basinal sediments in the Burdur region are late Miocene/early Pliocene in age (see Chapter 2) This is the best estimate of the onset of extension in the basin system. Throughout this chapter the late Miocene/early Pliocene to late Pliocene/ early Quaternary basinal sediments (the Burdur Formation) and tectonic events are collectively dated as Neogene for reasons of clarity and brevity and to separate them from the younger Quaternary events.

The geological structure of the Burdur-Acigöl-Baklan basin system was the subject of Chapters 5 and 6. The aim of this chapter is to describe and explain the nature of the change in tectonic style at the end of the Neogene and to provide a model for the deformation style observed which can be fitted into the general tectonic framework of the eastern Mediterranean. Firstly, however, consideration is given to seismicity associated with faulting in the basin system. 3 methods of studying seismicity are investigated. The first is the direct observation of twentieth century earthquake events and a summary of these is given. Such a study provides a useful insight into the surface geometries of active faults and short-term levels of seismicity. Secondly, the abundance of wet-sediment deformational horizons within the Burdur Formation is used to investigate whether or not present-day levels of seismicity can be extrapolated back to the Neogene. Finally, a geomorphological study of fault-controlled mountain fronts in the basin system provides information on the geographical distribution of fault activity over the past few

hundred thousand years. By comparing this geographical variation with recent earthquake observations, the reliability of recent seismicity in extrapolating back over geological time can further be assessed.

7.2. SEISMOLOGY.

7.2.1. Historical Seismology.

Earthquakes provide much information about a fault or fault system. The focal depth of the earthquake gives an indication of the thickness of the seismogenic layer of the crust (Jackson 1987). First motion analysis of seismic waves gives a fault plane solution which shows the geometry of the fault giving rise to the earthquake at source. This is further constrained by observations of fault breaks associated with the earthquake at the surface. Earthquake moment tensors (obtained by direct analysis of seismograms) can be used to indicate the strain across a deforming zone. However, instrumental earthquake magnitude data are only available for twentieth century earthquakes and strain rates for individual faults or fault systems calculated from such data should be treated with caution.

The Burdur region is seismically active, with 2 large earthquakes occurring this century (1914.10.3 and 1971.5.12). Both caused widespread damage. The earlier 1914.10.3 event was the larger of the 2 killing more than 4000 people and destroying 90% of the houses in Burdur. Altogether, earthquake and fire damage destroyed more than 17,000 houses within a northeast trending zone about 90km long and 30km wide defined by Duvar, Yasiköy, Ilyas, Kilinç, Gönen and Barla (Ambraseys and Finkel 1987). Damage caused by the 1971.5.12 event was more localized being restricted to some villages on the southeast side of the lake and to villages situated on the basin floor southwest of the lake. 57 people were killed in this event (Erinç et al. 1971). Ambraseys (1988) gives surface wave magnitudes of 7.0 and 6.2 and body wave magnitudes of 7.3 and 6.0 for the earlier and later events respectively. Both earthquakes gave rise to surface fault breaks. The 1914.10.3 event caused the submergence of the southeast coast of Lake Burdur for a length of 23km between Sandal Iskelesi of Burdur and Uz Köprü, west of Yaziköy. Halfway between these localities the level of the lake rose by about 1.5m threatening the road that runs along the coast (Ambraseys pers.comm.). The 1971.5.12 event

gave rise to surface cracks coinciding with parts of those of the earlier event along the southeast margin of the basin (Erinç et al. 1971). These were downthrown to the northwest by up to 30cm. No surface breaks occurred on the northwest side of the lake basin (Keightley 1975). Widespread liquefaction of sediment (mud volcanoes etc.) and rockfalls at the southern end of the Burdur basin were associated with this earthquake.

Surface fault breaks associated with both events would therefore tend to suggest that the Burdur basin is a fault-bounded graben with the major fault along its southeast margin.

Other historic seismic data from the study area include 2 surface wave magnitude 4.6 (body wave magnitude 5.3) shocks (1963.11.12) causing localized damage in the Tefenni area (Ambraseys 1988). There is no recorded historical seismicity associated with the large Acigöl fault scarp.

7.2.2. Pre-historical seismology.

A commonly observed consequence of seismic activity is the liquefaction of unconsolidated sediment. For modern earthquakes, this usually involves ground failures of Holocene fluvial, deltaic and aeolian deposits (Youd and Hoose 1977). Wet-sediment deformation structures will only occur where all of the following criteria are satisfied:

(a) A trigger capable of increasing the pore fluid pressure of the sediment until it exceeds its yield strength.

(b) A sediment susceptible to the above trigger.

(c) A force sufficient to deform the liquid-like deposit.

Suitable triggers include cyclic stresses (earthquakes, wind waves), impulsive forces (e.g. rapid loading of a landslide), increase in pore-fluid pressure related to groundwater charge up and the onset of fluidization (Allen 1986). The presence of wet-sediment deformation within the Burdur Formation attests to the availability of such triggers during the Neogene in the Burdur region. Wet-sediment deformation within the Burdur Formation manifests itself in many different ways.

Syn-sedimentary listric faults in the sediment cover are a reasonably common feature. These, however, do not form instantaneously and therefore cannot be related to individual seismic events. They occur in lake sediments which were initially horizontal and it would therefore appear that they are not related to slope instability. However, gradients can be brought about by normal block faulting in the basement beneath the sedimentary cover and their origin is, therefore, probably related to the readjustment of the sedimentary cover after block faulting events. Overturned cross-bedding is found in fan delta deposits at a few localities in the Burdur Formation. However, many triggers can account for such a style of deformation and it is not necessary to invoke seismic activity. By far the most commonly observed wet-sediment deformation structures in sediments from the Burdur Formation are ball-and-pillow type structures (Plate 7.1). These structures occur in sands and silts where overlying sediment has sunk forming a downwarp into the underlying layer. Continued sinking leads to the eventual disruption and partial break up of both beds sometimes with the movement of lower layer material into the upper horizon. They are always found along a single bedding horizon and are laterally extensive. Similar structures have been reported in young lacustrine sediments from seismically active zones (e.g. Hempton and Dewey 1983; Sims 1973, 1975). The structures from the Burdur Formation are described in more detail by Scott and Price (1988).

The ball-and-pillow structures from the Burdur Formation can be found at many localities and at various horizons. However they appear to be most common in the Günalan Member (see Chapter 2) from the northern end of the basin. They have a frequency within the sedimentary succession of about 1 deformed horizon every 25m. This is an approximate figure based on the number of horizons observed and the thickness of succession logged. Also, the deformed horizons are not regularly spaced but tend to occur in clusters of 2 or 3. This frequency of deformed horizons seems very low when compared with, for example, the Torridonian Sandstone, in which about half of the sediments have undergone some type of wet-sediment deformation (Allen 1986). A model predicting the amount of wet-sediment deformation in a pile of gradually accumulating potentially liquefiable sediment for a specific seismically active region is therefore necessary before such comparisons can be made.

The relationship between the maximum epicentral distance of liquefied sites and earthquake magnitude derived from Japanese earthquakes by

Kuribayashi and Tatsuoka (1975) takes the exponential form:

$$\log_{10}X = 0.87\ M - 4.5 \qquad \text{(eq.1)}$$

where X is the distance in kilometres and M, the magnitude. Ambraseys (1988) doubts whether X is a suitable measure of the distance of a site of liquefaction from the source of seismic energy release, but his curve, recalculated by redefining X as distance from the fault break (Ambraseys 1988; his Fig.67) is similar enough to that of Kuribayashi and Tatsuoka (1975) for the former to be used in this study. Using equation (1) Allen (1986) derived an equation to calculate the annual number of earthquakes which will induce liquefaction at a distance of X kilometres from their epicentres. This takes the double-exponential relationship:

$$N(X) = 10^{B} \exp - 1/M_{m} \left[0.499 \ln \left(X / 3.162\text{x}10^{-5} \right) \right] \qquad \text{(eq.2)}$$

where M_m is the mean earthquake magnitude and B, the logarithm of the annual total of earthquakes of all magnitudes. When combined with the sedimentation rate, the frequency of deformed horizons within a sedimentary succession (susceptible to deformation) at distance X from the palaeo-epicentre can be estimated. To apply this to deformation within the Burdur Formation we will firstly compute the variables M_m and B for historical seismicity and then extrapolate this back to the Neogene.

Alsan et al. (1975) published a catalogue of twentieth century earthquakes for Turkey and, using this, Båth (1979) made a preliminary study of seismic risk for different regions of the country. The seismic risk data has a reliable lower limit of M=4.5, but a straight-line relationship between the logarithm of the cumulative frequency and earthquake magnitude allows extrapolation to lower magnitudes (Fig.7.1). From this data values of 0.52 and 3.95 for M_m and B respectively are calculated for the region containing the Burdur Formation.

So, substituting B=3.95 and M_m=0.52 into equation (2) and taking X to be 20km (a reasonable mid-basin value), yields a value $N(X)=2.4\text{x}10^{-2}\ a^{-1}$. Assuming a reasonable instantaneous depositional rate for a fluvial sediment of $0.1m\ a^{-1}$ gives a periodicity of $0.24\ m^{-1}$ (or approximately one deformed horizon for every 4.2m of sediment). This must be considered to be an upper estimate as the region studied for seismic risk

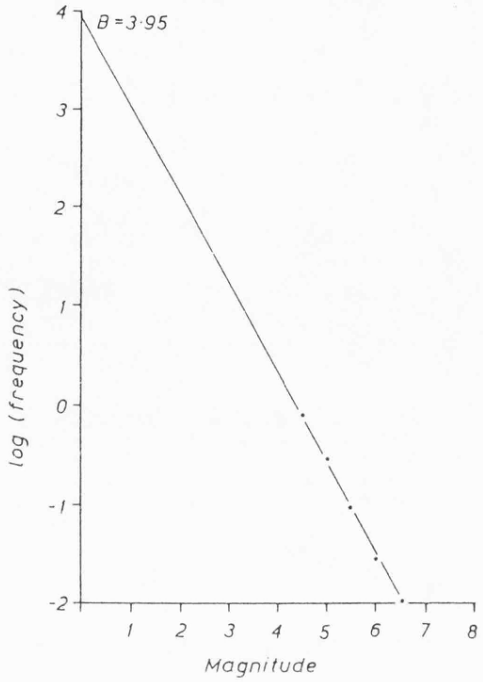

Fig.7.1. Frequency-magnitude graph of earthquakes in southwest Turkey. The data has a lower limit of M=4.5 but extrapolation back to lower magnitudes allows a value of B (the logarithm of the annual number of earthquakes) and M_m (the mean earthquake magnitude) to be calculated. Figures on the x-axis refer to the number of earthquakes greater than the value shown on the y-axis. Data is taken from Båth (1979).

FRONT. NO.	FAULT NAME	ORIENTATION	LENGTH (km)	MAXIMUM RELIEF(m)	Smf	Vf	LITHOLOGY
1	BURDUR FAULT	NE-SW	51.9	760	1.54	0.15	F,S,L,N
2	KUBUR FAULT	NE-SW	34.4	972	1.59	0.37	F,S,L
3	ACIGÖL FAULT	NE-SW	14.8	1197	1.17	0.13	L
4	MAYMUNDAGI FAULT (E)	ENE-WSW	6.1	779	1.14	0.20	F
5	MAYMUNDAGI FAULT (W)	E-W	8.2	808	1.25	0.18	F
6	BESPARMAK DAGI FAULT	NNE-SSW	36.5	723	1.42	0.26	F
7	BAKLAN FAULT (NW)	NE-SW	34.3	443	1.26	1.05	P,N
8	DINAR FAULT	NNW-SSE	58.2	1623	1.31	0.12	S,L

F = Eo-Oligocene Conglomerate S = Serpentinite
L = Basement Limestone P = Palaeozoic Metamorphics
N = Neogene Marls

Table 1. Geomorphological indices of fault controlled mountain fronts.

incorporates many active faults, not only the fault controlling the Neogene Burdur basin. However, it shows that deformed horizons in the Burdur Formation need not be common. Obviously, one will not find a deformed horizon every 4.2m within the succession as the abundance of potentially liquefiable sediments in the Burdur Formation is low; the basin fill is dominated by fine-grained lacustrine marl. When substituted into equation (2), figures published for seismicity in the Gulf of California by Lomnitz (1974) (M_m=0.5 and B=5) give a frequency of one deformed horizon per 1.15m. Californian seismicity can therefore account for more highly deformed successions such as the Torridonian Sandstone, a several kilometre thick pile of potentially liquefiable sediment (Allen 1986).

Clearly, twentieth century seismicity, extrapolated back to the Neogene, can account for the amount of deformation observed in the Burdur Formation. However, the fact that the deformation horizons are more common in the upper part of the succession (the Günalan Member) at the northern end of the basin requires explanation. A volcanic centre became active during the Lower Pliocene at the northern end of the basin and this evolved into an explosive maar-type volcano at about the time the Günalan Member was being deposited. Perhaps then, the deformation can be ascribed to seismic activity associated with this volcanic activity, rather than movements on normal faults. Again we can use the model described above to predict the amount of deformation associated with such activity. Firstly, the frequency of volcanic eruption must be known.

Maar volcanoes give rise to shallow explosive earthquakes due to phreatic eruption. A modern example of an explosive volcano is the Asama volcano from Japan. This volcano has been considerably active during the twentieth century, erupting 2301 times in 30 years. This gives an average of 77 eruptions a^{-1} (Minakami 1974), a frequency which we will extrapolate back to the Neogene of Burdur. (Counting up the number of air fall tuff and agglomerate horizons in the sedimentary succession at the northern end of the Burdur basin shows that there were 21 such periods of intense volcanic activity during the deposition of the Günalan Member (representing a time period of perhaps 2Ma)). A value of 1.89 for B in equation (2) is therefore obtained for an eruptive period. Explosive volcanic eruptions generally give rise to much lower magnitude earthquakes than fault movements. Most of the damage caused by such earthquakes is related to the detonation of air vibration rather than by

ground motion. A value for M_m of 0.5 will therefore be taken, bearing in mind that this is a maximum. Substituting these values into equation (2) gives an N(X) value of 1.7×10^{-4} a^{-1} for a site only 15km from the source of the eruption. (The distance of the volcanic centre from the majority of deformed horizons). If the sedimentation rate is 0.1m a^{-1} this would result in 1.7×10^{-3} deformed horizons per metre (or approximately 1 deformed horizon every vertical 600m of sediment). This is an upper estimate due to the maximum value of M_m taken and the value of B being for a particularly active period.

Clearly, volcanic eruptions cannot account for the deformation of sediment seen in the Burdur Formation. Also, Kuribayashi (1985) found that liquefaction of sediment does not occur at magnitudes of 3 or less. Most explosive volcanic eruptions give rise to earthquakes of less than magnitude 3. An alternative explanation for the localization of deformation to the upper part of the succession in the north is the fact that, due to the regional dip of the sediment, the upper part of the succession is nearest to the faulted Neogene basin margin. Also the Günalan Member is a succession of footwall-sourced alluvial fans. These are dominated by siltstones and sandstones, which are potentially liquefiable, as opposed to the lacustrine marls from lower in the succession. Finally, as a note of caution, one other mechanism which could give rise to deformational horizons is the rapid loading of an air fall volcaniclastic deposit, which would give rise to rapidly increasing pore fluid pressure and sediment failure (see Chapter 3; Figs.3.1, 3.2). However, at only 2 localities are there such deposits overlying deformed horizons and there is no evidence to suggest that volcaniclastic fall deposits could have been eroded from all the other localities.

The low frequency of wet-sediment deformation structures in potentially liquefiable successions of the Burdur Formation therefore places an upper limit on the level of seismicity active in the region during the Neogene.

7.3. GEOGRAPHICAL DISTRIBUTION OF FAULT ACTIVITY.

Several authors have studied recent fault history by considering the degradation of landforms with short survival times, such as fault scarps cutting alluvium (e.g. Bucknam and Anderson 1979; Nash 1981; Petersen 1985; Wallace 1977, 1980). Little attention has, however, been paid to

landforms with long survival times, such as high bedrock escarpments, which permit very approximate determinations of fault history but describe much longer time spans. Bull (1977, 1978) defined 2 geomorphological indices which describe the relative activity of a fault. The first is the mountain front sinuosity index (S_{mf}), which is defined as

$$S_{mf} = L_{mf} / L_s \qquad \text{(eq.3)}$$

where L_{mf} is the length of the mountain front and L_s is the straight line length of the mountain front. This index reflects the balance between uplift and erosion, with an active fault giving rise to a relatively straight mountain front and low S_{mf} values. The second index is the ratio of valley floor width to valley height, V_f, defined as

$$V_f = 2V_{fw} / (E_{ld} - E_{sc}) + (E_{rd} - E_{sc}) \qquad \text{(eq.4)}$$

where V_{fw} is the valley floor width, E_{ld} and E_{rd} are the elevations of the left and right valley divides respectively and E_{sc} is the elevation of the valley floor. These measurements are taken upstream from the front at a distance of 10% of the drainage basin length as suggested by Bull (1978). This index describes the down-cutting of a river in response to active uplift to form a V-shaped valley with a low V_f value.

The S_{mf} and V_f indices are also climate and lithology dependent. The effect of climate is the same for each mountain front but lithology must be taken into account when interpreting results. Table 1 shows results for each of the major basin-boundary faulted mountain fronts in the study area. S_{mf} values range from 1.14 to 1.59, V_f values from 0.12 to 1.05. Rockwell et al. (1985) showed that active faults from the western U.S.A. had average S_{mf} and V_f values of 1.14 and 0.63 respectively and less active faults averaged 2.04 and 1.05 respectively. Some of the higher values in the study area, especially those of Fault 1, can be explained by the rapid erosion of soft Neogene lithologies. The high S_{mf} values of Faults 1, 2 and 5 are partly explained by the fact that in each case several small en echelon faults were measured giving high L_{mf} and low L_s values. Nevertheless, most of the values obtained appear to fall into the range of active faults of Rockwell et al. (1985), who suggest that uplift rates of $0.4 mm a^{-1}$ are sufficient to keep S_{mf} values low. However, caution must be taken in comparing mountain front geomorphologies from

different areas in different lithologies. Within the study area the faults controlling the Acigöl basin (3 and 4) seem to have been the most active in the past few hundred thousand years, even though there is no recorded historical seismic event associated with this fault. As an aside, it is interesting to note that the alluvial fans on the SE side of the basin are smaller than those on the NW side suggesting tilting down to the SE. The Dinar fault also appears to be active and the relief associated with this structure suggests that it has had a relatively long history of uplift.

7.4. THE END-NEOGENE TECTONIC EVENT.

Enclosure 2 shows the distribution of Neogene and Quaternary sediments in the study area. The Neogene sediments cover a fairly large area, whereas those of the Quaternary are contained within narrow NE-SW trending grabens. This narrowing of the grabens at the end of the Neogene is best illustrated in the Burdur-Acigöl system. Fig.7.2 shows the structure of the southern part of the Burdur, Acigöl and Baklan basins based on seismic reflection data (see Chapter 5; Fig.5.7) and field mapping. Of interest is the fact that the fault controlling sedimentation in the Burdur basin during the Neogene moved towards the NW at the end of the Neogene to dissect the Neogene graben, creating a narrower Quaternary graben, the present-day Burdur basin. This phenomenon is not restricted to the study area. At the end of the Neogene both the Büyük Menderes and the Gediz Grabens (the 2 main E-W trending grabens in western Turkey) narrowed with the major fault moving into the hangingwall.

A possible explanation of this breaking-up of the end-Neogene topography throughout the study area and other parts of western Turkey is that the stresses in the upper elastic layer of the crust required to maintain the topography became too great (i.e. greater than the stresses which can be released during earthquakes) causing it to break up. Jackson and White (1989) showed that an upper limit to the size of rotating blocks in extending terranes is imposed by the thickness (or strength) of the outer elastic layer of the lithosphere. The following method of calculating the stress in the upper crust caused by topography (taken from Jackson and White 1989) illustrates this point.

The maximum shear stress, σ_{max}, required to support the topography of the

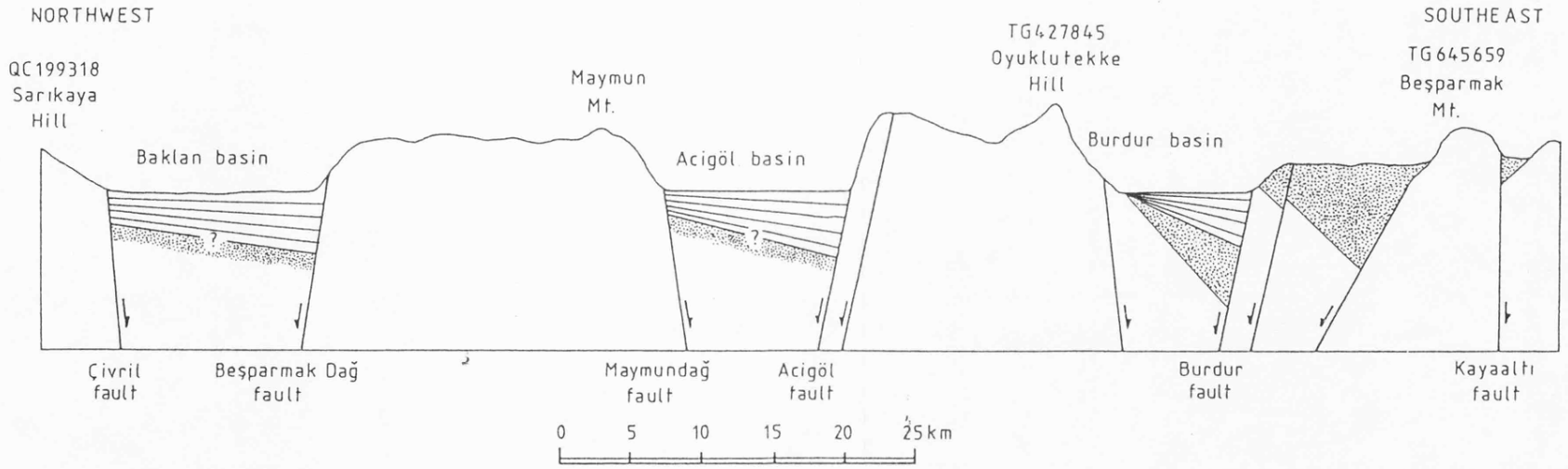

Fig.7.2. Simplified section across the southern part of the Burdur, Acigöl and Baklan basins. See enclosure 2 for location of section.

upper solid elastic layer of the crust, depends upon its thickness, T_e, and the topographic wavelength, λ. After McKenzie (1967),

$$\sigma_{max} = (\rho_B \, g \, \Delta t \, / \, 2) \, H(k') \qquad \text{(eq.5)}$$

where,

$$H(k') = \begin{cases} 1/e & \text{if } k'>2 \\ 3/4k' & \text{if } 1< k'<2 \\ 3/4k'^2 & \text{if } k'<1 \end{cases}$$

Δt is the effective amplitude of the topography, ρ_B, the basement density, g, the acceleration due to gravity and k', the dimensionless wave number, given by

$$k' = \pi \, T_e \, / \, \lambda \qquad \text{(eq.6)}$$

Δt is given by

$$\Delta t = h_B - h_e \qquad \text{(eq.7)}$$

where h_B is the basement amplitude and h_e, the height of the sedimentary and water column in the basin when normalised to basement density, given by

$$h_e = M_g \, / \, \rho_B \qquad \text{(eq.8)}$$

where M_g, the mass of the sedimentary and water column at the deepest point in the graben is given by

$$M_g = h_w \rho_w + h_w \rho^s - \phi^\circ \, (\rho_s - \rho_w) \, 1 \, \{ \exp(-a/1) - \exp(-b/1) \} \qquad \text{(eq.9)}$$

where h_w and h_s are the height of the water and sedimentary columns respectively, ρ_w and ρ_s, the density of water and the solid part of the sediment respectively, ϕ_o, the initial porosity, 1, the decay length (after Sclater and Christie 1980) and a and b, the depths of the sediment/water interface and the deepest part of the graben beneath the level at which $\phi = \phi_o$ respectively (Fig.7.3).

For the present-day situation in the Burdur region, λ = 26km. This is the

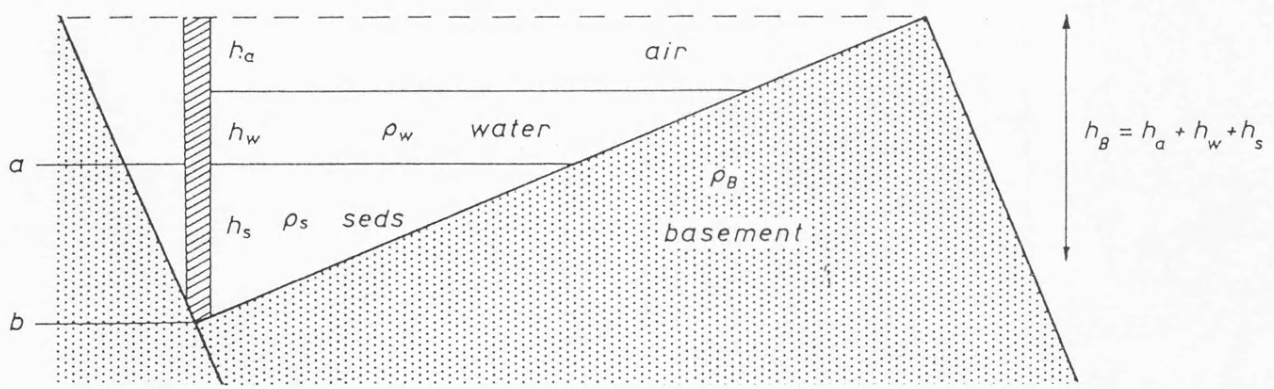

Fig.7.3. Cross-section illustrating the symbols used to calculate the effective basement topography when the graben is partly filled with sediment (thickness h_s) and water (thickness h_w) (after Jackson and White 1989).

distance between the Quaternary grabens on enclosure 2, or, more precisely, the distance between the Acigöl and Burdur Faults on Fig.7.2. T_e is taken as 8km as this is the approximate thickness of the elastic seismogenic upper crust in western Turkey (Jackson 1987). The following are the columnar thicknesses, taken from seismic data from the Burdur basin (Chapter 5) and topographic maps; h_a = 800m, h_w = 30m and h_s = 1450m. ρ_B is taken to be 2.85 Mg m^{-3}, ρ_s to be 2.70 Mg m^{-3}, l to be 1400m (for a sandstone/chalk mixture (see Sclater and Christie 1980)) and ϕ_o to be 70%. Substituting these values into equation (9) gives a value for M_g of 2.87×10^9 kg, giving an effective basement topography, Δt, of 1273m. Equation (5) then gives a σ_{max} value of 14MPa.

At the end of the Neogene, before the onset of the formation of the present-day grabens, the topographic wavelength was greater and a reasonable value for λ is 55km. This is the distance between the Neogene fault near Burdur and the most southeasterly Neogene exposures in the Acigöl region. Again seismic and topographic data gives columnar thicknesses; h_a = 800m and h_s = 1000m. These values when substituted for those used above give a σ_{max} value of 58MPa. This assumes that T_e was 8km at the end of the Neogene (i.e. no crustal thinning has occurred in the Quaternary). Perhaps a more realistic value of T_e for end-Neogene is 12km. This would give a σ_{max} value of 26MPa.

Obviously the σ_{max} values calculated above are only approximations. Nevertheless, it is apparent that the stress required to support the end-Neogene topography was greater than that required to support the present-day topography. Over an enormous scale range, the drops in shear stress associated with crustal earthquakes are remarkably uniform, being in the range 1-10MPa, with a logarithmic mean at 3MPa (Hanks 1977). Therefore at the end of the Neogene the supporting stresses became too great for the blocks to rotate coherently, and they broke up (i.e. became smaller). The present-day stresses in the crust also appear to be fairly high and cannot be dissipated by earthquakes. Large faults exist on the opposite sides of the Burdur and Acigöl basins (the Kubur and Maymundag Faults respectively). These prevent the blocks from moving coherently and reduce stress in the crust.

7.5. DEFORMATION OF BLOCKS.

7.5.1. Graben orientation

Another peculiarity of the basins in the study area is their NE-SW orientation. West of the study area are the Büyük Menderes, Kuçuk Menderes and Gediz Grabens, all E-W structures. However, as Fig.7.4 shows, the Burdur, Acigöl and Baklan Grabens have a similar orientation to the cross-grabens north of the Gediz Graben. They may, therefore be genetically related to these structures, interpreted by Sengör et al. (1985) and Sengör (1987) to be formed as a result of differential stretching in the hangingwall of the Gediz Graben.

It is likely that the NE-SW orientation of the grabens in the study area is an inherited feature, taking advantage of features in the palaeotectonic basement. Sengör et al. (1985) showed this for the Büyük, Kuçuk and Gediz Grabens and for the smaller cross-grabens north of the Gediz Graben, all of which follow the general fabric of the underlying Menderes Massif. Parallelism of normal fault arrays with basement fabric has also been documented by Laubach and Marshak (1987) for the autochthonous Caledonian foreland of NW Scotland where post-Caledonian faults nucleated on a steeply-dipping basement fabric. As with Sengör et al. (1985) and Sengör (1987) they interpret faults which are orthogonal to the main trend to be due to break up of the hangingwall of the main faults, which have listric geometry.

Plate 7.2 shows an enhanced Landsat 5 image (see Appendix II for details of enhancement technique) of the study area. A clear NE-SW fabric can be seen in areas of exposed basement lithologies. This is unlikely to be neotectonic as such a fabric is not seen in the uplifted Neogene sequences. In these areas the dominant fabric is NNE-SSW.

7.5.2. Regional σ_3 orientation.

Quaternary slip vectors from the study area indicate a general NW-SE extension direction (Chapter 5, Figs.5.5, 5.6). This is not in good agreement with the active N-S extension occurring throughout western Turkey and the Aegean shown by earthquake focal mechanisms (McKenzie 1978; Jackson and McKenzie 1984) and by the analysis of fault plane striae (Angelier et al. 1981). Fig.7.5 best illustrates the regional N-S

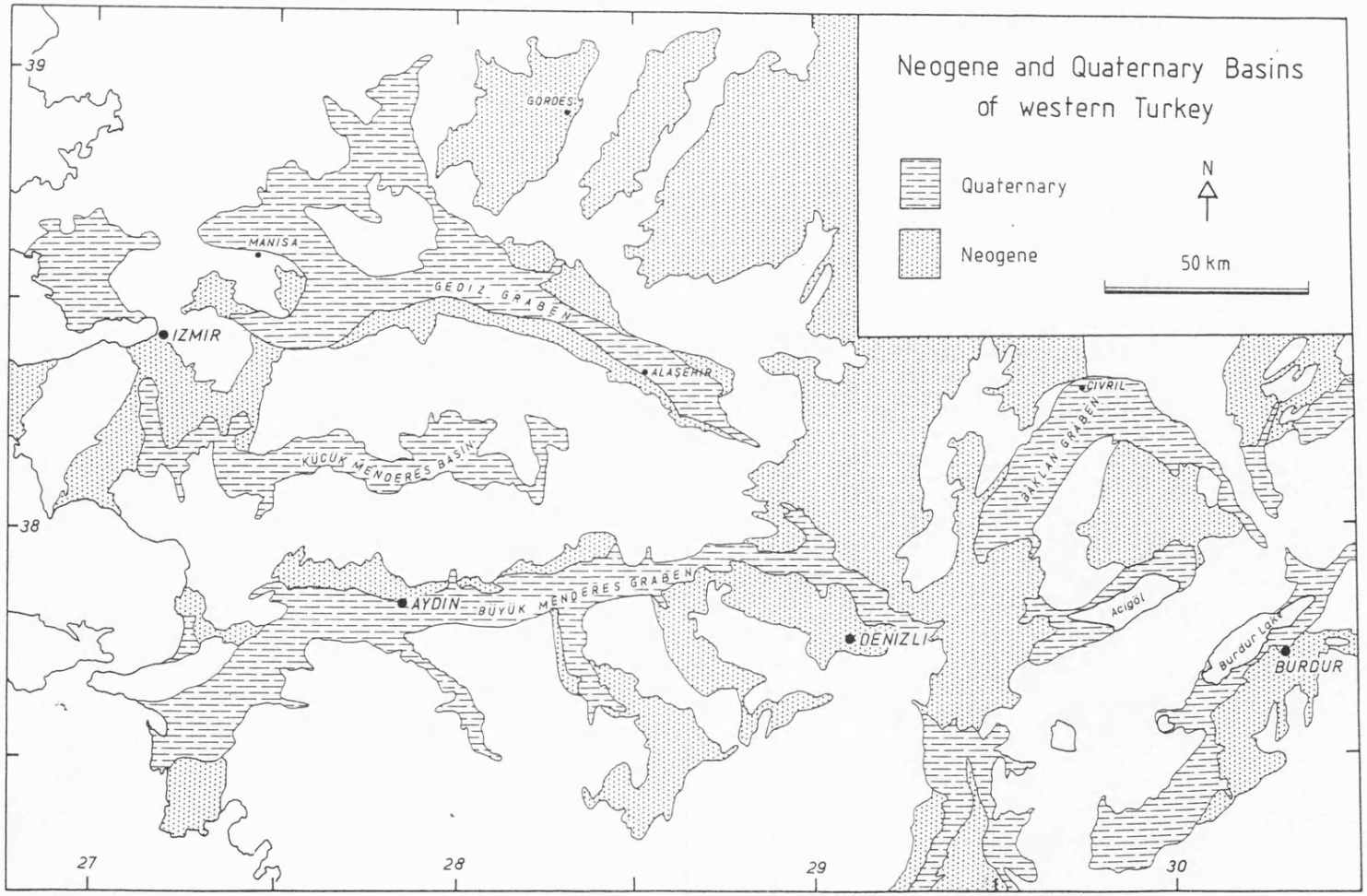

Taken from M.T.A. 1:500,000 Konya, Denizli, Izmir and Ankara sheets.

Fig.7.4. Map showing the distribution of Neogene and Quaternary basins in western Turkey.

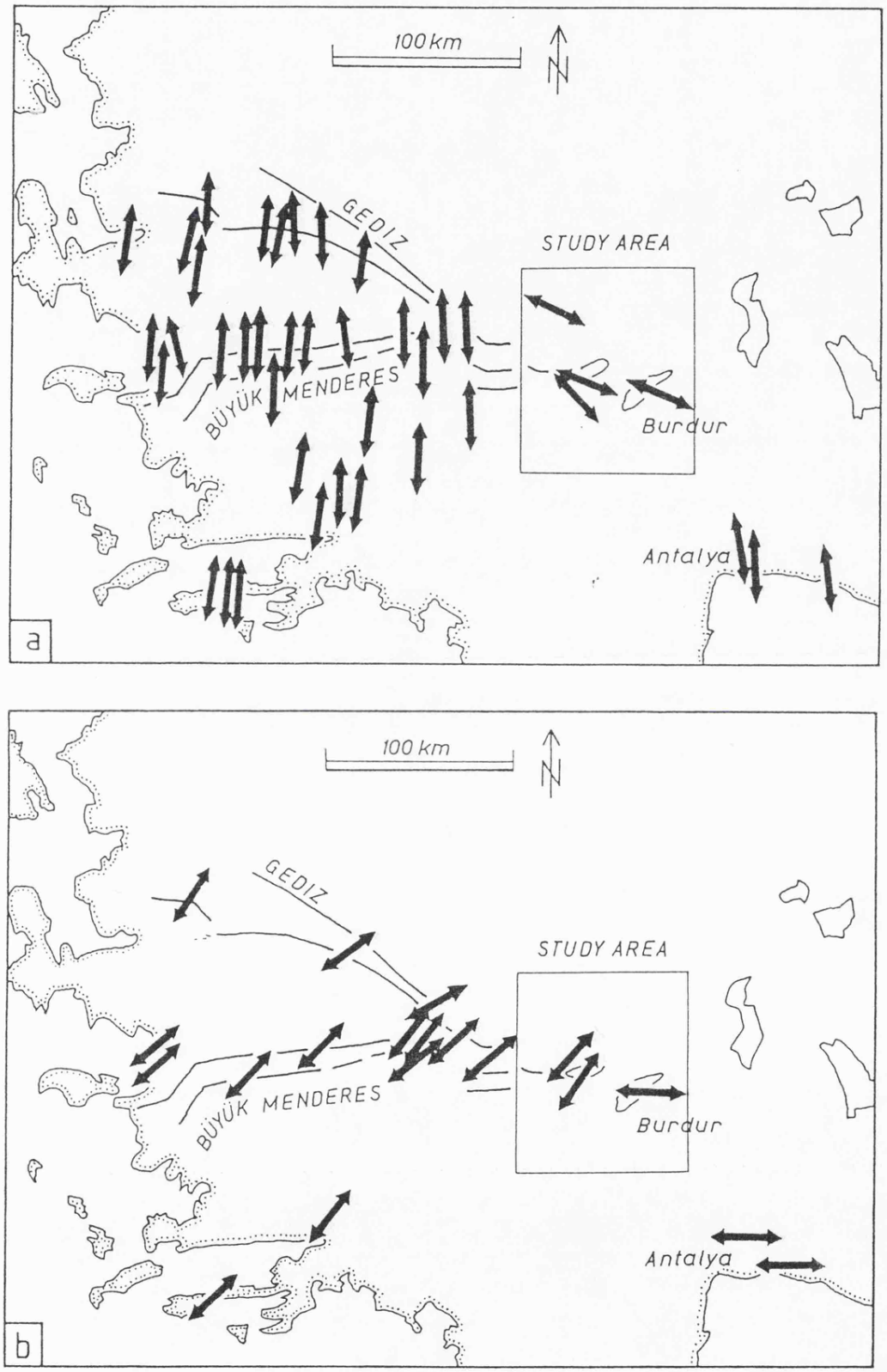

Fig.7.5. (a) Regional σ_3 orientation for faults of Pliocene age in southwest Turkey. Note the change from N-S to WNW-ESE in the study area. (b) Regional σ_3 orientation for faults of Quaternary age in southwest Turkey. (Both after Angelier et al. 1981).

extension with discrepant E-W slip vectors on the eastern edge of the deforming zone. The study area lies at the eastern edge of the Aegean-Western Anatolian Extensional Province in the Transition Zone of Sengör et al. (1985) and this discrepancy in extension direction may be some kind of "edge effect". However, it must clearly be accounted for in any model concerning the evolution of the Burdur-Acigöl-Baklan basin system.

7.5.3. Block rotations.

Rotations about horizontal axes since mid-Neogene times have allowed the study area to extend in a manner similar to the rotating domino model of Ransome et al. (1910). These rotations are easily detected by measuring the tilts of syn-rift basinal sediments. As well as rotations about horizontal axes, there is some evidence for rotations about vertical axes in the study area. Large rotations about vertical axes in taphrogens have become widely recognised in recent years, especially for the Aegean region (Laj et al. 1982; Kissel and Laj 1988; Kissel et al. 1984, 1985, 1986). Kissel and Poisson (1986) published palaeomagnetic data for Neogene formations from the Antalya basin and concluded that no significant rotations had occurred since at least 15Ma. However, samples of volcanics from the 4.5Ma Gölcük Member (see Chapter 2) from the NW end of the Burdur Formation show a 12.5° (±3°) clockwise rotation. This is the only locality in the study above the base of the Lycian nappes, the others occurring within the Antalya basin. Palaeomagnetic data from the Izmir region indicates an anticlockwise rotation of 29° (±11°) (Kissel et al. 1986). Although the timing of this rotation is poorly constrained a single K/Ar date of 7Ma from a sampled lava near Izmir and the fact that block-faulting is generally post-Tortonian suggest that the rotations have occurred since this date (Kissel and Laj 1988). Kissel et al. 1986 suggest that anticlockwise rotations from the Izmir region are representative of the whole of western Turkey above the Lycian nappes.

So, the local clockwise rotations near Burdur of approximately $3°Ma^{-1}$ may overprint a regional anticlockwise rotation of approximately $4°Ma^{-1}$, giving a net relative clockwise rotation of $7°Ma^{-1}$. If there is no overprint they must be treated separately.

7.5.4. Deformational models.

Any model describing active deformation for the study area must account for the discrepancy of slip-vector orientations, the basin orientation and geometry and the apparent clockwise rotations of crustal blocks. In the following section 2 basin evolution models, both potentially capable of producing the basin geometry of the study area, are described.

(a) Cross-graben model.

It has already been mentioned that the 3 basins of the study area are parallel to the cross-grabens north of the Gediz Graben and may therefore have formed in a similar manner. Sengör et al. (1985) and Sengör (1987) showed the faults controlling these grabens to be controlled by cross-faults which accommodate differential stretching in the hanging wall of the main Gediz Graben fault.

Enclosure 2 shows that the 3 NE-SW trending basins of the study area terminate in the NE against the Dinar Fault. So far little has been said about this structure. It may be a reactivated thrust fault as it is parallel and along strike from the Aksu thrust which is a palaeotectonic structure overlain by Pliocene sediments and marks the base of the eastern flank of the Isparta Angle (Sengör and Yilmaz 1981). However, there is no doubt as to its present nature as a normal fault because at many localities along the mountain front between Dinar and Civril (e.g. TH432301 and TH488462) slip planes can be observed with a normal dip slip component. It may be that the Dinar Fault is a major breakaway fault with the Burdur, Acigöl and Baklan basins forming due to differential stretch of the hanging wall along cross-faults (Fig.7.6).

(b) Rotational block model.

Several models have been proposed to explain the rotations about vertical axes often observed in regions of distributed deformation. A complex geometrical model involving strike-slip faults bounding an area deforming by rotations was proposed by Ron et al. (1984) and Garfunkel and Ron (1985). In this model surface area is conserved and stretching across the zone is balanced by shortening along strike. The 2-dimensional model proposed by McKenzie and Jackson (1983, 1986) is simpler because the surface area increases within the deforming zone during extension and there is no shortening along strike. Therefore the motions of rigid

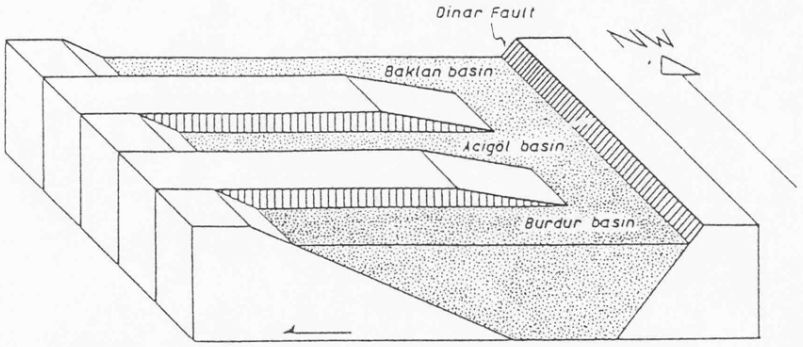

Fig.7.6. Block diagram illustrating the possible relationship between the Dinar Fault and the Burdur, Acigöl and Baklan basins. Differential stretch in the hangingwall of the Dinar Fault above a mid-crustal detachment has localised subsidence in the 3 basins.

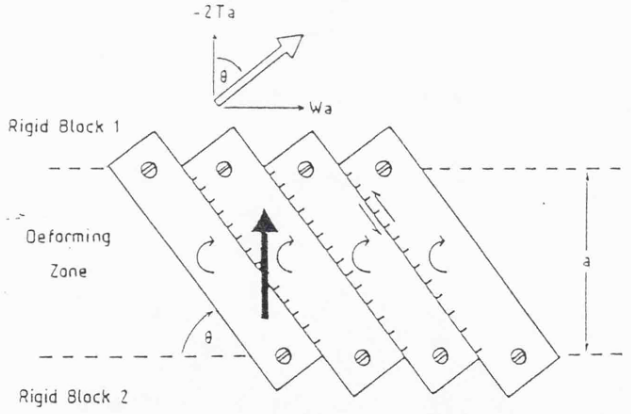

Fig.7.7. The pinned block model of McKenzie and Jackson (1986). The width of the deforming zone is a. The white arrow shows the motion of plate 1 relative to plate 2, with components -2Ta normal to the zone and Wa parallel to it. The black arrow indicates the position of the slip vector between adjacent blocks. Both normal and sinistral strike-slip motion occurs between these blocks. The blocks rotate in a clockwise direction.

plates bordering the deforming zone can more easily be related to deformation within the zone. The following is a brief description of the model of McKenzie and Jackson (1983, 1986) which is shown in Fig.7.7. 2 rigid plates are on either side of a deforming zone of width, a. If plate 1 moves in the direction of the white arrow relative to plate 2, there will be clockwise rotations of blocks within the deforming zone. These blocks are separated by normal faults with a sinistral strike-slip component in order to accommodate block rotations. The slip vector, shown by the black arrow, is perpendicular to the edge of the deforming zone. An important feature of the model is that the velocity vector of plate 1 (shown by the white arrow) is normal to the strike of the faults in the deforming zone. The velocity vector has a component Wa parallel to the edge of the deforming zone and -2Ta normal to it (Fig.7.7). The angle between the edge of the deforming zone and the faults within the zone, θ, will also be the angle between the velocity vector of plate 1 and -2Ta. McKenzie and Jackson (1983, 1986) showed that if the rotating blocks are pinned to the edge of the deforming zone then

$$d\theta/dt = W \qquad \text{(eq.10)}$$

and if they are floating then

$$d\theta/dt = W/2 \qquad \text{(eq.11)}$$

This model bears a striking resemblance to the situation in the study area. Here, NE-SW trending faults with approximately E-W slip vectors define clockwise-rotating blocks (Fig.7.8). If the model fits, then the slip vectors on the faults define a N-S trending deforming zone. The orientation of the faults dictates the velocity vector across this zone, which will have a dextral component with respect to the edge of the zone (Fig.7.7). Knowing values of a, θ and $d\theta/dt$ the model can be used to quantify the velocity vector across the deforming zone.

(i) The width of the deforming zone, a.

Geological data can be used to predict the width of the deforming zone. The zone will presumably incorporate all of the basement faults of the Burdur, Acigöl and Baklan basins and if it trends N-S it must be at least 90km wide to do so. Fig.7.5a shows that to the east and west of the deforming zone Pliocene slip vectors (from Angelier et al. 1981) indicate

N-S extension. The stations where N-S extension was computed define a zone 125km wide. As the deforming zone is unlikely to have had its extremities at these stations a value somewhat less than this is likely. Therefore a value of 100km is taken. It is interesting to note that Quaternary slip vectors to the east of the deforming zone are E-W trending (Fig.7.5b) perhaps showing that the zone has extended eastwards in the last 5Ma.

(ii) The angle θ.

Assuming a N-S trending deforming zone, the angle between the edge of the zone and the faults within the zone, θ, is about 45° (Fig.7.8). This angle is consistent for the Burdur, Acigöl and Baklan basins.

(iii) The rate of rotation, dθ/dt.

Palaeomagnetic data indicate a clockwise rotation rate of $3°Ma^{-1}$ within the deforming zone. This assumes that the local palaeomagnetic declination measured near to Burdur does not overprint the regional declination. The deforming zone rotates independently from any translation or rotation of the rigid boundary plates so there will be no overprinting.

Taking a = 100km, θ = 45° and $d\theta/dt = 3°Ma^{-1}$ equation (10) gives a slip vector of 3.0 cma^{-1}. This assumes that the blocks are pinned. If they are floating a value of $1.5cma^{-1}$ is obtained from equation (11). Previous applications of this model to deforming regions (e.g. McKenzie and Jackson 1983; Walcott 1984) favour the floating block model.

7.6. DISCUSSION.

Several lines of reasoning suggest that the cross-graben model cannot account for the style of deformation seen in the study area. Firstly, there is no evidence for a deepening of the "cross-grabens" towards the Dinar Fault. In fact, the Acigöl basin is not connected with the fault (see enclosure 2). This can perhaps be explained by invoking strain heterogeneities within the hanging wall basement blocks. Secondly, although major earthquakes have occurred on the faults controlling the "cross-grabens" (Ambraseys 1975, 1988) during the twentieth century,

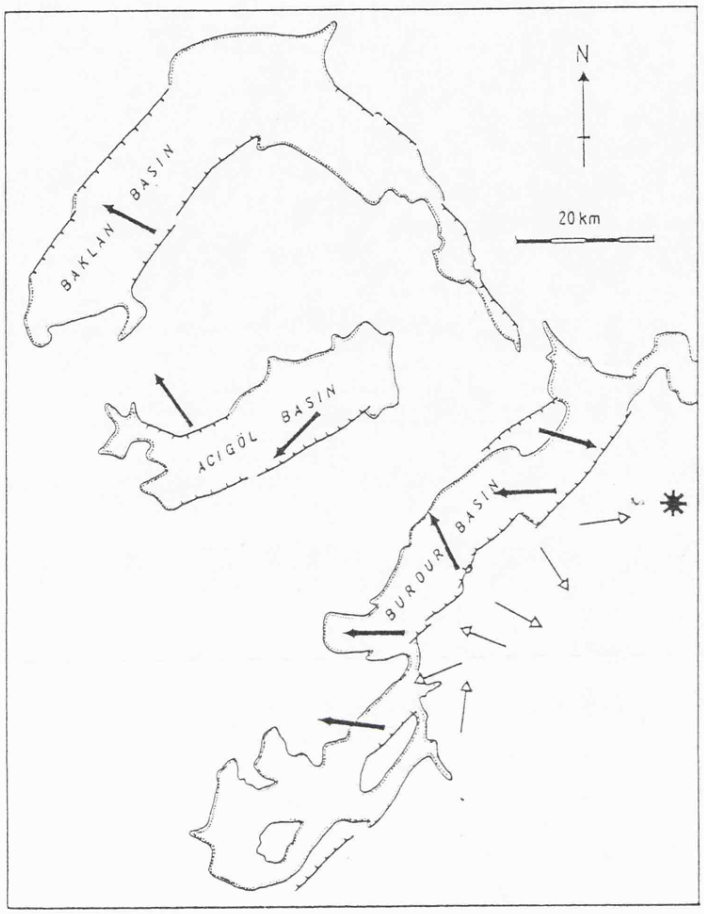

Fig.7.8. Orientation of σ_3 in the Burdur, Acigöl and Baklan basins. Black arrows indicate σ_3 orientation for basin-boundary faults and small arrows for faults within the Neogene Burdur Formation. Both are taken from σ_3 determinations presented in Chapter 5. The star indicates the position of the palaeomagnetic determination in 4.5Ma lavas undertaken by Kissel and Poisson (1986). Note the similarity between this figure and the pinned block model of McKenzie and Jackson (1986). (See text for a full discussion).

there is no record of major earthquakes on the Dinar Fault. This is surprising as the total theoretical seismic moment for the breakaway fault should be about 80% greater than that along the cross-faults (Sengör 1987). Finally, all the faults in the study area are normal and faults of opposing dip exist. There are Neogene tilts of about 10° in the Burdur region. So, if the Dinar Fault had a strike-parallel tilt of 10° one would expect some of the faults controlling the "cross-grabens" to have a reverse attitude.

If the rotational block model is to be accepted, the N-S trending deforming zone has to be interpreted in terms of the regional tectonic framework of the eastern Mediterranean. To the west of the deforming zone is the rapidly extending Aegean region with crustal thicknesses of 22-32km and to the east the relatively stable Anatolian plateau with a crustal thickness of 40-50km (Makris 1976; Makris and Vees 1977). The deforming zone is therefore a convenient boundary between these 2 regions of different tectonic character and crustal thickness. The dextral sense of motion of the velocity vector across the deforming zone also requires explanation.

If one considers the Aegean and Turkey as rigid bodies, a pole of rotation between these bodies can be calculated. Table 2 shows poles of rotation for the Aegean, Turkey and Africa. The Aegean-Africa pole was calculated by Le Pichon and Angelier (1979) from fault plane solutions of McKenzie (1978) and is probably inaccurate. The magnitude of their rotation, calculated from subduction rates in the Hellenic Trench, is also perhaps a minimum value due to an overestimate of the timing of onset of subduction. However, using this pole and that of Africa-Turkey (from Jackson and McKenzie 1984) an Aegean-Turkey pole can be calculated stereographically. This shows the Aegean to be rotating $19°/10^7$a clockwise with respect to Turkey about a pole situated in northern Italy, which predicts a $6.3 cma^{-1}$ velocity across the deforming zone with a predominantly sinistral component (Fig.7.9). Because the amount of rotation of the Aegean with respect to Africa is an underestimate the true pole of rotation between the Aegean and Turkey is probably nearer to the Aegean-Africa pole in southern Italy and the velocity across the deforming zone greater than $6.3 cma^{-1}$. This velocity will also be enhanced by the southward drift of the southern Aegean (Jackson and McKenzie 1988).

	Latitude	Longitude	Rate (°/10^7yr)	Source
Africa-Turkey	9.3	44.7	5.73	Jackson and McKenzie (1984)
Aegean-Africa	40.0	18.0	-23.10	Le Pichon and Angelier (1979
Aegean-Turkey	46.0	9.0	-19.00	Calculated from above

Table 2. Poles of rotation for the Aegean, Turkey and Africa.

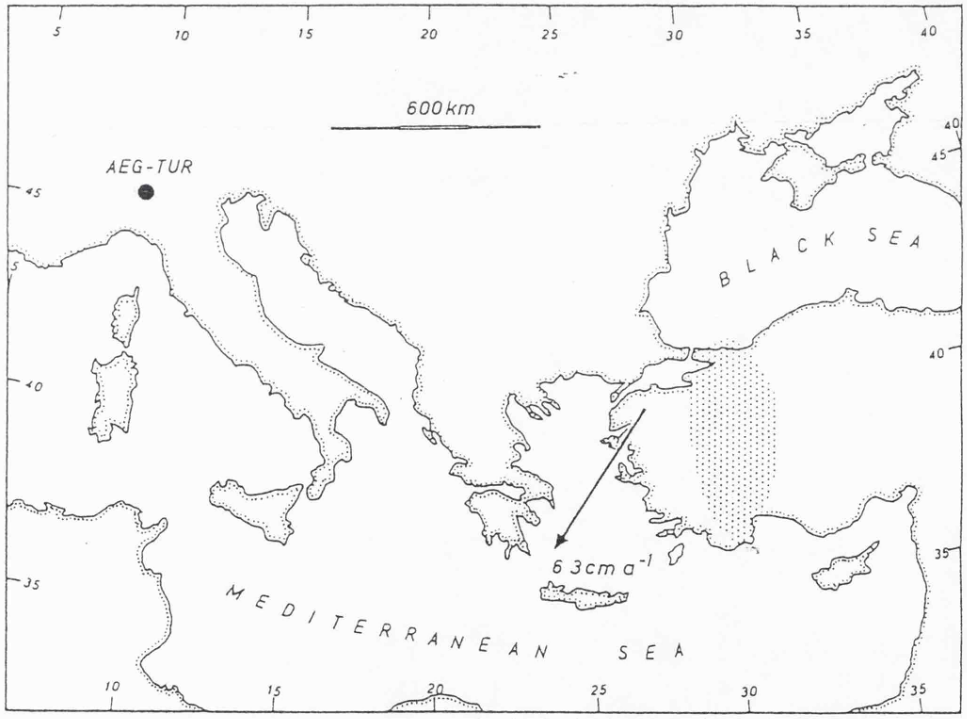

Fig.7.9. Map of the eastern Mediterranean region showing the position of the Aegean-Turkey pole of rotation calculated from Africa-Turkey (Jackson and McKenzie 1984) and Aegean-Africa (LePichon and Angelier 1979) poles. The black arrow shows the calculated velocity vector across the deforming zone , which is shown as a dotted region. Displacement across the deforming zone is sinistral.

The velocity vector across the deforming zone calculated from the rotations of rigid landmasses is therefore in disagreement with that predicted from the rotational block model. A sinistral velocity vector across the deforming zone with the grabens having a NE-SW orientation would give rise to anticlockwise block rotations in the deforming zone and the faults separating blocks within the zone would be compressional. This is clearly not the case, strongly suggesting that the sense of displacement across the zone cannot be calculated by considering the Aegean and Turkey as rigid rotating bodies. The Aegean, in particular, is a rapidly extending region which can be sub-divided into many smaller areas deforming independently from one another.

Kissel and Laj (1988) used palaeomagnetic data to show that the curvature of the Hellenic arc was brought about by opposing rotations at both ends of an originally E-W trending rectilinear arc. Although clockwise rotations in Greece occurred throughout the Plio-Quaternary (Kissel et al. 1986), anticlockwise rotations at the eastern end of the arc ended in the Tortonian. This is based on palaeomagnetic data from Rhodes (Laj et al. 1982). However, the inner arc in western Turkey appears to have rotated anticlockwise through the Plio-Quaternary (Kissel et al. 1986) and this rotation may be representative of the whole of western Turkey above the Lycian nappes as tentatively suggested by Kissel et al. (1986). Such a rotation against a stable Anatolian plateau would give the predicted dextral sense of motion across the deforming zone.

7.7. CONCLUSIONS.

The following conclusions, concerning the dynamic evolution of the Burdur-Acigöl-Baklan basin system, can be drawn from this study.

(a) The faults controlling the basin system are seismically active and have been since the onset of basin formation during the Neogene. Although difficult to quantify, wet-sediment deformation shows that levels of seismicity during the Neogene appear to have been lower than twentieth century levels. Wet-sediment deformation is too abundant to be induced by earthquakes associated with volcanic activity.

(b) The geomorphology of fault-controlled mountain fronts shows that

twentieth century seismicity (in terms of major earthquakes) cannot be extrapolated back for even the past few hundred thousand years. There is no historic record for major earthquakes associated with some of the most active faults in the area (e.g. the Acigöl and Maymundag Faults).

(c) The narrowing of the grabens at the end of the Neogene is due to the collapse of an unstable basement topography brought about by block-faulting. The stresses induced in the upper elastic layer of the crust by this topography are greater than stresses released during major earthquakes, causing the basins to break up into a more stable configuration. The lack of a simple half-graben domino-style geometry (i.e. the presence of large antithetic faults) is also accounted for by this topographic break up.

(d) The basin system formed in a N-S trending deforming zone between the actively extending Aegean area and the relatively stable Anatolian plateau. This deforming zone has a dextral sense of displacement across it and within the deforming zone basement blocks are rotating about vertical axes in a clockwise sense. This theory accounts for the discrepancy of stretching direction between the basin system and the major grabens of western Turkey (outside the deforming zone). Because of the non-rigid nature of western Turkey and the Aegean the dextral motion across the deforming zone is difficult to account for. It may be caused by the anticlockwise rotation of western Turkey.

7.8. REFERENCES.

Allen, J.R.L. 1986. Earthquake magnitude-frequency, epicentral distance and soft-sediment deformation in sedimentary basins. Sedimentary Geology, v.46, p.67-75.

Alsan, E., Tezuçan, L and Båth, M. 1975. An earthquake catalogue for the interval 1913-1970. Kandilli Observatory, Istanbul and Seismological Institute, Uppsala, Report No.7-75, 166pp. Also in: Tectonophysics, 1976, v.31, T13-T19.

Ambraseys, N.N. 1975. Studies in historical seismicity and tectonics. In: Geodynamics Today. Royal Society Publication, p.7-16.

Ambraseys, N.N. 1988. Engineering Seismology. Earthquake Engineering and Structural Dynamics, v.17, p.1-105.

Ambraseys, N.N. and Finkel, C. 1987. Seismicity of Turkey and neighbouring regions 1899-1915. Annales Geophysique, v.5b.

Angelier, J., Dumont, J.F., Karamanderesi, H., Poisson, A., Simsek, S. and Uysal, S. 1981. Analyses of fault mechanisms and expansion of southwestern Anatolia since the late Miocene. Tectonophysics, v.75, T1-T9.

Båth, M. 1979. Seismic risk in Turkey: a preliminary approach. Tectonophysics, v.54, T9-T16.

Bucknam, R.C. and Anderson, R.E. 1979. Estimation of fault-scarp ages from a scarp height-slope angle relationship. Geology, v.7, p.11-14.

Bull, W.B. 1977. Tectonic geomorphology of the Mojave Desrt. U.S. Geological Survey Contract Report 14-08-001-G-394, Office of Earthquakes, Volcanoes and Engineering, Menlo Park, California, 118pp.

Bull, W.B. 1978. Geomorphic tectonic activity classes of the south front of the San Gabriel Mountains, California. U.S. Geological Survey

Contract Report 14-08-001-G-394, Office of Earthquakes, Volcanoes and Engineering, Menlo Park, California, 59pp.

Curran, P.J. 1985. Principles of Remote Sensing. Longman, London, 282pp.

Drury, S.A. 1986. Remote sensing of geological structure in temperate agricultural terrains. Geological Magazine, v.123, p.113-121.

Erinç, S., Bener, M., Sungur, K. and Göçmen, K. 1971. 12 Mayis 1971 Burdur Depremi. Istanbul Üniversitesi Cografya Enstitüsü Yayinlari, No.66, 27pp.

Garfunkel, Z. and Ron, H. 1985. Block rotations and deformation by strike-slip faults: II. The properties of a type of macroscopic discontinuous deformation. Journal of Geophysical Research, v.90, p.8589-8602.

Hanks, T.C. 1977. Earthquake stress drops, ambient tectonic stress, and stresses that drive plate motions. Pure and Applied Geophysics, v.115, p.441-458.

Hempton, M.R. and Dewey, J.F. 1983. Earthquake-induced deformational structures in young lacustrine sediments, East Anatolian Fault, southeast Turkey. Tectonophysics, v.98, T7-T14.

Hunt, G.R. 1980. Electromagnetic radiation: the communication link, in remote sensing. In: Siegal, B.S. and Gillespie, A.R. (eds) Remote Sensing in Geology. Wiley, New York, p.5-45.

Jackson, J.A. 1987. Active normal faulting and crustal extension. In: Coward, M.P., Dewey, J.F. and Hancock, P.L. (eds) Continental Extensional Tectonics. Special Publication of the Geological Society of London, No. 28, p.3-17.

Jackson, J.A. and McKenzie, D.P. 1984. Active tectonics of the Alpine-Himalayan belt between western Turkey and Pakistan. Geophysical Journal of the Royal Astronomical Society, v.77, p.185-264.

Jackson, J.A. and McKenzie, D.P. 1988. The relationship between plate

motions and seismic moment tensors, and the rates of active deformation in the Mediterranean and Middle East. Geophysical Journal, v.93, p.45-73.

Jackson, J.A. and White, N.J. 1989. Normal faulting in the upper continental crust: observations from regions of active extension. Journal of Structural Geology, v.11, p.15-36.

Karaman, M.E. 1989. New aspects of plate boundaries between Aegean and Anatolian Plates. Terra Abstracts, v.1, p.56.

Keightley, W.O. 1975. Destructive earthquakesin Burdur and Bingol, Turkey: May 1971. National Research Council, Washington, D.C., 84pp.

Kissel, C. and Laj, C. 1988. The Tertiary geodynamical evolution of the Aegean arc: a palaeomagnetic reconstruction. Tectonophysics, v.146, p.183-201.

Kissel, C. and Poisson, A. 1987. Etude paléomagnétique préliminaire de formations néogènes du bassin d'Antalya (Taurides occidentales, Turquie). Comptes Rendus Académie des Sciences Paris, v.302(II-10), p.711-716.

Kissel, C., Jamet, M. and Laj, C. 1984. Palaeomagnetic evidence of Miocene and Pliocene rotational deformations of the Aegean Area. In: Dixon, J.E. and Robertson, A.H.F. (eds) The Geological Evolution of the Eastern Mediterranean. Special Publication of the Geological Society of London, No.17, p.669-679.

Kissel, C., Laj, C. and Muller, C. 1985. Tertiary geodynamical evolution of Northwestern Greece: palaeomagnetic results. Earth and Planetry Science Letters, v.72, p.190-204.

Kissel, C., Laj, C., Poisson, A., Savaşçin, Y., Simeakis, K. and Mercier, J.L. 1986. Paleomagnetic evidence for neogene rotational deformations in the Aegean domain. Tectonics, v.5, p.783-796.

Laj, C., Jamet, M., Sorel, D. and Valente, J.P. 1982. First paleomagnetic results from Mio-Pliocene series of the Hellenic sedimentary arc: Geodynamics of the Hellenic Arc and Trench. Tectonophysics, v.86,

p.45-67.

Laubach, S.E. and Marshak, S. 1987. Fault patterns generated during extensional deformation of crystalline basement, NW Scotland. In: Coward, M.P., Dewey, J.F. and Hancock, P.L. (eds) Continental Extensional Tectonics. Special Publication of the Geological Society of London, No.28, p.495-500.

Le Pichon, X. and Angelier, J. 1979. The Hellenic arc and trench system: a key to the neotectonic evolution of the eastern Mediterranean area. Tectonophysics, v.60, p.1-42.

Lomnitz, C. 1974. Global Tectonics and Earthquake Risk. Elsevier, Amsterdam, 320pp.

Makris, J. 1976. A dynamic model of the Hellenic arc deduced from geophysical data. Tectonophysics, v.36, p.339-346.

Makris, J. and Vees, R. 1977. Crustal structure of the central Aegean Sea and the islands of Evvia and Crete, Greece, obtained from refraction seismic experiments. Journal of Geophysics, v.42, p.329-341.

McKenzie, D.P. 1967. Some remarks on heat flow and gravity anomalies. Journal of Geophysical Research, v.72, p.6261-6273.

McKenzie, D.P. 1978. Active tectonics of the Alpine-Himalayan Belt: the Aegean Sea and surrounding regions. Geophysical Journal of the Royal Astronomical Society, v.55, p.217-254.

McKenzie, D.P. and Jackson, J.A. 1983. The relationship between strain rates, crustal thickening, paleomagnetism, finite strain and fault movements within a deforming zone. Earth and Planetry Science Letters, v.65, p.182-202.

McKenzie, D.P. and Jackson , J.A. 1986. A block model of distributed deformation by faulting. Journal of the Geological Society of London, v.143, p.349-353.

Minakami, T. 1974. Seismology of volcanoes in Japan. In: Civetta, L., Gasparini, P., Luongo, G. and Rapolla, A. (eds) Physical

Volcanology. Developements in Solid Earth Geophysics, No.6. Elsevier, p.1-28.

Nash, D.B. 1981. Fault: A FORTRAN program for modelling the degradation of active normal fault scarps. Computers and Geosciences, v.7, p.249-260.

Petersen, J.F. 1985. Equilibrium tendency in piedmont scarp denudation, Wasatch Front, Utah. In: Morisawa, M. and Hack, J.T. (eds) Tectonic Geomorphology. Allen and Unwin, Boston, p.209-233.

Ransome, F.L., Emmons, W.H. and Garry, G.H. 1910. Geology and ore deposits of the Bullfrog district, Nevada. Bulletin of the U.S. Geological Survey, No.407, 130pp.

Rockwell, K.R., Keller, A.K. and Johnson, D.L. 1985. Tectonic geomorphology of alluvial fans and mountain fronts near Ventura, California. In: Morisawa, M. and Hack, J.T. (eds) Tectonic Geomorphology. Allen and Unwin, Boston, p.183-207.

Ron, H., Freund, R., Garfunkel, Z. and Nur, A. 1984. Block rotation by strike-slip faulting: structural and paleomagnetic evidence. Journal of Geophysical Research, v.89, p.6256-6270.

Sclater, J.G. and Christie, P.A.F. 1980. Continental stretching: an explanation of the post mid-Cretaceous subsidence of the Central North Sea basin. Journal of Geophysical Research, v.85, p.3711-3739.

Scott, B. and Price, S. 1988. Earthquake-induced structures in young sediments. Tectonophysics, v.147, p.165-170.

Sengör, A.M.C. 1987. Cross-faults and differential stretching of hanging walls in regions of low-angle normal faulting: examples from Western Turkey. In: Coward, M.P., Dewey, J.F. and Hancock, P.L. (eds) Continental Extensional Tectonics. Special Publication of the Geological Society of London, No.28. p.575-589.

Sengör, A.M.C. and Yilmaz, Y. 1981. Tethyan evolution of Turkey: a plate tectonic approach. Tectonophysics, v.75, p.181-241.

Sengör, A.M.C., Görür, N. and Saroglu, F. 1985. Strike-slip faulting and related basin formation in zones of tectonic escape: Turkey as a case study. In: Biddle, K.T. and Christie-Blick, N. (eds) Strike-slip Deformation, Basin Formation and Sedimentation. Special Publication of the Society of Economic Paleontologists and Mineralogists, No.37, p.227-264.

Sims, J.D. 1973. Earthquake-induced structures in sediments of the Van Norman Lake, San Fernando, California. Science, v.1/2, p.161-163.

Sims, J.D. 1975. Determining earthquake recurrence intervals from deformational structures in young lacustrine sediments. Tectonophysics, v.29, p.144-152.

Walcott, R.I. 1984. The kinematics of the plate boundary through New Zealand: acomparison of short and long term deformations. Geophysical Journal of the Royal Astronomical Society, v.79, p.613-633.

Wallace, R.E. 1977. Profiles and ages of young fault scarps, north-central Nevada. Bulletin of the Geological Society of America, v.88, p.1267-1281.

Wallace, R.E. 1980. Degradation of the Hebgen Lake fault scarps of 1959. Geology, v.8, p.225-229.

Youd, L. and Hoose, S. 1977. Liquefaction susceptibility and geologic setting. Proceedings of the 6th World Conference on Earthquake Engineering, No.6, p.37-42.

Plate 7.1. Ball-and-pillow structures in normal graded sandstone beds. The coarse sandstone has penetrated downwards into the fine sandstone during sediment failure caused by pore fluid pressure of the sediment exceeding its yield strength. Such structures are probably earthquake-induced (see text for reasoning). Compare these with similar structures shown in Chapter 3 (Plate 3.4c.) which were caused by the rapid loading of an air fall agglomerate. The photograph shows part of a deformed horizon at TG653754, 1km southwest of Yakaköy.

Plate 7.1.

Plate 7.2. Landsat V TM (waveband 5) enhanced image of study area (see appendix 2 for enhancement technique).

CHAPTER EIGHT

SUMMARY OF CONCLUSIONS

The following conclusions can be made from this study:

(a) The Burdur Formation was deposited in a NE-SW trending intramontane basin, which had a half-graben structure. The major basin-boundary fault of this half-graben was along its SE margin. Dip profiles across the uplifted basinal succession suggest that this fault had a planar geometry at depth.

(b) Extension in the Burdur region began in late Miocene to early Pliocene times. This is indicated by a K-Ar (biotite) age of 4.6 ± 0.2Ma for lavas of the Lower Gölcük Member. These are believed to be synchronous with the oldest basinal sediments. However, a tentative biostratigraphic age of Pontian was obtained for the ostracode fauna of these sediments.

(c) The Burdur Formation was deposited in a closed basin. Rapid subsidence along the footwall margin is indicated by the poor developement of footwall-sourced fans. However, in the Kayi region, a thick footwall-sourced alluvial fan sequence developed. This was sourced in the relay structure between 2 left-stepping en echelon fault segments. Hangingwall-sourced fans were proximally confined to karstic depressions in the Mesozoic limestone, which formed much of the basin margins. However, palaeocurrents from the large stacked hangingwall-sourced fan sequence exposed in Kuruçay valley indicate a possible structural control at the basin margin.

(d) The scarcity of wet-sediment deformation in potentially-liquefiable sediments of the Burdur Formation shows that levels of seismicity in the Burdur region during the Pliocene were lower than twentieth century levels.

(e) Pliocene Lake Burdur was a deep saline lake. The Na/Ca ratio of lacustrine carbonates indicates that it had a salinity comparable to that of modern Lake Burdur (19 to 27 ‰). Inorganic carbonate precipitation was the dominant sedimentary process. Organic-rich marl

was deposited during times of increased rainfall and reduced evaporation (shown by an increase in $\delta^{18}O$). However, periods of increased evaporation of the order of a few thousand years (which may have been related to the solar cycle) gave rise to dolomitization. Organic-poor marl was deposited during times of reduced rainfall and increased evaporation (shown by a decrease in $\delta^{18}O$). The enrichment of $\delta^{13}C$ in the organic-poor marls was due to a fractionation between HCO_3^- and slowly released gaseous CO_2. Organic-rich / organic-poor cycles are well-developed. Spectral analysis indicates a periodicity of 19ka for these cycles. This is equivalent to the Earth's precessional cycle. It is therefore proposed that cyclic sedimentation in palaeolake Burdur was the result of orbitally-driven climatic change.

(f) Towards the end of the Pliocene the fault controlling the Burdur basin became inactive. Activity switched to a fault system in the hangingwall of the old fault and much of the Burdur Formation was uplifted in the footwall of this newly-formed fault system. This switch in fault activity gave rise to localised unconformities in the upper part of the Burdur Formation and an increase in block faulting activity caused widespread spring activity and the precipitation of the Yakaköy travertine. This end-Pliocene tectonic event gave rise to the present-day basin configuration of the study area (see (g)). The block faulted topography of this configuration induces less stress in the upper elastic layer of the crust than did the end-Pliocene basin topography. It is proposed that the break-up of the basins in the study area at the end of the Pliocene into the present-day configuration was necessary to release stresses built up in the crust.

(g) The Burdur, Acigöl and Baklan basins of the study area each have faulted margins on both sides. However, each of these basins is a half-graben with the major basin-boundary fault on the SE side. Evidence for the Burdur basin is from seismic data and recent surface fault breaks. Evidence for the Acigöl and Baklan basins is from geomorphological data and the avulsion of the Büyük Menderes river. The internal break-up of fault-bounded blocks for the reason outlined in (f) accounts for the presence of well-developed antithetic faults on the opposite basin margins. Bedding tilts and surface fault dips indicate a β value of 1.18 for the Burdur region since the onset of

extension. This, however, assumes that the faults have a planar geometry at depth. As a curvature of up to 40° at depth cannot be ruled out it may be an underestimate.

(h) The NW-SE extension direction of the study area (obtained from palaeostress studies of fault and striae populations) is in disagreement with the N-S extension direction of the Aegean region to the west. To the east of the study area is the relatively stable Anatolian plateau. It is proposed that the study area is within a N-S trending deforming zone between these 2 continental areas. The model adopted explains the orientation of extension within the zone, the clockwise rotations of fault-bounded blocks in the area (from earlier palaeomagnetic studies) and the NE-SW orientation of the grabens in the deforming zone. However, the model requires a dextral motion across the deforming zone. Rapid extension in the northern Aegean predicts a sinistral motion as the southern Aegean is moving southwards. The anticlockwise rotation of western Turkey may resolve this discrepancy.

APPENDIX I.

OSTRACODE FAUNA OF THE BURDUR FORMATION.

Sample MP29. Lower Akdere Road Section (Unit 55) TG607759.

AKDERE MEMBER

Candona (Typhlocypris) fossulata POKORNY, 1952.
Candona nobilis (SNEJDER, 1963)

Sample MP4. Upper Akdere Road Section (Unit 3) TG609749.

AKDERE MEMBER

Ilyocypris bradyi SARS, 1890
Cyprideis tuberculata (MEHES, 1908)
Candona (Typhlocypris) fossulata POKORNY, 1952
Candona (Candona) altoides PETKOVSKI, 1961
Candona (Candona) candida (MULLER, 1776)
Candona (Candona) decimai FREELS, 1980
Candona (Candona) burdurensis FREELS, 1980
Heterocypris (non adult)

Sample MP28. Upper Akdere Road Section (Unit 4) TG609749.

AKDERE MEMBER

Candona (Typhlocypris) fossulata POKORNY, 1952
Candona nobilis (SNEJDER, 1963)
Candona (Candona) cf. decimai FREELS, 1980
Candona (Candona) cf. burdurensis FREELS, 1980

Sample MP27. Upper Akdere Road Section (Unit 7) TG609749.

AKDERE MEMBER

Candona (Typhlocypris) eremita (VEJDOVSKY, 1880)
Candona (Caspiocypris) erzurumensis FREELS, 1980
Cyprideis sp. (non adult)

Sample MP26. Upper Akdere Road Section (Unit 7) TG609749.

AKDERE MEMBER

Candona (Candona) decimai FREELS, 1980
Candona (Candona) cf. altoides PETKOVSKI, 1961
Candona (Candona) burdurensis FREELS, 1980

Sample MP25. Upper Akdere Road Section (Unit 8) TG609749.

AKDERE MEMBER

Candona (Candona) decimai FREELS, 1980

Candona (Candona) cf. altoides PETKOVSKI, 1961

Candona (Candona) burdurensis FREELS, 1980

Sample MP5. Upper Akdere Road Section (Unit 13) TG609749.

AKDERE MEMBER

Candona (Candona) decimai FREELS, 1980

Candona (Candona) altoides PETKOVSKI, 1961

Candona nobilis (SNEJDER, 1963)

Candona (Candona) xanthica FREELS, 1980

Candona (Caspiocypris) erzurumensis FREELS, 1980

Candona (Typhlocypris) fossulata POKORNY, 1952

Candona (Typhlocypris) amblygonica FREELS, 1980

Sample MP6. Upper Akdere Road Section (Unit 17) TG609749.

AKDERE MEMBER

Candona (Candona) decimai FREELS, 1980

Candona nobilis (SNEJDER, 1963)

Candona (Candona) cf. xanthica FREELS, 1980

Candona (Caspiocypris) erzurumensis FREELS, 1980

Candona (Typhlocypris) fossulata POKORNY, 1952

Candona (Typhlocypris) amblygonica FREELS, 1980

Ilyocypris bradyi SARS, 1890

Cyprideis seminulum seminulum (REUSS, 1850)

Heterocypris salina salina (BRADY, 1868)

Sample MP24. Upper Akdere Road Section (Unit 24) TG609749.

AKDERE MEMBER

Heterocypris salina salina (BRADY, 1868)

The following samples are not from logged sections:

Sample MP8. TG600929.

ÇENDIK MEMBER

Cyprideis pontica KRSTIC, 1970

Cyprideis seminulum seminulum (REUSS, 1850)

Heterocypris salina barneri (LUTTIG, 1955)

Zonocypris membranae membranae (LIVENTAL, 1937)

Candona (Candona) decimai FREELS, 1980

Candona (Candona) altoides PETKOVSKI, 1961
Candona nobilis (SNEJDER, 1963)
Ilyocypris bradyi SARS, 1890
Ilyocypris gibba (RAMDOHR, 1808)

Sample MP23. TG424596.
ÇENDIK MEMBER
"Pontocythere" bayramensis TUNOGLU and GÖKÇEN, 1985
Candona (Candona) altoides PETKOVSKI, 1961
Candona nobilis (SNEJDER, 1963)
Candona cf. namanganica (SNEJDER, 1959)
Candona (Typhlocypris) fossulata POKORNY, 1952
Ilyocypris bradyi SARS, 1890

Sample MP19. TG383688.
QUATERNARY
Candona (Candona) angulata (MULLER, 1900)
Candona (Candona) neglecta SARS, 1888
Candona parallela pannonica ZALANYI, 1959
Candona (Typhlocypris) eremita (VEJDOVSKY, 1880)
Candona (Typhlocypris) amblygonica FREELS, 1980
Limnocythere cf. inopinata (BAIRD, 1843)

Sample MP20. TG662756.
YAKAKÖY TRAVERTINE
Candona parallela pannonica ZALANYI, 1959
Ilyocypris bradyi SARS, 1890
Prionocypris zenkeri (CHYZER and TOTH, 1858)
Candona (Pontoniella) acuminata (ZALANYI, 1929)
Candona (Pontoniella) loczyi (ZALANYI, 1929)
Candona (Pontoniella) saxagintae STANCHEVA, 1981

Sample MP10. TG420409.
AKDERE MEMBER
Candona nobilis (SNEJDER, 1963)
Candona parallela pannonica ZALANYI, 1959
Candona (Candona) cf. altoides PETKOVSKI, 1961
Prionocypris zenkeri (CHYZER and TOTH, 1858)
Ilyocypris bradyi SARS, 1890
Heterocypris cf. salina salina (BRADY, 1868)

Sample MP13. TG439488.

AKDERE MEMBER

Heterocypris salina salina (BRADY, 1868)
Heterocypris vialovi (SNEJDER, 1961)
Candona (Candona) cf. candida (MULLER, 1776)
Candona (Candona) decimai FREELS, 1980
Prionocypris cf. zenkeri (CHYZER and TOTH, 1858)
Ilyocypris bradyi SARS, 1890

Sample MP18. TG603665.

AKDERE MEMBER

Heterocypris salina salina (BRADY, 1869)
Heterocypris vialovi (SNEJDER, 1961)
Heterocypris salina barneri (LUTTIG, 1955)
Prionocypris zenkeri (CHYZER and TOTH, 1858)
Candona (Candona) xanthica FREELS, 1980
Candona nobilis (SNEJDER, 1963)
Candona (Candona) decimai FREELS, 1980
Candona (Candona) altoides PETKOVSKY, 1961

Sample MP21. TG530682.

AKDERE MEMBER

Ilyocypris bradyi SARS, 1890
Candona (Candona) candida (MULLER, 1776)
Candona cf. nobilis (SNEJDER, 1963)
Candona (Candona) xanthica FREELS, 1890
Candona (Typhlocypris) eremita (VEJDOVSKY, 1880)
Candona (Candona) cf. erzerumensis FREELS, 1980

Sample MP22. TG671757.

GÜNALAN MEMBER

Heterocypris salina salina (BRADY, 1869)
Heterocypris salina barneri (LUTTIG, 1955)
Heterocypris viavoli (SNEJDER, 1961)
Candona parallela pannonica ZALANYI, 1929
Prionocypris zenkeri (CHYZER and TOTH, 1858)
Candona (Typhlocypris) fossulata POKORNY, 1952
Candona cf. nobilis (SNEJDER, 1963)
Candona (Candona) xanthica FREELS, 1980

APPENDIX II.

Plate 7.2 (Chapter 7) was generated on the I²S system 600 at B.G.S. in Keyworth using a single-waveband Landsat 5 Thematic Mapper image. Molecular water absorbs electromagnetic energy in a number of narrow infrared wavebands due to the stretching and bending of H-O-H bonds (Hunt 1980). Waveband 5 was chosen for enhancement because the wavelength it measures (λ=1.55-1.75μm) partially overlaps the water absorption peak centred on 1.4μm and hence, it records changes in water content. This is ideal for the poorly-vegetated Neogene, since any variation should be a result of solar irradiance, which varies with slope angle and azimuth to produce shadows. In any non-vegetated or evenly-vegetated (i.e. see Drury 1986) region the variation in intensity of waveband 5 represents a sun-illuminated topography. To introduce the effect of an artificial sunset the image was processed by directional filtering. A convolution was performed on the original image based on a square matrix of variously weighted cells, whose dimensions are equivalent to image pixels. The central cell of the matrix overlies each pixel in turn, and the process of convolution calculates new intensities based on the cell values and the intensities of the pixels overlain by the matrix (Curran 1985). In Plate 7.2 an artificial sunset from the NE is used by performing a convolution with the following matrix:

$$\begin{pmatrix} 1 & 1 & 1 \\ -1 & 0 & 1 \\ -1 & -1 & -1 \end{pmatrix}$$

This matrix has the effect of removing any variations due to vegetation but many distinctive features may be the remnants of agricultural boundaries, evaporation lines on a playa (see, for example, Acigöl) or roads.

Sedimentation and Neotectonics of the Burdur Region, southwest Turkey.

Simon Paul Price.

The NE-SW trending Burdur-Acigöl-Baklan basin system of southwest Turkey represents the present-day configuration of a system initiated in late Miocene / early Pliocene times. During the Pliocene a half-graben, controlled by a NW-dipping planar fault system, developed in the area around Burdur. The Burdur Formation was deposited in this half-graben. Rapid subsidence is indicated by the lack of a well-developed footwall-sourced fan system. However, larger fans developed in the relay structures between en echelon fault segments. The centre of the basin was occupied by a deep saline lake. Orbitally-driven climatic change was the dominant control on sedimentation in this lake. The scarcity of wet-sediment deformation within the Burdur Formation suggests that levels of Pliocene seismicity were lower than twentieth century levels.

Towards the end of the Pliocene the fault system controlling the Burdur basin became inactive and renewed faulting took place in the hangingwall of the old system. This event gave rise to the present-day configuration of narrow basins in the study area and was due to instability of the end-Pliocene topography. Both margins of the present-day Burdur, Acigöl and Baklan basins are faulted. In each case the major throw is on the fault on the southeast margin. A β value of 1.18 calculated for the Burdur region assumes a planar fault geometry. As a curvature of up to 40° at depth cannot be ruled out this must be considered a minimum estimate.

Each of the Burdur, Acigöl and Baklan basins is extending in a NW-SE direction (compared to the N-S extension direction of the Aegean). It is proposed that the basins are within a N-S trending deforming zone between the rapidly-extending Aegean region (to the west) and the relatively stable Anatolian plateau (to the east). The model adopted explains the clockwise rotation of fault-bounded blocks in the Burdur region. The dextral motion across the deforming zone, predicted by the model, may be a result of the anticlockwise rotation of western Turkey.


LEICESTER UNIVERSITY LIBRARY